Tuning the Biophysical and Biochemical Cues of Fibrin Microthread Scaffolds Towards the Treatment of Volumetric Muscle Loss

A Dissertation
Submitted to the Faculty of

WORCESTER POLYTECHNIC INSTITUTE

in partial fulfillment of the requirements for the

Degree of Doctor of Philosophy in
Biomedical Engineering

August 20, 2020

By

Meagan Eva Carnes

Approved by:

George D. Pins, Ph.D.
Professor, Advisor
Biomedical Engineering
Worcester Polytechnic Institute

Raymond L. Page, Ph.D.
Professor of Practice
Biomedical Engineering
Worcester Polytechnic Institute

Jeannine M. Coburn, Ph.D.
Assistant Professor
Biomedical Engineering
Worcester Polytechnic Institute

Tanja Dominko, D.V.M., Ph.D.
Professor
Biology and Biotechnology
Worcester Polytechnic Institute

Jonathan M. Grasman, Ph.D.
Assistant Professor
Biomedical Engineering
New Jersey Institute of Technology

Acknowledgements

First, I would like to thank my advisor, George Pins, Ph.D., for his unwavering support and guidance. His mentorship has allowed me to become an independent scientist, and for that I am very grateful. I will miss our many long meetings in your office discussing research, IPAs, skiing, politics, and of course baseball. I truly cannot thank you enough for everything!

I would like to thank my dissertation committee Ray Page, Ph.D., Tanja Dominko, D.V.M., Ph.D., Jeannine Coburn, Ph.D., and Jon Grasman, Ph.D. I am thankful for the time, support, and guidance they provided throughout my Ph.D.; their constructive feedback strengthened my work and helped me become a better scientist. Many thanks to the rest of the BME faculty, Gateway staff, and IGERT faculty and staff for the support, technical assistance, and training you have provided me. I feel blessed to have been a part of this supportive community.

I was lucky to have great educators along the way who sparked my interest in science and research. I owe special thanks to Frank Buono, who encouraged me to never settle as a line cook when you can be a chef; this inspired me to become an independent scientist. Thanks to Ashok Ramasubramanian, Ph.D., for allowing me to gain hands-on research experience in his lab.

I owe a huge thanks to my fellow graduate students, past and present, with whom I've shared countless good conversations, laughs, hugs, tears, and beers. This experience truly would not have been the same without you, and I am thankful for the lifelong friendships we have formed. A special thanks to my fellow IGERT and Pins lab peers for providing technical assistance, feedback, and emotional support. I also owe a huge thanks to the undergraduate students who have helped me along the way; I'm sure I would still be in the lab right now had it not been for your help!

Finally, I would like to thank my biggest supporters: my family and friends. Andrew, you've always been one of my biggest supporters through my Ph.D. and life! I am so thankful to have had you by my side through this long and challenging journey and am grateful for your unwavering support, love, and friendship. To my mom and dad, Joanne and Kevin, thank you for a lifetime of support and encouragement! You helped me through some of my most challenging times in graduate school, from reconstructive ankle surgery year one to a thyroidectomy year six and everything in between. I would also like to thank my sister and brother, Amy and Michael, and my soon-to-be family, the Thistles, for their unwavering support. Thanks to my friends for the encouragement and much needed distractions throughout. The road to my Ph.D. has been long and challenging, but incredibly rewarding. I am thankful to have been on this journey with you all! Thank you all!

Table of Contents

Table of Figures

Table of Tables

Abbreviations

1° HRP crosslinked – Microthreads crosslinked via primary co-extrusion method
1°/2° HRP crosslinked – Microthreads crosslinked via primary and secondary methods
2° HRP crosslinked – Microthreads crosslinked via secondary post-processing method
2D – Two-dimensional
3D – Three-dimensional
AChR – Acetylcholine receptor
ASCs – Adipose-derived stem cells
AFM – Atomic force microscopy
ANOVA – Analysis of variance
AU – Arbitrary units
ATR – Attenuated total reflectance
BSA – Bovine serum albumin
BMP-2 – Bone morphogenetic protein-2
C-SFM – Conditioned serum free medium
CD31 – Cluster of differentiation 31
CEP – ω-[2-carboxyethyl]pyrrole
CLI – Critical limb ischemia
Co-inc – Microthreads co-extruded with fibroblast growth factor 2
CT – Computed tomography
DI – Deionized
dH_2O – Deionized water
DMEM – Dulbecco's Modified Eagle medium
ECs – Endothelial cells
ECM – Extracellular matrix
EDC – 1-ethyl-3-(3-dimethylaminopropyl) carbodiimide
EDC – Microthreads crosslinked with EDC
EDC then HEP 1000 – Microthreads EDC crosslinked then adsorbed with 1000 μg/mL heparin
EDCn – Microthreads EDC crosslinked in neutral buffer
EDC HEP 10 – Microthreads conjugated with 10 μg/mL heparin via EDC crosslinking
EDC HEP 100 – Microthreads conjugated with 100 μg/mL heparin via EDC crosslinking
EDC HEP 1000 – Microthreads conjugated with 1000 μg/mL heparin via EDC crosslinking
EDL – Extensor digitorum longus
ELISA – Enzyme-linked immunosorbent assay

EMG – Needle electromyography
EtO – Ethylene oxide
F-actin – Filamentous actin
FBS – Fetal bovine serum
FGF – Fibroblast growth factor
FGF2 – Fibroblast growth factor 2
FGF6 – Fibroblast growth factor 6
FFMT – Free functional muscle transfer
FFT – Fast fourier transform
FITC – Fluorescein isothiocyanate
FTIR – Fourier transform infrared spectroscopy
FWHM -- Full width half maximum
GAG – Glycosaminoglycan
GFP – Green fluorescent protein
GNDF – Glial-derived neurotrophic factor
HA – Hyaluronic acid
HBS – HEPES buffered saline
HEPES – N-[2-Hydroxyethyl]piperazine-N'-[2-ethanesulfonic acid]
HGF – Hepatocyte growth factor
HRP – Horseradish peroxidase
ID – inner diameter
IGF – Insulin-like growth factor
IGF-1 – Insulin-like growth factor 1
IGF-2 – Insulin-like growth factor 2
IL-1β – Interleukin 1β
IL-6 – Interleukin 6
IM – Intramuscular
iPSCs – Induced pluripotent stem cells
IQR – Inner quartile range
K_d – Equilibrium dissociation constant
LD – *Latissimus dorsi*
M1 – Pro-inflammatory macrophage
M2 – Alternatively activated (anti-inflammatory) macrophage
MAPKs – Mitogen-activated protein kinases
MDPCs – Muscle-derived progenitor cells
MES – 2-(N-morpholino)ethanesulfonic acid
MES 5.0 – Fibrin microthreads etched in MES buffer with pH 5.0
MES 5.5 – Fibrin microthreads etched in MES buffer with pH 5.5
MMPs – Matrix metalloproteinases
MRI – Magnetic resonance imaging
mRNA – Messenger ribonucleic acid
MSCs – Mesenchymal stem cells
MTM – Maximum tangent modulus
MyHC – Myosin heavy chain
NCS – Nerve conduction study

NGF – Nerve growth factor
NHS – N-hydroxysuccinimide
NMJ – Neuromuscular junction
NO – Nitric oxide
Pax7 – Paired box gene 7
PBS – Phosphate buffered saline
PCL – Poly(ε-caprolactone)
PDGF – Platelet derived growth factor
PDMS – Polydimethylsiloxane
PECAM – Platelet endothelial cell adhesion molecules
PEG – Polyethylene glycol
PGA – Poly(glycolic acid)
PLA/PLLA – Poly(lactic acid)
PLGF – Placental growth factor
PLG/PLGA – Poly-lactic-*co*-glycolic acid
PP – Polypropylene
PRP – Platelet rich plasma
PSCs – Perivascular stem cells
PU – Polyurethane
ROS – Reactive oxygen species
Rq – Root mean square roughness
RT – Room temperature
RT-qPCR – Quantitative reverse transcription polymerase chain reaction
S1P – Sphingosine-1-phosphate
SA – Surface area
SAF – Strain at failure
SC – Satellite cell
SDF-1α – Stromal cell-derived factor 1-α
SEM – Scanning electron microscopy
SEM – Standard error of the mean
SFM – Serum free medium
SIS – Small intestinal submucosa
TA – *Tibialis anterior*
TCP – Tissue culture plastic
TBS – Tris buffered saline
TEMG – Tissue engineered muscle graft
TGF-β – Transforming growth factor-β
TNF-α – Tumor necrosis factor-α
UBM – Urinary bladder matrix
UNX – Uncrosslinked fibrin microthreads
UNX 1° HRP – Uncrosslinked microthreads co-incorporated with HRP
UNX 2° H_2O_2 – Uncrosslinked microthreads in H_2O_2 post-processing bath
UNX HEP 10 – Uncrosslinked microthreads passively adsorbed with 10 μg/mL heparin
UNX HEP 1000 – Uncrosslinked microthreads passively adsorbed with 1000 μg/mL heparin
UTS – Ultimate tensile strength

UV – Ultraviolet
VEGF – Vascular endothelial growth factor
VML – Volumetric muscle loss
vWF – von Willebrand factor

Abstract

65.8 million Americans suffer from musculoskeletal injuries annually, with treatment costs exceeding 176 billion dollars. These injuries can cause volumetric muscle loss (VML), where severe musculoskeletal injury results in poor functional recovery. Due to the severity of VML injuries, the extracellular matrix (ECM) surrounding myofibers is destroyed. This normally provides mechanical support, topographic alignment cues, and bioactive signaling molecules, such as fibroblast growth factor 2 (FGF2), to orchestrate regeneration. The current standard of care for treating VML is autologous tissue transfer, but this procedure is unable to restore function and can result in complications including infection and graft failure. Thus, an unmet clinical need remains to develop a treatment that restores function to VML injuries. Towards this, tissue engineered scaffolds are being developed to enhance functional muscle regeneration by incorporating biophysical and biochemical cues that mimic native skeletal muscle tissue composition, architecture, mechanics, and bioactive signaling. In this thesis, we developed strategies to tune the biophysical and biochemical cues of fibrin microthreads, a cylindrical fibrous scaffold that mimics the structure of a muscle fiber. The goal of this project was to develop fibrin microthreads with anisotropic surface features, robust mechanical properties, and physiologically relevant, sustained release of FGF2 to direct the cellular processes that will ultimately enhance functional skeletal muscle regeneration in VML injuries. We developed a method to etch microthreads in an acidic buffer, and found this created aligned, sub-micron surface features on microthreads while maintaining microthread bulk mechanical properties. Microthreads etched in acidic buffer enhanced myoblast alignment and filamentous stress fiber organization compared to control microthreads. Next, we developed enzymatic crosslinking strategies using horseradish peroxidase (HRP) by either incorporating crosslinkers during microthread production or in a post-processing bath. Varying incorporation strategies enabled the development of HRP crosslinked microthreads with enhanced tensile strengths and a decreased rate of plasmin-mediated degradation, while maintaining myoblast viability. Finally, we evaluated the effect of co-incorporating FGF2 within microthreads or passively adsorbing FGF2 to heparin-conjugated microthreads, mimicking FGF2 sequestration in ECM. Fibrin microthreads demonstrated sustained release of FGF2 over one week and enhanced myoblast proliferation and outgrowth *in vitro*. We expect the strategic engineering of biophysical and biochemical cues through the development of aligned topographic features, enzymatic crosslinking, and sustained FGF2 delivery will further develop fibrin microthread scaffolds towards the goal of creating a treatment that restores function following VML injuries.

Chapter 1: Overview

1.1 INTRODUCTION

A total of 65.8 million Americans suffer from musculoskeletal injuries annually, with treatment costs exceeding 176 billion dollars.[1-5] These injuries can cause volumetric muscle loss (VML), where severe musculoskeletal injury results in scar tissue deposition and poor functional recovery.[6, 7] Because of the complex and large-scale nature of VML injuries, treatment options remain limited and have substantial disadvantages. The current standard of care for VML is autologous tissue transfer, where a muscle flap is excised from an undamaged muscle and grafted into the injury site.[8-11] While this has been moderately successful in restoring some function, muscle flaps remain unable to effectively restore muscle function.[11-14] Additionally, a high instance of muscle flap procedures result in complications including up to 10% graft failure, infection, and donor site morbidity related to tissue necrosis.[10, 11, 15, 16] Often a revision surgery or amputation of the affected limb is required.[10, 11, 15, 16] *As such, a clinical need remains for the development of an alternative treatment that will restore function in VML injuries.*

Skeletal muscle regeneration is a highly coordinated process that is driven by native biochemical and biophysical cues of the tissue. In the case of small-scale injuries, skeletal muscle is capable of endogenous repair through activation of muscle progenitor cells, or satellite cells (SCs), which proliferate and differentiate to form mature myotubes that restore contractile function to damaged muscle tissue.[17] The basement membrane surrounding muscle fibers provides mechanical support, contact guidance cues, and growth factor reservoirs that are necessary for skeletal muscle regeneration. Skeletal muscle extracellular matrix (ECM) surrounding myofibers has a highly aligned and fibrous architecture, which provides these contact guidance cues and plays an important role in dictating muscle tissue structure, function, and repair.[18] Upon initial injury, disruption of the basement membrane initiates release of heparan sulfate proteoglycan-bound growth factors within this matrix, including fibroblast

growth factor 2 (FGF2).[19-23] FGF2 is responsible for stimulating the proliferation and migration of activated SCs,[24-27] and is present in injured muscle tissue 2-8 days after injury.[28] In the case of VML injuries, however, the basement membrane and connective tissue are destroyed. Without these biophysical and biochemical cues to guide regeneration, VML injuries fill with scar tissue and are unable to direct functional repair. *A treatment which replaces the biophysical and biochemical cues of the ECM that are destroyed in VML may guide functional skeletal muscle regeneration after VML injuries.*

To overcome the limitations of current clinical treatments for VML injuries, tissue engineered biomaterial scaffolds are under development with the goal of preventing scar tissue formation and enhancing functional muscle regeneration. Skeletal muscle tissue engineering and regenerative medicine present a promising therapeutic strategy by repairing or replacing the damaged muscle with a combination of instructive biomaterial scaffolds, biologically active molecules, and cells.[29, 30] Tissue engineered scaffolds are three-dimensional (3D) constructs that recapitulate the native ECM milieu, creating a synthetic microenvironment to locally control cellular functions and guide regeneration. To accomplish this, scaffolds must incorporate biophysical and biochemical cues that mimic native tissue composition, architecture, mechanics, and bioactive signaling. Scaffolds that guide skeletal muscle regeneration must facilitate the formation of aligned myotubes parallel to the force conduction pathway to maximize functional regeneration. These scaffolds must (1) provide mechanical support to the regenerating tissue, (2) promote aligned myotube formation, and (3) deliver growth factors to promote myogenesis and angiogenesis.[31] While progress has been made towards this*, an unmet need remains for a scaffold capable of meeting all of these needs simultaneously.*[32, 33]

Towards this goal, our laboratory developed fibrin microthreads, a novel scaffold resembling the architecture of native muscle fibers. This scaffold approximates the fibrillar structure of native skeletal muscle ECM, which allows it to provide structural support and promote cellular alignment.[34] These scaffolds have been chemically crosslinked with 1-ethyl-3-(3-dimethyl aminopropyl) carbodiimide (EDC) to strengthen their structural properties and resistance to proteolytic degradation,[35] and used to deliver growth factors such as hepatocyte growth factor (HGF).[36, 37] Fibrin microthreads have been shown to be a promising therapeutic treatment for VML injuries.[37, 38] In an *in vivo* murine model of VML, treatment with EDC

crosslinked and HGF-loaded fibrin microthreads promoted the recovery of force production after 60 days following injury.[37] However, challenges such as limited scaffold degradation and rapid release of HGF from the microthreads likely contributed to the lack of full functional regeneration of the tissue, and necessitate the development of strategies to further tune scaffold mechanical properties, and to control degradation rates and release of myogenic growth factors.

1.2 OVERALL GOAL and HYPOTHESIS

The overall objective of this dissertation was to develop fibrin microthread scaffolds with both biophysical and biochemical signaling cues that mimic native skeletal muscle tissue properties.

Specifically, the goal of this project was to develop a fibrin microthread scaffold with anisotropic surface features, robust mechanical properties, and sustained release of FGF2 towards the ultimate goal of restoring function in VML injuries.

To systematically test this, the project was divided into three specific aims. In Specific Aim 1, we developed a method to create aligned, grooved features on the surface of fibrin microthreads to enhance myoblast alignment. We placed fibrin microthreads into 2-(N-morpholino)ethane-sulfonic acid (MES) acidic buffer and evaluated the effect of buffer pH on the generation of these features. In Specific Aim 2 we developed enzymatic crosslinking strategies using horseradish peroxidase (HRP) to enhance scaffold mechanical properties and decrease the rate of plasmin-mediated degradation while maintaining myoblast viability. We studied the effect of varying HRP and hydrogen peroxide (H_2O_2) incorporation strategies on the resulting crosslink density and structural properties of fibrin microthreads by incorporating crosslinking agents during or after microthread production. In Specific Aim 3, we developed fibrin microthreads with sustained release of FGF2 to enhance myoblast proliferation and outgrowth *in vitro*. We evaluated two incorporation strategies, covalently conjugating heparin to fibrin microthreads, mimicking FGF2 sequestration in the basement membrane, and mixing FGF2 within microthreads prior to extrusion for their ability to create sustained release of FGF2. We expect the strategic engineering of biophysical and biochemical cues including aligned topographic features, enzymatic crosslinking, and sustained delivery of FGF2 will further

develop fibrin microthread scaffolds towards the goal of creating a treatment for VML capable of enhancing functional skeletal muscle regeneration.

1.3 SPECIFIC AIM 1: CREATE AND CHARACTERIZE ANISOTROPIC SURFACE TOPOGRAPHY ON FIBRIN MICROTHREADS TO ENHANCE MYOBLAST ALIGNMENT

To regenerate functional muscle tissue, engineered scaffolds should impart topographical features to induce myoblast alignment by a phenomenon known as contact guidance. Myoblast alignment is an essential step towards myotube formation, which is guided *in vivo* by extracellular matrix structure and micron-scale grooves between adjacent muscle fibers.[18] Fibrin microthread scaffolds mimic the morphological architecture of native muscle tissue and have demonstrated promise as an implantable scaffold for treating skeletal muscle injuries.[37, 39] While these scaffolds promote modest myoblast alignment, it is not sufficient to generate highly functional muscle tissue. In Chapter 3 of this dissertation we develop and characterize a new method of etching the surface of fibrin microthreads to incorporate aligned, sub-micron grooves which promote myoblast alignment. To generate these topographic features, we placed fibrin microthreads into MES acidic buffer and evaluated the effect of buffer pH on the generation of these features. Surface characterization with atomic force microscopy and scanning electron microscopy indicated the generation of aligned, sub-micron sized grooves on microthreads in MES buffer with pH 5.0. Microthreads etched with surface features had tensile mechanical properties comparable to controls, indicating that surface treatment does not inhibit scaffold bulk properties. Our data demonstrates that etching threads in MES buffer with pH 5.0 enhanced alignment and filamentous actin stress fiber organization of myoblasts on the surface of scaffolds. The ability to tune topographic features on the surfaces of scaffolds independent of mechanical properties provides a valuable tool for designing microthread-based scaffolds to enhance regeneration of functional muscle tissue. *Carnes, M. E. and Pins, G. D. Etching anisotropic surface topography onto fibrin microthread scaffolds for guiding myoblast alignment. Journal of Biomedical Materials Research Part B* ***2020****; 108(5): 2308-2319.*

1.4 SPECIFIC AIM 2: ENZYMATICALLY CROSSLINK FIBRIN MICROTHREADS WITH HORSERADISH PEROXIDASE TO ENHANCE MECHANICAL PROPERTIES AND DECREASE DEGRADATION RATE WHILE MAINTAINING MYOBLAST VIABILITY

Horseradish peroxidase (HRP) has been investigated as a catalyst to crosslink tissue engineered hydrogels because of its mild reaction conditions and ability to modulate the mechanical properties of the matrix.[40, 41] Here we report the results of the first study investigating the use of HRP to crosslink fibrin scaffolds. In Chapter 4 we examined the effect of varying HRP and hydrogen peroxide (H_2O_2) incorporation strategies on the resulting crosslink density and structural properties of fibrin in a microthread scaffold format. Primary and secondary scaffold modification techniques were evaluated to crosslink fibrin microthread scaffolds. The incorporation of crosslinking agents into the precursor solutions during extrusion of microthreads was considered a primary (1º) modification method, while soaking microthreads in a post-processing crosslinker bath was considered a secondary (2º) method of scaffold modification. Fibrin microthreads were enzymatically crosslinked through primary, secondary, or a combination of both approaches. All fibrin microthread scaffolds crosslinked with HRP and H_2O_2 via primary and/or secondary methods exhibited an increase in dityrosine crosslink density compared to uncrosslinked control microthreads, demonstrated by scaffold fluorescence. Fourier transform infrared spectroscopy indicated the formation of isodityrosine bonds in 1º HRP crosslinked microthreads. Characterization of tensile mechanical properties revealed that all HRP crosslinked microthreads were significantly stronger than control microthreads. Primary (1º) HRP crosslinked microthreads also demonstrated significantly slower degradation than control microthreads, suggesting that incorporating HRP and H_2O_2 during extrusion yields scaffolds with increased resistance to proteolytic degradation. Finally, cells seeded on HRP crosslinked microthreads retained a high degree of viability, demonstrating that HRP crosslinking yields biocompatible scaffolds suitable for tissue engineering. The goal of this work was to facilitate the logical design of enzymatically crosslinked fibrin microthreads with tunable structural properties, enabling their application for engineered tissue constructs with varied mechanical and structural properties. *Carnes, M. E., Gonyea, C. R., Mooney, R. G., Njihia, J. W., Coburn, J. M.,*

and Pins, G. D. Horseradish peroxidase-catalyzed crosslinking of fibrin microthread scaffolds. Tissue Engineering Part C: Methods. ***2020****; 26(6): 316-331.*

1.5 SPECIFIC AIM 3: DEVELOP FIBRIN MICROTHREADS WITH FIBROBLAST GROWTH FACTOR 2 RELEASE PROFILES TO ENHANCE MYOBLAST PROLIFERATION AND OUTGROWTH

FGF2's pleiotropic effect on promoting myogenesis, angiogenesis, and innervation make it an ideal growth factor for treating VML injuries. To mitigate challenges with FGF2 delivery such as supraphysiological dosing and short *in vivo* half-life,[42, 43] bioinspired conjugation strategies have been investigated using heparin to mimic sequestration of FGF2 in the ECM.[19, 44-46] While the therapeutic potential of sustained FGF2 delivery has been demonstrated, it has primarily been performed in hydrogel scaffolds, which lack biophysical cues such as mechanical support and aligned contact guidance.[47-49] Fibrin is an ideal scaffold material for incorporating FGF2, as it binds with high affinity to FGF2 and protects it from proteolytic degradation.[50] The sustained delivery of FGF2 from scaffolds with robust mechanical properties and topographic alignment cues has yet to be explored for treating VML. The goal of this aim was to develop an instructive fibrin microthread scaffold with physiologically relevant, sustained release of FGF2. To accomplish this, we covalently coupled heparin to fibrin microthreads, creating a biomimetic conjugation strategy analogous to FGF2 sequestration in the basement membrane. We also evaluated whether incorporation of FGF2 within fibrin microthreads by mixing prior to extrusion would yield sustained release of FGF2. We hypothesized that heparin conjugated and co-incorporated fibrin microthreads would provide sustained release of FGF2 from the scaffold and enhance *in vitro* myoblast proliferation and outgrowth. Toluidine blue staining and fourier transform infrared spectroscopy confirmed heparin conjugation to fibrin microthreads by demonstrating increased dye uptake and amide bond peaks with increasing heparin concentration, respectively. FGF2 release kinetics revealed that fibrin microthreads conjugated with heparin had sustained release of FGF2 over one week. A Transwell®-based proliferation assay revealed that FGF2 released from fibrin microthread scaffolds remained bioactive, stimulating myoblast proliferation over a period of four days *in vitro*. Finally, a 3D outgrowth assay suggests that FGF2-loaded fibrin microthreads may promote increased outgrowth onto

fibrin microthreads. Sustained release of FGF2 from fibrin microthreads addresses limitations in the field and enable the development of a scaffold that synergistically provides biochemical and biophysical cues. We anticipate that the combined effect of fibrin microthread mechanical properties, topographic alignment cues, and FGF2 will be an effective scaffold to enhance the regeneration of functional muscle tissue in VML injuries. *Carnes, M. E. and Pins, G. D. Sustained release of FGF2 from fibrin microthread scaffolds for skeletal muscle tissue engineering. In preparation 2020.*

1.6 REFERENCES

1. National Hospital Discharge Survey (NHDS). *Center for Disease Control* **2010**.
2. National Hospital Ambulatory Medical Care Survey Outpatient Department (NHAMCS_OP). *Center for Disease Control* **2010**.
3. National Hospital Ambulatory Medical Care Survey Emergency Department (NHAMCS_ED). *Center for Disease Control* **2010**.
4. National Ambulatory Medical Care Survey (NAMCS). *Center for Disease Control* **2010**.
5. Medical Expenditures Panel Survey (MEPS), Agency for Healthcare Research and Quality, U.S. Department of Health and Human Services, 1996-2011. **2011**.
6. Devore, D. I., Walters, T.J., Christy, R.J., Rathbone, C.R., Hsu, J.R., Baer, D.G., and Wenke, J.C., For Combat Wounded: Extremity Trauma Therapies From the USAISR. *Military Medicine* **2011,** *176* (6), 660-663.
7. Surgeons, A. S. o. P., 2014 Plastic Surgery Statistics Report. Statistics, A. N. C. o. P. S. P., Ed. 2014.
8. Grogan, B. F.; Hsu, J. R.; Consortium, S. T. R., Volumetric Muscle Loss. *J Am Acad Orthop Sur* **2011,** *19*, S35-S37.
9. Doi, K.; Hattori, Y.; Tan, S. H.; Dhawan, V., Basic science behind functioning free muscle transplantation. *Clin Plast Surg* **2002,** *29* (4), 483-95, v-vi.
10. Eckardt, A., Microsurgical reconstruction in the head and neck region: an 18-year experience with 500 consecutive cases. *Journal of Cranio-Maxillofacial Surgery* **2003,** *31* (4), 197-201.
11. Lin, C. H.; Lin, Y. T.; Yeh, J. T.; Chen, C. T., Free functioning muscle transfer for lower extremity posttraumatic composite structure and functional defect. *Plast Reconstr Surg* **2007,** *119* (7), 2118-26.
12. Pochini, A. D., Andreoli, C.V., Belangero, P.S., Figueiredo, E.A., Terra, B.B., Cohen, C., Andrade, M.D., Cohen, M., Ejnisman, B., Clinical Considerations for the Surgical Treatment of Pectoralis Major Muscle Ruptures Based on 60 Cases: a Prospecitve Study and Literature Review. *Amer J of Sports Med* **2014,** *42* (1), 95-102.
13. Äärimaa, V., Rantanen, J., Heikkilä, J., Helttula, I. and Orava, S., Rupture of the Pectoralis Major Muscle. *Amer J of Sports Med* **2004,** *32* (5), 1256-1262.
14. Riccio, M.; Zingaretti, N.; Verdini, F.; Marchesini, A.; De Francesco, F.; Parodi, P. C., Functional donor-site morbidity after soleus muscle-flap procedure in the treatment of lower limb severe injuries. *Handchir Mikrochir Plast Chir* **2019,** *51* (6), 453-463.
15. Bianchi, B.; Copelli, C.; Ferrari, S.; Ferri, A.; Sesenna, E., Free flaps: outcomes and complications in head and neck reconstructions. *J Craniomaxillofac Surg* **2009,** *37* (8), 438-42.

16. Lawson, R.; Levin, L. S., Principles of free tissue transfer in orthopaedic practice. *The Journal of the American Academy of Orthopaedic Surgeons* **2007,** *15* (5), 290-9.
17. Rudnicki, M. A., Le Grand, F., McKinnell, I., Kuang, S., The molecular regulation of muscle stem cell function. *Cold Spring Harb. Symp. Quant. Biol.* ` **2008,** *73*, 323-331.
18. Gillies, A. R.; Lieber, R. L., Structure and function of the skeletal muscle extracellular matrix. *Muscle & nerve* **2011,** *44* (3), 318-31.
19. Folkman, J.; Klagsbrun, M.; Sasse, J.; Wadzinski, M.; Ingber, D.; Vlodavsky, I., A heparin-binding angiogenic protein--basic fibroblast growth factor--is stored within basement membrane. *The American journal of pathology* **1988,** *130* (2), 393-400.
20. Bashkin, P.; Doctrow, S.; Klagsbrun, M.; Svahn, C. M.; Folkman, J.; Vlodavsky, I., Basic fibroblast growth factor binds to subendothelial extracellular matrix and is released by heparitinase and heparin-like molecules. *Biochemistry* **1989,** *28* (4), 1737-43.
21. Sanes, J. R., The basement membrane/basal lamina of skeletal muscle. *J Biol Chem* **2003,** *278* (15), 12601-4.
22. Charge, S. B. P., Rudnicki, M.A., Cellular and Molecular Regulation of Muscle Regeneration. *Physiol Rev* **2004,** *84*, 209-238.
23. Cornelison, D. D.; Olwin, B. B.; Rudnicki, M. A.; Wold, B. J., MyoD(-/-) satellite cells in single-fiber culture are differentiation defective and MRF4 deficient. *Dev Biol* **2000,** *224* (2), 122-37.
24. Sheehan, S. M.; Allen, R. E., Skeletal muscle satellite cell proliferation in response to members of the fibroblast growth factor family and hepatocyte growth factor. *J Cell Physiol* **1999,** *181* (3), 499-506.
25. Jarvinen, T. A.; Jarvinen, T. L.; Kaariainen, M.; Kalimo, H.; Jarvinen, M., Muscle injuries: biology and treatment. *Am J Sports Med* **2005,** *33* (5), 745-64.
26. Cornelison, D. D.; Filla, M. S.; Stanley, H. M.; Rapraeger, A. C.; Olwin, B. B., Syndecan-3 and syndecan-4 specifically mark skeletal muscle satellite cells and are implicated in satellite cell maintenance and muscle regeneration. *Dev Biol* **2001,** *239* (1), 79-94.
27. Cornelison, D. D.; Wilcox-Adelman, S. A.; Goetinck, P. F.; Rauvala, H.; Rapraeger, A. C.; Olwin, B. B., Essential and separable roles for Syndecan-3 and Syndecan-4 in skeletal muscle development and regeneration. *Genes Dev* **2004,** *18* (18), 2231-6.
28. Do, M. K.; Suzuki, T.; Gerelt, B.; Sato, Y.; Mizunoya, W.; Nakamura, M.; Ikeuchi, Y.; Anderson, J. E.; Tatsumi, R., Time-coordinated prevalence of extracellular HGF, FGF2 and TGF-beta3 in crush-injured skeletal muscle. *Anim Sci J* **2012,** *83* (10), 712-7.
29. Langer, R.; Vacanti, J. P., Tissue engineering. *Science* **1993,** *260* (5110), 920-6.
30. Nakayama, K. H.; Shayan, M.; Huang, N. F., Engineering Biomimetic Materials for Skeletal Muscle Repair and Regeneration. *Advanced healthcare materials* **2019,** *8* (5), e1801168.
31. Gilbert, P. M.; Havenstrite, K. L.; Magnusson, K. E.; Sacco, A.; Leonardi, N. A.; Kraft, P.; Nguyen, N. K.; Thrun, S.; Lutolf, M. P.; Blau, H. M., Substrate elasticity regulates skeletal muscle stem cell self-renewal in culture. *Science* **2010,** *329* (5995), 1078-81.
32. Qazi, T. H.; Mooney, D. J.; Pumberger, M.; Geißler, S.; Duda, G. N., Biomaterials based strategies for skeletal muscle tissue engineering: Existing technologies and future trends. *Biomaterials* **2015,** *53*, 502-521.
33. Grasman, J. M.; Zayas, M. J.; Page, R. L.; Pins, G. D., Biomimetic scaffolds for regeneration of volumetric muscle loss in skeletal muscle injuries. *Acta Biomater* **2015,** *25*, 2-15.
34. Cornwell, K. G.; Pins, G. D., Discrete crosslinked fibrin microthread scaffolds for tissue regeneration. *J Biomed Mater Res A* **2007,** *82* (1), 104-12.
35. Grasman, J. M.; Page, R. L.; Dominko, T.; Pins, G. D., Crosslinking strategies facilitate tunable structural properties of fibrin microthreads. *Acta Biomater* **2012,** *8* (11), 4020-30.
36. Grasman, J. M., Page, R. L., and Pins, G. D., Design of an In Vitro Model of Cell Recruitment for Skeletal Muscle Regeneration Using Hepatocyte Growth Factor-Loaded Fibrin Microthreads. *Tissue Eng Part A* **2017,** *23* (15-16), 773-783.

37. Grasman, J. M.; Do, D. M.; Page, R. L.; Pins, G. D., Rapid release of growth factors regenerates force output in volumetric muscle loss injuries. *Biomaterials* **2015,** *72*, 49-60.
38. Page, R. L.; Malcuit, C.; Vilner, L.; Vojtic, I.; Shaw, S.; Hedblom, E.; Hu, J.; Pins, G. D.; Rolle, M. W.; Dominko, T., Restoration of skeletal muscle defects with adult human cells delivered on fibrin microthreads. *Tissue engineering. Part A* **2011,** *17* (21-22), 2629-40.
39. Page, R. L.; Malcuit, C.; Vilner, L.; Vojtic, I.; Shaw, S.; Hedblom, E.; Hu, J.; Pins, G. D.; Rolle, M. W.; Dominko, T., Restoration of Skeletal Muscle Defects with Adult Human Cells Delivered on Fibrin Microthreads. *Tissue Eng Part A* **2011,** *17* (21), 2629-2640.
40. Khanmohammadi, M.; Dastjerdi, M. B.; Ai, A.; Ahmadi, A.; Godarzi, A.; Rahimi, A.; Ai, J., Horseradish peroxidase-catalyzed hydrogelation for biomedical applications. *Biomater Sci* **2018,** *6* (6), 1286-1298.
41. Partlow, B. P.; Applegate, M. B.; Omenetto, F. G.; Kaplan, D. L., Dityrosine Cross-Linking in Designing Biomaterials. *Acs Biomater Sci Eng* **2016,** *2* (12), 2108-2121.
42. Simons, M.; Bonow, R. O.; Chronos, N. A.; Cohen, D. J.; Giordano, F. J.; Hammond, H. K.; Laham, R. J.; Li, W.; Pike, M.; Sellke, F. W.; Stegmann, T. J.; Udelson, J. E.; Rosengart, T. K., Clinical trials in coronary angiogenesis: issues, problems, consensus: An expert panel summary. *Circulation* **2000,** *102* (11), E73-86.
43. Simons, M.; Ware, J. A., Therapeutic angiogenesis in cardiovascular disease. *Nat Rev Drug Discov* **2003,** *2* (11), 863-71.
44. Yang, H. S.; Bhang, S. H.; Hwang, J. W.; Kim, D. I.; Kim, B. S., Delivery of basic fibroblast growth factor using heparin-conjugated fibrin for therapeutic angiogenesis. *Tissue Eng Part A* **2010,** *16* (6), 2113-9.
45. Jeon, O.; Ryu, S. H.; Chung, J. H.; Kim, B. S., Control of basic fibroblast growth factor release from fibrin gel with heparin and concentrations of fibrinogen and thrombin. *Journal of Controlled Release* **2005,** *105* (3), 249-259.
46. Sakiyama-Elbert, S. E.; Hubbell, J. A., Development of fibrin derivatives for controlled release of heparin-binding growth factors. *J Control Release* **2000,** *65* (3), 389-402.
47. Zisch, A. H., Schenk, U., Schense, J. C., Sakiyama-Elbert, S. E., and Hubbell, J. A., Covalently conjugated VEGF–fibrin matrices for endothelialization. *J Control Release* **2001,** *72*, 101-113.
48. Borselli, C.; Storrie, H.; Benesch-Lee, F.; Shvartsman, D.; Cezar, C.; Lichtman, J. W.; Vandenburgh, H. H.; Mooney, D. J., Functional muscle regeneration with combined delivery of angiogenesis and myogenesis factors. *Proc Natl Acad Sci U S A* **2010,** *107* (8), 3287-92.
49. Richardson, T. P., Peters, M. C., Ennett, A. B., and Mooney, D. J., Polymeric system for dual growth factor delivery. *Nature Biotechnology* **2001,** *19*, 1029-1034.
50. Sahni, A.; Baker, C. A.; Sporn, L. A.; Francis, C. W., Fibrinogen and fibrin protect fibroblast growth factor-2 from proteolytic degradation. *Thromb Haemost* **2000,** *83* (5), 736-41.

Chapter 2: Background[1]

2.1 CLINICAL NEED: VOLUMETRIC MUSCLE LOSS

A total of 65.8 million Americans suffer from musculoskeletal injuries annually, with treatment costs exceeding 176 billion dollars.[2-6] Although these injuries are not commonly life threatening, they profoundly impact the quality of life of patients. Musculoskeletal conditions are highly debilitating, comprising the second highest global volume of years lived with disability.[7] It is estimated that these injuries result in an additional 326 billion dollars annually in lost productivity.[8] Severe musculoskeletal injuries can lead to volumetric muscle loss (VML), where extensive musculoskeletal damage and tissue loss result in permanent loss of function.[9-10] VML injuries can result from sports injuries, surgical resection, and traumatic events such as car accidents and combat injury. In particular, musculoskeletal injuries sustained in combat present a unique challenge because they lead to the highest number of disabled war fighters and have the largest disability costs.[11]

While the rate of combat mortality for U.S. Warfighters has dropped significantly since World War II, there has been a marked increase in the number of soldiers who suffer from extraordinary injuries, such as blast injuries, which impart extensive damage to the head, neck and extremities.[12] 54% of all soldiers wounded on the battlefield suffer from at least one musculoskeletal extremity injury, with 53% of these injuries involving soft tissue damage.[9, 13] Combat-related extremity injuries cause the greatest number of disabled soldiers.[11] Injured soldiers incur an average of 4.2 wounds, making extremity injuries the primary cause for hospitalization and evacuation from theater.[11] VML injuries also result in significant long-term disability that does not improve over time.[14-15] These extremity wounds also represent the largest projected disability costs of combat injuries.[11, 16] The projected lifetime disability costs of a soldier with VML is $341,200 USD per individual.[15] Extremity injuries account for 69% of

resource utilization, making them not only the most common injuries but also some of the most expensive to treat.[16]

Due to the complex and large-scale nature of VML injuries, current treatment options remain limited and have substantial disadvantages. In the case of small-scale injuries or strains, muscle is capable of endogenous regeneration and complete functional restoration. However, this ability is abated in VML, where the native biophysical and biochemical signaling cues are no longer present to facilitate regeneration. These injuries are concamitant with denervation and the destruction of native vasculature, further limiting regeneration. Currently physical therapy is the only targeted treatment for VML injuries, and it has shown limited success in improving muscle strength.[17-19] The current standard of care for VML is autologous tissue transfer, where a muscle flap is excised from an undamaged muscle and grafted into the injury site.[20-23] This procedure is commonly referred to as a free functional muscle transfer (FFMT). While FFMT has been moderately successful in salvaging limbs and restoring some muscle function, muscle flaps remain unable to completely restore muscle function.[23-26] This procedure is also complicated and time consuming to perform and requires the expertise of skilled orthopedic and microvascular surgeons, which may limit its widespread use.[20, 27] Additionally, a high instance of muscle flap procedures result in complications such as infection, graft failure, and donor site morbidity due to tissue necrosis.[22-23, 28-29] Often a revisionary surgery or amputation of the affected limb is required.[22-23, 28-29] Thus, a clinical need exists for the development of an alternative treatment that will restore function in VML injuries.

2.2 SKELETAL MUSCLE ANATOMY

Skeletal muscle is the most abundant tissue in the human body, making up approximately 40-45% of total body mass.[30] This tissue is primarily responsible for generating a series of discrete uniaxial forces that enable locomotion. It consists of hierarchically organized myofibers, vasculature, nerves, and connective tissue (**Figure 2.1**). Myofibers are elongated, cylindrical, multi-nucleated fibers that act as the functional unit of skeletal muscle. Myofibers are generated by the fusion of myoblasts to form multi-nucleated tubes, ranging in diameter from 10 - 100 μm depending on muscle location and function.[30-32] As these myofibers mature, their nuclei become oriented along the periphery just below the sarcolemma, the plasma membrane of the myofiber.

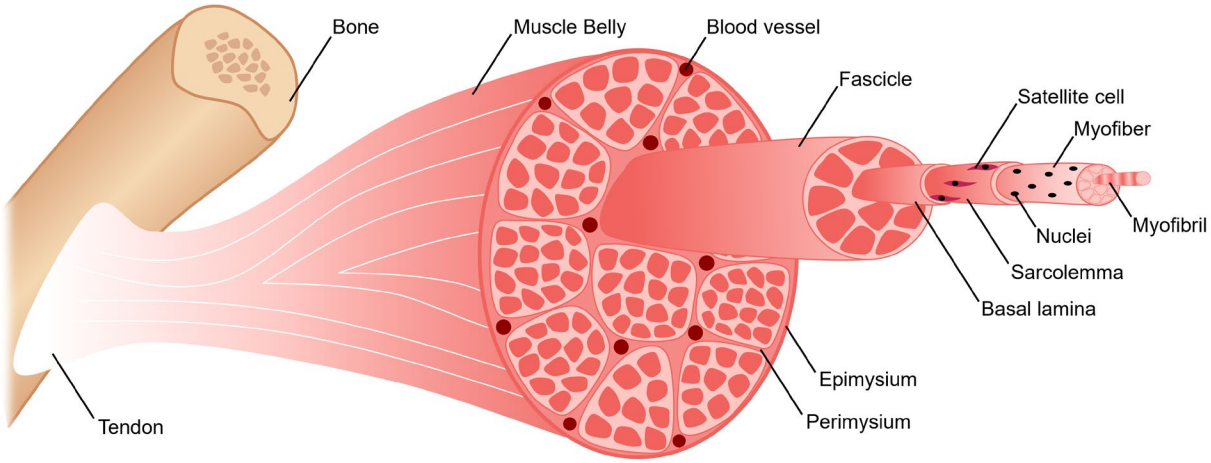

Figure 2.1. Skeletal muscle anatomy. Skeletal muscle is a highly aligned tissue with a hierarchically organized, cable-like structure.

Myofibers consist of myofibrils with repeating sarcomeres, the contractile unit of skeletal muscle. Sarcomeres contain contractile proteins thin filament actin and thick filament myosin. Within skeletal muscle tissue, parallel myofibers are bundled together to form fascicles, which are encased by perimysium. Subsequently, parallel bundles of fascicles are bundled together to form the muscle belly, which is surrounded by epimysium. Surrounding each myofiber is endomysial connective tissue known as the basement membrane and basal lamina. The perimysium, epimysium, and endomysium together provide structural support to the tissue while aiding in force transmission and synchronous contraction. The basal lamina is composed of proteins including type IV collagen, fibronectin, and laminin-2.[33-34] It also consists of glycosaminoglycans (GAGs) and proteoglycans, such as heparan sulfate, which act as reservoirs for growth factors essential for myogenesis, including hepatocyte growth factor (HGF) and fibroblast growth factor 2 (FGF2).[33-35] Heparan sulfate is also involved in HGF binding to its cell surface receptor, c-Met, by controlling the binding of HGF and regulating the cell's mitogenic activity.[36] It also significantly enhances FGF2 signaling, binding to both the growth factor and its receptor, forming a ternary complex.[37-38] Structural evaluation of skeletal muscle basement membrane shows an aligned organization of architecture, including perimysial collagen bundles approximately 0.5-1 μm in diameter that run parallel to muscle fibers.[34]

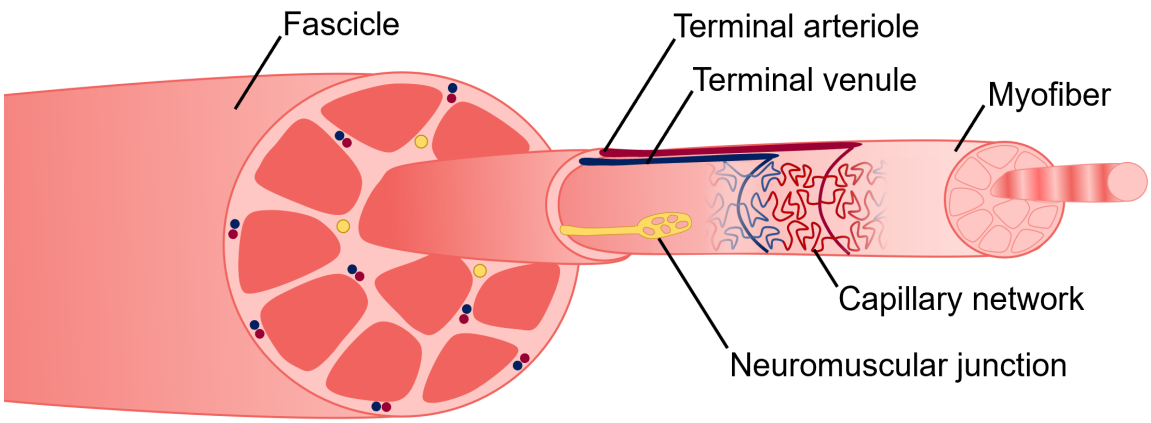

Figure 2.2. Anatomy of skeletal muscle vasculature and neuromuscular junctions. Arterioles, venules, and neurons run adjacent and parallel to myofibers.

Just below the basal lamina and above the sarcolemma is where satellite cells (SCs), muscle-specific resident stem cells, are located.[39] In healthy skeletal muscle, SCs typically account for only about 2-7% of the total myonuclei.[40] They are identified by the expression of transcription factor paired box 7 (Pax7) and have been found to be necessary for skeletal muscle regeneration.[41-44] Upon injury, SCs leave their quiescent state and become activated to enter the cell cycle.[45] They proliferate and differentiate to form multi-nucleated myotubes, which mature to form myofibers. SCs are also capable self-renewing by maintaining a stem-like population.[46] A more detailed explanation of the role of SCs in skeletal muscle regeneration will be explored in Section 2.3.

To allow for voluntary locomotion, skeletal muscle is highly innervated. Motor neurons extend from the central nervous system and branch extensively throughout the muscle tissue to contact individual myofibers at a neuromuscular junction (NMJ) (**Figure 2.2**). The NMJ is the site at which an action potential from the motor neuron is converted to a muscle contraction. Contraction is initiated by acetylcholine release from the presynaptic axon, which subsequently binds to the myofiber and depolarizes the membrane. Membrane depolarization results in an action potential which travels down the length of the myofiber and initiates the release of calcium ions. Calcium binding within the myofibril results in an actin/myosin-mediated power stroke and muscle contraction. To meet its high metabolic demands, skeletal muscle tissue is also highly vascularized. An organized branching structure with capillary networks running parallel

to the myofibers allow for optimal nutrient and oxygen exchange (**Figure 2.2**). Capillary networks in skeletal muscle are dense, with approximately 600 capillaries/mm^2.[47] This results in 40 μm distance between capillaries, and thus a 20 μm distance for oxygen diffusion.[47]

2.3 SKELETAL MUSCLE REGENERATION

After acute injury, endogenous repair of skeletal muscle follows a highly coordinated regenerative process involving three separate but overlapping phases: destruction/inflammatory, repair, and remodeling (**Figure 2.3 A-E**).

2.3.1 Destruction/Inflammatory Phase

During the inflammatory phase, remodeling of damaged tissue and release of cytokines to promote regeneration are largely facilitated by immune cells including macrophages and neutrophils, and occurs within the first 1-2 weeks after injury.[48] Immediately upon injury damaged myofibers, blood vessels, and neurons undergo necrosis. This is due to membrane damage which permits an influx of extracellular calcium and triggers autodigestion via calcium-dependent proteases such as calpains.[31, 49-51] In addition to cellular damage, disruption of the blood vessels and basement membrane surrounding myofibers also occurs upon injury. Mechanical injury to the basement membrane releases growth factors sequestered by proteoglycans within this ECM including HGF, FGF2, and transforming growth factor β (TGF-β) over a period of two weeks post-injury (**Figure 2.3 C**).[33-35, 52] The release of both intracellular contents and sequestered ECM growth factors, as well as activation of the complement cascade, stimulate resident mononuclear cells within the muscle tissue.[33, 51, 53] These cells then chemotactically recruit circulating leucocytes to the site of injury.[53] Neutrophils are the first sub-population of leucocytes to arrive, typically within the first few hours after injury.[54] These phagocytes are most active during the first 24 hours post-injury and aid in clearing necrotic cellular debris. While they act as a source of pro-inflammatory cytokines,[55-56] they may also generate oxygen free radicals and ultimately induce tissue damage.[57] During the inflammatory phase TGF-β is released into the wound site by platelets. TGF-β acts as an immunomodulator, attracting and activating monocytes and macrophages to the injury.[58] Next, macrophages infiltrate and become the predominant cell type at the injury within several days. They can be

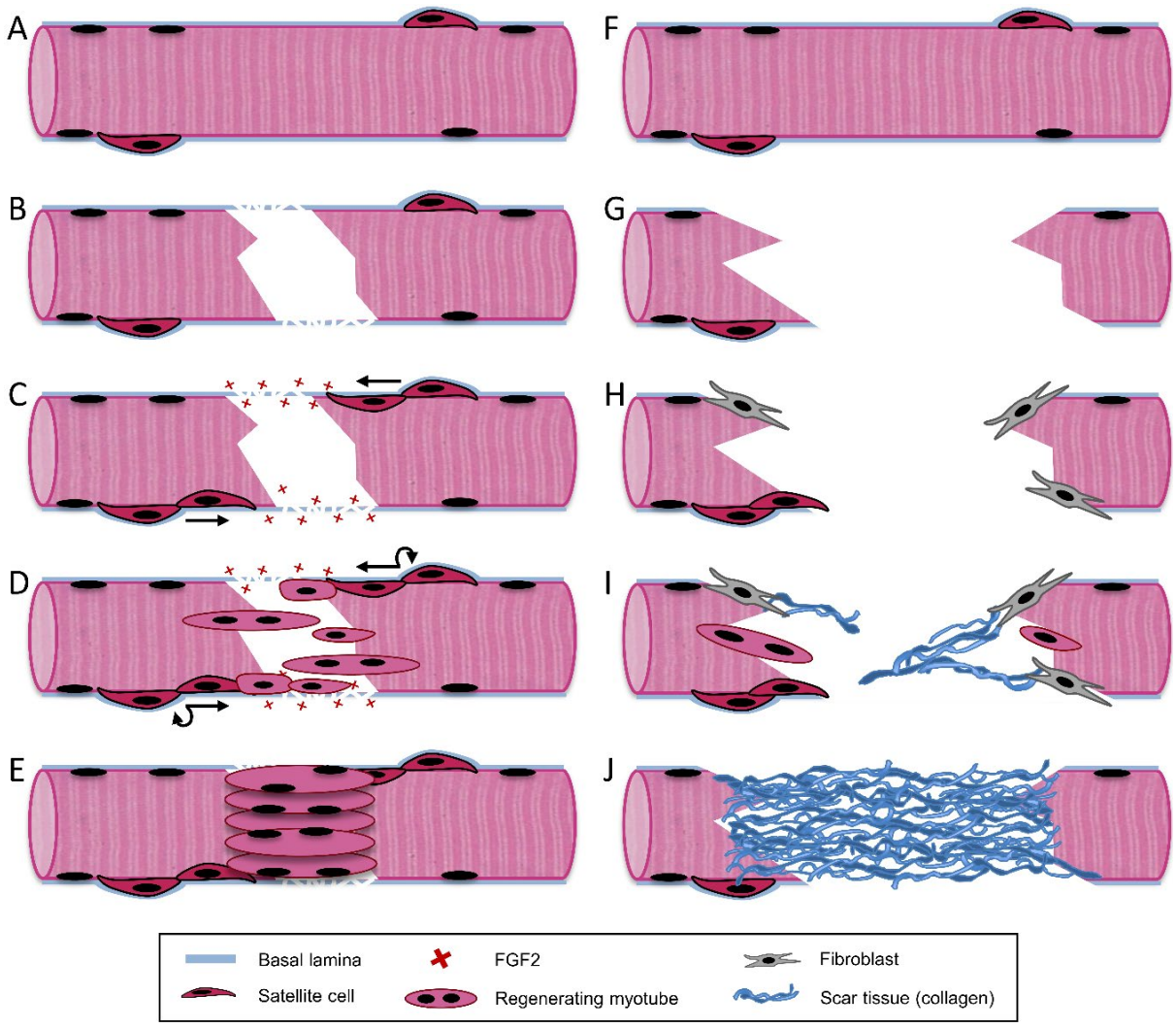

Figure 2.3. Skeletal muscle regeneration. Differences in regeneration following small scale skeletal muscle injuries (A-E) vs. volumetric muscle loss (F-J). Healthy muscle tissue (A) incurs a small-scale injury, which damages the myofiber and its surrounding basal lamina (B). The disrupted basal lamina releases sequestered growth factors including fibroblast growth factor 2 (FGF2) and satellite cells are activated, proliferating and migrating into the wound site along the basal lamina (C). Satellite cells begin fusing to form myotubes while simultaneously self-renewing (D). Resulting tissue is fully recovered, with aligned myotubes (E). Healthy muscle tissue (F) incurs a large-scale VML injury, which destroys the majority of native basal lamina and satellite cells (G). Without these cues, satellite cell-mediated regeneration is diminished, and fibroblasts begin infiltrating the wound (H). The injury is characterized by sparse and misaligned myoblast infiltration and collagen deposition (I), resulting in scar tissue formation and decrease in muscle function(J).

classified into two distinct and sequential subpopulations: classically activated pro-inflammatory (M1) and alternatively activated anti-inflammatory (M2) macrophage.[59-60] Pro-inflammatory M1 macrophages are first to arrive after neutrophils and continue to phagocytose debris and release

reactive oxygen species and pro-inflammatory cytokines.[61-62] These paracrine factors stimulate resident SC proliferation and mobilization.[63-64] M1 macrophages are eventually replaced by M2 macrophages, which have been associated with promoting SC exit from the cell cycle and commitment to differentiation.[63, 65] Some of the secreted growth factors and cytokines that play an important role in this phase of regeneration are tumor necrosis factor-α (TNF- α), fibroblast growth factor 2 (FGF2), insulin-like growth factor (IGF), interleukin -1β (IL-1β), and interleukin 6 (IL-6).[55-56, 61-62]

2.3.2 Repair Phase

The repair phase of skeletal muscle takes place 1- 4 weeks post-injury and involves the activation and proliferation of SCs (**Figure 2.3 D**) and their subsequent differentiation into mature muscle tissue (**Figure 2.3 E**).[66] Upon initial injury, disruption of the basement membrane initiates the release of heparan sulfate proteoglycan-bound growth factors within this matrix, including HGF and FGF2.[33, 35, 56, 67-68] HGF is released from the basement membrane by physical disruption and nitric oxide (NO)-mediated activation of matrix metalloproteinases (MMPs), which release HGF from the basement membrane.[69-72] HGF is released immediately upon injury, and its presence in muscle wounds peaks 2-4 days post-injury.[52] HGF has been shown to be the predominant growth factor capable of activating SCs to re-enter the cell cycle.[36, 69, 73-76] SCs express HGF's receptor c-Met, allowing it to bind and stimulate SC activation.[69, 73] In addition to promoting activation, HGF is also responsible for promoting SC proliferation and migration.[56] FGF2 is another growth factor responsible for the proliferation and migration of activated SCs.[31, 77-79] FGF2 has been shown to be present in muscle wound fluid 2-8 days after injury, and peaks around 6-8 days.[52] In addition to HGF and FGF2, numerous other growth factors are responsible for promoting SC proliferation and migration, including TGF-β and platelet-derived growth factor (PDGF).[55-56] TGF-β presence in muscle injuries has been shown to peak around 12 - 14 days post-injury.[52] SCs gives rise to quiescent SCs and committed myogenic progenitors, allowing for both self-renewal and the sub-population primarily responsible for muscle regeneration. SCs reside below the basement membrane on the periphery of skeletal muscle myofibers, which provides instructive biophysical contact guidance cues for their migration into the wound margin in response to injury.[80-81] SCs are guided by the basement membrane

surrounding necrotic myofibers to facilitate aligned cell division, migration, and fusion into myofibers.[81-82] These mechanisms are driven in part by the aligned topographical cues provided by the basement membrane.

Next, muscle progenitor cells begin to differentiate, expressing myosin heavy chains (MyHCs) and fusing together to form multinucleated myotubes. Regenerating myofibers can be identified by their characteristic centrally located nuclei. While HGF, FGF2, TGF-β, and PDGF are essential during early phases of muscle regeneration, they are known to inhibit subsequent differentiation into mature muscle.[74, 83-86] This highlights the importance of the highly regulated and temporal expression of growth factors throughout skeletal muscle regeneration. Other growth factors, including insulin-like growth factor 1 (IGF-1) and 2 (IGF-2), stimulate both proliferation and differentiation of SCs.[55-56, 87-89]

The success of muscle regeneration is also highly dependent on effective revascularization and reinnervation of the tissue, which occur concurrently during the repair phase. While SC-mediated activation, proliferation, and differentiation can take place in denervated muscle tissue, subsequent tissue maturation of newly regenerating myofibers is dependent on the presence of nerves.[90] Nerve activity has been shown to be crucial for skeletal muscle maturation because it provides electrical stimulation to the tissue.[91] Innervation also promotes the switch from fast to slow MyHC in regenerating muscle.[91] Additionally, revascularization of muscle tissue is paramount for successful regeneration. Upon injury, endothelial cells (ECs) sprout and form tubular structures in the direction of growth factor stimuli. Pericytes and smooth muscle cells are responsible for forming a layer over the ECs to stabilize the new vessels. Newly formed capillaries provide the oxygen required for aerobic metabolism, which is necessary for myofiber generation and maturation.[31] Additionally, the proximity of vasculature to SCs *in vivo* allows ECs to act upon SCs via paracrine growth factor signaling, stimulating their proliferation.[92] Growth factors play a critical role in promoting revascularization and innervation of skeletal muscle. For example, FGF2 has been shown to stimulate endothelial migration and sprouting, as well as pericyte and smooth muscle cell migration. FGF2 also stimulates the formation of more mature vessels than other proangiogenic growth factors such as vascular endothelial growth factor (VEGF).[93] Additionally, FGF2 has

been shown to have neurotrophic activity, stimulating the synthesis and secretion of nerve growth factor (NGF) and promoting neuronal survival and outgrowth.[55, 94-97]

2.3.3 Remodeling Phase

The final phase of regeneration is the remodeling phase, which occurs 2-6 weeks post-injury.[48] This phase consists of regenerating myofiber maturation and ECM remodeling. The basement membrane acts to guide maturing myofibers.[98] Regenerating myotubes within the basal lamina may not fuse, causing the formation of small fiber clusters. Alternatively, fibers may fuse at only one extremity, causing forked fibers. Myofiber maturation is also highly dependent on revascularization of the tissue and the generation of neuromuscular junctions. Muscle begins to regain its contractile function during this phase.

The formation and remodeling of scar tissue due to fibrosis also takes place during tissue remodeling. In addition to chemotactically recruiting inflammatory cells, TGF-β also stimulates the synthesis of ECM molecules including fibronectin, collagens, and proteoglycans.[58, 99-100] Fibroblasts are attracted to the wound site by TGF-β and increase the synthesis of ECM proteins.[100] TGF-β is also responsible for inhibiting ECM protease production and stimulating protease inhibitor production, making it responsible for the reconstruction of the basement membrane surrounding damaged myofibers.[101] Additionally, FGF2 is also known to stimulate fibroblast migration and proliferation.[102] Repair and replacement of connective tissue ECM that was damaged during injury is important because it provides stability for the regenerating muscle tissue. ECM is also important for enhancing muscle tensile strength as well as myofiber-tendon junctions.[103] However, an over-production of ECM often remodels into scar tissue and can inhibit muscle regeneration. The degree of scar tissue formation often increases with increasing severity and size of injury and is associated with poor functional outcomes. The role of scar tissue formation on tissue regeneration will be discussed further in Section 2.3.4 below.

2.3.4 Limited capacity for regeneration in VML injuries

Although SC-mediated regeneration is effective in most muscle injuries, this is not the case in large-scale VML injuries. Due to the magnitude of these injuries, the basement membrane is typically compromised or destroyed, ablating native biophysical and biochemical

cues necessary for SCs to facilitate regeneration (**Figure 2.3 G**). With the basement membrane removed, the population of resident SCs is severely depleted. Thus, VML injuries appear to have a limited invasion of myoblasts into the injury site.[31] Additionally, the growth factor population that is sequestered within the basement membrane is also destroyed, which significantly limits their ability to guide regenerative processes such as SC-mediated myogenesis, the inflammatory response, revascularization, and reinnervation.[104-105] The biophysical cues provided by the basement membrane are also significantly limited upon VML injury. During normal regeneration, the basement membrane provides instructive biophysical contact guidance cues for SC aligned cell division and migration into the wound margin in response to injury.[80-82] However, when this ECM is removed in VML injuries, SCs have a limited capacity to migrate into the wound and undergo aligned cell division and myotube fusion. Lateral migration of SCs outside the basement membrane is more likely to occur in VML injuries, where the basement membrane has been disrupted.[106] In addition to limited contact guidance cues and signaling, these large-scale injuries also have a lack of mechanical support.[107]

With limited muscle regeneration, fibroblast-mediated collagen I deposition dominates the healing response and generates non-functional scar tissue in the wound (**Figure 2.3 H-J**). When M1 and M2 macrophage populations are depleted within a muscle injury, regeneration is impaired and fibrotic scar tissue is deposited.[104] Alternatively, a chronic inflammatory response can lead to dysregulation of growth factor expression and result in limited regeneration and fibrosis.[105] Scar tissue fills the void, bridging the remaining muscle fibers at each end of the injury to facilitate force transduction along the muscle.[108] In small-scale injuries, scar tissue can act as a conduit to aid in myogenesis. However, in VML injuries ECM deposition occurs quicker than myofiber formation and generates a dense scar tissue cap that inhibits myofibers from bridging the wound.[30, 108] This can yield the formation of myotendinous junctions between adjacent myofibers and scar tissue.[108] Ultimately, fibrous tethering within VML injuries restricts torque production and range of motion, resulting in permanent loss of function in these injuries.[17]

The extent to which VML injuries revascularize and reinnervate is vital for muscle regeneration and is also highly dependent on the extent of the injury. Often extensive skeletal muscle injuries include injury to the vasculature and neural networks surrounding the muscle tissue. Among the military population with VML lower limb injuries, 14% also had a nerve

injury, and 5% had a vascular injury.[15] A nerve injury in conjunction with VML has also been observed in a murine animal model of skeletal muscle injury.[109] When a VML defect comprising 20% of the tibialis anterior (TA) muscle of Lewis rats was created, it yielded axotomy of 69% of the motoneurons innervating that muscle.[109] Without reinnervation, injured muscle tissues lack action potential-mediated muscle contractions, inducing atrophy. Reduced NMJ formation has also been associated with a depleted number of SCs in the injury.[110] Revascularization is also vital to VML injury, but often poses challenges. The degree to which skeletal muscle injuries revascularize depends on the severity of the injury; in larger VML defects there is limited revascularization because of a greater degree of scar tissue deposition.[111] Dense scar tissue can impede the ingrowth of neurons and vasculature and limit oxygen diffusion, yielding denervated and ischemic muscle.[112-113]

2.4 BIOMATERIAL STRATEGIES FOR SKELETAL MUSCLE REGENERATION

To overcome the limitations of current clinical treatments for VML injuries, tissue engineered biomaterial scaffolds are under development with the goal of preventing scar tissue formation and enhancing functional muscle regeneration. Skeletal muscle tissue engineering and regenerative medicine present a promising therapeutic treatment by repairing or replacing the damaged muscle with a combination of instructive biomaterial scaffolds, biologically-active molecules, and cells.[114-115] Tissue engineered scaffolds are three-dimensional (3D) constructs that recapitulate the native ECM milieu, creating a synthetic microenvironment to locally control cellular functions and guide regeneration. To accomplish this, scaffolds must incorporate biophysical and biochemical cues that mimic native tissue composition, architecture, mechanics, and bioactive signaling. Biophysical cues include scaffold topography, porosity, and mechanics, while biochemical cues comprise the spatial and temporal control over the presentation of bioactive molecules. Scaffolds are made of synthetic or natural materials with demonstrated biocompatibility such that the scaffold will not cause toxicity, injury, or immunological rejection when implanted in living tissue. Biocompatible scaffolds allow for the incorporation of cells and biologically-active molecules such as proteins, peptides, growth factors, cytokines, transgenes, and messenger ribonucleic acid (mRNA).

Skeletal muscle tissue engineering can be broadly classified into one of three approaches: *in situ*, *in vivo*, and *in vitro* tissue engineering (**Figure 2.4, Table 2.1**).[30, 116] These treatments range in complexity and can act by enhancing endogenous regeneration or by generating engineered tissues to replace damaged muscle. *In situ* tissue engineering involves the implantation of an acellular biomaterial scaffold into the injury that can direct endogenous regeneration. Strategic engineering of biophysical and biochemical cues allows the scaffold to instruct host cell recruitment, activation, proliferation, and differentiation. Slightly more complex, *in vivo* tissue engineering involves seeding instructive biomaterial scaffolds with cells immediately prior to transplantation, where they can then participate in regeneration. While this approach limits the manipulation of cells prior to transplantation and preserves their efficacy, it can leave them susceptible to low viability, retention, and immune rejection.[30, 117-118] Finally, *in vitro* tissue engineering involves the development and implantation of a functional tissue engineered construct. This is achieved by combining scaffolds, biological factors, and cells and culturing these constructs *in vitro* until the cells differentiate into contractile myofibers. Differentiation is often achieved through a combination of biochemical cues, mechanical stimulation, and electrical stimulation. While *in vitro* tissue engineered constructs have greater functionality prior to implantation than those developed through *in situ* and *in vivo* techniques, they have several significant drawbacks. While they display some functionality, these contractile forces are often significantly lower than what is seen in native muscle tissue.[107] Additionally, due

Table 2.1. Comparison of tissue engineering approaches. Based off Table 1 in reference [119].

	In situ	*In vivo*	*In vitro*
Off-the-shelf availability	Likely	Possible	Not possible
Scalability	Easier	Difficult	Most difficult
Ease of clinical translation	Easier	Complex	Complex
Cost-effectiveness	More	Less	Least
Disease modeling	No	No	Yes
Drug screening modeling	No	No	Yes

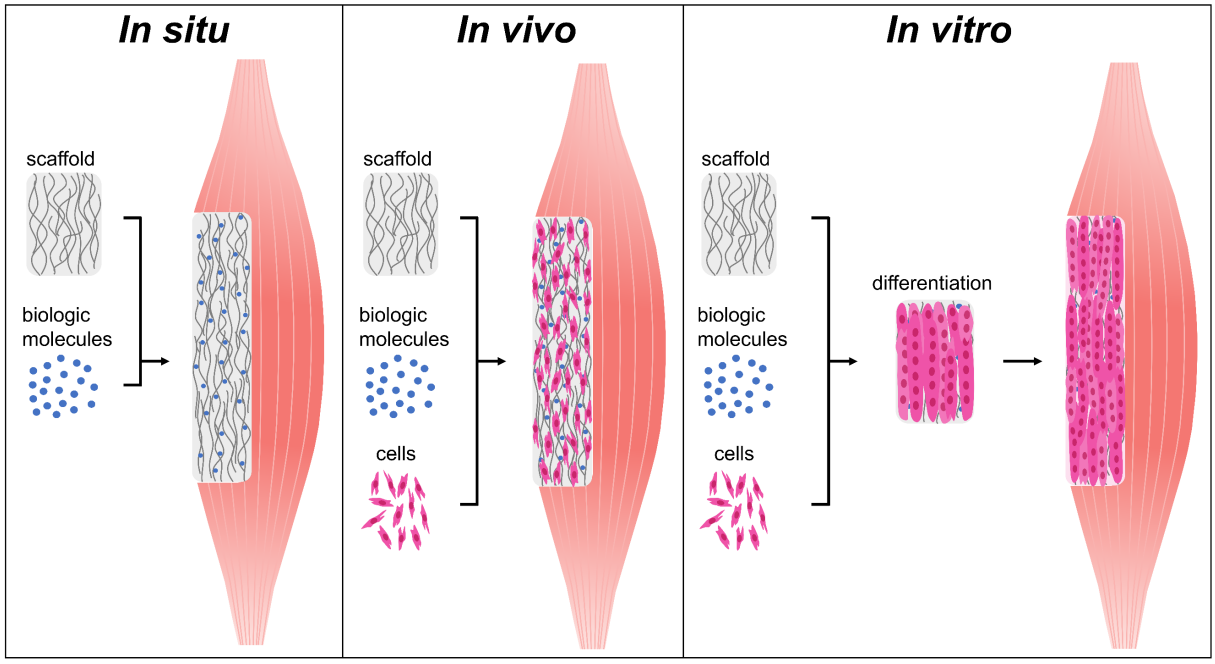

Figure 2.4. Skeletal muscle tissue engineering approaches. *In situ* tissue engineering relies on endogenous regeneration guided by an acellular scaffold with instructive biophysical and biochemical cues. *In vivo* tissue engineering transplants a scaffold, biologic factors, and cells, creating a synthetic niche and delivering cells to aid in regeneration. *In vitro* tissue engineering utilizes the same factors but first differentiates the cells *in vitro* into a functional construct prior to implantation.

to oxygen and nutrient diffusion limitations these constructs are often size-limited or require the development of a complex vascular network to support extended cell viability. Herein we review past and current skeletal muscle tissue engineering strategies, with a focus on the use of instructive biomaterial scaffolds. This chapter will not cover scaffold-free approaches to treating VML such as rehabilitation regimes, autologous grafts, or minced muscle grafts delivered without a biomaterial scaffold. It will also not include cellular, drug, gene, or growth factor injections unless they are delivered using a biomaterial carrier. Additionally, this chapter will focus exclusively on the treatment of muscle injuries and not include treatments for genetic diseases such as Duchenne muscular dystrophy. While this chapter focuses on VML resection injuries, it also evaluates muscle injuries induced from critical limb ischemia (CLI), crush, and myotoxin injuries, which present a different pathophysiology and capacity for functional recovery than VML injuries.[120] Preclinical and clinical *in situ*, *in vivo*, and *in vitro* tissue

engineering strategies will be reviewed, with a focus on the biophysical and biochemical cues of these scaffolds that guide regeneration.

2.4.1 In situ strategies: Acellular scaffolds to promote endogenous regeneration

In situ tissue engineering utilizes acellular biomaterial scaffolds to direct endogenous regeneration. Tissue engineered scaffolds employ biophysical and biochemical cues to recapitulate native ECM structure, creating a synthetic microenvironment to locally control host cellular functions and guide regeneration. Implantation of an acellular scaffold offers unique advantages over cell-based strategies, including faster and simpler fabrication and storage. By not delivering cells the culture time for these scaffolds is eliminated, yielding faster fabrication, streamlined delivery workflows and operations, the potential for long term storage and off-the-shelf capabilities. Additionally, these factors result in the production of scaffolds that often have lower regulatory barriers and a quicker path to commercialization (**Table 2.1**).[121] For this strategy to be effective, strategic engineering of the biomaterial scaffold is paramount to develop a synthetic niche capable of directing endogenous regeneration. This section will focus on the strategies utilized for skeletal muscle scaffold development, with a focus on biomaterial selection and biophysical and biochemical cues used to modulate these materials.

2.4.1.1 Biomaterial selection: Synthetic, natural, and hybrid polymers

Most biomaterials fall into one of two classes, synthetic or natural, which both offer distinct advantages and drawbacks. Synthetic scaffolds are easy, consistent, and inexpensive to fabricate and can be manufactured to have detailed geometries down to the nanoscale. They can also be engineered to have precise and tunable degradation profiles and mechanical properties. Conjugation of biomolecules such as growth factors is also possible, and their release from the scaffolds can be finely tuned by altering conjugation strategies or scaffold degradation rates. Synthetic polymers offer additional benefits, such as the ability to be electrically conductive.[122-124] Synthetic scaffolds that have been used for skeletal muscle tissue engineering include poly(ε-caprolactone) (PCL), poly(glycolic acid) (PGA), polylactic acid (PLA, PLLA), and copolymer poly-lactic-*co*-glycolic acid (PLG, PLGA), polyurethane (PU), polyethylene glycol (PEG), and polypropylene (PP). However, use of synthetic biomaterials comes at a cost. These polymers are

often associated with low cell attachment, limiting their use without functionalization of a natural biopolymer. Additionally, synthetic scaffolds have limited biocompatibility and have been shown to elicit a pro-inflammatory immune response upon implantation.[117]

In contrast, natural polymers are highly biocompatible and contain native signaling cues which aid in promoting cellular attachment, proliferation, and differentiation. They also contain native functional groups suitable for growth factor conjugation and are naturally degraded upon implantation. Natural biopolymers include collagen, fibrin, alginate, laminin, silk fibroin, hyaluronic acid (HA), decellularized ECM, chitosan, keratin, and gelatin. While biopolymer scaffold porosity, topography, and mechanics can be modified, there is less precision and tunability than with synthetic scaffolds. Biopolymers are also subject to inherent biologic variability due to material sourcing. Both synthetic and natural biomaterials can be made into an ideal scaffold through strategic incorporation of biophysical and biochemical cues designed to create a synthetic microenvironment conducive to skeletal muscle tissue regeneration.

2.4.1.2 Biophysical cues

An ideal biomaterial scaffold should match native tissue mechanical properties, degrade at a rate that matches the rate of new tissue regeneration, and contain 3D topographical features and porosity to direct cellular alignment and allow for cellular infiltration. These features can be accomplished through the incorporation of instructive biophysical cues (**Figure 2.5**). Scaffold strength and stiffness should be optimized to match native tissue mechanics to create a synthetic niche that exposes cells to physiologically relevant forces. Myoblasts respond to mechanical stimuli through mechanotranduction, informing their proliferation, adhesion, and differentiation. Substrate stiffness does not affect the propensity for myoblasts to assemble into myotubes, but it was shown to have an important role on the development of myosin/actin striations.[125] Myoblasts cultured on substrates with a modulus of 12 kPa, which matches the elasticity of native resting muscle tissue, were found to have significantly increased striations, indicating a more functional and mature cellular phenotype.[125] Scaffold biodegradation is another biophysical cue that must match the kinetics of skeletal muscle regeneration and new tissue ingrowth.[126] Rapid degradation can lead to voids within the tissue and compromised regeneration, while slow degradation can invoke a chronic inflammatory response, scar tissue deposition, and encapsulation.[127] Both

scaffold mechanics and degradation are commonly controlled by material choice and crosslinking. Hydrogels, sponges, fibers, composites and devitalized ECM are among the most commonly exploited conformations for biomaterial scaffolds. These systems are all able to create a 3D environment that provides suitable porosity, topographical cues, and mechanical properties to support tissue regeneration.

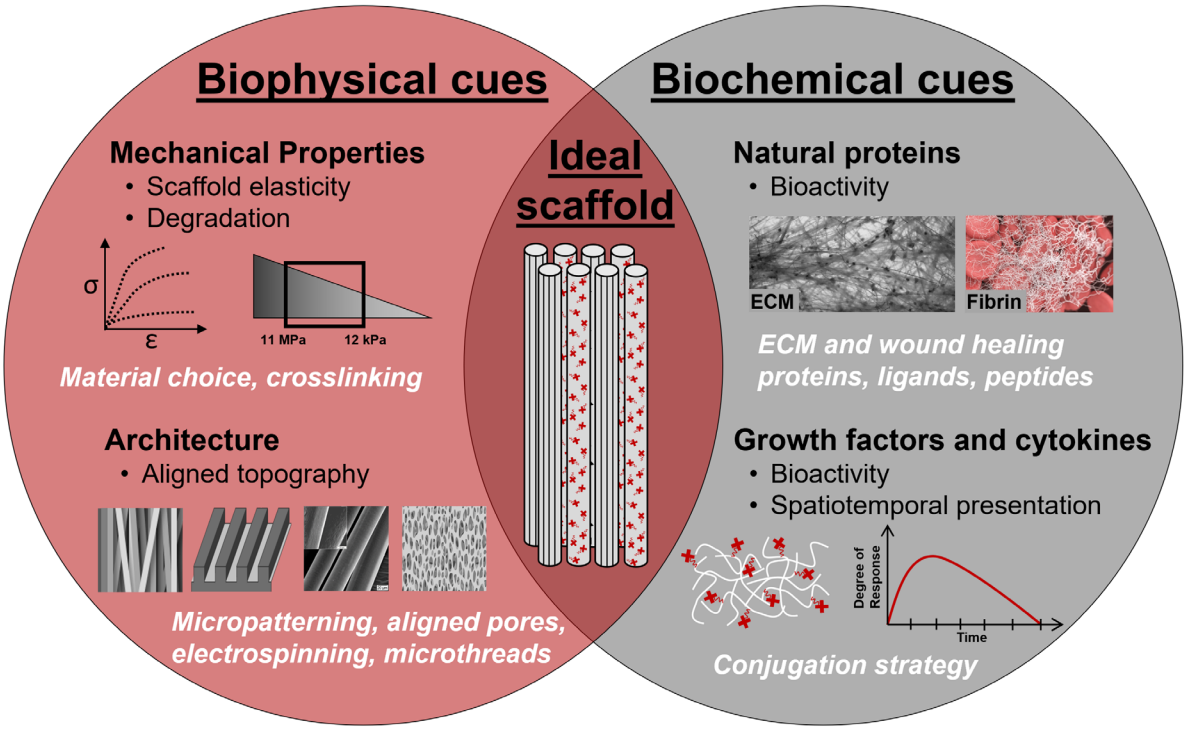

Figure 2.5. The role of biophysical and biochemical cues in designing biomaterials for skeletal muscle tissue engineering. Biophysical cues include scaffold mechanics, degradation and architectural morphology. Biochemical cues include exploiting natural molecules, and spatiotemporal delivery of biomolecules such as growth factors. In concert, biophysical and biochemical cues allow for the generation of scaffolds that effectively recapitulate a cellular microenvironment conducive for regeneration. Image concept adapted from [126].

2.4.1.2.1 Decellularized ECM

One of the most commonly exploited acellular scaffolds is decellularized ECM. Decellularized ECM is a scaffold prepared by removing cells from source mammalian tissue or whole organs, leaving behind the native ECM with preserved structural and chemical composition. Decellularized ECM has been used as a biomaterial because it contains the native

ligands, ECM proteins, and growth factors found in skeletal muscle which are known to play an instrumental role in SC chemotaxis and proliferation, the inflammatory response, myotube differentiation and, ultimately, functional tissue regeneration.[64, 128-130] These ECM molecules include collagens, laminin, fibronectin, heparin sulfate, chondroitin sulfate, HA, VEGF, FGF2, and TGF-β.[131-134] The goal for these scaffolds is that upon implantation into a muscle injury, they will become infiltrated by cells that release proteases which degrade the scaffold, releasing native growth factors and ECM proteins that promote host cell infiltration.[64] Decellularized ECM is harvested from a variety of source tissues, including dermis, skeletal muscle, small intestinal submucosa (SIS), and urinary bladder matrix (UBM).[128-129] Different source tissues provide varying structural organization and chemical composition.[135] The process by and extent to which ECM is decellularized can also yield varying physical and chemical properties, and contribute to the varying degrees of remodeling seen after implantation.[136-138] This may explain the conflicting reports in the literature of decellularized ECM inflammatory response, induction of fibrosis, and ability to promote muscle fiber regeneration upon implantation.

Early studies investigating the use of xenogeneic SIS and homologous muscle ECM found that implanted scaffolds promoted a strong angiogenic response despite variable contractile function and the persistent deposition of collagenous connective tissue.[139-141] In one study, Badylak's group observed that upon implantation into rodent partial resection models, both SIS and muscle ECM scaffolds induced constructive remodeling characterized by robust mononuclear cell infiltration and myogenesis, although no contractile analysis was performed to evaluate muscle function.[135, 142] Corona et al. implanted a syngeneic muscle ECM scaffold into a partially resected rat TA muscle and saw recovery of one third of the original force deficit was restored after two months post-injury, despite histological analysis showing overwhelming fibrosis at the implantation site.[143] The authors hypothesize that the ECM scaffold prevented muscle fiber damage and acted as a structural reinforcement to transmit forces across the injury. Another study evaluated a syngeneic muscle ECM scaffold to treat a rodent TA VML defect model and found that at two weeks post-implantation, the scaffold elicited a pro-inflammatory response with a large quantity of macrophages surrounding the implant.[144] At eight weeks after treatment little to no myosin^{+} muscle fibers were present, and increased collagen 1 was observed. Upon stimulation, TA muscles treated with muscle ECM demonstrated a 17% increase in torque

compared to those with an injury and no treatment. More recent studies utilizing a UBM ECM scaffold to treat rodent and porcine VML injuries found that injuries treated with scaffolds demonstrated limited myogenesis, fibrotic deposition, and chronic functional deficits at terminal timepoints.[145-146] Discrepancies in the existing literature regarding whether or not ECM scaffolds promote constructive remodeling in preclinical models may be due in part to differences in ECM sources, decellularization protocols, differences in anatomy, and the severity of preclinical VML models.

Decellularized ECM is the first tissue engineered scaffold to be clinically evaluated for treating VML injury. A 2010 case study treated a persistent combat-induced quadriceps injury 3.5 years post-injury with an acellular porcine SIS ECM scaffold and subsequent physical therapy.[18] At 16 weeks post operatively a modest improvement in isokinetic muscle function was demonstrated, as well as new soft tissue observed via computed tomography (CT) at 36 weeks post-operatively. A 2014 study by Sicari et al. evaluated the use of UBM ECM in five male patients with extremity VML injuries incurred at least six months prior that maintained a minimum of 25% functional deficit compared to the contralateral uninjured limb.[121] At six months post-surgery magnetic resonance imaging (MRI) and histological evaluation of biopsies both showed the presence of vascularization and islands of muscle cells. Furthermore, three of the five patients showed a 20% functional improvement of the affected limb. A follow-up study of eight patients with VML, including the five from the previous study[121], used electrodiagnostic evaluations with nerve conduction studies (NCS) and needle electromyography (EMG) to demonstrate restoration of nerve tissue as it relates to variable functional outcomes in ECM-treated VML injuries.[147] The study found that five of the eight patients treated with ECM scaffolds demonstrated improvements in electrical activity evaluated through NCS and EMG as well as improved muscle strength, compared to the pretreatment condition. Most recently, a 13-patient study was conducted to evaluate the ability of ECM bioscaffolds and physical therapy to improve force production, range-of-motion, and function in a range of VML extremity injuries,[148] which also included five patients from the previous study.[121] Patients demonstrated an average improvement of 37.3% in strength, 27.1% in range-of-motion tasks, and 271.8% in functional task performance at six months post-operatively. The authors acknowledged that debridement of scar tissue during surgery and the effect of mechanical transduction via the ECM

scaffold may have contributed to these modest functional gains. They also observed the formation of muscle tissue at the injury site through histology of biopsied tissue and MRI or CT imaging. Despite some promising results, the clinical use of decellularized ECM remains limited due to variable outcomes among patients and the limited understanding of the mechanisms by which these acellular scaffolds mediate muscle regeneration.

2.4.1.2.2 Hydrogels, sponges, and meshes

Hydrogels, sponges, and meshes are used as alternative acellular scaffolds to decellularized ECM because they allow for more precise control of the scaffold material, mechanics, degradation, and porosity. Porosity is a critical biophysical cue to control in tissue engineered scaffolds because of its role in permitting cellular infiltration and oxygen and nutrient diffusion. Porosity is commonly achieved through the use of hydrogels, sponges, and fibrous meshes. Pore sizes typically range from 10 to 500 μm, and larger macropores typically permit greater cell viability and migration.[149] Injectable *in situ* polymerizing collagen and decellularized ECM hydrogel scaffolds were evaluated for their ability to treat critical limb ischemia (CLI) in a rat hindlimb ischemia model.[150] They found that decellularized ECM hydrogels promoted increased the number of $MyoD^+$ cells recruited to the injury and blood vessel density compared to the collagen hydrogel. More recent work delivering a laminin 111-enriched fibrin hydrogel to a murine VML defect demonstrated an infiltration of macrophages and ECs into the hydrogels at two weeks post-injury, but did not report increases in peak isometric torque at four weeks post-injury compared to the untreated negative control.[151] Sponge-based scaffolds can be generated by freeze-drying polymer solutions or hydrogels, creating a porous microstructure. Freeze-dried collagen sponges implanted into a partial resection of the vastus lateralis muscle in a rabbit model qualitatively demonstrated less scar tissue formation and a greater number, diameter, and length of myofibers at 24 weeks post-injury compared to the untreated control.[152] Lyophilized, highly porous sponges made of gelatin, collagen, and laminin 111 and crosslinked with 1-ethyl-3-(3-dimethyl aminopropyl) carbodiimide (EDC) have also been evaluated in a 10% resection of the gastrocnemius-soleus complex of mice.[153] At two weeks post-injury protein lysates from sponge-treated muscles showed significantly higher expression of MyoD and desmin compared to untreated muscles, suggesting an increase in myogenic activity at the injury site due to

scaffold-mediated regeneration. In addition to hydrogels and sponges, fibrous meshes are also highly porous scaffolds that permit cellular infiltration. Fibrous meshes of PLLA with an average fiber diameter of 150 μm and pore size of 50–100 μm demonstrated host cell infiltration in rat TA VML defects. Histological evaluation of TA muscles at one, two, three, and four weeks demonstrated an influx of Von Willebrand factor $(vWF)^+$ ECs and $Pax7^+$ muscle progenitor cells into the fibrous mesh scaffolds over time.[154] While acellular hydrogels, sponges, and meshes permit cellular infiltration upon injury into VML defects, these scaffolds have not demonstrated aligned myofibers or significant gains in muscle function. This may be due in part to the lack of instructive topographical alignment cues that these scaffolds provide due to their isotropic nature. This has motivated a thrust of skeletal muscle tissue engineering research that focuses on the development of anisotropic scaffolds with aligned architectural features.

2.4.1.2.3 Aligned scaffolds

Incorporation of instructive biophysical cues such as anisotropic surface topography is a commonly exploited technique to promote cell alignment in skeletal muscle tissue engineering. Myoblast alignment is an essential step towards myotube formation, which is guided *in vivo* by ECM structure and micron-scale grooves between adjacent muscle fibers. Many strategies have been explored to create scaffolds with anisotropic surface topography, including patterned substrates,[155-162] electrospun fibers,[123-124, 156, 163-166] microthreads,[167-169] and aligned pores.[170-172] A review describes these methods in detail and their ability to align and differentiate myoblasts *in vitro*, as this falls outside of the scope of this chapter.[173] These methods are also commonly employed to generate *in vitro* tissue engineered skeletal muscle, which will be discussed in Section 2.4.3. Nakayama and colleagues evaluated the therapeutic benefit of aligned nanofibrillar collagen scaffolds and rehabilitative exercise on the treatment of VML.[174] Ablated murine TA muscles were treated with either aligned or randomly oriented collagen nanofibers, and animals were randomly assigned to either voluntary cage running or no rehabilitation regime during recovery. After 21 days post-treatment, muscle treated with both random and aligned nanofibers exhibited significantly higher myofiber cross sectional area than those left untreated or treated with a decellularized ECM scaffold. Additionally, they noted significantly higher perfused vascular density in muscles treated with the aligned nanofibers compared with those treated with

the randomly-oriented nanofibers. This study warrants further investigation of anisotropically aligned scaffolds. Use of these scaffolds in conjunction with biochemical cues and cells will be discussed in later sections of this chapter.

2.4.1.3 Biochemical cues

Biochemical cues are often strategically incorporated into scaffolds for skeletal muscle tissue engineering as a method to further regulate cellular functions including survival, attachment, proliferation, migration, and differentiation into myotubes. These include biologically active molecules such as proteins, peptides, growth factors, cytokines, transgenes, and mRNA. Strategic design of biomaterial-based scaffolds must take place to protect these molecules from degradation, maintain their native conformation, and preserve their bioactivity. Biomaterial scaffolds should also be designed to carefully control spatiotemporal presentation, biomolecule release kinetics, and local concentrations. For example, genetic substances can be delivered via viral or non-viral vectors, such as liposomes and synthetic particles, engineered to translocate into the cell or nucleus.

2.4.1.3.1 Growth factors and cytokines

Growth factors and cytokines are among some of the most commonly investigated biologic molecules to treat skeletal muscle injuries due to their instrumental role in facilitating native regeneration (reviewed in Section 2.3).[55] Early clinical trials using bolus injections of growth factors such as VEGF and FGF2 to treat cardiovascular disease had limited success.[175-177] This is likely attributed to the bolus delivery method, which provided initial supraphysiological growth factor concentrations followed by rapid degradation, preventing sustained presentation of these factors for the necessary time frame.[178-179] Delivering growth factors via biomaterial carriers prevents their denaturation and mediates their release, which is controlled by scaffold degradation and/or diffusion through the matrix. They are often incorporated into biomaterials through physical entrapment, ionic interactions, or covalent coupling.[127, 179] Engineering these scaffolds to control growth factor release kinetics allows for the delivery of optimized concentrations, localized delivery, and increased therapeutic efficiency.

Several researchers have investigated the ability of growth factor-loaded scaffolds to promote skeletal muscle regeneration in ischemic and VML injury models.[154, 180-191] VEGF-loaded hydrogel scaffolds have been investigated for their ability to promote angiogenesis in hindlimb injuries.[180-183] Silva et al. confirmed that VEGF delivered to a TA ischemic murine injury via alginate hydrogel was present at physiologically relevant levels for up to 15 days post-injection, compared to only three days after delivery of VEGF via bolus injection.[180] Sustained delivery of VEGF via alginate hydrogels resulted in significantly higher blood vessel density and tissue perfusion compared to no treatment and bolus VEGF delivery. Another study evaluated the sustained delivery of VEGF from alginate hydrogels for the treatment of an ischemic murine TA injury.[181] After seven days post-injury, VEGF delivery resulted in 50% innervated motor end plates compared to 5% in the blank alginate gel, likely due to the significant increase in glial-derived neurotrophic factor (GDNF) and NGF expression levels compared to uninjured muscle. Hydrogel-mediated VEGF also resulted in significantly higher number of vessels (cluster of differentiation 31 $(CD31)^+$) and mature vessels (smooth muscle $actin^+$) after 14 days compared to blank hydrogels. To generate a more controlled release of VEGF from alginate hydrogels, Lee et al. encapsulated VEGF within PLGA microspheres, creating a sustained release of VEGF over three weeks.[182] These composite scaffolds generated significantly higher platelet endothelial cell adhesion molecules (PECAM) expression than bolus VEGF or VEGF-loaded alginate hydrogels, indicating the formation of functional microvessels. Another study evaluated the ability of VEGF-coated collagen matrices to stimulate repair in a rabbit lower leg osteotomy with soft tissue contusion injury, and found VEGF scaffolds resulted in 73% recovery of muscle strength compared to 53% recovery of no treatment control group after 30 days post-injury.[183]

IGF-1 has also been used to treat VML injuries because of its important role in stimulating myoblast survival, proliferation, and differentiation.[154, 184] Hammers et al. found that a controlled release of IGF-1 from (PEG)ylated fibrin gels implanted into a murine hindlimb ischemia injury stimulated significantly higher force production 14 days post-injury compared to bolus IGF-1 and blank hydrogel treatments.[184] Other researchers implanted IGF-1-loaded gelatin porous sponges into TA muscle of rats and after two weeks found a four-fold increase in the number of $Pax7^+$ infiltrated cells and significantly greater number of muscle fibers compared to control blank hydrogels.[154]

Another commonly utilized growth factor for promoting skeletal muscle regeneration is FGF2.[154, 185-187] In a rabbit hind limb ischemia injury model, FGF2-loaded gelatin hydrogels had significantly greater tissue blood flow, number of arterioles, and vascular density four weeks after treatment.[185] Other researchers have delivered sustained FGF2 release from ionic gelatin hydrogels covalently crosslinked with PLG, which yielded significantly greater capillary density ($CD31^+$) and blood flow compared to bolus FGF2 injection at eight weeks after ischemic hindlimb injury.[186] Murine TA muscles implanted with FGF2-loaded gelatin sponges found a significant increase in the number of $Pax7^+$ infiltrated cells and significantly greater number of muscle fibers compared to control blank hydrogels.[154]

Our laboratory delivered HGF adsorbed to EDC-crosslinked fibrin microthread scaffolds in a murine VML defect.[188] Surgical resection of 30 mg of the TA muscle yielded approximately 50% reduction in force immediately after injury, and was immediately filled with fibrin microthreads that were EDC crosslinked and passively adsorbed with 40 ng/mL of HGF. At 60 days post-injury, this treatment resulted in an increase of over 200% of twitch and tetanic force production, compared to the 150% and 130% increases seen from treatment with fibrin microthreads or fibrin gel with no HGF delivery. HGF fibrin microthreads resulted in a significantly higher recovered force production than injuries that received no treatment or treatment with a fibrin hydrogel alone. This work has been recently acknowledged as the only study of growth factor-based repair that evaluated functional recovery in an appropriate VML injury model.[192] Histological analysis showed myofibers adjacent to implanted EDC crosslinked microthreads, indicating that the aligned microthread architecture likely guides myofiber ingrowth and alignment.[188] This motivates the future development of scaffolds with biophysical cues such as aligned topography in conjunction with the delivery of biochemical cues such as growth factors. Overall, the delivery of a single myogenic or angiogenic growth factor to skeletal muscle injuries yields improvements in regeneration, but it remains unclear which growth factors, concentrations, and delivery strategies yield the best results, and warrants further investigation.

Toward the goal of recapitulating *in vivo* regeneration, several studies also assessed the synergistic presentation of multiple growth factors. While delivery of a single growth factor has shown promising results for promoting skeletal muscle regeneration and angiogenesis, this

strategy represents a drastically simplified version of the complex, spatiotemporal presentation of multiple factors during regeneration. Through the development of more complex biomaterials systems, the release kinetics of multiple factors in a spatiotemporal manner that mimics *in vivo* presentation and concentration will likely enhance regenerative outcomes.[127, 193] The first preclinical work evaluating delivery of multiple growth factors for skeletal muscle repair investigated the co-stimulatory effect of IGF-1 and VEGF delivered to ischemic rodent hindlimbs via an injectable alginate hydrogel.[189] Despite the limited control over release kinetics that this scaffold provided, the co-delivery of 3 μg each of these factors from the alginate hydrogel stimulated significantly higher blood perfusion seven weeks after ligation compared to the blank hydrogel and bolus IGF-1/VEGF treatments. Injuries treated with the IGF-1/VEGF hydrogel also had significantly larger myofiber diameters and number of centrally located nuclei compared to blank gels, which are hallmarks of regenerating muscle. Another study evaluated the therapeutic potential of stromal cell-derived factor-1 α (SDF-1α) alone or in combination with IGF-1 to treat an ischemic skeletal muscle injury in rodents.[190] Co-delivery of these factors in a PEGylated fibrin hydrogel yielded significant improvements in revascularization ($CD31^+$ cells/fiber) and functional recovery (maximum tetanic force production) at 14 days post-injury compared to treatment with blank hydrogel, which was not achieved by the delivery of SDF-1α alone. Matsui et al. investigated gelatin hydrogel granules to deliver FGF2 alongside a mix of growth factors isolated from platelet-activated platelet rich plasma (PRP), which included PDGF, VEGF, TGF- β, and FGF2.[191] One week after implantation into a murine hindlimb ischemic injury the combination treatment yielded a significantly higher number of blood vessels compared to no treatment, which was not achieved by delivery of FGF2 or the PRP-isolated growth factor mixture alone. The combination treatment also significantly enhanced blood reperfusion compared to hydrogels with just FGF2 or PRP-isolated growth factors. As biomaterial scaffolds advance to allow for more precise spatiotemporal delivery of multiple growth factors, this strategy will better mimic the complex *in vivo* temporal presentation during regeneration and will likely yield greater therapeutic, functional outcomes.

2.4.1.3.2 Genetic substances

Another thrust of research focuses on the delivery of genetic material including cDNA and mRNA. Gene therapy strategies transfer genetic material into host cells to treat genetic diseases or injury. This treatment often utilizes engineering of viral and non-viral vectors to safely and efficiently transfer genetic material into cell nuclei. These strategies include adenovirus, adeno-associated virus, retrovirus, lentivirus, liposomes, synthetic particles, and polymer-based scaffolds, and display varying degrees of immunogenicity and transfection efficiency. These approaches are typically limited to injections that do not control vector spatiotemporal presentation. To make gene therapy treatments more effective, researchers recently utilized biomaterial-based delivery systems to provide localized and sustained delivery of these therapies. Biomaterial scaffolds can help deliver genetic cargo by preserving genetic structures, protecting them from nuclease-mediated degradation, and controlling their release from the scaffold. By modulating scaffold properties such as molecular weight, porosity or crosslinking, a localized and sustained release of genetic material can be mediated through diffusion or scaffold degradation.[194-195] This delivery strategy has the potential to increase transfection efficiency and expression, ultimately improving the therapeutic effectiveness of these treatments.

One study evaluated the delivery of adenoviral vectors and plasmids encoding FGF2 and FGF6 transgenes delivered in collagen-gelatin scaffolds to excisional quadriceps defects in rats.[196] At 21 days after injury they found that treatment with FGF2 transgenes increased the arteriole density by 11-fold and myotube marker CD56 expression 20-fold compared to controls. They also note that the delivery of recombinant FGF2 protein was unable to produce equivalent responses, highlighting the benefit of a gene delivery strategy for treating skeletal muscle injury. Another gene therapy study delivered plasmid FGF4 cDNA within a gelatin hydrogel scaffold to treat hindlimb ischemia in rabbits.[197] The hydrogel preserved the plasmid structure allowing for improved transfection efficiency compared to naked FGF4 gene. Ischemic injuries treated with hydrogel-FGF4 had significantly less severe tissue damage and more pronounced vascular responsiveness to adenosine at four weeks compared to injuries treated with a naked FGF4 gene.

An alternative strategy to the delivery of plasmids and viruses is mRNA-based delivery. This method is advantageous because it does not present the risks of genome integration or

insertional mutagenesis that other gene therapy strategies have, but it can be limited based on the conventional delivery method of direct solution-based injection. Biomaterial-based delivery of mRNA allows for localized and controlled release of cargo. Recently, Zaitseva et al. evaluated the delivery of modified mRNA encoding HGF through crosslinked nanofibrillar collagen scaffolds to a murine skeletal muscle injury.[198] After 20% ablation of the TA muscle, scaffolds were implanted to fill the defect void. At two weeks after implantation, capillary density ($CD31^+$) was observed in injuries treated with the HGF mRNA than by control scaffolds loaded with firefly luciferase-mRNA. As the use of biomaterial-based delivery of genetic substances continues to be implemented, it is likely that this strategy will continue to be investigated for skeletal muscle regeneration. However, cost, immunogenicity, and safety remain concerns regarding this relatively new approach.[115]

2.4.1.3.3 Small molecules

Small molecules are another class of biologic molecules that have been investigated for skeletal muscle regeneration. These organic compounds are typically under 800 Da in size which allows them to readily diffuse across the cell membrane, unlike macromolecules.[199] Small molecules can be produced using synthetic chemistry, allowing for diverse structures and lower manufacturing costs compared to larger molecules such as recombinant growth factors. They work by regulating biological targets such as receptors or enzymes to modulate specific cellular effects. These effects can be reversed and temporally controlled to allow for rapid activation or inhibition. However, small molecules are often delivered orally or via direct injection and the risk of off-target events where proteins with similar conformations are affected can be problematic.[199] To address this, biomaterial-based delivery of small molecules to localize treatment to target tissues is something that is recently being explored. One study investigated the use of a PLGA thin film to deliver FTY720 to a full thickness VML defect in the spinotrapezius muscle of mice.[200] FTY720 is a small molecule agonist of sphingosine-1-phosphate (S1P), a bioactive signaling lipid produced by red blood cells, platelets, and ECs.[200] Receptors of S1P are highly expressed on anti-inflammatory monocytes and have been shown to leverage pro-regenerative effects.[201] The authors demonstrated that three days after injury localized delivery of FTY720 had a higher percentage of anti-inflammatory monocyte and

macrophage infiltration into the injury compared to defects treated with the PLGA film alone.[200] They also found significantly higher blood vessel density ($CD31^+$) in the defect region in mice treated with FTY720 compared to those treated with a blank scaffold control. Another group also found angiogenic effects with the biomaterial-based delivery of small molecule CEP03, derived from ω-[2-carboxyethyl]pyrrole (CEP) protein adducts.[202] CEP protein adducts are a product of lipid oxidation and accumulate during inflammation and wound healing, but as-is face limitations of protein delivery including high cost and manufacturing challenges. CEP03 was encapsulated in Matrigel, an ECM generated by carcinoma cells *in vitro*, injected intramuscularly into the gastrocnemius muscle of mice with hind limb ischemia. Fourteen days after treatment with CEP03, a significant increase in relative mean perfusion ratio (ischemic/unoperated leg) and microvessel density ($CD31^+$) was observed compared with injuries treated with Matrigel alone. Ongoing work developing biomaterials to spatiotemporally deliver small molecules has the potential to increase their therapeutic potential and make this a more commonly investigated approach to treating skeletal muscle injury.

2.4.2 In vivo strategies: Utilizing biomaterials to improve cell delivery

While acellular *in situ* tissue engineering strategies reviewed in Section 2.4.1 have demonstrated success in promoting endogenous skeletal muscle regeneration through recruitment of host cell populations, there are conflicting studies described in the literature that question whether this strategy will facilitate full functional recovery after the large-scale injuries incurred from VML.[64, 203] Corona et al. hypothesized that restricted host SC infiltration into the VML defect is primary limitation to the success of this strategy, as they noted a low number of $Pax7^+$ SCs within a defect treated with an acellular ECM scaffold.[203] Thus, one of the most commonly explored approaches for skeletal muscle regeneration involves the delivery of cells. While early research focused on the direct intramuscular injection of cell suspensions, this simplistic delivery technique has several significant limitations including poor retention, survival, and immune rejection of transplanted cells.[30, 204] However, the recent development of biomaterial-based delivery systems with strategic biophysical and biochemical signaling cues creates a synthetic microenvironment conducive for cell survival and engraftment upon transplantation. The first study to evaluate the efficiency of SCs delivered via a polymer scaffold found 3-fold higher

engraftment of cells into host muscle compared to those delivered via conventional direct injection.[205] Biomaterial delivery systems may also regulate cell fate, stemness and, ultimately, participation in regeneration. *In vivo* tissue engineering involves seeding instructive biomaterial scaffolds with cells immediately prior to transplantation, where they can then provide host cells with paracrine signaling and/or participate in regeneration.[117] By limiting the culture time and manipulation of cells prior to their transplantation, their efficacy can be preserved.[30]

2.4.2.1 Cell source

A range of cell types have been utilized for skeletal muscle tissue engineering including SCs, myoblasts, muscle-derived precursor cells (MDPCs), mesenchymal stem cells (MSCs), perivascular stem cells (PSCs), adipose-derived stem cells (ASCs) and induced pluripotent stem cells (iPSCs).[206-208] SCs are a common cell type utilized for tissue engineering because of their essential role as the resident progenitor cell in native tissue regeneration. However, population heterogeneity and purification remain challenges and sources of variability regarding their functional regenerative potential. Additionally, expansion of SCs *in vitro* results in senescence and loss of proliferative capability, limiting their clinical utility.[209] Thus, there is a tradeoff where increased SC manipulation yields a more purified population but with generally lower regenerative potential.[127] Other muscle-derived cell populations including myoblasts and MDPCs expressing various stem cell markers have also demonstrated regenerative potential, but pose similar challenges regarding cell engraftment, survival, and immunologic rejection.[206] MSCs, including ASCs and PSCs, are also commonly used because they are easily isolated from bone marrow, fat, and umbilical cord tissues, among others.[206] MSCs are pluripotent and give rise to mesodermal tissues including skeletal muscle as well as ectodermal and endodermal tissues. This may permit MSCs to simultaneously participate in peripheral nerve repair and angiogenesis which both play critical roles in skeletal muscle repair. ASCs are a particularly attractive cell type because they are isolated with a simple, high yield procedure and can be expanded quickly, differentiate into myotubes, and evade the host immune system to prevent rejection.[207] These various cell types used for skeletal muscle tissue engineering have been reviewed in detail previously.[206-208] Another important concern is whether cellular therapies are derived from autologous or allogeneic sources. Autologous cells present minimal immunogenicity concerns,

while allogeneic and xenogeneic cells may require immunosuppressive treatment that potentially limits important native responses that direct skeletal muscle regeneration.[210]

2.4.2.2 Hydrogel-based delivery

Hydrogels are one of the most commonly implemented scaffolds for cell delivery-based strategies because cells can be easily mixed into precursor solutions prior to polymerization, and they can be cast directly into the injury, filling irregularly shaped voids. Researchers have used hydrogel scaffolds to deliver myoblasts,[211-212] MDPCs,[213-215] minced muscle grafts,[216-217] MSCs,[218] ASCs,[219-220] and a combination of cell types.[221-222] Beier et al. injected 1 million male primary myoblasts suspended in a fibrin matrix into a female rodent anterior gracilis muscle defect and found male nuclei within host female muscle fibers two weeks after delivery.[212] Other studies delivered MDPCs in fibrin[213, 215] and HA[214] hydrogels to partially resected rodent TA muscles, and found that treatment supported reduced fibrosis,[213] increased myogenesis and vascularization,[213] and partial restoration of muscle contractile function when delivered progressively via multiple injections over time.[215] Rossi et al. evaluated the delivery of either SCs or MDPCs via a HA hydrogel and found that SCs improved the number of new myofibers and resulted in a significantly higher tetanic force generated compared to delivery of MDPCs alone.[214] Other researchers utilized collagen[216, 221] and laminin-111 supplemented HA[217] hydrogels as a vehicle to deliver minced muscle grafts to rodent TA VML injuries.[216-217] Ward et al. found that 50% less minced muscle graft tissue was needed to regain the same functional improvement when delivered in a collagen hydrogel compared to the 100% minced muscle graft.[216] Another study delivering 50% minced muscle grafts with a laminin-111 supplemented HA hydrogel found a 42% improvement in peak tetanic torque production after eight weeks compared to unrepaired limbs. However, this was not a significant improvement compared to delivery of the 50% minced muscle grafts alone. It is not clear if a scaffold is necessary for the delivery of minced muscle grafts, as these cells remain largely contained by their native ECM that remains partially intact.

Several researchers utilized ASCs for skeletal muscle tissue engineering.[219-220] Aurora et al. delivered human ASCs encapsulated in a composite scaffold of PEGylated platelet free plasma hydrogel with porcine ECM to a rodent TA VML injury.[219] Two weeks after injury the

composite scaffold with ASCs resulted in the transplanted cells localized to the injury site and a significantly higher vessel density compared to treatment with acellular composite scaffolds. Another study delivering ASCs in a collagen hydrogel to a similar TA defect found injuries treated with ASC-loaded hydrogels had significantly higher blood flow restoration compared to the hydrogel alone treatment after eight weeks post-injury.[220] It is clear that ASCs encapsulated within hydrogel scaffolds are a promising technology for promoting angiogenesis in VML defects.

Finally, the effect of co-delivery of multiple cell types has also been evaluated.[221-222] One group used composite scaffolds of PLLA/PLGA sponges and fibrin hydrogel to co-deliver ECs and fibroblasts to a defect created in the linea-alba of male nude mice, and 10 days after injury found more neovascularization and significantly higher perfusion than treatment with acellular fibrin hydrogels.[222] While hydrogel delivery systems are easy to deliver and aid in localized cell retention, they are limited due to their weak mechanics and lack of aligned topographical cues necessary to promote functional muscle regeneration.

2.4.2.3 Decellularized ECM-based delivery

Another commonly investigated scaffold for *in vivo* tissue engineering strategies is decellularized ECM.[223-230] Early work studied the delivery of acellular or autologous myoblast-seeded decellularized muscle ECM to the *obliqui abdominis* muscle of rats.[224] Researchers found that myoblast-seeded scaffolds demonstrated abundant blood vessels after two months, while acellular scaffolds were completely replaced by scar tissue. Another study used decellularized muscle ECM to deliver male SC-derived myoblasts to a full-thickness abdominal wall defect in female rats and found the persistence of male myoblasts in the implanted patches after nine months.[225] This work suggests that decellularized ECM scaffolds may facilitate the retention of transplanted cells at the injury site. Quarta et al. evaluated whether MDPCs (expressing bioluminescent reporter protein luciferase) encapsulated in decellularized muscle ECM enhanced skeletal muscle regeneration.[228] The researchers discovered that injecting a MDPC suspension directly into ECM scaffolds resulted in inefficient retention within the scaffold, and instead incorporated MDPCs into an ECM hydrogel and microinjected the cell-seeded hydrogel into the bulk decellularized ECM scaffold. MDPCs were delivered alone or in combination with muscle

resident cells, a heterogeneous population of fibro-adipogenic progenitors, macrophages, and ECs, to a TA VML injury in mice. ECM scaffolds that co-delivered MDPCs and a muscle resident cell population yielded approximately 40 times higher bioluminescence than scaffolds that delivered MDPCs alone. This suggests that the heterogeneous resident cell population supports MDPC viability within the implanted scaffolds. Additionally, injuries treated with ECM scaffolds co-seeded with MDPCs and muscle resident cells demonstrated active and passive length-tension relationships that were equivalent to control uninjured muscle.[229] Injuries treated with co-seeded scaffolds also exhibited less fibrosis compared to untreated injuries and treatment with scaffolds alone.

Other researchers utilized decellularized ECM scaffolds to deliver minced muscle autografts.[226-227] An allogeneic decellularized muscle ECM scaffold was used to deliver minced muscle autograft tissue to a rat lower-limb VML injury.[226] After 12 weeks, treatment with minced muscle-loaded ECM scaffolds significantly increased contractile force recovery compared to untreated injury controls. Treated injuries also demonstrated increased MyoD expression and less fibrous scar tissue formation than those left untreated. Goldman et al. created VML defects in the TA of rats and used a UBM ECM scaffold to deliver minced muscle grafts at a dose of 50% of the total defect mass.[227] At eight weeks post-injury, this treatment resulted in a 28.2% significant increase in peak isometric torque compared to the no repair control, whereas treatment with an acellular UBM ECM scaffold did not result in a significant improvement. These studies indicate that decellularized ECM may serve as an effective method to deliver and retain minced muscle tissue within VML defects.

Finally, decellularized ECM has also been used to deliver MSCs.[223, 230] Merritt et al. implanted decellularized muscle ECM into a full-thickness defect in the lateral gastrocnemius of Lewis rats.[223] Seven days after implantation, bone marrow-derived MSCs were injected into the implanted ECM. After 42 days an 85% functional recovery was observed in muscles treated with MSC-loaded ECM scaffolds with respect to the contralateral uninjured muscle. However, this functional improvement was not significantly greater than treatment with the acellular ECM scaffold. Muscles treated with MSC-seeded scaffolds had significantly more blood vessels and myofibers than those treated with acellular ECM scaffolds. Another study used human umbilical cord MSCs delivered in a porcine decellularized cardiac ECM because the researchers

hypothesized that both components could promote macrophage polarization toward a pro-regenerative M2 phenotype.[230] Rodent TA defects were treated with MSCs, ECM scaffolds, or MSC-loaded ECM scaffolds. Muscle injuries treated with MSC-loaded ECM scaffolds had the highest recorded isometric torque at four and eight weeks post-injury compared to treatment with MSCs alone and ECM scaffolds alone. At two weeks post-implantation, the MSC-loaded ECM treatment group had a significantly higher population of CD206+ macrophages, indicative of pro-regenerative M2 polarization. Finally, histological evaluation of treated muscle found treatment with MSC-loaded ECM had higher new muscle fiber regeneration and lower collagen deposition compared to MSCs alone or ECM scaffolds alone. Taken together, varying degrees of success have been demonstrated by using decellularized ECM scaffolds as cell delivery vehicles and may be attributed to differences in ECM sources and decellularization protocols as well as differences in the anatomy and severity of preclinical VML models.

2.4.2.4 Microfiber-based delivery

While hydrogel, sponge, and decellularized ECM scaffolds have effectively delivered cells to VML injuries, these methods lack aligned topographical cues that have been shown to direct cellular processes that promote improved functional skeletal muscle regeneration. While the use of anisotropic topography has been widely adopted to generate aligned myotubes *in vitro*, few studies have used aligned scaffolds as a cell delivery vehicle to treat *in vivo* VML defects.[231] Page et al. investigated the ability of an aligned fibrin microthread scaffold seeded with human MDPCs to restore function in a mouse TA partial resection VML injury.[231] Tissue sections explanted two days and two weeks post-implantation stained with human nuclear antigen revealed that implanted cells had migrated into the host tissue. After 30 days, the percent of collagen was significantly reduced and muscle area was significantly higher in muscles treated with MDPC-seeded fibrin microthreads compared to injuries that received no treatment. After 120 days post-treatment, mice receiving treatment with MDPC-loaded microthreads had significant improvements in tetanic force generation upon electrical stimulation compared to untreated injuries. This study suggests that fibrin microthreads in combination with MDPCs are a promising scaffold for treating VML defects. A recent study performed a meta-analysis of 44 studies that evaluated quantitative functional capacity after treatment of VML injuries by using a

random-effects model to evaluate the effect size, which indicates treatment effectiveness.[232] The findings from the Page et al. study had the third highest effect size of the 44 studies that met the inclusion criteria, meaning it resulted in one of the highest improvements in functional capacity. This further validates that an aligned microfiber-based scaffold in conjunction with MDPCs is a promising therapeutic treatment for VML and should be further explored.

2.4.2.5 Growth factor-loaded scaffolds

As discussed previously (Section 2.4.1.3.1), growth factors are among the most commonly investigated therapeutic molecules for treating skeletal muscle defects due to their role in orchestrating native regeneration.[55] Incorporation of growth factors within scaffolds allows for control over their release kinetics, localized delivery and concentration, and therapeutic effectiveness. Delivering cells within a growth factor-loaded biomaterial scaffold creates a synthetic niche that more accurately mimics ECM and its native signaling molecules. This growth factor-enriched microenvironment may prevent cultured myoblasts from undergoing apoptosis, losing their myogenic potential, and having low transplantation efficiency, which are the major bottlenecks of traditional cell injection-based approaches. Incorporation of growth factors within cell delivery scaffolds may also promote transplanted cell activation, proliferation, migration, and differentiation. Hagiwara et al. implanted FGF2 and green fluorescent protein $(GFP)^+$ myoblast-loaded gelatin hydrogel microspheres into a rat thigh muscle injury.[233] After four weeks, muscle injuries treated with FGF2 and myoblast-loaded scaffolds had significantly higher GFP expression compared to the delivery of myoblasts alone or in combination with blank microspheres. Furthermore, this co-treatment strategy yielded significantly higher expression of myogenin and reduced expression of MyoD1, suggesting that this approach promotes myoblast differentiation.

Studies also investigated the delivery of cells from biomaterial scaffolds containing multiple growth factors.[234-239] Complex biomaterials systems that release multiple factors in a spatiotemporal manner mimicking *in vivo* GF presentation will create a more conducive cellular microenvironment and likely enhance regenerative outcomes.[127, 193] Several studies specifically investigated the delivery of IGF-1 and VEGF in tandem.[234-236] One study evaluated the co-stimulatory effect of IGF-1 and VEGF by delivering these factors, along with GFP^+ primary

myoblasts, in an alginate scaffold.[234] After myotoxin injury to the murine TA muscle and subsequent hindlimb ischemia, scaffolds were implanted into the injuries. Antibody staining against GFP revealed that after three days of treatment mice implanted with myoblast seeded scaffolds releasing IGF-1/VEGF had a 25.5-fold increase in GFP fibers/mm^2 over bolus injection of GFP$^+$ myoblasts. Scaffolds delivering myoblasts and IGF-1/VEGF also demonstrated the highest recovery of normalized tetanic force compared to all other experimental conditions evaluated. Co-delivery of IGF-1 and VEGF with myoblasts also appeared to have an angiogenic effect on treated muscle injuries, improving blood perfusion after six weeks, compared to those treated with acellular IGF-1/VEGF-loaded scaffolds. Another group used a shape-memory alginate scaffold with IGF-1/VEGF and autologous MDPCs to treat myotoxin and ischemic injuries in TA muscles of mice.[235] Scaffolds delivering IGF-1/VEGF and MDPCs improved transplanted cell engraftment and contractile function after six weeks, with the treatment promoting 90% recovery of the tetanic contractile forces relative to unoperated controls. Another study by Pumberger et al. sought to increase the paracrine signaling of transplanted MSCs by incorporating IGF-1 and VEGF into implanted porous alginate cryogels.[236] The authors hypothesized that stimulation with IGF-1/VEGF would increase MSC paracrine secretion and induce muscle regeneration without the need for transplanted cells to engraft into the host tissue and directly participate in this process. A crush injury to a rat left soleus muscle was induced, followed by implantation of the MSC-loaded scaffold adjacent to the injured muscle. After 56 days post-injury a significant increase in tetanic contraction and muscle fiber density was observed in injuries treated with MSC-loaded scaffolds with IGF-1/VEGF compared to the blank alginate cryogel control treatment. Incorporation of both IGF-1 and VEGF into biomaterial scaffolds clearly demonstrates their co-stimulatory effect on cell engraftment, angiogenesis, and functional muscle regeneration.[234-236]

Other researchers evaluated FGF2 in tandem with HGF[237] or IGF-1.[238-239] Hill et al. implanted alginate scaffolds containing SCs, HGF, and FGF2 into murine TA laceration injuries to assess their ability to promote muscle regeneration.[237] Myoblasts delivered on scaffolds releasing HGF/FGF2 had notably higher engraftment into the regenerating muscle compared to myoblasts delivered via bolus injection or acellular HGF/FGF2 loaded scaffolds. Two studies from the Christ lab recently evaluated the co-stimulatory effect of keratin hydrogels loaded with

MDPCs, FGF2, and IGF-1 for the treatment of VML defects in rat TA[238] and mouse latissimus dorsi (LD) VML defects.[239] Eight weeks after implantation into TA VML defects, acellular keratin hydrogels incorporated with IGF-1 was the only treatment group that significantly improved functional recovery compared to injuries with no repair.[238] Overall, injuries treated with acellular scaffolds demonstrated greater functional improvements compared to MDPC-seeded scaffolds. A similar result was observed when these scaffolds were implanted in the mouse LD injury.[239] Acellular keratin hydrogels loaded with FGF2/IGF-1 enabled significantly improved recovery of contractile force compared to the same FGF2/IGF-1 loaded scaffold seeded with MDPCs. From these studies, it is clear that FGF2 in combination with HGF or IGF-1 has a co-stimulatory effect in treating muscle injuries, but it remains unclear whether the addition of cells is necessary to further enhance skeletal muscle regeneration. Additional optimization of biomaterial carriers, growth factor incorporation strategies, and cell loading methods are necessary to maximize the functional regenerative potential of *in vivo* tissue engineering strategies.

2.4.2.6 Genetically modified cells

Another recent strategy to enhance muscle regeneration in VML injuries is the delivery of scaffolds loaded with transfected myoblasts that upregulate myogenic or angiogenic gene expression. While gene therapy is commonly employed, it can be limited by low efficiency and transient transgene expression. These limitations are often due to delivery modality. In addition to utilizing biomaterial-based strategies to more efficiently deliver genetic payloads (reviewed in Section 2.4.1.3.2), researchers investigated the delivery of transfected cells encapsulated within biomaterial scaffolds.[240-243] Researchers transfected myoblasts,[241-242] mesoangioblasts,[240] and ASCs[243] to express growth factors involved in muscle regeneration including VEGF,[242-243] SDF-1, FGF2,[241] placental growth factor (PLGF).[240] Fuoco et al. transduced mesoangioblasts with a lentivector encoding PLGF and encapsulated them within a photopolymerizable PEG-fibrinogen hydrogel.[240] This cell-loaded hydrogel was implanted to replace an 80% ablation of the TA in mice. $MyHC^+$ muscle fiber number and size increased with time after injury through six months when muscle fibers appeared fully mature. Grip and tread mill tests revealed that mice whose injuries were treated with transfected myoblasts expressing PLGF demonstrated strength and

running resistances almost equivalent to uninjured mice. Another group transfected myoblasts with plasmid vectors carrying human FGF2 cDNA.[241] Myoblasts overexpressing FGF2 were encapsulated in an alginate scaffold and implanted into a crush injury of the rat soleus muscle. After four days post-injury, injuries treated with FGF2 overexpressing myoblasts had a significantly higher number of proliferating cells, lower number of apoptotic cells, and two-fold increase in microvessel formation compared to control animals receiving myoblasts overexpressing luciferase. Despite this, functional analysis at 14 days post-injury did not show a significant increase in muscle force as a result of treatment with FGF2 overexpressing myoblasts. This may be due to evaluating contractile function only two weeks after treatment. Shevchenko et al. transduced human ASCs with recombinant adeno-associated virus encoding human VEGF, encapsulated them in Matrigel, and injected them into the TA, gastrocnemius, and biceps femoris muscles of mice that underwent ischemic injury.[243] The authors assessed the viability of transplanted cells seven days after intramuscular injection and found the presence of transplanted cells throughout the muscle tissue. After 12 days, injuries treated with VEGF overexpressing ASCs reached 80-90% higher blood perfusion than those treated with non-genetically modified ASCs. Zhou and colleagues transfected myoblasts with VEGF or SDF-1 using a lipofectamine transfection reagent.[242] These transfected cells were seeded onto collagen scaffolds and then implanted into rat muscle defects. Implanted conditions include collagen scaffolds and cells transfected with VEGF, SDF-1, or a combination of cells transfected with either VEGF or SDF-1. At two weeks post-injury, microvessel density of the injured tissue was significantly higher in the muscles treated with both VEGF and SDF-1 transfected cells compared to just VEGF, SDF-1, or non-transfected cells. This indicates the synergistic effect of delivering cells transfected with both VEGF and SDF-1. Future work to address challenges including immunogenicity, transfection efficiency, and expression may help expand the use of this promising strategy. Additionally, further optimization of biomaterial carriers to provide a suitable synthetic microenvironment to support cell viability and engraftment will be critical areas of investigation.

2.4.3 In vitro strategies: Developing mature tissue constructs prior to implantation

While *in vivo* tissue engineering strategies reviewed in Section 2.4.2 have resulted in functional regeneration of skeletal muscle defects, this approach has some distinct limitations.

Despite reducing the manipulation of cells prior to transplantation and preserving their efficacy, this approach still leaves cells susceptible to low viability, retention, and immune rejection.[30, 117-118] *In vitro* tissue engineering also involves cell delivery, but instead through the development and implantation of a functional tissue engineered muscle graft (TEMG). This is achieved by combining scaffolds, biological factors, and cells, creating cultured constructs *in vitro* that permit cell differentiation into myofibers. Differentiation is often achieved through a combination of biophysical and biochemical cues as well as mechanical and electrical stimulation. Biomaterial scaffolds with strategic biophysical and biochemical cues create a synthetic microenvironment conducive to cell expansion, differentiation, and ultimately enhanced tissue regeneration. TEMG have the added benefit of being suitable for *in vitro* disease modeling and drug screening.[244-245]

While *in vitro* TEMG have greater functionality prior to implantation than constructs developed through *in situ* and *in vivo* tissue engineering strategies, they have several notable limitations. Although TEMGs can generate contractile force, it is often significantly lower than that observed in native muscle tissue.[107] Additionally, oxygen and nutrient diffusion limitations within these constructs often limit their size or require the development of a complex vascular network to support extended cell viability. Prolonged *in vitro* culture times make TEMG clinical scalability, cost-effectiveness, off-the-shelf availability, and regulatory compliance more challenging than *in situ* and *in vivo* tissue engineering approaches. Implanted TEMGs have resulted in varied degrees of skeletal muscle regeneration, which is likely due to vast assortment of scaffold biomaterials, cell types, culture time and conditions, construct sizes, stimulation regimes, custom bioreactors, and preclinical models evaluated.[50]

2.4.3.1 Aligned scaffolds

One of the most facile methods of generating functional TEMG constructs is by utilizing scaffolds with anisotropic surface features to guide aligned myoblast orientation and differentiation. Strategies to generate aligned features are discussed in detail in Section 2.4.1.2.3. TEMG constructs have primarily utilized fibrous scaffolds[246-248] and aligned pores.[171] The Grayson lab developed hydrogel microfibers by electrospinning co-extruded solutions of fibrinogen and sodium alginate, where the latter acts as a sacrificial structure that when dissolved creates a porous fibrin microfiber.[50, 246] They generated TEMGs by seeding these hydrogel

microfibers with ASCs[246] or myoblasts[247], and evaluated their ability to regenerate murine VML defects. ASC seeded fibrin microfiber bundles were implanted into a fully resected TA and extensor digitorum longus (EDL) muscle injury.[246] Injuries treated with ASC seeded TEMGs demonstrated minimal fibrosis and significantly more MHC+ cells compared to those treated with acellular fibrin microfiber scaffolds. TEMGs made of fibrin microfibers and myoblasts were also evaluated in a separate study for their ability to participate in skeletal muscle regeneration after a partial ablation of the murine TA.[247] At four weeks post-injury measurements of maximal isometric torque indicated that defects treated with myoblast TEMGs and acellular fibrin microfiber scaffolds demonstrated complete functional recovery, while untreated defects demonstrated a 30% torque deficit compared to uninjured muscles. Another group generated TEMGs by co-culturing myoblasts and ECs on aligned nanofibrillar collagen scaffolds.[248] *In vitro*, co-cultured aligned nanofibrillar scaffolds generated constructs with longer myotubes, more synchronized contractility, and higher secretion of angiogenic cytokines compared to randomly oriented scaffolds. After nine days of *in vitro* culture, aligned scaffolds co-seeded with myoblasts and ECs were implanted into a murine partial TA resection injury. Organized myofibers and increased vascular perfusion were observed in muscles treated with aligned TEMGs compared to muscles that received TEMGs with randomly oriented scaffolds. Finally, Kroehne et al. used a controlled freeze-drying process of collagen gels to create aligned pores 20-50 μm in width.[171] When seeded with myoblasts, the anisotropic pore structure enabled aligned myotube formation *in vitro*. Upon implantation into a murine TA and EDL resection injury, the TEMG generated force when electrically stimulated. Because of its simplicity and effectiveness, aligned scaffolds continue to be a commonly investigated method of generating TEMGs with aligned myotubes, contractility, and the ability to promote skeletal muscle regeneration *in vivo*.[171, 246-248]

2.4.3.2 Mechanical and electrical stimulation

Another commonly employed method for generating mature and contractile TEMGs is the use of external stimuli such as electrical or mechanical stimulation. These methods create culture conditions that mimic *in vivo* stimuli and initiate the activation of intracellular signaling pathways involved in skeletal muscle development.[249] Mechanical stimulation regimes mimic

uniaxial strains experienced during daily movement and exercise, while electrical stimulation induces muscle contraction and mimics motor neuron electrical synapses. It is well known that immobility (lack of mechanical stimulation) and denervation (lack of electrical stimulation) can cause muscle atrophy.[250-251] Thus, researchers utilized mechanical and electrical stimulation to promote myoblast fusion, alignment, hypertrophy, and contractile TEMGs *in vitro*.[252-258] A range of uniaxial mechanical stimulation regimes have been applied to TEMGs, including static and cyclic stretch. Static stretching (or tension culture) provides a single strain at the beginning of a culture period, while cyclic stretching applies periodic strain pulses to TEMGs. Researchers have evaluated different frequencies, amplitudes, and "exercise" durations of cyclic stretch. Similar variables are modified in the development of cyclic electrical stimulation regimes. It is important to note the important role that bioreactors play in the application of these stimulation regimes. Bioreactors are often custom built to control culture parameters as well as provide controlled and precise application of external stimuli.

Electrical stimulation has been used to generate TEMGs that promote myofiber formation when implanted *in vivo*.[252] Serena et al. seeded MDPCs in a porous collagen sponge and used stainless steel electrodes to apply a cyclic electrical stimulation regime (33 mHz square wave with 70 mM/cm impulses) starting three days after cell seeding.[252] When MDPC seeded collagen constructs were allowed to mature *in vitro* for seven days, the investigators found that TEMGs that received electrical stimulation had significantly higher expression of MyoD and desmin compared to unstimulated control TEMGs. After one week, TEMGs were implanted into the TA of syngeneic mice. Ten days after treatment, TEMGs were excised and found to contain desmin+ cells and new myofiber formation. While electrical stimulation is a commonly exploited technique for generating mature muscle tissue *in vitro*, more studies evaluating the ability of these constructs to facilitate functional muscle regeneration upon *in vivo* implantation must be conducted.

Cyclic mechanical conditioning is also commonly utilized to generate mature TEMGs prior to implantation into VML injuries.[253-258] Moon et al. seeded decellularized ECM with MDPCs and used a linear motor to create cyclic uniaxial 10% strain, which stretched the constructs three times/min for the first five minutes of every hour.[253] The authors found that one week of mechanical preconditioning generated TEMGs with cellular maturation and

organization. Preconditioned TEMGs were implanted subcutaneously into the LD of mice. Histological analysis revealed that preconditioned TEMGs demonstrate cellular alignment after one week of implantation. After four weeks, preconditioned TEMGs generated specific force that was 1% of native tissue upon stimulated tetanic contraction, where TEMGs with no preconditioning did not generate detectable contractile force. Machingal et al. used this same mechanical pre-conditioning regime to stimulate their TEMGs of decellularized UBM seeded with MDPCs in a custom bioreactor for one week.[254] TEMGs were then implanted into a 50% resection injury of the LD muscle in mice. After two months, muscles treated with mechanically pre-conditioned TEMGs generated a maximum tetanic force representing 72% of native LD muscle. This is a marked improvement compared to the 50% observed in muscles left untreated or implanted with an acellular UBM scaffold. Corona et al. further investigated these findings by evaluating three versions of the UBM/MDPC TEMG developed by Machingal et al., including (1) a TEMG with short culture time and no pre-conditioning, (2) a TEMG with mechanical pre-conditioning, and (3) a TEMG with pre-conditioning and a second application of MDPCs.[255] Two months after implantation in the same LD model described previously,[254] muscle defects that received the TEMG with pre-conditioning and second application of MDPCs had twice the magnitude of functional recovery relative to the other two conditions evaluated.[255] These TEMGs have also been implanted into a more clinically relevant, larger LD defect in an immune competent rat.[256] Two months after injury, *ex vivo* functional assessment showed that muscle defects implanted with pre-conditioned TEMGs had significantly higher contractile force recovery than those treated with an acellular UBM scaffold or untreated controls. This TEMG with the same cyclic mechanical pre-conditioning protocol has also been evaluated for its ability to stimulate regeneration in murine TA defects, and displayed high variability in functional regeneration.[257-258] Collectively, these studies demonstrate the variability that the VML muscle injury implantation model, anatomical location, and size contribute to observed functional improvements.[259] Future investigations of various scaffold materials and cyclic mechanical stimulation regimes may allow for further TEMG maturation and functionality.

In addition to cyclic mechanical pre-conditioning, many researchers have incorporated static mechanical stimulation to provide uniaxial tension to TEMGs *in vitro*.[245, 260-263] However, many TEMGs generated with passive tension have not been evaluated *in vivo* for treating muscle

defects, but instead have been developed for *in vitro* tissue modeling and drug screening.[245, 261-263] Juhas et al. casted a Matrigel/fibrin matrix seeded with myoblasts into cylindrical polydimethylsiloxane (PDMS) molds with Velcro tabs at either end which acted as gel attachment sites and facilitated uniaxial tension.[260] After two weeks in culture, these TEMGs had a high density of aligned myofibers encased in laminin, and generated twitch and tetanic contractions upon electrical stimulation. Differentiated and undifferentiated TEMGs were both implanted into a dorsal skinfold window chamber in nude mice to evaluate their ability to survive and promote vascularization. Two weeks after implantation, TEMGs were saturated with host vessels, and vessels in pre-differentiated TEMGs appeared to align with myofibers in a manner that mirrors native tissue organization. Functional analysis of explanted TEMGs demonstrated a 3.8-fold increase in specific force from one to two weeks post-implantation. The ability of TEMGs generated with passive tension to treat VML injuries requires future investigation and will allow us to better understand how these constructs may contribute to skeletal muscle regeneration.

2.4.3.3 Angiogenesis and innervation

The ability of TEMGs to integrate into host vasculature and become innervated is essential for their survival and ability to promote functional muscle regeneration. Vascularization of these constructs is important because oxygen and nutrient diffusion limitations can inhibit their survival and prohibit the creation of large constructs necessary to treat large-scale VML injuries. To promote angiogenesis, researchers developed pre-vascularized TEMGs *in vitro* prior to implantation to allow for extended cell viability. This is often achieved through co-culture, where multiple cell types are used to generate TEMGs instead of myoblasts alone. To facilitate the formation of NMJs and prevent denervation-related muscle atrophy of implanted TEMGs, researchers investigated whether pre-forming these structures in TEMGs prior to implantation would accelerate these connections upon *in vivo* implantation.[264] Additionally, nerve activity has been shown to be essential for skeletal muscle maturation because it provides electrical stimulation and promotes the switch from fast to slow MyHC in regenerating muscle.[91] The development of TEMGs with vasculature and/or NMJs allows for the development of constructs

that better mimic native skeletal muscle tissue and increase graft integration and success upon implantation.

Several researchers developed pre-vascularized TEMGs and evaluated their ability to participate in skeletal muscle regeneration *in vivo*.[247-248, 265-268] Li et al. created TEMGs with collagen hydrogels seeded with adipose-derived microvessels with or without myoblasts.[265] Upon implantation into a full thickness biceps femoris defect, vascularized constructs were unable to prevent fibrosis and did not support muscle regeneration; this may suggest the supportive role that vascularization plays in muscle regeneration. Other researchers utilized co- and tri-cultures to generate vascularized TEMGs.[247-248, 266-267] Nakayama et al. seeded myoblasts and ECs on aligned nanofibrillar collagen scaffolds.[248] Vascularized TEMGs yielded twice as many donor-derived myofibers and a significantly higher perfused vascular density compared to acellular scaffolds after implantation in a murine partial TA resection injury. Another group used an electrospun fibrin scaffold co-seeded 1:1 with human ECs and ASCs and cultured the TEMG *in vitro* for 11 days to form aligned vessels.[247] The researchers implanted these vascularized TEMGs into murine VML defects and found that the implanted human vessels anastomosed with host vasculature and were perfusable. However, little host vessel infiltration into the TEMG was observed, possibly because of the formation of a fibrous capsule around the implanted TEMG. Others researchers evaluated a triculture system of myoblasts, fibroblasts, and ECs to generate TEMGs.[266-267] Koffler et al. seeded myoblasts, fibroblasts, and ECs on decellularized SIS ECM, and found three weeks of culture promoted the formation of vessels with branched networks and multinucleated myofibers.[266] These TEMGs were implanted into a full thickness segment of the abdominal wall of nude mice, and after 14 days exhibited branched vessel networks that permitted higher perfusion than TEMGs of only myoblasts. Similarly, Shandalov et al. created TEMGs by seeding a PLLA/PLGA scaffold with a tri-culture of myoblast, fibroblasts, and ECs that was cultured *in vitro* for ten days.[267] One week after implantation into a full thickness abdominal wall defect, tri-culture generated TEMGs demonstrated functional vascular perfusion and anastomosis with host vessels. An alternative strategy by Lee et al. developed sheets of myoblasts on a thermosensitive hydrogel transfected with VEGF plasmids.[268] The authors seeded myoblasts on a Tetronic-tyramine-RGD hydrogel. The cells were transfected with VEGF plasmids with poly(b-amino ester) nanoparticles. Transfected cells formed significantly more

capillaries *in vitro* than non-transfected cells. Upon implantation into a mouse ischemia model, muscles treated with transfected cell sheets had significantly enhanced capillary and arteriole density relative to non-transfected cell sheets, indicating the ability of these transfected cells to promote angiogenesis in the injury site. As *in vitro* tissue engineering strategies continue to be developed, it is necessary to continue the development of strategies to enhance vascularization of these constructs to ensure their survival after transplantation.

Other researchers have sought to form NMJs *in vitro* to accelerate innervation upon implantation.[264] One study evaluated the ability of agrin to create acetylcholine receptor clusters on TEMGs of myoblast-seeded fibrin hydrogels.[264] Agrin-supplemented TEMGs were implanted subcutaneously into nude rats with the common peroneal nerve embedded within the construct. Agrin-supplemented TEMGs enhanced contacts with host nerves and developed more mature vasculature compared to TEMGs without agrin. However, these constructs did not generate aligned myotubes, likely due to the isotropic nature of the fibrin hydrogel scaffold. Applying agrin supplementation to scaffolds with unidirectional cues may allow for the generation of more mature, innervated TEMGs. The development of TEMGs with a combination of vasculature and NMJs would allow for a more biomimetic construct and one that is likely to have higher survival, anastomosis, and innervation upon implantation.

2.5 CONCLUSIONS AND FUTURE DIRECTIONS

This chapter summarized the current tissue engineering approaches investigated to treat VML defects, with a focus on biomaterials-based strategies. *In situ*, *in vivo*, and *in vitro* tissue engineering strategies offer diverse approaches for treating VML injuries and have demonstrated varied success. The variability of the outcomes is likely a result of the assortment of design factors, including the use of numerous different preclinical defect models and assessment strategies. Many factors impact these models, including the choice of animal, muscle, and the method of generating muscle injury. While mice and rats are the most commonly utilized pre-clinical animal models because of the ease of conducting high throughput studies with standardized injury models, they typically create defects that are orders of magnitude smaller than those seen clinically. More recently, researchers have used larger preclinical animal models including dogs[139] and pigs[269], which generate defects on a more clinically relevant scale.[270]

Additionally, muscles in varying anatomical locations have different functions, anatomy, and mechanical loading, which can influence regenerative outcomes.[270] Musculoskeletal injury methods also vary and include myotoxic agents, hindlimb ischemia, and partial or total resection models. While myotoxic agents and hindlimb ischemia can yield significant functional deficits, these injuries retain native ECM, vasculature, and nerve structure. Thus, these injuries have a pathophysiology that is different than that of destructive VML injuries.[192] Finally, researchers utilize a broad range of metrics to evaluate VML regeneration from qualitative histology to quantitative muscle functional analyses. Functional analyses are more useful in assessing regenerative outcomes as a clinically feasible treatment, because VML is characterized by a persistent loss of function. Ultimately, the use of a more standardized preclinical animal model and corresponding functional assessment technique will help to make results more comparable across the field.

Initially, tissue engineering scaffolds were simple scaffolds that provided mechanical support to injuries or encapsulated cells for more efficient delivery. More recently, they have progressed to more complex materials that recapitulate the ECM native milieu to locally control host cellular functions and guide functional regeneration. To accomplish this, scaffolds strategically combine biophysical and biochemical cues such as mechanics, topography, and biologically active molecules. In the future, scaffolds that concurrently incorporate multiple both biophysical and biochemical cues will more accurately recapitulate native skeletal muscle tissue and likely lead to greater functional improvements. For example, a scaffold that provides mechanical stability, alignment cues, and spatiotemporal control over the presentation of bioactive molecules would provide both biophysical and biochemical cues that promote functional skeletal muscle regeneration. Another important consideration is engineering these scaffolds to promote vascularization and innervation, as both are paramount to normal muscle function and successful regeneration.

Currently, clinical investigations have been limited to decellularized ECM scaffolds. Ultimately, *in situ* tissue engineering strategies implanting acellular scaffolds will likely be the first clinically available therapeutic for VML. They have off-the-shelf capabilities and simpler scalability, cost-effectiveness, and path to FDA approval.[119] However, challenges still remain regarding scalability of constructs for large defects and stability of incorporated biologic

molecules. Cellular-based strategies have increased complexity compared to acellular strategies. To avoid immune rejection autologous cell sourcing is necessary. This poses significant challenges with manufacturing and maintaining cell plasticity. There is still an unresolved conflict in the literature as to whether cell-based strategies are necessary for treating VML defects. Further research into the mechanisms that govern endogenous regeneration may elucidate mechanisms by which biomaterial-based treatments can successfully in promote functional skeletal muscle in VML injuries.

In this thesis, we investigated fibrin microthreads as an instructive scaffold with both biophysical and biochemical signaling cues that mimic the native skeletal muscle tissue properties that are destroyed in large-scale VML injuries. Specifically, we sought to develop a fibrin microthread scaffold with anisotropic surface features, robust mechanical properties, and sustained release of FGF2 towards the ultimate goal of restoring function in VML injuries. Anisotropic surface features were investigated to promote enhanced myoblast alignment, which is essential for generating functional muscle tissue. To control scaffold mechanical properties and decrease the rate of plasmin-mediated regeneration, we crosslinked fibrin microthreads with horseradish peroxidase (HRP). To enhance the biochemical cues of this scaffold, we loaded microthreads with FGF2 to improve myoblast proliferation and migration. Ultimately, we hypothesize that improving the biophysical and biochemical cues of fibrin microthreads will create a scaffold that enhances functional muscle regeneration after VML injuries.

2.6 ACKNOWLEDGEMENTS

This research was funded in part by NIH R15 HL137145 (GDP) and NSF DGE IGERT 1144804 (MEC).

2.7 REFERENCES

1. Carnes, M. E.; Pins, G. D., Skeletal Muscle Tissue Engineering: Biomaterials-Based Strategies for the Treatment of Volumetric Muscle Loss. *Bioengineering* **2020,** *7* (3), 85.
2. National Hospital Discharge Survey (NHDS). *Center for Disease Control* **2010**.
3. National Hospital Ambulatory Medical Care Survey Outpatient Department (NHAMCS_OP). *Center for Disease Control* **2010**.
4. National Hospital Ambulatory Medical Care Survey Emergency Department (NHAMCS_ED). *Center for Disease Control* **2010**.
5. National Ambulatory Medical Care Survey (NAMCS). *Center for Disease Control* **2010**.

6. Medical Expenditures Panel Survey (MEPS), Agency for Healthcare Research and Quality, U.S. Department of Health and Human Services, 1996-2011. **2011**.
7. Disease, G. B. D.; Injury, I.; Prevalence, C., Global, regional, and national incidence, prevalence, and years lived with disability for 328 diseases and injuries for 195 countries, 1990-2016: a systematic analysis for the Global Burden of Disease Study 2016. *Lancet* **2017,** *390* (10100), 1211-1259. DOI: 10.1016/S0140-6736(17)32154-2.
8. Corso, P.; Finkelstein, E.; Miller, T.; Fiebelkorn, I.; Zaloshnja, E., Incidence and lifetime costs of injuries in the United States. *Inj Prev* **2015,** *21* (6), 434-40. DOI: 10.1136/ip.2005.010983rep.
9. Devore, D. I., Walters, T.J., Christy, R.J., Rathbone, C.R., Hsu, J.R., Baer, D.G., and Wenke, J.C., For Combat Wounded: Extremity Trauma Therapies From the USAISR. *Military Medicine* **2011,** *176* (6), 660-663.
10. Surgeons, A. S. o. P., 2014 Plastic Surgery Statistics Report. Statistics, A. N. C. o. P. S. P., Ed. 2014.
11. Masini, B. D.; Waterman, S. M.; Wenke, J. C.; Owens, B. D.; Hsu, J. R.; Ficke, J. R., Resource utilization and disability outcome assessment of combat casualties from Operation Iraqi Freedom and Operation Enduring Freedom. *Journal of orthopaedic trauma* **2009,** *23* (4), 261-6. DOI: 10.1097/BOT.0b013e31819dfa04.
12. Greer, M. A.; Miklos-Essenberg, M. E.; Harrison-Weaver, S., A review of 41 upper extremity war injuries and the protective gear worn during Operation Enduring Freedom and Operation Iraqi Freedom. *Mil Med* **2006,** *171* (7), 595-7. DOI: 10.7205/milmed.171.7.595.
13. Owens, B. D.; Kragh, J. F., Jr.; Wenke, J. C.; Macaitis, J.; Wade, C. E.; Holcomb, J. B., Combat wounds in operation Iraqi Freedom and operation Enduring Freedom. *The Journal of trauma* **2008,** *64* (2), 295-9. DOI: 10.1097/TA.0b013e318163b875.
14. Rivera, J. C.; Corona, B. T., Muscle-related Disability Following Combat Injury Increases With Time. *US Army Med Dep J* **2016**, 30-4.
15. Corona, B. T.; Rivera, J. C.; Owens, J. G.; Wenke, J. C.; Rathbone, C. R., Volumetric muscle loss leads to permanent disability following extremity trauma. *J Rehabil Res Dev* **2015,** *52* (7), 785-92. DOI: 10.1682/JRRD.2014.07.0165.
16. Cross, J. D.; Ficke, J. R.; Hsu, J. R.; Masini, B. D.; Wenke, J. C., Battlefield orthopaedic injuries cause the majority of long-term disabilities. *The Journal of the American Academy of Orthopaedic Surgeons* **2011,** *19 Suppl 1*, S1-7.
17. Garg, K.; Ward, C. L.; Hurtgen, B. J.; Wilken, J. M.; Stinner, D. J.; Wenke, J. C.; Owens, J. G.; Corona, B. T., Volumetric muscle loss: persistent functional deficits beyond frank loss of tissue. *J Orthop Res* **2015,** *33* (1), 40-6. DOI: 10.1002/jor.22730.
18. Mase, V. J., Jr.; Hsu, J. R.; Wolf, S. E.; Wenke, J. C.; Baer, D. G.; Owens, J.; Badylak, S. F.; Walters, T. J., Clinical application of an acellular biologic scaffold for surgical repair of a large, traumatic quadriceps femoris muscle defect. *Orthopedics* **2010,** *33* (7), 511. DOI: 10.3928/01477447-20100526-24.
19. Aurora, A.; Garg, K.; Corona, B. T.; Walters, T. J., Physical rehabilitation improves muscle function following volumetric muscle loss injury. *BMC Sports Sci Med Rehabil* **2014,** *6* (1), 41. DOI: 10.1186/2052-1847-6-41.
20. Grogan, B. F.; Hsu, J. R.; Consortium, S. T. R., Volumetric Muscle Loss. *J Am Acad Orthop Sur* **2011,** *19*, S35-S37. DOI: Doi 10.5435/00124635-201102001-00007.
21. Doi, K.; Hattori, Y.; Tan, S. H.; Dhawan, V., Basic science behind functioning free muscle transplantation. *Clin Plast Surg* **2002,** *29* (4), 483-95, v-vi. DOI: 10.1016/s0094-1298(02)00020-2.
22. Eckardt, A., Microsurgical reconstruction in the head and neck region: an 18-year experience with 500 consecutive cases. *Journal of Cranio-Maxillofacial Surgery* **2003,** *31* (4), 197-201.
23. Lin, C. H.; Lin, Y. T.; Yeh, J. T.; Chen, C. T., Free functioning muscle transfer for lower extremity posttraumatic composite structure and functional defect. *Plast Reconstr Surg* **2007,** *119* (7), 2118-26. DOI: 10.1097/01.prs.0000260595.85557.41.

24. Riccio, M.; Zingaretti, N.; Verdini, F.; Marchesini, A.; De Francesco, F.; Parodi, P. C., Functional donor-site morbidity after soleus muscle-flap procedure in the treatment of lower limb severe injuries. *Handchir Mikrochir Plast Chir* **2019,** *51* (6), 453-463. DOI: 10.1055/a-0972-1247.
25. Pochini, A. D., Andreoli, C.V., Belangero, P.S., Figueiredo, E.A., Terra, B.B., Cohen, C., Andrade, M.D., Cohen, M., Ejnisman, B., Clinical Considerations for the Surgical Treatment of Pectoralis Major Muscle Ruptures Based on 60 Cases: a Prospecitve Study and Literature Review. *Amer J of Sports Med* **2014,** *42* (1), 95-102.
26. Äärimaa, V., Rantanen, J., Heikkilä, J., Helttula, I. and Orava, S., Rupture of the Pectoralis Major Muscle. *Amer J of Sports Med* **2004,** *32* (5), 1256-1262.
27. Diwan, A.; Eberlin, K. R.; Smith, R. M., The principles and practice of open fracture care, 2018. *Chin J Traumatol* **2018,** *21* (4), 187-192. DOI: 10.1016/j.cjtee.2018.01.002.
28. Bianchi, B.; Copelli, C.; Ferrari, S.; Ferri, A.; Sesenna, E., Free flaps: outcomes and complications in head and neck reconstructions. *J Craniomaxillofac Surg* **2009,** *37* (8), 438-42. DOI: 10.1016/j.jcms.2009.05.003.
29. Lawson, R.; Levin, L. S., Principles of free tissue transfer in orthopaedic practice. *The Journal of the American Academy of Orthopaedic Surgeons* **2007,** *15* (5), 290-9. DOI: 10.5435/00124635-200705000-00007.
30. Qazi, T. H.; Mooney, D. J.; Pumberger, M.; Geißler, S.; Duda, G. N., Biomaterials based strategies for skeletal muscle tissue engineering: Existing technologies and future trends. *Biomaterials* **2015,** *53*, 502-521. DOI: 10.1016/j.biomaterials.2015.02.110.
31. Jarvinen, T. A.; Jarvinen, T. L.; Kaariainen, M.; Kalimo, H.; Jarvinen, M., Muscle injuries: biology and treatment. *Am J Sports Med* **2005,** *33* (5), 745-64. DOI: 10.1177/0363546505274714.
32. Jarvinen, T. A.; Jarvinen, T. L.; Kaariainen, M.; Aarimaa, V.; Vaittinen, S.; Kalimo, H.; Jarvinen, M., Muscle injuries: optimising recovery. *Best Pract Res Clin Rheumatol* **2007,** *21* (2), 317-31. DOI: 10.1016/j.berh.2006.12.004.
33. Sanes, J. R., The basement membrane/basal lamina of skeletal muscle. *J Biol Chem* **2003,** *278* (15), 12601-4. DOI: 10.1074/jbc.R200027200.
34. Gillies, A. R.; Lieber, R. L., Structure and function of the skeletal muscle extracellular matrix. *Muscle & nerve* **2011,** *44* (3), 318-31. DOI: 10.1002/mus.22094.
35. Folkman, J.; Klagsbrun, M.; Sasse, J.; Wadzinski, M.; Ingber, D.; Vlodavsky, I., A heparin-binding angiogenic protein--basic fibroblast growth factor--is stored within basement membrane. *The American journal of pathology* **1988,** *130* (2), 393-400.
36. Naka, D.; Ishii, T.; Shimomura, T.; Hishida, T.; Hara, H., Heparin modulates the receptor-binding and mitogenic activity of hepatocyte growth factor on hepatocytes. *Experimental cell research* **1993,** *209* (2), 317-24. DOI: 10.1006/excr.1993.1316.
37. Roghani, M.; Moscatelli, D., Basic fibroblast growth factor is internalized through both receptor-mediated and heparan sulfate-mediated mechanisms. *J Biol Chem* **1992,** *267* (31), 22156-62.
38. Rapraeger, A. C., Syndecan-regulated receptor signaling. *The Journal of cell biology* **2000,** *149* (5), 995-8.
39. Mauro, A., Satellite cell of skeletal muscle fibers. *J Biophys Biochem Cytol* **1961,** *9*, 493-5. DOI: 10.1083/jcb.9.2.493.
40. Rudnicki, M. A.; Le Grand, F.; McKinnell, I.; Kuang, S., The molecular regulation of muscle stem cell function. *Cold Spring Harb Symp Quant Biol* **2008,** *73*, 323-31. DOI: 10.1101/sqb.2008.73.064.
41. von Maltzahn, J.; Jones, A. E.; Parks, R. J.; Rudnicki, M. A., Pax7 is critical for the normal function of satellite cells in adult skeletal muscle. *P Natl Acad Sci USA* **2013,** *110* (41), 16474-16479. DOI: 10.1073/pnas.1307680110.
42. Sambasivan, R.; Yao, R.; Kissenpfennig, A.; Van Wittenberghe, L.; Paldi, A.; Gayraud-Morel, B.; Guenou, H.; Malissen, B.; Tajbakhsh, S.; Galy, A., Pax7-expressing satellite cells are indispensable for adult skeletal muscle regeneration. *Development* **2011,** *138* (17), 3647-56. DOI: 10.1242/dev.067587.

43. Lepper, C.; Partridge, T. A.; Fan, C. M., An absolute requirement for Pax7-positive satellite cells in acute injury-induced skeletal muscle regeneration. *Development* **2011,** *138* (17), 3639-46. DOI: 10.1242/dev.067595.
44. Murphy, M. M.; Lawson, J. A.; Mathew, S. J.; Hutcheson, D. A.; Kardon, G., Satellite cells, connective tissue fibroblasts and their interactions are crucial for muscle regeneration. *Development* **2011,** *138* (17), 3625-37. DOI: 10.1242/dev.064162.
45. Cosgrove, B. D.; Sacco, A.; Gilbert, P. M.; Blau, H. M., A home away from home: challenges and opportunities in engineering in vitro muscle satellite cell niches. *Differentiation* **2009,** *78* (2-3), 185-94. DOI: 10.1016/j.diff.2009.08.004.
46. Moss, F. P.; Leblond, C. P., Satellite cells as the source of nuclei in muscles of growing rats. *Anat Rec* **1971,** *170* (4), 421-35. DOI: 10.1002/ar.1091700405.
47. Hermansen, L.; Wachtlova, M., Capillary density of skeletal muscle in well-trained and untrained men. *J Appl Physiol* **1971,** *30* (6), 860-3. DOI: 10.1152/jappl.1971.30.6.860.
48. Grefte, S.; Kuijpers-Jagtman, A. M.; Torensma, R.; Von den Hoff, J. W., Skeletal muscle development and regeneration. *Stem Cells Dev* **2007,** *16* (5), 857-68. DOI: 10.1089/scd.2007.0058.
49. Grasman, J. M.; Zayas, M. J.; Page, R. L.; Pins, G. D., Biomimetic scaffolds for regeneration of volumetric muscle loss in skeletal muscle injuries. *Acta Biomater* **2015,** *25*, 2-15. DOI: 10.1016/j.actbio.2015.07.038.
50. Gilbert-Honick, J.; Grayson, W., Vascularized and Innervated Skeletal Muscle Tissue Engineering. *Advanced healthcare materials* **2020,** *9* (1), e1900626. DOI: 10.1002/adhm.201900626.
51. Ciciliot, S.; Schiaffino, S., Regeneration of mammalian skeletal muscle. Basic mechanisms and clinical implications. *Curr Pharm Des* **2010,** *16* (8), 906-14. DOI: 10.2174/138161210790883453.
52. Do, M. K.; Suzuki, T.; Gerelt, B.; Sato, Y.; Mizunoya, W.; Nakamura, M.; Ikeuchi, Y.; Anderson, J. E.; Tatsumi, R., Time-coordinated prevalence of extracellular HGF, FGF2 and TGF-beta3 in crush-injured skeletal muscle. *Anim Sci J* **2012,** *83* (10), 712-7. DOI: 10.1111/j.1740-0929.2012.01057.x.
53. Tidball, J. G., Inflammatory cell response to acute muscle injury. *Med Sci Sports Exerc* **1995,** *27* (7), 1022-32. DOI: 10.1249/00005768-199507000-00011.
54. Fielding, R. A.; Manfredi, T. J.; Ding, W.; Fiatarone, M. A.; Evans, W. J.; Cannon, J. G., Acute phase response in exercise. III. Neutrophil and IL-1 beta accumulation in skeletal muscle. *Am J Physiol* **1993,** *265* (1 Pt 2), R166-72. DOI: 10.1152/ajpregu.1993.265.1.R166.
55. Husmann, I.; Soulet, L.; Gautron, J.; Martelly, I.; Barritault, D., Growth factors in skeletal muscle regeneration. *Cytokine Growth Factor Rev* **1996,** *7* (3), 249-58.
56. Charge, S. B. P., Rudnicki, M.A., Cellular and Molecular Regulation of Muscle Regeneration. *Physiol Rev* **2004,** *84*, 209-238.
57. Toumi, H.; Best, T. M., The inflammatory response: friend or enemy for muscle injury? *Br J Sports Med* **2003,** *37* (4), 284-6. DOI: 10.1136/bjsm.37.4.284.
58. Wahl, S. M.; Hunt, D. A.; Wakefield, L. M.; McCartney-Francis, N.; Wahl, L. M.; Roberts, A. B.; Sporn, M. B., Transforming growth factor type beta induces monocyte chemotaxis and growth factor production. *Proceedings of the National Academy of Sciences* **1987,** *84* (16), 5788-5792.
59. Mantovani, A.; Sozzani, S.; Locati, M.; Allavena, P.; Sica, A., Macrophage polarization: tumor-associated macrophages as a paradigm for polarized M2 mononuclear phagocytes. *Trends Immunol* **2002,** *23* (11), 549-555. DOI: Pii S1471-4906(02)02302-5
Doi 10.1016/S1471-4906(02)02302-5.
60. Martinez, F. O.; Sica, A.; Mantovani, A.; Locati, M., Macrophage activation and polarization. *Front Biosci* **2008,** *13*, 453-61. DOI: 10.2741/2692.
61. Saclier, M.; Yacoub-Youssef, H.; Mackey, A. L.; Arnold, L.; Ardjoune, H.; Magnan, M.; Sailhan, F.; Chelly, J.; Pavlath, G. K.; Mounier, R.; Kjaer, M.; Chazaud, B., Differentially activated macrophages orchestrate myogenic precursor cell fate during human skeletal muscle regeneration. *Stem Cells* **2013,** *31* (2), 384-96. DOI: 10.1002/stem.1288.

62. Philippou, A.; Maridaki, M.; Theos, A.; Koutsilieris, M., Cytokines in muscle damage. *Adv Clin Chem* **2012,** *58*, 49-87. DOI: 10.1016/b978-0-12-394383-5.00010-2.
63. Tidball, J. G.; Dorshkind, K.; Wehling-Henricks, M., Shared signaling systems in myeloid cell-mediated muscle regeneration. *Development* **2014,** *141* (6), 1184-96. DOI: 10.1242/dev.098285.
64. Badylak, S. F.; Dziki, J. L.; Sicari, B. M.; Ambrosio, F.; Boninger, M. L., Mechanisms by which acellular biologic scaffolds promote functional skeletal muscle restoration. *Biomaterials* **2016,** *103*, 128-36. DOI: 10.1016/j.biomaterials.2016.06.047.
65. Cantini, M.; Giurisato, E.; Radu, C.; Tiozzo, S.; Pampinella, F.; Senigaglia, D.; Zaniolo, G.; Mazzoleni, F.; Vitiello, L., Macrophage-secreted myogenic factors: a promising tool for greatly enhancing the proliferative capacity of myoblasts in vitro and in vivo. *Neurol Sci* **2002,** *23* (4), 189-94. DOI: 10.1007/s100720200060.
66. Huard, J.; Lu, A.; Mu, X.; Guo, P.; Li, Y., Muscle Injuries and Repair: What's New on the Horizon! *Cells, tissues, organs* **2016,** *202* (3-4), 227-236. DOI: 10.1159/000443926.
67. Bashkin, P.; Doctrow, S.; Klagsbrun, M.; Svahn, C. M.; Folkman, J.; Vlodavsky, I., Basic fibroblast growth factor binds to subendothelial extracellular matrix and is released by heparitinase and heparin-like molecules. *Biochemistry* **1989,** *28* (4), 1737-43.
68. Cornelison, D. D.; Olwin, B. B.; Rudnicki, M. A.; Wold, B. J., MyoD(-/-) satellite cells in single-fiber culture are differentiation defective and MRF4 deficient. *Dev Biol* **2000,** *224* (2), 122-37. DOI: 10.1006/dbio.2000.9682.
69. Wozniak, A. C.; Anderson, J. E., Nitric oxide-dependence of satellite stem cell activation and quiescence on normal skeletal muscle fibers. *Dev Dyn* **2007,** *236* (1), 240-50. DOI: 10.1002/dvdy.21012.
70. Tatsumi, R.; Liu, X.; Pulido, A.; Morales, M.; Sakata, T.; Dial, S.; Hattori, A.; Ikeuchi, Y.; Allen, R. E., Satellite cell activation in stretched skeletal muscle and the role of nitric oxide and hepatocyte growth factor. *Am J Physiol Cell Physiol* **2006,** *290* (6), C1487-94. DOI: 10.1152/ajpcell.00513.2005.
71. Tatsumi, R.; Allen, R. E., Active hepatocyte growth factor is present in skeletal muscle extracellular matrix. *Muscle & nerve* **2004,** *30* (5), 654-8. DOI: 10.1002/mus.20114.
72. Anderson, J. E.; Wozniak, A. C., Satellite cell activation on fibers: modeling events in vivo--an invited review. *Can J Physiol Pharmacol* **2004,** *82* (5), 300-10. DOI: 10.1139/y04-020.
73. Allen, R. E.; Sheehan, S. M.; Taylor, R. G.; Kendall, T. L.; Rice, G. M., Hepatocyte growth factor activates quiescent skeletal muscle satellite cells in vitro. *J Cell Physiol* **1995,** *165* (2), 307-12. DOI: 10.1002/jcp.1041650211.
74. Gal-Levi, R.; Leshem, Y.; Aoki, S.; Nakamura, T.; Halevy, O., Hepatocyte growth factor plays a dual role in regulating skeletal muscle satellite cell proliferation and differentiation. *Biochim Biophys Acta* **1998,** *1402* (1), 39-51.
75. Tatsumi, R.; Anderson, J. E.; Nevoret, C. J.; Halevy, O.; Allen, R. E., HGF/SF is present in normal adult skeletal muscle and is capable of activating satellite cells. *Dev Biol* **1998,** *194* (1), 114-28. DOI: 10.1006/dbio.1997.8803.
76. Tatsumi, R.; Hattori, A.; Ikeuchi, Y.; Anderson, J. E.; Allen, R. E., Release of hepatocyte growth factor from mechanically stretched skeletal muscle satellite cells and role of pH and nitric oxide. *Mol Biol Cell* **2002,** *13* (8), 2909-18. DOI: 10.1091/mbc.E02-01-0062.
77. Sheehan, S. M.; Allen, R. E., Skeletal muscle satellite cell proliferation in response to members of the fibroblast growth factor family and hepatocyte growth factor. *J Cell Physiol* **1999,** *181* (3), 499-506. DOI: 10.1002/(SICI)1097-4652(199912)181:3<499::AID-JCP14>3.0.CO;2-1.
78. Cornelison, D. D.; Filla, M. S.; Stanley, H. M.; Rapraeger, A. C.; Olwin, B. B., Syndecan-3 and syndecan-4 specifically mark skeletal muscle satellite cells and are implicated in satellite cell maintenance and muscle regeneration. *Dev Biol* **2001,** *239* (1), 79-94. DOI: 10.1006/dbio.2001.0416.
79. Cornelison, D. D.; Wilcox-Adelman, S. A.; Goetinck, P. F.; Rauvala, H.; Rapraeger, A. C.; Olwin, B. B., Essential and separable roles for Syndecan-3 and Syndecan-4 in skeletal muscle development and regeneration. *Genes Dev* **2004,** *18* (18), 2231-6. DOI: 10.1101/gad.1214204.

80. Mourikis, P.; Relaix, F., Activated Muscle Satellite Cells Chase Ghosts. *Cell stem cell* **2016,** *18* (2), 160-2. DOI: 10.1016/j.stem.2016.01.008.
81. Webster, M. T.; Manor, U.; Lippincott-Schwartz, J.; Fan, C. M., Intravital Imaging Reveals Ghost Fibers as Architectural Units Guiding Myogenic Progenitors during Regeneration. *Cell stem cell* **2016,** *18* (2), 243-52. DOI: 10.1016/j.stem.2015.11.005.
82. Serrano, A. L.; Munoz-Canoves, P., Regulation and dysregulation of fibrosis in skeletal muscle. *Experimental cell research* **2010,** *316* (18), 3050-8. DOI: 10.1016/j.yexcr.2010.05.035.
83. Yablonka-Reuveni, Z.; Seger, R.; Rivera, A. J., Fibroblast growth factor promotes recruitment of skeletal muscle satellite cells in young and old rats. *J Histochem Cytochem* **1999,** *47* (1), 23-42. DOI: 10.1177/002215549904700104.
84. Yeh, H. J.; Jin, J. J.; Wang, Y. X.; Zhou, J. Q.; Lin, X. H.; Mu, X. J.; Li, W. Y., [Effect of expression of exogenous PDGF-A chain on growth and transformation of CHO cells]. *Shi Yan Sheng Wu Xue Bao* **1989,** *22* (4), 455-65.
85. Lafyatis, R.; Lechleider, R.; Roberts, A. B.; Sporn, M. B., Secretion and transcriptional regulation of transforming growth factor-beta 3 during myogenesis. *Mol Cell Biol* **1991,** *11* (7), 3795-803. DOI: 10.1128/mcb.11.7.3795.
86. Clegg, C. H.; Linkhart, T. A.; Olwin, B. B.; Hauschka, S. D., Growth factor control of skeletal muscle differentiation: commitment to terminal differentiation occurs in G1 phase and is repressed by fibroblast growth factor. *The Journal of cell biology* **1987,** *105* (2), 949-56. DOI: 10.1083/jcb.105.2.949.
87. Allen, R. E.; Boxhorn, L. K., Regulation of skeletal muscle satellite cell proliferation and differentiation by transforming growth factor-beta, insulin-like growth factor I, and fibroblast growth factor. *J Cell Physiol* **1989,** *138* (2), 311-5. DOI: 10.1002/jcp.1041380213.
88. Engert, J. C.; Berglund, E. B.; Rosenthal, N., Proliferation precedes differentiation in IGF-I-stimulated myogenesis. *The Journal of cell biology* **1996,** *135* (2), 431-40. DOI: 10.1083/jcb.135.2.431.
89. Coolican, S. A.; Samuel, D. S.; Ewton, D. Z.; McWade, F. J.; Florini, J. R., The mitogenic and myogenic actions of insulin-like growth factors utilize distinct signaling pathways. *J Biol Chem* **1997,** *272* (10), 6653-62. DOI: 10.1074/jbc.272.10.6653.
90. Slater, C. R., Schiaffino, S., Innervation of regenerating muscle. *Skeletal muscle repair and regeneration* **2008**, 303-334.
91. Kalhovde, J. M.; Jerkovic, R.; Sefland, I.; Cordonnier, C.; Calabria, E.; Schiaffino, S.; Lomo, T., "Fast" and "slow" muscle fibres in hindlimb muscles of adult rats regenerate from intrinsically different satellite cells. *The Journal of physiology* **2005,** *562* (Pt 3), 847-57. DOI: 10.1113/jphysiol.2004.073684.
92. Christov, C.; Chretien, F.; Abou-Khalil, R.; Bassez, G.; Vallet, G.; Authier, F. J.; Bassaglia, Y.; Shinin, V.; Tajbakhsh, S.; Chazaud, B.; Gherardi, R. K., Muscle satellite cells and endothelial cells: close neighbors and privileged partners. *Mol Biol Cell* **2007,** *18* (4), 1397-409. DOI: 10.1091/mbc.e06-08-0693.
93. Nillesen, S. T.; Geutjes, P. J.; Wismans, R.; Schalkwijk, J.; Daamen, W. F.; van Kuppevelt, T. H., Increased angiogenesis and blood vessel maturation in acellular collagen-heparin scaffolds containing both FGF2 and VEGF. *Biomaterials* **2007,** *28* (6), 1123-31. DOI: 10.1016/j.biomaterials.2006.10.029.
94. Baird, A., Fibroblast growth factors: activities and significance of non-neurotrophin neurotrophic growth factors. *Curr Opin Neurobiol* **1994,** *4* (1), 78-86.
95. Unsicker, K.; Reichert-Preibsch, H.; Wewetzer, K., Stimulation of neuron survival by basic FGF and CNTF is a direct effect and not mediated by non-neuronal cells: evidence from single cell cultures. *Brain Res Dev Brain Res* **1992,** *65* (2), 285-8.
96. Sakiyama-Elbert, S. E.; Hubbell, J. A., Development of fibrin derivatives for controlled release of heparin-binding growth factors. *J Control Release* **2000,** *65* (3), 389-402.
97. Jungnickel, J.; Haase, K.; Konitzer, J.; Timmer, M.; Grothe, C., Faster nerve regeneration after sciatic nerve injury in mice over-expressing basic fibroblast growth factor. *J Neurobiol* **2006,** *66* (9), 940-8. DOI: 10.1002/neu.20265.

98. Schmalbruch, H., The morphology of regeneration of skeletal muscles in the rat. *Tissue Cell* **1976,** *8* (4), 673-92. DOI: 10.1016/0040-8166(76)90039-2.
99. Ignotz, R. A.; Massague, J., Transforming growth factor-beta stimulates the expression of fibronectin and collagen and their incorporation into the extracellular matrix. *J Biol Chem* **1986,** *261* (9), 4337-45.
100. Roberts, A. B.; Joyce, M. E.; Bolander, M. E.; Sporn, M. B., Transforming Growth-Factor-Beta (Tgf-Beta) - a Multifunctional Effector of Both Soft and Hard Tissue Regeneration. *Int Congr Ser* **1990,** *925*, 89-101.
101. Edwards, D. R.; Murphy, G.; Reynolds, J. J.; Whitham, S. E.; Docherty, A. J.; Angel, P.; Heath, J. K., Transforming growth factor beta modulates the expression of collagenase and metalloproteinase inhibitor. *EMBO J* **1987,** *6* (7), 1899-904.
102. Cornwell, K. G.; Pins, G. D., Enhanced proliferation and migration of fibroblasts on the surface of fibroblast growth factor-2-loaded fibrin microthreads. *Tissue Eng Part A* **2010,** *16* (12), 3669-77. DOI: 10.1089/ten.TEA.2009.0600.
103. Lehto, M.; Jarvinen, M.; Nelimarkka, O., Scar formation after skeletal muscle injury. A histological and autoradiographical study in rats. *Arch Orthop Trauma Surg* **1986,** *104* (6), 366-70.
104. Segawa, M.; Fukada, S.; Yamamoto, Y.; Yahagi, H.; Kanematsu, M.; Sato, M.; Ito, T.; Uezumi, A.; Hayashi, S.; Miyagoe-Suzuki, Y.; Takeda, S.; Tsujikawa, K.; Yamamoto, H., Suppression of macrophage functions impairs skeletal muscle regeneration with severe fibrosis. *Experimental cell research* **2008,** *314* (17), 3232-44. DOI: 10.1016/j.yexcr.2008.08.008.
105. Kharraz, Y.; Guerra, J.; Mann, C. J.; Serrano, A. L.; Munoz-Canoves, P., Macrophage plasticity and the role of inflammation in skeletal muscle repair. *Mediators Inflamm* **2013,** *2013*, 491497. DOI: 10.1155/2013/491497.
106. Watt, D. J.; Morgan, J. E.; Clifford, M. A.; Partridge, T. A., The Movement of Muscle Precursor Cells between Adjacent Regenerating Muscles in the Mouse. *Anat Embryol* **1987,** *175* (4), 527-536. DOI: Doi 10.1007/Bf00309688.
107. Bian, W.; Bursac, N., Tissue engineering of functional skeletal muscle: challenges and recent advances. *IEEE Eng Med Biol Mag* **2008,** *27* (5), 109-13. DOI: 10.1109/MEMB.2008.928460.
108. Turner, N. J.; Badylak, S. F., Regeneration of skeletal muscle. *Cell and tissue research* **2012,** *347* (3), 759-74. DOI: 10.1007/s00441-011-1185-7.
109. Corona, B. T.; Flanagan, K. E.; Brininger, C. M.; Goldman, S. M.; Call, J. A.; Greising, S. M., Impact of volumetric muscle loss injury on persistent motoneuron axotomy. *Muscle & nerve* **2018,** *57* (5), 799-807. DOI: 10.1002/mus.26016.
110. Liu, W.; Chakkalakal, J. V., The composition, development, and regeneration of neuromuscular junctions. In *Current topics in developmental biology*, Elsevier: 2018; Vol. 126, pp 99-124.
111. Grounds, M. D., Towards understanding skeletal muscle regeneration. *Pathol Res Pract* **1991,** *187* (1), 1-22. DOI: 10.1016/S0344-0338(11)81039-3.
112. Nguyen, F.; Guigand, L.; Goubault-Leroux, I.; Wyers, M.; Cherel, Y., Microvessel density in muscles of dogs with golden retriever muscular dystrophy. *Neuromuscular disorders : NMD* **2005,** *15* (2), 154-63. DOI: 10.1016/j.nmd.2004.11.002.
113. Juhas, M.; Bursac, N., Engineering skeletal muscle repair. *Curr Opin Biotechnol* **2013,** *24* (5), 880-6. DOI: 10.1016/j.copbio.2013.04.013.
114. Langer, R.; Vacanti, J. P., Tissue engineering. *Science* **1993,** *260* (5110), 920-6. DOI: 10.1126/science.8493529.
115. Nakayama, K. H.; Shayan, M.; Huang, N. F., Engineering Biomimetic Materials for Skeletal Muscle Repair and Regeneration. *Advanced healthcare materials* **2019,** *8* (5), e1801168. DOI: 10.1002/adhm.201801168.
116. Stern-Straeter, J.; Riedel, F.; Bran, G.; Hormann, K.; Goessler, U. R., Advances in skeletal muscle tissue engineering. *In Vivo* **2007,** *21* (3), 435-44.

117. Sicari, B. M., Londono, R., and Badylak, S. F., Strategies for skeletal muscle tissue engineering: seed vs. soil. *J. Mater. Chem. B* **2015,** *3*, 7881-7895.
118. Tedesco, F. S.; Cossu, G., Stem cell therapies for muscle disorders. *Curr Opin Neurol* **2012,** *25* (5), 597-603. DOI: 10.1097/WCO.0b013e328357f288.
119. Sengupta, D.; Waldman, S. D.; Li, S., From in vitro to in situ tissue engineering. *Ann Biomed Eng* **2014,** *42* (7), 1537-45. DOI: 10.1007/s10439-014-1022-8.
120. Corona, B. T.; Wenke, J. C.; Ward, C. L., Pathophysiology of Volumetric Muscle Loss Injury. *Cells, tissues, organs* **2016,** *202* (3-4), 180-188. DOI: 10.1159/000443925.
121. Sicari, B. M.; Rubin, J. P.; Dearth, C. L.; Wolf, M. T.; Ambrosio, F.; Boninger, M.; Turner, N. J.; Weber, D. J.; Simpson, T. W.; Wyse, A.; Brown, E. H.; Dziki, J. L.; Fisher, L. E.; Brown, S.; Badylak, S. F., An acellular biologic scaffold promotes skeletal muscle formation in mice and humans with volumetric muscle loss. *Science translational medicine* **2014,** *6* (234), 234ra58. DOI: 10.1126/scitranslmed.3008085.
122. Dong, R.; Ma, P. X.; Guo, B., Conductive biomaterials for muscle tissue engineering. *Biomaterials* **2020,** *229*, 119584. DOI: 10.1016/j.biomaterials.2019.119584.
123. Chen, M. C.; Sun, Y. C.; Chen, Y. H., Electrically conductive nanofibers with highly oriented structures and their potential application in skeletal muscle tissue engineering. *Acta Biomater* **2013,** *9* (3), 5562-72. DOI: 10.1016/j.actbio.2012.10.024.
124. Ku, S. H.; Lee, S. H.; Park, C. B., Synergic effects of nanofiber alignment and electroactivity on myoblast differentiation. *Biomaterials* **2012,** *33* (26), 6098-104. DOI: 10.1016/j.biomaterials.2012.05.018.
125. Engler, A. J.; Griffin, M. A.; Sen, S.; Bonnemann, C. G.; Sweeney, H. L.; Discher, D. E., Myotubes differentiate optimally on substrates with tissue-like stiffness: pathological implications for soft or stiff microenvironments. *The Journal of cell biology* **2004,** *166* (6), 877-87. DOI: 10.1083/jcb.200405004.
126. Lanza, R.; Langer, R.; Vacanti, J. P.; Atala, A., *Principles of tissue engineering*. Academic press: 2020.
127. Cezar, C. A.; Mooney, D. J., Biomaterial-based delivery for skeletal muscle repair. *Adv Drug Deliv Rev* **2015,** *84*, 188-97. DOI: 10.1016/j.addr.2014.09.008.
128. Badylak, S. F., The extracellular matrix as a biologic scaffold material. *Biomaterials* **2007,** *28* (25), 3587-3593. DOI: 10.1016/j.biomaterials.2007.04.043.
129. Badylak, S. F.; Freytes, D. O.; Gilbert, T. W., Extracellular matrix as a biological scaffold material: Structure and function. *Acta Biomater* **2009,** *5* (1), 1-13. DOI: 10.1016/j.actbio.2008.09.013.
130. Garg, K.; Ward, C. L.; Corona, B. T., Asynchronous inflammation and myogenic cell migration limit muscle tissue regeneration mediated by a cellular scaffolds. *Inflamm Cell Signal* **2014,** *1* (4). DOI: 10.14800/ics.530.
131. Wolf, M. T.; Dearth, C. L.; Sonnenberg, S. B.; Loboa, E. G.; Badylak, S. F., Naturally derived and synthetic scaffolds for skeletal muscle reconstruction. *Adv Drug Deliv Rev* **2014,** *84*, 208-221. DOI: 10.1016/j.addr.2014.08.011.
132. VoytikHarbin, S. L.; Brightman, A. O.; Kraine, M. R.; Waisner, B.; Badylak, S. F., Identification of extractable growth factors from small intestinal submucosa. *Journal of Cellular Biochemistry* **1997,** *67* (4), 478-491. DOI: Doi 10.1002/(Sici)1097-4644(19971215)67:4<478::Aid-Jcb6>3.0.Co;2-P.
133. Brown, B.; Lindberg, K.; Reing, J.; Stolz, D. B.; Badylak, S. F., The basement membrane component of biologic scaffolds derived from extracellular matrix. *Tissue Eng* **2006,** *12* (3), 519-526. DOI: DOI 10.1089/ten.2006.12.519.
134. Marcal, H.; Ahmed, T.; Badylak, S. F.; Tottey, S.; Foster, L. J. R., A comprehensive protein expression profile of extracellular matrix biomaterial derived from porcine urinary bladder. *Regenerative medicine* **2012,** *7* (2), 159-166. DOI: 10.2217/Rme.12.6.

135. Wolf, M. T.; Daly, K. A.; Reing, J. E.; Badylak, S. F., Biologic scaffold composed of skeletal muscle extracellular matrix. *Biomaterials* **2012,** *33* (10), 2916-2925. DOI: 10.1016/j.biomaterials.2011.12.055.
136. Brown, B. N.; Freund, J. M.; Han, L.; Rubin, J. P.; Reing, J. E.; Jeffries, E. M.; Wolf, M. T.; Tottey, S.; Barnes, C. A.; Ratner, B. D.; Badylak, S. F., Comparison of three methods for the derivation of a biologic scaffold composed of adipose tissue extracellular matrix. *Tissue Eng Part C Methods* **2011,** *17* (4), 411-21. DOI: 10.1089/ten.TEC.2010.0342.
137. Faulk, D. M.; Carruthers, C. A.; Warner, H. J.; Kramer, C. R.; Reing, J. E.; Zhang, L.; D'Amore, A.; Badylak, S. F., The effect of detergents on the basement membrane complex of a biologic scaffold material. *Acta Biomater* **2014,** *10* (1), 183-193. DOI: 10.1016/j.actbio.2013.09.006.
138. Reing, J. E.; Brown, B. N.; Daly, K. A.; Freund, J. M.; Gilbert, T. W.; Hsiong, S. X.; Huber, A.; Kullas, K. E.; Tottey, S.; Wolf, M. T.; Badylak, S. F., The effects of processing methods upon mechanical and biologic properties of porcine dermal extracellular matrix scaffolds. *Biomaterials* **2010,** *31* (33), 8626-8633. DOI: 10.1016/j.biomaterials.2010.07.083.
139. Turner, N. J.; Yates, A. J.; Weber, D. J.; Qureshi, I. R.; Stolz, D. B.; Gilbert, T. W.; Badylak, S. F., Xenogeneic Extracellular Matrix as an Inductive Scaffold for Regeneration of a Functioning Musculotendinous Junction. *Tissue Eng Pt A* **2010,** *16* (11), 3309-3317. DOI: 10.1089/ten.tea.2010.0169.
140. Valentin, J. E.; Turner, N. J.; Gilbert, T. W.; Badylak, S. F., Functional skeletal muscle formation with a biologic scaffold. *Biomaterials* **2010,** *31* (29), 7475-7484. DOI: 10.1016/j.biomaterials.2010.06.039.
141. Merritt, E. K.; Hammers, D. W.; Tierney, M.; Suggs, L. J.; Walters, T. J.; Farrar, R. P., Functional Assessment of Skeletal Muscle Regeneration Utilizing Homologous Extracellular Matrix as Scaffolding. *Tissue Eng Pt A* **2010,** *16* (4), 1395-1405. DOI: 10.1089/ten.tea.2009.0226.
142. Sicari, B. M.; Agrawal, V.; Siu, B. F.; Medberry, C. J.; Dearth, C. L.; Turner, N. J.; Badylak, S. F., A Murine Model of Volumetric Muscle Loss and a Regenerative Medicine Approach for Tissue Replacement. *Tissue Eng Pt A* **2012,** *18* (19-20), 1941-1948. DOI: 10.1089/ten.tea.2012.0475.
143. Corona, B. T.; Wu, X.; Ward, C. L.; McDaniel, J. S.; Rathbone, C. R.; Walters, T. J., The promotion of a functional fibrosis in skeletal muscle with volumetric muscle loss injury following the transplantation of muscle-ECM. *Biomaterials* **2013,** *34* (13), 3324-35. DOI: 10.1016/j.biomaterials.2013.01.061.
144. Garg, K.; Ward, C. L.; Rathbone, C. R.; Corona, B. T., Transplantation of devitalized muscle scaffolds is insufficient for appreciable de novo muscle fiber regeneration after volumetric muscle loss injury. *Cell and tissue research* **2014,** *358* (3), 857-873. DOI: 10.1007/s00441-014-2006-6.
145. Aurora, A.; Roe, J. L.; Corona, B. T.; Walters, T. J., An acellular biologic scaffold does not regenerate appreciable de novo muscle tissue in rat models of volumetric muscle loss injury. *Biomaterials* **2015,** *67*, 393-407. DOI: 10.1016/j.biomaterials.2015.07.040.
146. Greising, S. M.; Rivera, J. C.; Goldman, S. M.; Watts, A.; Aguilar, C. A.; Corona, B. T., Unwavering Pathobiology of Volumetric Muscle Loss Injury. *Sci Rep* **2017,** *7* (1), 13179. DOI: 10.1038/s41598-017-13306-2.
147. Han, N.; Yabroudi, M. A.; Stearns-Reider, K.; Helkowski, W.; Sicari, B. M.; Rubin, J. P.; Badylak, S. F.; Boninger, M. L.; Ambrosio, F., Electrodiagnostic Evaluation of Individuals Implanted With Extracellular Matrix for the Treatment of Volumetric Muscle Injury: Case Series. *Physical therapy* **2016,** *96* (4), 540-549. DOI: 10.2522/ptj.20150133.
148. Dziki, J., Badylak, S., Yabroudi, M., Sicari, B., Ambrosio, F., Stearns, K., Turner, N., Wyse, A., Boninger, M.L., Brown, E.H., and Rubin, J.P., An acellular biologic scaffold treatment for volumetric muscle loss: results of a 13-patient cohort study. *Nature Regenerative Medicine* **2016,** *1*, 16008.
149. Hill, E.; Boontheekul, T.; Mooney, D. J., Designing scaffolds to enhance transplanted myoblast survival and migration. *Tissue Eng* **2006,** *12* (5), 1295-304. DOI: 10.1089/ten.2006.12.1295.

150. DeQuach, J. A.; Lin, J. E.; Cam, C.; Hu, D.; Salvatore, M. A.; Sheikh, F.; Christman, K. L., Injectable skeletal muscle matrix hydrogel promotes neovascularization and muscle cell infiltration in a hindlimb ischemia model. *European cells & materials* **2012,** *23*, 400.
151. Marcinczyk, M.; Dunn, A.; Haas, G.; Madsen, J.; Scheidt, R.; Patel, K.; Talovic, M.; Garg, K., The Effect of Laminin-111 Hydrogels on Muscle Regeneration in a Murine Model of Injury. *Tissue Eng Pt A* **2019,** *25* (13-14), 1001-1012.
152. Kin, S.; Hagiwara, A.; Nakase, Y.; Kuriu, Y.; Nakashima, S.; Yoshikawa, T.; Sakakura, C.; Otsuji, E.; Nakamura, T.; Yamagishi, H., Regeneration of skeletal muscle using in situ tissue engineering on an acellular collagen sponge scaffold in a rabbit model. *ASAIO journal* **2007,** *53* (4), 506-513.
153. Haas, G. J.; Dunn, A. J.; Marcinczyk, M.; Talovic, M.; Schwartz, M.; Scheidt, R.; Patel, A. D.; Hixon, K. R.; Elmashhady, H.; McBride-Gagyi, S. H., Biomimetic sponges for regeneration of skeletal muscle following trauma. *J Biomed Mater Res A* **2019,** *107* (1), 92-103.
154. Ju, Y. M., Atala, A., Yoo, J. J., Lee, S. J., In situ regeneration of skeletal muscle tissue through host cell recruitment. *Acta Biomater* **2014,** *10*, 4332-4339.
155. Huang, N. F.; Lee, R. J.; Li, S., Engineering of aligned skeletal muscle by micropatterning. *Am J Transl Res* **2010,** *2* (1), 43-55.
156. Huang, N. F., Patel, S., Thakar, R.G., Wu, J., Hsiao, B.S., Chu, B., Lee, R.J., and Li, S., Myotube Assembly on Nanofibrous and Micropatterned Polymers. *Nano Letters* **2006,** *6* (3), 537-542.
157. Charest, J. L.; Garcia, A. J.; King, W. P., Myoblast alignment and differentiation on cell culture substrates with microscale topography and model chemistries. *Biomaterials* **2007,** *28* (13), 2202-10. DOI: 10.1016/j.biomaterials.2007.01.020.
158. Wang, P. Y.; Yu, H. T.; Tsai, W. B., Modulation of alignment and differentiation of skeletal myoblasts by submicron ridges/grooves surface structure. *Biotechnology and bioengineering* **2010,** *106* (2), 285-94. DOI: 10.1002/bit.22697.
159. Monge, C.; Ren, K.; Berton, K.; Guillot, R.; Peyrade, D.; Picart, C., Engineering muscle tissues on microstructured polyelectrolyte multilayer films. *Tissue Eng Part A* **2012,** *18* (15-16), 1664-76. DOI: 10.1089/ten.TEA.2012.0079.
160. Flemming, R. G., Murphy, C.J., Abrams, G.A., Goodman, S.L., Nealey, P.F, Effects of synthetic micro- and nano-structures surfaces on cell behavior. *Biomaterials* **1999,** *20*, 573-588.
161. Zhao, Y.; Zeng, H.; Nam, J.; Agarwal, S., Fabrication of skeletal muscle constructs by topographic activation of cell alignment. *Biotechnology and bioengineering* **2009,** *102* (2), 624-31. DOI: 10.1002/bit.22080.
162. Bian, W.; Liau, B.; Badie, N.; Bursac, N., Mesoscopic hydrogel molding to control the 3D geometry of bioartificial muscle tissues. *Nature protocols* **2009,** *4* (10), 1522-34. DOI: 10.1038/nprot.2009.155.
163. Choi, J. S.; Lee, S. J.; Christ, G. J.; Atala, A.; Yoo, J. J., The influence of electrospun aligned poly(epsilon-caprolactone)/collagen nanofiber meshes on the formation of self-aligned skeletal muscle myotubes. *Biomaterials* **2008,** *29* (19), 2899-906. DOI: 10.1016/j.biomaterials.2008.03.031.
164. Li, W., Mauck, R.L., Cooper, J.A., Yuan, X., and Tuan, R.S., Engineering controllable anisotropy in electrospun biodegradable nanofibrous scaffolds for musculoskeletal tissue engineering. *Journal of Biomechanics* **2007,** *40*, 1686-1693. DOI: 10.1016/j.jbiomech.2006.09.004.
165. Aviss, K. J.; Gough, J. E.; Downes, S., Aligned electrospun polymer fibres for skeletal muscle regeneration. *European cells & materials* **2010,** *19*, 193-204.
166. Zhang, S.; Liu, X.; Barreto-Ortiz, S. F.; Yu, Y.; Ginn, B. P.; DeSantis, N. A.; Hutton, D. L.; Grayson, W. L.; Cui, F. Z.; Korgel, B. A.; Gerecht, S.; Mao, H. Q., Creating polymer hydrogel microfibres with internal alignment via electrical and mechanical stretching. *Biomaterials* **2014,** *35* (10), 3243-51. DOI: 10.1016/j.biomaterials.2013.12.081.
167. Cornwell, K. G.; Pins, G. D., Discrete crosslinked fibrin microthread scaffolds for tissue regeneration. *J Biomed Mater Res A* **2007,** *82* (1), 104-12. DOI: 10.1002/jbm.a.31057.

168. O'Brien, M. P.; Carnes, M. E.; Page, R. L.; Gaudette, G. R.; Pins, G. D., Designing Biopolymer Microthreads for Tissue Engineering and Regenerative Medicine. *Curr Stem Cell Rep* **2016,** *2* (2), 147-157. DOI: 10.1007/s40778-016-0041-9.
169. Pins, G. D.; Silver, F. H., A self-assembled collagen scaffold suitable for use in soft and hard tissue replacement. *Materials Science and Engineering: C* **1995,** *3* (2), 101-107. DOI: 10.1016/0928-4931(95)00109-3.
170. Jana, S.; Cooper, A.; Zhang, M., Chitosan scaffolds with unidirectional microtubular pores for large skeletal myotube generation. *Advanced healthcare materials* **2013,** *2* (4), 557-61. DOI: 10.1002/adhm.201200177.
171. Kroehne, V.; Heschel, I.; Schugner, F.; Lasrich, D.; Bartsch, J. W.; Jockusch, H., Use of a novel collagen matrix with oriented pore structure for muscle cell differentiation in cell culture and in grafts. *J Cell Mol Med* **2008,** *12* (5A), 1640-8. DOI: 10.1111/j.1582-4934.2008.00238.x.
172. Ma, P. X.; Zhang, R., Microtubular architecture of biodegradable polymer scaffolds. *J Biomed Mater Res* **2001,** *56* (4), 469-77.
173. Jana, S.; Levengood, S. K.; Zhang, M., Anisotropic Materials for Skeletal-Muscle-Tissue Engineering. *Adv Mater* **2016,** *28* (48), 10588-10612. DOI: 10.1002/adma.201600240.
174. Nakayama, K. H.; Alcazar, C.; Yang, G.; Quarta, M.; Paine, P.; Doan, L.; Davies, A.; Rando, T. A.; Huang, N. F., Rehabilitative exercise and spatially patterned nanofibrillar scaffolds enhance vascularization and innervation following volumetric muscle loss. *NPJ Regen Med* **2018,** *3*, 16. DOI: 10.1038/s41536-018-0054-3.
175. Simons, M.; Annex, B. H.; Laham, R. J.; Kleiman, N.; Henry, T.; Dauerman, H.; Udelson, J. E.; Gervino, E. V.; Pike, M.; Whitehouse, M. J.; Moon, T.; Chronos, N. A., Pharmacological treatment of coronary artery disease with recombinant fibroblast growth factor-2: double-blind, randomized, controlled clinical trial. *Circulation* **2002,** *105* (7), 788-93.
176. Simons, M.; Ware, J. A., Therapeutic angiogenesis in cardiovascular disease. *Nat Rev Drug Discov* **2003,** *2* (11), 863-71. DOI: 10.1038/nrd1226.
177. Henry, T. D.; Annex, B. H.; McKendall, G. R.; Azrin, M. A.; Lopez, J. J.; Giordano, F. J.; Shah, P. K.; Willerson, J. T.; Benza, R. L.; Berman, D. S.; Gibson, C. M.; Bajamonde, A.; Rundle, A. C.; Fine, J.; McCluskey, E. R.; Investigators, V., The VIVA trial: Vascular endothelial growth factor in Ischemia for Vascular Angiogenesis. *Circulation* **2003,** *107* (10), 1359-65.
178. Simons, M.; Bonow, R. O.; Chronos, N. A.; Cohen, D. J.; Giordano, F. J.; Hammond, H. K.; Laham, R. J.; Li, W.; Pike, M.; Sellke, F. W.; Stegmann, T. J.; Udelson, J. E.; Rosengart, T. K., Clinical trials in coronary angiogenesis: issues, problems, consensus: An expert panel summary. *Circulation* **2000,** *102* (11), E73-86.
179. Lee, K.; Silva, E. A.; Mooney, D. J., Growth factor delivery-based tissue engineering: general approaches and a review of recent developments. *J R Soc Interface* **2011,** *8* (55), 153-70. DOI: 10.1098/rsif.2010.0223.
180. Silva, E. A.; Mooney, D. J., Spatiotemporal control of vascular endothelial growth factor delivery from injectable hydrogels enhances angiogenesis. *J Thromb Haemost* **2007,** *5* (3), 590-8. DOI: 10.1111/j.1538-7836.2007.02386.x.
181. Shvartsman, D.; Storrie-White, H.; Lee, K.; Kearney, C.; Brudno, Y.; Ho, N.; Cezar, C.; McCann, C.; Anderson, E.; Koullias, J.; Tapia, J. C.; Vandenburgh, H.; Lichtman, J. W.; Mooney, D. J., Sustained delivery of VEGF maintains innervation and promotes reperfusion in ischemic skeletal muscles via NGF/GDNF signaling. *Molecular therapy : the journal of the American Society of Gene Therapy* **2014,** *22* (7), 1243-53. DOI: 10.1038/mt.2014.76.
182. Lee, J.; Bhang, S. H.; Park, H.; Kim, B. S.; Lee, K. Y., Active Blood Vessel Formation in the Ischemic Hindlimb Mouse Model Using a Microsphere/Hydrogel Combination System. *Pharm Res-Dordr* **2010,** *27* (5), 767-774. DOI: 10.1007/s11095-010-0067-0.

183. Frey, S. P.; Jansen, H.; Raschke, M. J.; Meffert, R. H.; Ochman, S., VEGF improves skeletal muscle regeneration after acute trauma and reconstruction of the limb in a rabbit model. *Clin Orthop Relat Res* **2012,** *470* (12), 3607-14. DOI: 10.1007/s11999-012-2456-7.
184. Hammers, D. W., Sarathy, A., Pham, C.B., Drinnan, C.T., Farrar, R.P., and Suggs, L.J., Controlled Release of IGF-1 From a Biodegradable Matrix Improves Functional Recovery of Skeletal Muscle from Ischemia/Reperfusion. *Biotechnology and bioengineering* **2011,** *109* (4), 1051-1059.
185. Doi, K.; Ikeda, T.; Marui, A.; Kushibiki, T.; Arai, Y.; Hirose, K.; Soga, Y.; Iwakura, A.; Ueyama, K.; Yamahara, K.; Itoh, H.; Nishimura, K.; Tabata, Y.; Komeda, M., Enhanced angiogenesis by gelatin hydrogels incorporating basic fibroblast growth factor in rabbit model of hind limb ischemia. *Heart Vessels* **2007,** *22* (2), 104-8. DOI: 10.1007/s00380-006-0934-0.
186. Layman, H.; Spiga, M. G.; Brooks, T.; Pham, S.; Webster, K. A.; Andreopoulos, F. M., The effect of the controlled release of basic fibroblast growth factor from ionic gelatin-based hydrogels on angiogenesis in a murine critical limb ischemic model. *Biomaterials* **2007,** *28* (16), 2646-54. DOI: 10.1016/j.biomaterials.2007.01.044.
187. Yasuda, Y.; Koyama, H.; Tabata, Y.; Fujihara, Y.; Oba, M.; Uchinuma, E.; Takato, T., Controlled delivery of bFGF remodeled vascular network in muscle flap and increased perfusion capacity via minor pedicle. *J Surg Res* **2008,** *147* (1), 132-7. DOI: 10.1016/j.jss.2007.10.009.
188. Grasman, J. M.; Do, D. M.; Page, R. L.; Pins, G. D., Rapid release of growth factors regenerates force output in volumetric muscle loss injuries. *Biomaterials* **2015,** *72*, 49-60. DOI: 10.1016/j.biomaterials.2015.08.047.
189. Borselli, C.; Storrie, H.; Benesch-Lee, F.; Shvartsman, D.; Cezar, C.; Lichtman, J. W.; Vandenburgh, H. H.; Mooney, D. J., Functional muscle regeneration with combined delivery of angiogenesis and myogenesis factors. *Proc Natl Acad Sci U S A* **2010,** *107* (8), 3287-92. DOI: 10.1073/pnas.0903875106.
190. Rybalko, V. Y.; Pham, C. B.; Hsieh, P. L.; Hammers, D. W.; Merscham-Banda, M.; Suggs, L. J.; Farrar, R. P., Controlled delivery of SDF-1alpha and IGF-1: CXCR4(+) cell recruitment and functional skeletal muscle recovery. *Biomater Sci* **2015,** *3* (11), 1475-86. DOI: 10.1039/c5bm00233h.
191. Matsui, M.; Tabata, Y., Enhanced angiogenesis by multiple release of platelet-rich plasma contents and basic fibroblast growth factor from gelatin hydrogels. *Acta Biomater* **2012,** *8* (5), 1792-1801.
192. Passipieri, J. A.; Christ, G. J., The Potential of Combination Therapeutics for More Complete Repair of Volumetric Muscle Loss Injuries: The Role of Exogenous Growth Factors and/or Progenitor Cells in Implantable Skeletal Muscle Tissue Engineering Technologies. *Cells, tissues, organs* **2016,** *202* (3-4), 202-213. DOI: 10.1159/000447323.
193. Chen, F. M.; Zhang, M.; Wu, Z. F., Toward delivery of multiple growth factors in tissue engineering. *Biomaterials* **2010,** *31* (24), 6279-308. DOI: 10.1016/j.biomaterials.2010.04.053.
194. Stilhano, R. S.; Madrigal, J. L.; Wong, K.; Williams, P. A.; Martin, P. K.; Yamaguchi, F. S.; Samoto, V. Y.; Han, S. W.; Silva, E. A., Injectable alginate hydrogel for enhanced spatiotemporal control of lentivector delivery in murine skeletal muscle. *J Control Release* **2016,** *237*, 42-9. DOI: 10.1016/j.jconrel.2016.06.047.
195. Falco, E. E.; Wang, M. O.; Thompson, J. A.; Chetta, J. M.; Yoon, D. M.; Li, E. Z.; Kulkami, M. M.; Shah, S.; Pandit, A.; Roth, J. S.; Fisher, J. P., Porous EH and EH-PEG scaffolds as gene delivery vehicles to skeletal muscle. *Pharm Res* **2011,** *28* (6), 1306-16. DOI: 10.1007/s11095-010-0358-5.
196. Doukas, J.; Blease, K.; Craig, D.; Ma, C.; Chandler, L. A.; Sosnowski, B. A.; Pierce, G. F., Delivery of FGF genes to wound repair cells enhances arteriogenesis and myogenesis in skeletal muscle. *Molecular therapy : the journal of the American Society of Gene Therapy* **2002,** *5* (5 Pt 1), 517-27. DOI: 10.1006/mthe.2002.0579.
197. Kasahara, H.; Tanaka, E.; Fukuyama, N.; Sato, E.; Sakamoto, H.; Tabata, Y.; Ando, K.; Iseki, H.; Shinozaki, Y.; Kimura, K.; Kuwabara, E.; Koide, S.; Nakazawa, H.; Mori, H., Biodegradable gelatin

hydrogel potentiates the angiogenic effect of fibroblast growth factor 4 plasmid in rabbit hindlimb ischemia. *J Am Coll Cardiol* **2003,** *41* (6), 1056-62. DOI: 10.1016/s0735-1097(02)03007-3.
198. Zaitseva, T. S.; Alcazar, C.; Zamani, M.; Hou, L.; Sawamura, S.; Yakubov, E.; Hopkins, M.; Woo, Y. J.; Paukshto, M. V.; Huang, N. F., Aligned Nanofibrillar Scaffolds for Controlled Delivery of Modified mRNA. *Tissue Eng Part A* **2019,** *25* (1-2), 121-130. DOI: 10.1089/ten.TEA.2017.0494.
199. Jung, D. W.; Williams, D. R., Reawakening atlas: chemical approaches to repair or replace dysfunctional musculature. *ACS Chem Biol* **2012,** *7* (11), 1773-90. DOI: 10.1021/cb3003368.
200. San Emeterio, C. L.; Olingy, C. E.; Chu, Y.; Botchwey, E. A., Selective recruitment of non-classical monocytes promotes skeletal muscle repair. *Biomaterials* **2017,** *117*, 32-43. DOI: 10.1016/j.biomaterials.2016.11.021.
201. Awojoodu, A. O.; Ogle, M. E.; Sefcik, L. S.; Bowers, D. T.; Martin, K.; Brayman, K. L.; Lynch, K. R.; Peirce-Cottler, S. M.; Botchwey, E., Sphingosine 1-phosphate receptor 3 regulates recruitment of anti-inflammatory monocytes to microvessels during implant arteriogenesis. *Proc Natl Acad Sci U S A* **2013,** *110* (34), 13785-90. DOI: 10.1073/pnas.1221309110.
202. Hou, L.; Yang, G.; Tang, S.; Alcazar, C.; Joshi, P.; Strassberg, Z.; Kim, M.; Kawamura, M.; Woo, Y. J.; Shrager, J.; Ding, S.; Huang, N. F., Small Molecule Derived From Carboxyethylpyrrole Protein Adducts Promotes Angiogenesis in a Mouse Model of Peripheral Arterial Disease. *J Am Heart Assoc* **2018,** *7* (18), e009234. DOI: 10.1161/JAHA.118.009234.
203. Corona, B. T.; Greising, S. M., Challenges to acellular biological scaffold mediated skeletal muscle tissue regeneration. *Biomaterials* **2016,** *104*, 238-46. DOI: 10.1016/j.biomaterials.2016.07.020.
204. Smythe, G. M.; Hodgetts, S. I.; Grounds, M. D., Problems and solutions in myoblast transfer therapy. *J Cell Mol Med* **2001,** *5* (1), 33-47. DOI: 10.1111/j.1582-4934.2001.tb00136.x.
205. Boldrin, L.; Elvassore, N.; Malerba, A.; Flaibani, M.; Cimetta, E.; Piccoli, M.; Baroni, M. D.; Gazzola, M. V.; Messina, C.; Gamba, P.; Vitiello, L.; De Coppi, P., Satellite cells delivered by micro-patterned scaffolds: a new strategy for cell transplantation in muscle diseases. *Tissue Eng* **2007,** *13* (2), 253-62. DOI: 10.1089/ten.2006.0093.
206. Sicari, B. M.; Dearth, C. L.; Badylak, S. F., Tissue Engineering and Regenerative Medicine Approaches to Enhance the Functional Response to Skeletal Muscle Injury. *Anatomical Record-Advances in Integrative Anatomy and Evolutionary Biology* **2014,** *297* (1), 51-64. DOI: 10.1002/ar.22794.
207. Pantelic, M. N.; Larkin, L. M., Stem Cells for Skeletal Muscle Tissue Engineering. *Tissue Eng Part B-Re* **2018,** *24* (5), 373-391. DOI: 10.1089/ten.teb.2017.0451.
208. McCullagh, K. J.; Perlingeiro, R. C., Coaxing stem cells for skeletal muscle repair. *Adv Drug Deliv Rev* **2015,** *84*, 198-207. DOI: 10.1016/j.addr.2014.07.007.
209. Montarras, D.; Morgan, J.; Collins, C.; Relaix, F.; Zaffran, S.; Cumano, A.; Partridge, T.; Buckingham, M., Direct isolation of satellite cells for skeletal muscle regeneration. *Science* **2005,** *309* (5743), 2064-7. DOI: 10.1126/science.1114758.
210. Swijnenburg, R.-J.; Schrepfer, S.; Govaert, J. A.; Cao, F.; Ransohoff, K.; Sheikh, A. Y.; Haddad, M.; Connolly, A. J.; Davis, M. M.; Robbins, R. C., Immunosuppressive therapy mitigates immunological rejection of human embryonic stem cell xenografts. *Proceedings of the National Academy of Sciences* **2008,** *105* (35), 12991-12996.
211. van Wachem, P. B.; Brouwer, L. A.; van Luyn, M. J., Absence of muscle regeneration after implantation of a collagen matrix seeded with myoblasts. *Biomaterials* **1999,** *20* (5), 419-26.
212. Beier, J. P.; Stern-Straeter, J.; Foerster, V. T.; Kneser, U.; Stark, G. B.; Bach, A. D., Tissue engineering of injectable muscle: three-dimensional myoblast-fibrin injection in the syngeneic rat animal model. *Plast Reconstr Surg* **2006,** *118* (5), 1113-21; discussion 1122-4. DOI: 10.1097/01.prs.0000221007.97115.1d.
213. Matthias, N.; Hunt, S. D.; Wu, J. B.; Lo, J.; Callahan, L. A. S.; Li, Y.; Huard, J.; Darabi, R., Volumetric muscle loss injury repair using in situ fibrin gel cast seeded with muscle-derived stem cells (MDSCs). *Stem Cell Res* **2018,** *27*, 65-73. DOI: 10.1016/j.scr.2018.01.008.

214. Rossi, C. A.; Flaibani, M.; Blaauw, B.; Pozzobon, M.; Figallo, E.; Reggiani, C.; Vitiello, L.; Elvassore, N.; De Coppi, P., In vivo tissue engineering of functional skeletal muscle by freshly isolated satellite cells embedded in a photopolymerizable hydrogel. *Faseb J* **2011,** *25* (7), 2296-304. DOI: 10.1096/fj.10-174755.
215. Kim, J. H.; Ko, I. K.; Atala, A.; Yoo, J. J., Progressive Muscle Cell Delivery as a Solution for Volumetric Muscle Defect Repair. *Sci Rep-Uk* **2016,** *6*. DOI: ARTN 38754 10.1038/srep38754.
216. Ward, C. L.; Ji, L.; Corona, B. T., An Autologous Muscle Tissue Expansion Approach for the Treatment of Volumetric Muscle Loss. *Biores Open Access* **2015,** *4* (1), 198-208. DOI: 10.1089/biores.2015.0009.
217. Goldman, S. M.; Henderson, B. E. P.; Walters, T. J.; Corona, B. T., Co-delivery of a laminin-111 supplemented hyaluronic acid based hydrogel with minced muscle graft in the treatment of volumetric muscle loss injury. *PLOS ONE* **2018,** *13* (1), e0191245. DOI: 10.1371/journal.pone.0191245.
218. Pereira, T.; Armada-da Silva, P. A. S.; Amorim, I.; Rema, A.; Caseiro, A. R.; Gartner, A.; Rodrigues, M.; Lopes, M. A.; Bartolo, P. J.; Santos, J. D.; Luis, A. L.; Mauricio, A. C., Effects of Human Mesenchymal Stem Cells Isolated from Wharton's Jelly of the Umbilical Cord and Conditioned Media on Skeletal Muscle Regeneration Using a Myectomy Model. *Stem Cells International* **2014,** *2014*. DOI: Artn 376918 10.1155/2014/376918.
219. Aurora, A.; Wrice, N.; Walters, T. J.; Christy, R. J.; Natesan, S., A PEGylated platelet free plasma hydrogel based composite scaffold enables stable vascularization and targeted cell delivery for volumetric muscle loss. *Acta Biomater* **2018,** *65*, 150-162. DOI: 10.1016/j.actbio.2017.11.019.
220. Huang, H.; Liu, J.; Hao, H.; Chen, D.; Zhizhong, L.; Li, M.; Song, H.; Xiang, R.; Jiang, C.; Fu, X.; Han, W., Preferred M2 Polarization by ASC-Based Hydrogel Accelerated Angiogenesis and Myogenesis in Volumetric Muscle Loss Rats. *Stem Cells Int* **2017,** *2017*, 2896874. DOI: 10.1155/2017/2896874.
221. Goldman, S. M.; Henderson, B. E. P.; Corona, B. T., Evaluation of bone marrow mononuclear cells as an adjunct therapy to minced muscle graft for the treatment of volumetric muscle loss injuries. *Stem Cell Res Ther* **2017,** *8*. DOI: ARTN 142 10.1186/s13287-017-0589-z.
222. Lesman, A.; Koffler, J.; Atlas, R.; Blinder, Y. J.; Kam, Z.; Levenberg, S., Engineering vessel-like networks within multicellular fibrin-based constructs. *Biomaterials* **2011,** *32* (31), 7856-7869. DOI: 10.1016/j.biomaterials.2011.07.003.
223. Merritt, E. K.; Cannon, M. V.; Hammers, D. W.; Le, L. N.; Gokhale, R.; Sarathy, A.; Song, T. J.; Tierney, M. T.; Suggs, L. J.; Walters, T. J.; Farrar, R. P., Repair of traumatic skeletal muscle injury with bone-marrow-derived mesenchymal stem cells seeded on extracellular matrix. *Tissue Eng Part A* **2010,** *16* (9), 2871-81. DOI: 10.1089/ten.TEA.2009.0826.
224. Conconi, M. T.; De Coppi, P.; Bellini, S.; Zara, G.; Sabatti, M.; Marzaro, M.; Zanon, G. F.; Gamba, P. G.; Parnigotto, P. P.; Nussdorfer, G. G., Homologous muscle acellular matrix seeded with autologous myoblasts as a tissue-engineering approach to abdominal wall-defect repair. *Biomaterials* **2005,** *26* (15), 2567-74. DOI: 10.1016/j.biomaterials.2004.07.035.
225. De Coppi, P.; Bellini, S.; Conconi, M. T.; Sabatti, M.; Simonato, E.; Gamba, P. G.; Nussdorfer, G. G.; Parnigotto, P. P., Myoblast-acellular skeletal muscle matrix constructs guarantee a long-term repair of experimental full-thickness abdominal wall defects. *Tissue Eng* **2006,** *12* (7), 1929-36. DOI: 10.1089/ten.2006.12.1929.
226. Kasukonis, B.; Kim, J.; Brown, L.; Jones, J.; Ahmadi, S.; Washington, T.; Wolchok, J., Codelivery of Infusion Decellularized Skeletal Muscle with Minced Muscle Autografts Improved Recovery from Volumetric Muscle Loss Injury in a Rat Model. *Tissue Eng Part A* **2016,** *22* (19-20), 1151-1163. DOI: 10.1089/ten.TEA.2016.0134.

227. Goldman, S. M.; Corona, B. T., Co-delivery of micronized urinary bladder matrix damps regenerative capacity of minced muscle grafts in the treatment of volumetric muscle loss injuries. *PLOS ONE* **2017,** *12* (10), e0186593. DOI: 10.1371/journal.pone.0186593.
228. Quarta, M.; Cromie, M.; Chacon, R.; Blonigan, J.; Garcia, V.; Akimenko, I.; Hamer, M.; Paine, P.; Stok, M.; Shrager, J. B.; Rando, T. A., Bioengineered constructs combined with exercise enhance stem cell-mediated treatment of volumetric muscle loss. *Nature communications* **2017,** *8*, 15613. DOI: 10.1038/ncomms15613.
229. Quarta, M.; Cromie Lear, M. J.; Blonigan, J.; Paine, P.; Chacon, R.; Rando, T. A., Biomechanics show stem cell necessity for effective treatment of volumetric muscle loss using bioengineered constructs. *NPJ Regen Med* **2018,** *3*, 18. DOI: 10.1038/s41536-018-0057-0.
230. Qiu, X.; Liu, S.; Zhang, H.; Zhu, B.; Su, Y.; Zheng, C.; Tian, R.; Wang, M.; Kuang, H.; Zhao, X.; Jin, Y., Mesenchymal stem cells and extracellular matrix scaffold promote muscle regeneration by synergistically regulating macrophage polarization toward the M2 phenotype. *Stem Cell Res Ther* **2018,** *9* (1), 88. DOI: 10.1186/s13287-018-0821-5.
231. Page, R. L.; Malcuit, C.; Vilner, L.; Vojtic, I.; Shaw, S.; Hedblom, E.; Hu, J.; Pins, G. D.; Rolle, M. W.; Dominko, T., Restoration of Skeletal Muscle Defects with Adult Human Cells Delivered on Fibrin Microthreads. *Tissue Eng Part A* **2011,** *17* (21), 2629-2640.
232. Greising, S. M.; Corona, B. T.; McGann, C.; Frankum, J. K.; Warren, G. L., Therapeutic Approaches for Volumetric Muscle Loss Injury: A Systematic Review and Meta-Analysis. *Tissue Eng Part B Rev* **2019,** *25* (6), 510-525. DOI: 10.1089/ten.TEB.2019.0207.
233. Hagiwara, K.; Chen, G.; Kawazoe, N.; Tabata, Y.; Komuro, H., Promotion of muscle regeneration by myoblast transplantation combined with the controlled and sustained release of bFGFcpr. *J Tissue Eng Regen Med* **2016,** *10* (4), 325-33. DOI: 10.1002/term.1732.
234. Borselli, C.; Cezar, C. A.; Shvartsman, D.; Vandenburgh, H. H.; Mooney, D. J., The role of multifunctional delivery scaffold in the ability of cultured myoblasts to promote muscle regeneration. *Biomaterials* **2011,** *32* (34), 8905-14. DOI: 10.1016/j.biomaterials.2011.08.019.
235. Wang, L.; Cao, L.; Shansky, J.; Wang, Z.; Mooney, D.; Vandenburgh, H., Minimally invasive approach to the repair of injured skeletal muscle with a shape-memory scaffold. *Molecular therapy : the journal of the American Society of Gene Therapy* **2014,** *22* (8), 1441-9. DOI: 10.1038/mt.2014.78.
236. Pumberger, M.; Qazi, T. H.; Ehrentraut, M. C.; Textor, M.; Kueper, J.; Stoltenburg-Didinger, G.; Winkler, T.; von Roth, P.; Reinke, S.; Borselli, C.; Perka, C.; Mooney, D. J.; Duda, G. N.; Geissler, S., Synthetic niche to modulate regenerative potential of MSCs and enhance skeletal muscle regeneration. *Biomaterials* **2016,** *99*, 95-108. DOI: 10.1016/j.biomaterials.2016.05.009.
237. Hill, E.; Boontheekul, T.; Mooney, D. J., Regulating activation of transplanted cells controls tissue regeneration. *Proc Natl Acad Sci U S A* **2006,** *103* (8), 2494-9. DOI: 10.1073/pnas.0506004103.
238. Passipieri, J. A.; Baker, H. B.; Siriwardane, M.; Ellenburg, M. D.; Vadhavkar, M.; Saul, J. M.; Tomblyn, S.; Burnett, L.; Christ, G. J., Keratin Hydrogel Enhances In Vivo Skeletal Muscle Function in a Rat Model of Volumetric Muscle Loss. *Tissue Eng Part A* **2017**. DOI: 10.1089/ten.TEA.2016.0458.
239. Baker, H. B.; Passipieri, J. A.; Siriwardane, M.; Ellenburg, M. D.; Vadhavkar, M.; Bergman, C. R.; Saul, J. M.; Tomblyn, S.; Burnett, L.; Christ, G. J., Cell and Growth Factor-Loaded Keratin Hydrogels for Treatment of Volumetric Muscle Loss in a Mouse Model. *Tissue Eng Part A* **2017,** *23* (11-12), 572-584. DOI: 10.1089/ten.TEA.2016.0457.
240. Fuoco, C.; Rizzi, R.; Biondo, A.; Longa, E.; Mascaro, A.; Shapira-Schweitzer, K.; Kossovar, O.; Benedetti, S.; Salvatori, M. L.; Santoleri, S.; Testa, S.; Bernardini, S.; Bottinelli, R.; Bearzi, C.; Cannata, S. M.; Seliktar, D.; Cossu, G.; Gargioli, C., In vivo generation of a mature and functional artificial skeletal muscle. *EMBO Mol Med* **2015,** *7* (4), 411-22. DOI: 10.15252/emmm.201404062.
241. Stratos, I.; Madry, H.; Rotter, R.; Weimer, A.; Graff, J.; Cucchiarini, M.; Mittlmeier, T.; Vollmar, B., Fibroblast growth factor-2-overexpressing myoblasts encapsulated in alginate spheres increase

proliferation, reduce apoptosis, induce adipogenesis, and enhance regeneration following skeletal muscle injury in rats. *Tissue Eng Part A* **2011,** *17* (21-22), 2867-77. DOI: 10.1089/ten.tea.2011.0239.
242. Zhou, W.; He, D. Q.; Liu, J. Y.; Feng, Y.; Zhang, X. Y.; Hua, C. G.; Tang, X. F., Angiogenic gene-modified myoblasts promote vascularization during repair of skeletal muscle defects. *J Tissue Eng Regen Med* **2015,** *9* (12), 1404-16. DOI: 10.1002/term.1692.
243. Shevchenko, E. K.; Makarevich, P. I.; Tsokolaeva, Z. I.; Boldyreva, M. A.; Sysoeva, V. Y.; Tkachuk, V. A.; Parfyonova, Y. V., Transplantation of modified human adipose derived stromal cells expressing VEGF165 results in more efficient angiogenic response in ischemic skeletal muscle. *Journal of translational medicine* **2013,** *11*, 138. DOI: 10.1186/1479-5876-11-138.
244. Madden, L.; Juhas, M.; Kraus, W. E.; Truskey, G. A.; Bursac, N., Bioengineered human myobundles mimic clinical responses of skeletal muscle to drugs. *Elife* **2015,** *4*, e04885. DOI: 10.7554/eLife.04885.
245. Vandenburgh, H.; Shansky, J.; Benesch-Lee, F.; Barbata, V.; Reid, J.; Thorrez, L.; Valentini, R.; Crawford, G., Drug-screening platform based on the contractility of tissue-engineered muscle. *Muscle & nerve* **2008,** *37* (4), 438-447. DOI: 10.1002/mus.20931.
246. Gilbert-Honick, J.; Ginn, B.; Zhang, Y.; Salehi, S.; Wagner, K. R.; Mao, H. Q.; Grayson, W. L., Adipose-derived Stem/Stromal Cells on Electrospun Fibrin Microfiber Bundles Enable Moderate Muscle Reconstruction in a Volumetric Muscle Loss Model. *Cell Transplant* **2018**, 963689718805370. DOI: 10.1177/0963689718805370.
247. Gilbert-Honick, J.; Iyer, S. R.; Somers, S. M.; Lovering, R. M.; Wagner, K.; Mao, H. Q.; Grayson, W. L., Engineering functional and histological regeneration of vascularized skeletal muscle. *Biomaterials* **2018,** *164*, 70-79. DOI: 10.1016/j.biomaterials.2018.02.006.
248. Nakayama, K. H.; Quarta, M.; Paine, P.; Alcazar, C.; Karakikes, I.; Garcia, V.; Abilez, O. J.; Calvo, N. S.; Simmons, C. S.; Rando, T. A.; Huang, N. F., Treatment of volumetric muscle loss in mice using nanofibrillar scaffolds enhances vascular organization and integration. *Commun Biol* **2019,** *2*. DOI: ARTN 170
10.1038/s42003-019-0416-4.
249. Rangarajan, S.; Madden, L.; Bursac, N., Use of flow, electrical, and mechanical stimulation to promote engineering of striated muscles. *Ann Biomed Eng* **2014,** *42* (7), 1391-405. DOI: 10.1007/s10439-013-0966-4.
250. Booth, F., Time course of muscular atrophy during immobilization of hindlimbs in rats. *Journal of Applied Physiology* **1977,** *43* (4), 656-661.
251. Herbison, G.; Jaweed, M.; Ditunno, J., Muscle atrophy in rats following denervation, casting, inflammation, and tenotomy. *Archives of physical medicine and rehabilitation* **1979,** *60* (9), 401-404.
252. Serena, E.; Flaibani, M.; Carnio, S.; Boldrin, L.; Vitiello, L.; De Coppi, P.; Elvassore, N., Electrophysiologic stimulation improves myogenic potential of muscle precursor cells grown in a 3D collagen scaffold. *Neurol Res* **2008,** *30* (2), 207-14. DOI: 10.1179/174313208X281109.
253. Moon du, G.; Christ, G.; Stitzel, J. D.; Atala, A.; Yoo, J. J., Cyclic mechanical preconditioning improves engineered muscle contraction. *Tissue Eng Part A* **2008,** *14* (4), 473-82. DOI: 10.1089/tea.2007.0104.
254. Machingal, M. A.; Corona, B. T.; Walters, T. J.; Kesireddy, V.; Koval, C. N.; Dannahower, A.; Zhao, W. X.; Yoo, J. J.; Christ, G. J., A Tissue-Engineered Muscle Repair Construct for Functional Restoration of an Irrecoverable Muscle Injury in a Murine Model. *Tissue Eng Pt A* **2011,** *17* (17-18), 2291-2303. DOI: 10.1089/ten.tea.2010.0682.
255. Corona, B. T.; Machingal, M. A.; Criswell, T.; Vadhavkar, M.; Dannahower, A. C.; Bergman, C.; Zhao, W. X.; Christ, G. J., Further Development of a Tissue Engineered Muscle Repair Construct In Vitro for Enhanced Functional Recovery Following Implantation In Vivo in a Murine Model of Volumetric Muscle Loss Injury. *Tissue Eng Pt A* **2012,** *18* (11-12), 1213-1228. DOI: 10.1089/ten.tea.2011.0614.

256. Passipieri, J. A.; Hu, X.; Mintz, E.; Dienes, J.; Baker, H. B.; Wallace, C. H.; Blemker, S. S.; Christ, G. J., In Silico and In Vivo Studies Detect Functional Repair Mechanisms in a Volumetric Muscle Loss Injury. *Tissue Eng Part A* **2019,** *25* (17-18), 1272-1288. DOI: 10.1089/ten.tea.2018.0280.
257. Corona, B. T.; Ward, C. L.; Baker, H. B.; Walters, T. J.; Christ, G. J., Implantation of in vitro tissue engineered muscle repair constructs and bladder acellular matrices partially restore in vivo skeletal muscle function in a rat model of volumetric muscle loss injury. *Tissue Eng Part A* **2014,** *20* (3-4), 705-15. DOI: 10.1089/ten.TEA.2012.0761.
258. Mintz, E. L.; Passipieri, J. A.; Franklin, I. R.; Toscano, V. M.; Afferton, E. C.; Sharma, P. R.; Christ, G. J., Long-Term Evaluation of Functional Outcomes Following Rat Volumetric Muscle Loss Injury and Repair. *Tissue Eng Part A* **2020,** *26* (3-4), 140-156. DOI: 10.1089/ten.TEA.2019.0126.
259. Wu, X.; Corona, B. T.; Chen, X.; Walters, T. J., A standardized rat model of volumetric muscle loss injury for the development of tissue engineering therapies. *Biores Open Access* **2012,** *1* (6), 280-90. DOI: 10.1089/biores.2012.0271.
260. Juhas, M.; Engelmayr, G. C.; Fontanella, A. N.; Palmer, G. M.; Bursac, N., Biomimetic engineered muscle with capacity for vascular integration and functional maturation in vivo. *P Natl Acad Sci USA* **2014,** *111* (15), 5508-5513. DOI: 10.1073/pnas.1402723111.
261. Morimoto, Y.; Kato-Negishi, M.; Onoe, H.; Takeuchi, S., Three-dimensional neuron-muscle constructs with neuromuscular junctions. *Biomaterials* **2013,** *34* (37), 9413-9419. DOI: 10.1016/j.biomaterials.2013.08.062.
262. Wang, L.; Shansky, J.; Vandenburgh, H., Induced Formation and Maturation of Acetylcholine Receptor Clusters in a Defined 3D Bio-Artificial Muscle. *Mol Neurobiol* **2013,** *48* (3), 397-403. DOI: 10.1007/s12035-013-8412-z.
263. Gholobova, D.; Decroix, L.; Van Muylder, V.; Desender, L.; Gerard, M.; Carpentier, G.; Vandenburgh, H.; Thorrez, L., Endothelial Network Formation Within Human Tissue-Engineered Skeletal Muscle. *Tissue Eng Pt A* **2015,** *21* (19-20), 2548-2558. DOI: 10.1089/ten.tea.2015.0093.
264. Ko, I. K.; Lee, B. K.; Lee, S. J.; Andersson, K. E.; Atala, A.; Yoo, J. J., The effect of in vitro formation of acetylcholine receptor (AChR) clusters in engineered muscle fibers on subsequent innervation of constructs in vivo. *Biomaterials* **2013,** *34* (13), 3246-55. DOI: 10.1016/j.biomaterials.2013.01.029.
265. Li, M. T.; Ruehle, M.; Stevens, H.; Servies, N.; Willett, N.; Karthikeyakannan, S.; Warren, G. L.; Guldberg, R.; Krishnan, L. N., Skeletal myoblast-seeded vascularized tissue scaffolds in the treatment of a large volumetric muscle defect in the rat biceps femoris muscle. *Tissue Eng Part A* **2017**. DOI: 10.1089/ten.TEA.2016.0523.
266. Koffler, J.; Kaufman-Francis, K.; Shandalov, Y.; Egozi, D.; Pavlov, D. A.; Landesberg, A.; Levenberg, S., Improved vascular organization enhances functional integration of engineered skeletal muscle grafts. *Proc Natl Acad Sci U S A* **2011,** *108* (36), 14789-94. DOI: 10.1073/pnas.1017825108.
267. Shandalov, Y.; Egozi, D.; Koffler, J.; Dado-Rosenfeld, D.; Ben-Shimol, D.; Freiman, A.; Shor, E.; Kabala, A.; Levenberg, S., An engineered muscle flap for reconstruction of large soft tissue defects. *Proc Natl Acad Sci U S A* **2014,** *111* (16), 6010-5. DOI: 10.1073/pnas.1402679111.
268. Lee, J.; Jun, I.; Park, H. J.; Kang, T. J.; Shin, H.; Cho, S. W., Genetically engineered myoblast sheet for therapeutic angiogenesis. *Biomacromolecules* **2014,** *15* (1), 361-72. DOI: 10.1021/bm401605f.
269. Ward, C. L.; Pollot, B. E.; Goldman, S. M.; Greising, S. M.; Wenke, J. C.; Corona, B. T., Autologous minced muscle grafts improve muscle strength in a porcine model of volumetric muscle loss injury. *Journal of orthopaedic trauma* **2016,** *30* (12), e396-e403.
270. Sarrafian, T. L.; Bodine, S. C.; Murphy, B.; Grayson, J. K.; Stover, S. M., Extracellular matrix scaffolds for treatment of large volume muscle injuries: A review. *Veterinary Surgery* **2018,** *47* (4), 524-535.

Chapter 3: Etching Anisotropic Surface Topography onto Fibrin Microthread Scaffolds for Guiding Myoblast Alignment[1]

3.1 INTRODUCTION

Biophysical cues such as scaffold topography are important regulators for directing cellular alignment, differentiation, and migration, as well as for guiding tissue regeneration. Tissue engineering of skeletal muscle often exploits biophysical cues to mimic the structure of native muscle tissue. Skeletal muscle is a highly aligned and hierarchically organized tissue responsible for uniaxial force transduction and voluntary locomotion. Efficient muscle contraction results from this aligned tissue structure, where bundles of parallel multinucleated myotubes synchronously contract. Initial myoblast alignment is an essential step prior to myotube formation and maturation and is known to be guided by micron-scale grooves between adjacent muscle fibers by a phenomenon known as contact guidance. The native extracellular matrix (ECM) surrounding muscle fibers has a highly aligned and fibrous architecture, which provides contact guidance cues and plays an important role in dictating muscle tissue structure and function.[2] Incorporation of instructive biophysical cues such as micropatterning anisotropic surface topography is a commonly exploited technique to promote myoblast alignment and myotube formation on engineered scaffolds to ultimately enhance functional tissue regeneration.

Many strategies have been explored to create scaffolds with anisotropic surface topography, including patterned substrates,[3-10] electrospun fibers,[4, 11-16] microthreads,[17-19] and aligned pores.[20-22] Electrospun fibers are one of the most commonly employed methods of generating aligned fibrous scaffolds due to their facile production method, rapid fabrication, and control over fiber thickness and orientation.[23-25] Aligned electrospun nano- and microfiber scaffolds have been made from a range of synthetic and natural polymers, and have been shown to stimulate myoblast adhesion, alignment, expression of myogenic proteins, and differentiation

into myotubes.[4, 11-16] Despite this, electrospun scaffolds are limited by tight fiber packing, which impedes cellular infiltration into the scaffold and challenges their clinical utility as a 3D implantable scaffold.[26-28] Discrete polymer microthreads also mimic the morphological architecture of native muscle tissue and have the unique capability of being hierarchically organized into complex 3D scaffolds, such as bundles or composites, eliminating common drawbacks of electrospun fiber scaffolds such as cellular infiltration.[18, 29-31] In addition to tunable mechanical properties, degradation rate, and presentation of biochemical signals, microfibers have also been modified to incorporate nanoscale surface features for the purpose of further stimulating cellular alignment.[16, 32-34]

Our laboratory developed a strategy for creating discrete fibrin microthreads, approximately 100 μm in diameter.[17] These scaffolds have robust and tunable mechanical properties compared to fibrin hydrogel-based systems[17, 32, 35] as well as morphological properties that mimic native tissue architecture, making them an attractive platform technology for tissue engineering applications.[18] Scaffold tensile properties have been modified through changes in production parameters[32], and through crosslinking with ultraviolet energy[17] or carbodiimide chemistry.[35] Fibrin microthreads have also been modified to incorporate growth factors such as fibroblast growth factor 2 (FGF-2)[36] and hepatocyte growth factor (HGF)[30] to enhance cellular functions such as proliferation and migration. Additionally, their cylindrical form mimics the native fibril structure of ECM scaffolds and has been shown to promote alignment of a variety of cell types, including myoblasts.[17, 29, 32, 37]

Fibrin microthreads have shown great promise as an implantable scaffold for treatment of critical-size skeletal muscle defects.[30, 31] Critical sized, non-healing defects in the tibialis anterior of mice were created by excising muscle tissue. Muscle injuries treated with microthreads that were bundled and seeded with primary muscle-derived cells significantly reduced collagen deposition in the wound site, enhanced ingrowth of new muscle tissue, and improved functional muscle regeneration compared to the untreated control 10 weeks after injury.[31] Bundles of fibrin microthreads crosslinked and loaded with HGF have also been evaluated using this *in vivo* skeletal muscle defect model.[30] HGF-loaded microthreads significantly increased the number of myogenin-positive cells in the wound 14 days after injury and significantly enhanced muscle force production 60 days post-injury. This enhanced muscle regeneration may be attributed to the

biomimetic morphology of the microthread scaffold, as fibrin hydrogel implants did not promote functional muscle regeneration. Immunohistochemical analysis of tissue explants revealed that myofibers were located adjacent to microthreads and had a high number of nuclei per myofiber, demonstrating that these scaffolds promote myoblast ingrowth and maturation *in vivo*. Although microthreads have been shown to guide aligned muscle regeneration in muscle defects, *in vitro* characterization of myoblast alignment reveals that only approximately 40% of cells on fibrin microthreads are aligned along the long axis of the microthread.[32] As such, there remains a significant unmet need to generate highly oriented skeletal muscle tissue, and necessitates exploration of new strategies to further enhance myoblast alignment on these scaffolds.

The goal of the present study is to develop and characterize a new method of imparting grooved, aligned features onto the surface of fibrin microthread scaffolds to enhance myoblast alignment. Initial studies in our lab showed that when microthreads were placed into a 2-(N-morpholino)ethane-sulfonic acid (MES) acidic buffer prior to carbodiimide crosslinking, they displayed surface features with anisotropically aligned grooves parallel to the long axis of microthreads. Here we evaluate the effect of MES buffer pH on the generation of anisotropic surface features, scaffold tensile properties, and myoblast alignment. We hypothesized that anisotropic surface topography would promote myoblast alignment along the long axis of the microthread, thus making these microthreads a promising scaffold to enhance functional skeletal muscle regeneration.

3.2 MATERIALS and METHODS

3.2.1 Fibrin microthread extrusion

Fibrin microthreads were formed by 3D printing, co-extruding fibrinogen and thrombin as previously described.[17] Briefly, fibrinogen isolated from bovine plasma (MP Biomedicals) was dissolved in HEPES (N-[2-Hydroxyethyl]piperazine-N'-[2-ethanesulfonic acid]) buffered saline (HBS, 20 mM HEPES, 0.9% NaCl, pH 7.4) to a concentration of 70 mg/mL and stored at -20°C until use. Thrombin isolated from bovine plasma (Sigma) was dissolved in HBS at 40 U/mL and stored at -20°C until use. To produce microthreads, fibrinogen and thrombin solutions were thawed to room temperature, and thrombin was mixed with a 40 mM $CaCl_2$ solution to form a 6 U/mL working solution. Equal volumes of fibrinogen and thrombin solutions were

taken up separately into 1 mL syringes and inserted into the tip of a blending applicator (Micromedics Inc., St. Paul, MN; SA-3670). The solutions were mixed in the blending applicator and extruded through polyethylene tubing (BD, Sparks, MD) with an inner diameter of 0.86 mm into a 10 mM HEPES buffer bath (pH 7.4) in a Teflon coated pan. Threads were extruded at 0.225 mL/min using a dual syringe pump. After microthreads were incubated for 10-15 min to allow for polymerization, the scaffolds were removed and stretched to approximately 300% of their initial drawn length and hung overnight to dry under the tension of their own weight.

3.2.2 Microthread etching

To create anisotropic grooved features on the surface of fibrin microthreads, microthreads were first suspended in 1-well dishes by inserting them between two slatted polydimethylsiloxane (PDMS) columns placed on the edges of the dish (**Figure 3.1**). Approximately 13 - 5cm long microthreads were suspended in each 1-well dish. 30 mL of 50 mM 2-(N-morpholino)ethane-sulfonic acid (MES) at a pH of 5.0 or 5.5 was added to 1 well dishes for a period of 15 minutes. Additional timepoints of 30 minutes and 1 hour were initially tested, but no difference in surface features were observed and therefore these conditions are not reported in this chapter. After 15 minutes, MES buffer was removed and microthreads were rinsed three times for five minutes with deionized (DI) water. Microthreads were then allowed to air dry. Control microthreads were treated with DI water instead of MES buffer.

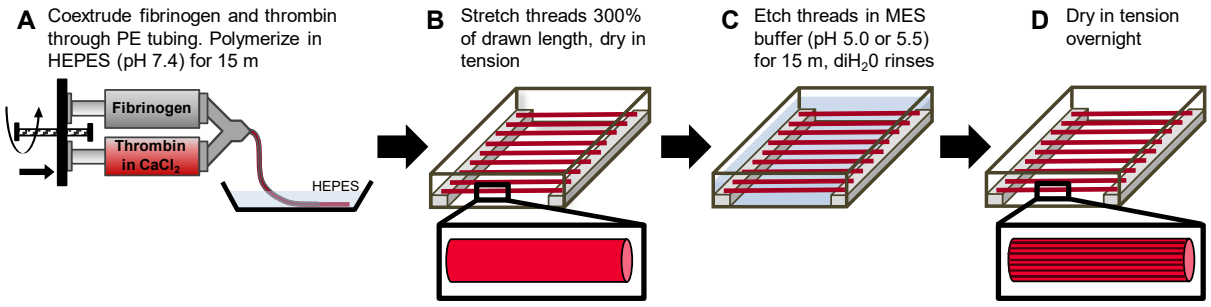

Figure 3.1. Method of MES etching of fibrin microthreads. Fibrin microthreads are made by 3D printing of fibrinogen and thrombin into HEPES buffer (A). Threads are stretched 300% of initial drawn length and hung to dry in tension (B). MES buffer (pH 5.0 or 5.5) is added to threads for 15 minutes, followed by three 5-minute dH_20 rinses (C). Threads are left to dry in tension overnight (D).

3.2.3 Surface characterization

To characterize the surface topography of MES-etched fibrin microthreads, atomic force microscopy (AFM) was used to visualize microthread surface features (NaioAFM, Switzerland). 10 µm x 10 µm images were taken of thread surfaces using constant force contact mode and a MikroMasch HQ: CSC17 contact mode cantilever (**Figure 3.2 A**) Gwyddion software was utilized to flatten gross thread curvature with inputted average thread diameter using the revolve arc feature (**Figure 3.2 B - C**). Root mean square roughness (Rq) and surface area (SA) were acquired using the "Statistical quantities" tool in Gwyddion software on curve-flattened images. Average maximum height of roughness and mean spacing of profile irregularities were acquired by evaluating 5 horizontal lines evenly spaced across each original unflattened image at 1, 3, 5, 7, and 9 µm. The "Calculate roughness parameters" tool in Gwyddion was used to determine roughness parameters, and the five values for each image were averaged.

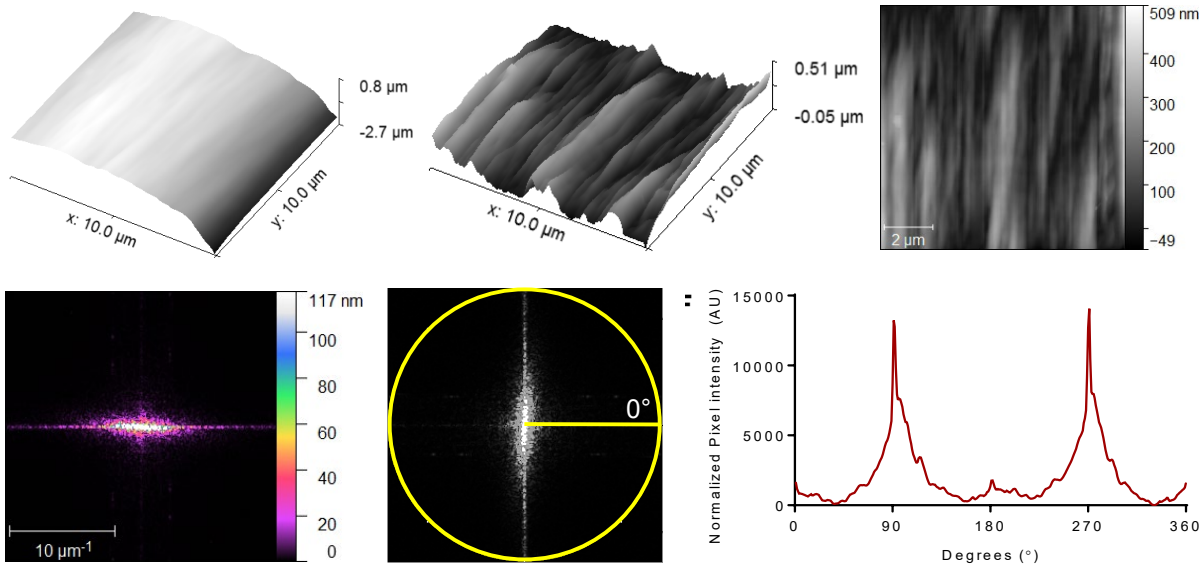

Figure 3.2. Method of AFM image analysis for MES-etched fibrin microthreads. Original AFM images of the microthread surface (A) are flattened with Gwyddion software using average thread diameter (B). Flattened images can also be represented in 2D (C). 2D fast Fourier transforms (FFT) of flattened surfaces are performed (D). FFT outputs are binarized and rotated 90°. A yellow circle and line demonstrate circular angle pixel analysis (E). Radial pixel analysis results in a plot of pixel intensity at each degree, where high peaks at 90° and 270° indicate anisotropic surface topography consistent with the long axis of the microthread (F).

Anisotropy of scaffolds were characterized by performing a Fast Fourier Transform

(FFT).[38] Fourier transform converts an image from the spatial domain to the frequency domain. It represents the rate of change of pixel intensities across an image, with low frequencies in the center and high frequencies furthest from the center of the transform. Fourier transforms with frequencies along one axis represent surfaces with a high degree of surface alignment. FFT of each flattened AFM image were generated using Gwyddion (**Figure 3.2 D).** ImageJ (NIH) was used to convert FFT images to 16 bit and rotate 90°. Oval Profile ImageJ plug-in was used to further evaluate topography by summing pixels along each degree of a circle created around an FFT plot (**Figure 3.2 E**). Pixel intensity values for each FFT plot were normalized so that data for all samples could be compared. These values can then be plotted to show changes in pixel intensity over 360° (**Figure 3.2 F**). Narrow, high peaks represent a high degree of alignment.

Etched microthreads were also imaged with scanning electron microscopy (SEM) to characterize thread morphology and surface topography. Air-dried threads were mounted on aluminum stubs (Ted Pella, Redding, CA) coated with double-sided carbon tape and sputter coated with a thin layer or gold-palladium for 1 minute. Images were acquired with 5 kV accelerating voltage using a Phenom G1 benchtop SEM (Thermo Fisher Scientific, Waltham, MA).

3.2.4 Mechanical characterization of etched microthreads

Mechanical analysis of etched fibrin microthreads was performed using methods described previously.[35] Individual microthreads were attached with medical grade silicone adhesive to vellum paper frames with precut windows of 2.0 cm, which defined the region of loading. The 2.0 cm was the distance between the adhesive spots on the two edges of the vellum frame window and was used as the initial gauge length for testing. Silicone glue was allowed to cure for at least 12 hours. Microthreads adhered to vellum frames were hydrated in phosphate buffered saline (PBS) (pH 7.4, room temperature) for one hour prior to testing. Hydrated microthreads diameters were measured using a calibrated reticule with a 10x objective on a Nikon Eclipse E600 upright microscope (Nikon, Melville, NY). To define the cross-sectional area, microthreads were assumed to be cylindrical and three diameter measurements were taken along the length of each microthread and averaged.

After hydration, microthreads were securely mounted in the grips of an ElectroPuls

E1000 uniaxial testing machine (Instron, Norwood, MA) and a 1 N load cell. Once secured, the 2 edges of each vellum frame were cut, and the microthreads were uniaxially loaded until failure at a 50% strain rate (10 mm/min). Force and displacement were recorded continuously through each test at 10 Hz frequency. Engineering stress was calculated as the recorded force divided by the initial cross-sectional area of the microthread. Strain was calculated as the increased extension from the initial 2.0 cm gauge length. A MATLAB (MathWorks, Natick, MA) script was written to analyze the ultimate tensile strength (UTS), maximum tangent modulus (MTM), strain at failure (SAF), and load at failure for each sample. The MTM was defined as the highest linear region in the stress-strain curve for each sample that corresponds to 20% of the total length of each test. Outliers were identified as any microthreads whose wet diameters or load at failure were 1.5 times greater than the inner quartile range (IQR) (average wet diameter +/- 1.5(IQR)) and were subsequently removed from further analysis, as previously described.[32, 35]

3.2.5 Cell culture

C2C12 Immortalized mouse myoblasts (ATCC CRL-1772, Manassas, VA) were cultured in complete medium, consisting of a 1:1 (v/v) ratio of high glucose Dulbecco's modified Eagle Medium (DMEM, Gibco, Thermo Fisher Scientific) and Ham's F12 (Gibco), supplemented with 4 mM L-glutamine, 10% fetal bovine serum (FBS, HyClone, Logan, UT), 100 U/mL penicillin, 100 µg/mL streptomycin (Thermo Fisher Scientific, Waltham, MA), and 2.5 µg/mL amphotericin-B (Thermo Fisher Scientific) as described previously.[35] Cells were incubated at 37°C with 5% CO2 and maintained at a density below 70% confluence using standard cell culture techniques. Cell passage was carried out using 0.25% trypsin-EDTA (Corning, Corning, NY).

3.2.6 Nuclear alignment of myoblasts on etched microthreads

A cell alignment assay was conducted to determine myoblast alignment on microthread scaffolds as previously described.[32] Briefly, three individual microthreads of the same condition were attached to a PDMS ring (inner diameter 3.4") with medical grade silicone adhesive. Microthreads were sterilized in 70% ethanol for at least 2 hours and rinsed 3 times with DI water. Rings were placed on top of 13 mm diameter circular Nunc Thermanox™ coverslips (Thermo Fisher Scientific) elevated in 6-well dishes by a PDMS post. Immediately prior to

seeding, microthreads were rehydrated with 150 µL of PBS for 1 hour. After 1 hour, PBS was aspirated and 100 µL of a 100,000 cells/mL cell suspension in complete medium supplemented with 50 µg/mL aprotinin was added to the top of the coverslip. After a 4 hour incubation, PDMS rings with seeded microthreads were moved to a new 6-well plate with fresh medium and allowed to incubate for an additional 20 hours. After 24 hours, microthreads were fixed in 4% paraformaldehyde and stained with Hoechst 33342 to visualize C2C12 myoblast nuclei.

Microthreads were imaged using a fluorescent microscope (Zeiss Axiovert 200M microscope, Carl Zeiss, Germany). Fluorescent images were analyzed by thresholding greyscale images in ImageJ and carrying out the particle analysis function within ImageJ to obtain the orientation of the long axis of the nucleus with respect to the microthread, as previously described.[32] Cells with nuclei on the edge of the microthread or in contact with another cell were excluded from analysis. All other nuclei orientations were normalized to fall between 0° and 90°, binned in 15° increments, and plotted on a circular histogram using a custom MATLAB script. The script displayed total nuclei within each increment and calculated kurtosis using the kurtosis MATLAB function.

3.2.7 Cytoskeletal organization of myoblasts on single and bundled etched microthreads

Groups of five microthreads were bundled together by hydrating scaffolds dropwise with PBS until microthreads adhered together, as previously described.[39] Three individual microthreads or one bundle were attached to 25 x 25 mm glass coverslips with medical grade silicone adhesive and placed in 6-well plates for sterilization and culturing. Single or bundled microthreads were sterilized in 70% ethanol for at least 2 hours and rinsed 3 times with DI water. Immediately prior to seeding, microthreads were rehydrated with 200 µL of PBS for 1 hour. After 1 hour, PBS was aspirated and 200 µL of a 250,000 cells/mL cell suspension in complete medium supplemented with 50 µg/mL aprotinin was added to the top of the coverslip. After 4 hours of incubation, 3 mL of fresh medium was added to each well to completely submerge the single or bundled microthreads and allowed to incubate for an additional 20 hours. After 24 hours, samples were fixed in 4% paraformaldehyde and stained with Alexa fluor 488 phalloidin and Hoechst 33342 following manufacturer's instructions to visualize C2C12 myoblast filamentous actin (F-actin) and nuclei, respectively. Single and bundled microthreads were

imaged using a Zeiss Axiovert 200M microscope and confocal microscope (TCS SP5 Point Scanning Confocal, Leica, Germany), respectively.

3.2.8 Statistical analyses

Statistical analyses were performed using Graphpad Prism 7 software. For mechanical testing, nuclear alignment, and roughness parameter data, statistical differences were determined by one-way ANOVA ($p < 0.05$) with Dunnett's pairwise multiple comparisons post hoc analysis, or by Kruskal Wallis ($p < 0.05$) with Tukey's pairwise multiple comparisons post hoc analysis if ANOVA assumptions were not met. Two-way ANOVA ($p < 0.05$) with Dunnett's pairwise multiple comparisons post hoc analysis was used to evaluate FWHM and maximum pixel intensity of FFT plots. Values reported are means ± standard error of the mean (SEM) unless otherwise stated.

3.3 RESULTS

3.3.1 Etching imparts anisotropic surface features on fibrin microthreads as a function of pH

Anisotropic grooved features were created on the surface of fibrin microthreads by incubating microthreads in MES buffer, where buffer pH was an important regulator in the generation of surface features. SEM images of fibrin microthreads showed amorphous surface features on control microthreads (dH_2O) and those placed in MES buffer with a pH of 5.5 (MES 5.5), while microthreads placed in a more acidic MES buffer with a pH of 5.0 (MES 5.0) exhibited highly aligned, grooved surface features parallel to the long axis of the microthread (**Figure 3.3 A - C**). Preliminary studies evaluating a wide range of buffer pH conditions showed that all MES buffer with a pH below 5.0 resulted in microthread degradation, and all MES buffer with a pH above 5.5 exhibited amorphous surface features comparable to those observed at pH 5.5. For this reason, further analyses were limited to microthreads incubated in MES buffers with pH of 5.0 and 5.5.

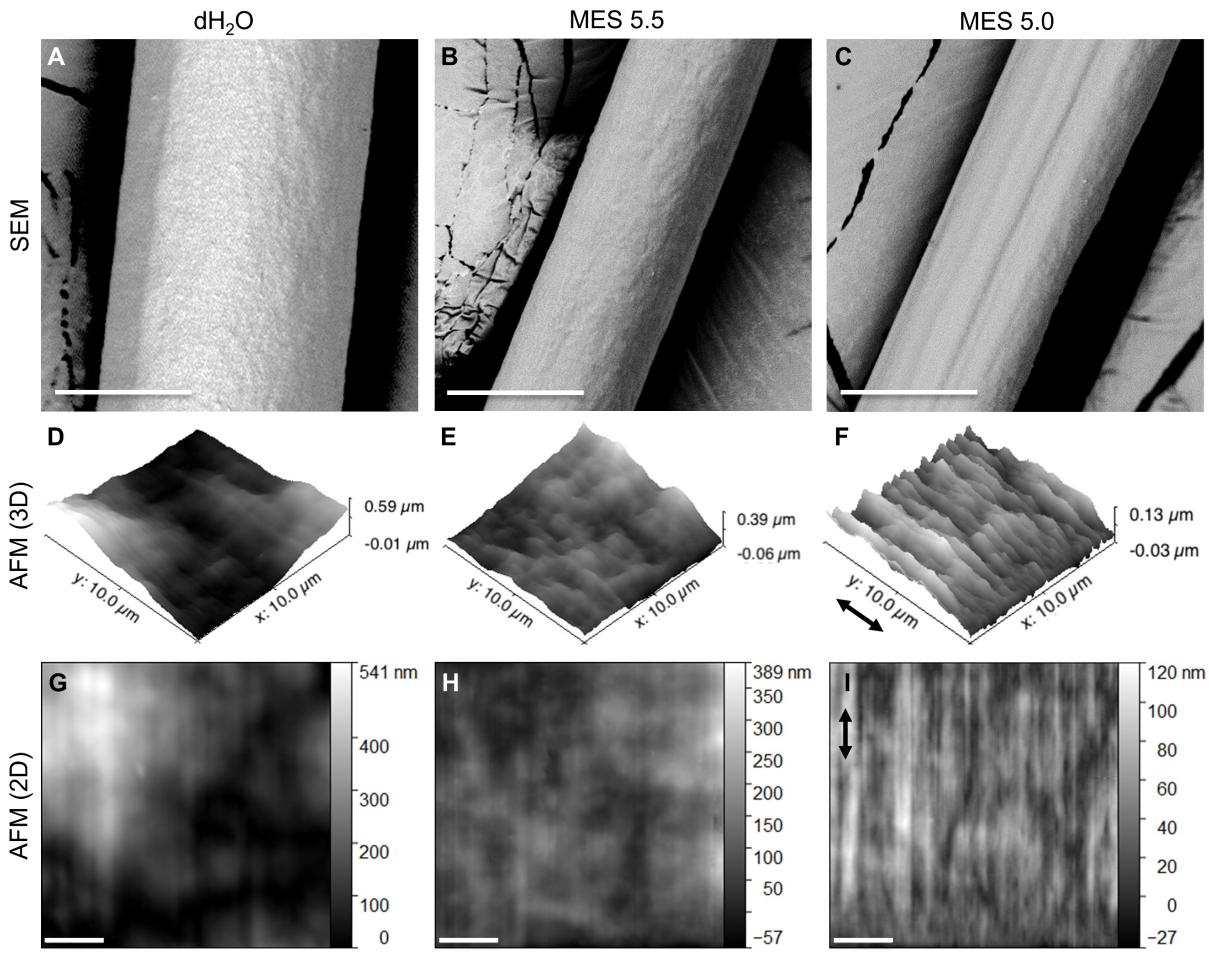

Figure 3.3. Surface characterization of etched fibrin microthreads. Representative SEM images of control dH_2O microthreads (A) and MES-etched microthreads with pH 5.5 (B) and pH 5.0 (C). 10 µm x 10 µm 3D (D-F) and 2D (G-I) AFM images of fibrin microthread surfaces. Control dH_2O microthreads (D, G) and threads etched in MES pH 5.5 (E, H) do not demonstrate aligned surface features. Microthreads etched in MES pH 5.0 buffer (F, I) have grooved, anisotropic surface characteristics along the long axis of the thread, indicated by black arrows. Scale bar is 20 µm on SEM images and 2 µm on 2D AFM images.

Characterization of microthread surfaces with AFM confirmed our initial observations with SEM. Images of microthread surfaces (10 µm x 10 µm) showed nanoscale surface features, which appeared amorphous on dH_2O and MES 5.5 microthreads, but highly anisotropic on MES 5.0 microthreads (**Figure 3.3 D - I**). Additionally, these anisotropic grooved features on MES 5.0 microthreads were consistent with the long axis of the microthreads, as indicated by the black arrows in **Figure 3.3**. Anisotropy of microthread surfaces were characterized by performing a FFT followed by a radial pixel summation of flattened AFM images to generate normalized pixel intensity plots, where high, narrow peaks at 90° and 270° indicate anisotropic surface features

consistent with the long axis of the microthread (**Figure 3.2 F).** All microthread conditions exhibited characteristic peaks at 90° and 270°, indicating the presence of anisotropic features (**Figure 3.4 A**). Normalized pixel intensity plots were quantified for peak height and steepness of peaks at 90° and 270°. MES 5.0 microthreads had significantly higher pixel intensity at the 270° peak than dH_2O microthreads (**Figure 3.4 B**). Peak steepness was evaluated by calculating full width half maximum (FWHM) for the two peaks. No differences in FWHM were observed between microthread conditions (**Figure 3.4 C).**

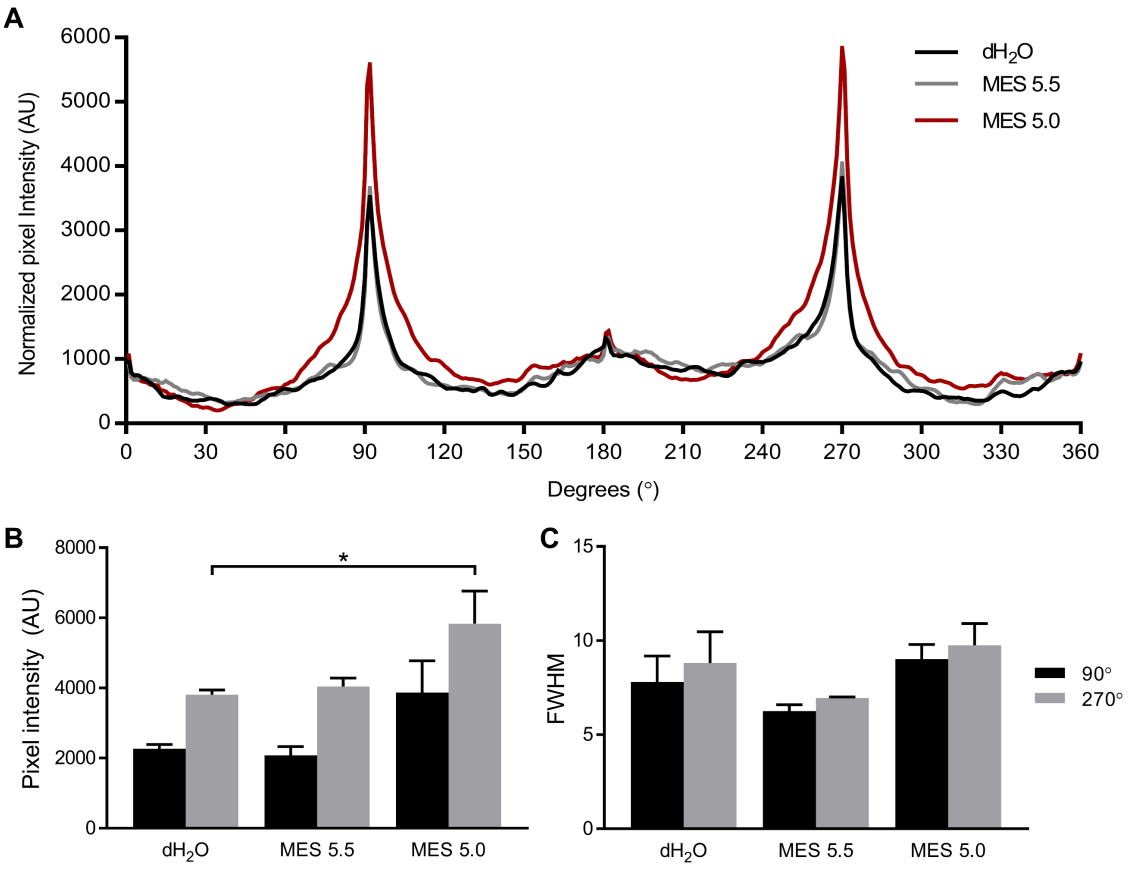

Figure 3.4. Alignment analysis of AFM surface topography. Average normalized pixel intensities of 2D FFT plots of flattened AFM images have sharp spikes at 90° and 270°, which indicate aligned topography in the direction of the long axis of the microthread for all conditions (A). Pixel intensity values for the three conditions at peaks (90° and 270°) were compared and show significantly higher peak at 270° in the MES 5.0 microthread compared to control dH_2O microthreads (B). Full width half maximum (FWHM) of each pixel intensity plot was evaluated to assess the steepness of the peaks (C). * indicates statistical significance between corresponding groups using two-way ANOVA with Dunnett's pairwise multiple comparisons post hoc analysis ($p < 0.05$, $N \geq 3$ experimental replicates).

Standardized AFM roughness parameters were also evaluated to further characterize the surface properties of the microthreads. Surface area and roughness were evaluated from flattened AFM images. No significant changes between microthread etching conditions were observed (**Figure 3.5 A, C**). To elucidate information about the scale of observed surface features, average maximum height of roughness and mean spacing of profile irregularities were evaluated from a 5 line average of roughness parameters (**Figure 3.5 B, D**). Average maximum height of roughness was 38.9 +/- 12 nm for MES 5.0 microthreads, 25.0 +/- 0.7 nm for MES 5.5 microthreads, and 33.9 +/- 6.8 nm for dH_2O control microthreads. This provided important information about the depth scale of surface features. Mean spacing of profile irregularities provided information about the width scale of these features and was found to range tightly between 646 - 676 nm for all 3 microthread conditions.

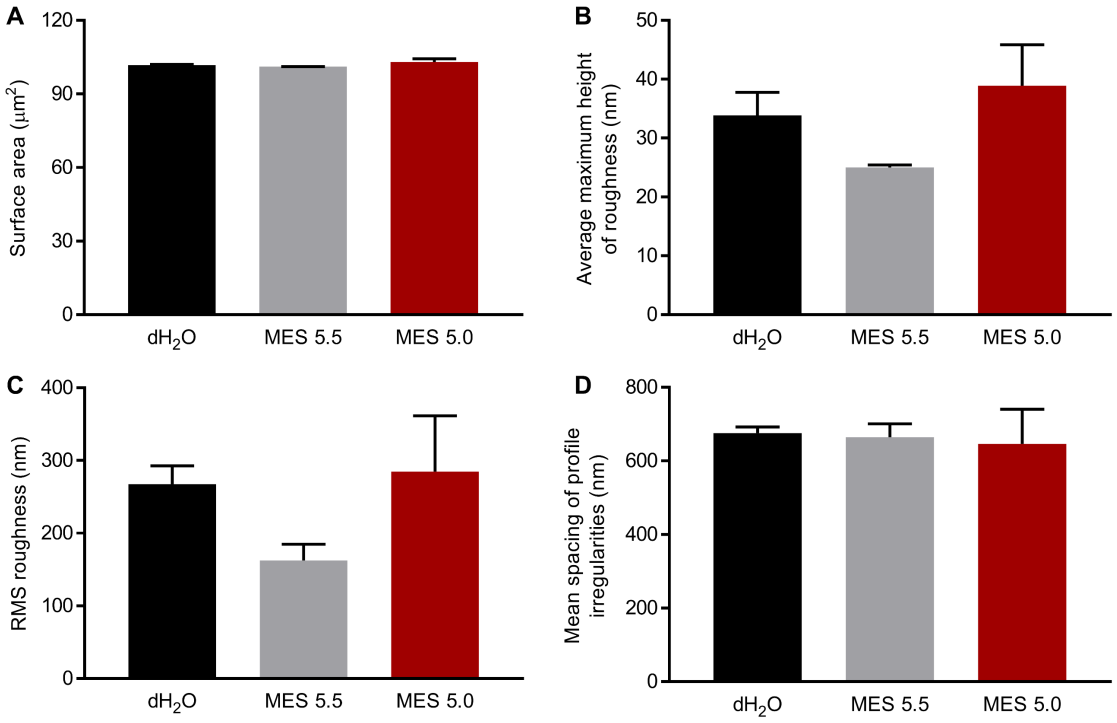

Figure 3.5. Analysis of microthread surface area, roughness, and feature dimensions. Gwyddion software was used to calculate average parameters for each 10 μm x 10 μm AFM image. Surface area (A) and RMS roughness (C) were evaluated with the general statistics tool in Gwyddion on AFM arc-subtracted images. Average maximum height of roughness (B) and mean spacing of profile irregularities (D) provide height and width information about observed surface features. These were calculated from 5-line averages of the Gwyddion line roughness analysis tool. No statistically significant differences in surface area and roughness parameters were found. ($N \geq 3$ experimental replicates).

3.3.2 Etching does not attenuate the tensile mechanical properties of fibrin microthreads

Scaffold mechanical properties serve as another biophysical cue that regulates muscle cell adhesion, proliferation, and differentiation.[40] Tensile mechanical testing was performed on MES etched fibrin microthreads to ensure that this treatment to impart anisotropic surface features did not significantly decrease scaffold mechanical properties. Microthreads were uniaxially loaded at a 50% strain rate until failure to determine their mechanical properties. Prior to testing, diameter measurements of hydrated microthreads were taken. There were no significant differences found between MES 5.0, MES 5.5, and dH_2O fibrin microthread diameters (**Figure 3.6 D**). Stress-strain curves of all microthread conditions exhibited initial toe regions where with increasing elongation there was small increase in stress, similar to previously published work evaluating fibrin microthread tensile properties.[32]

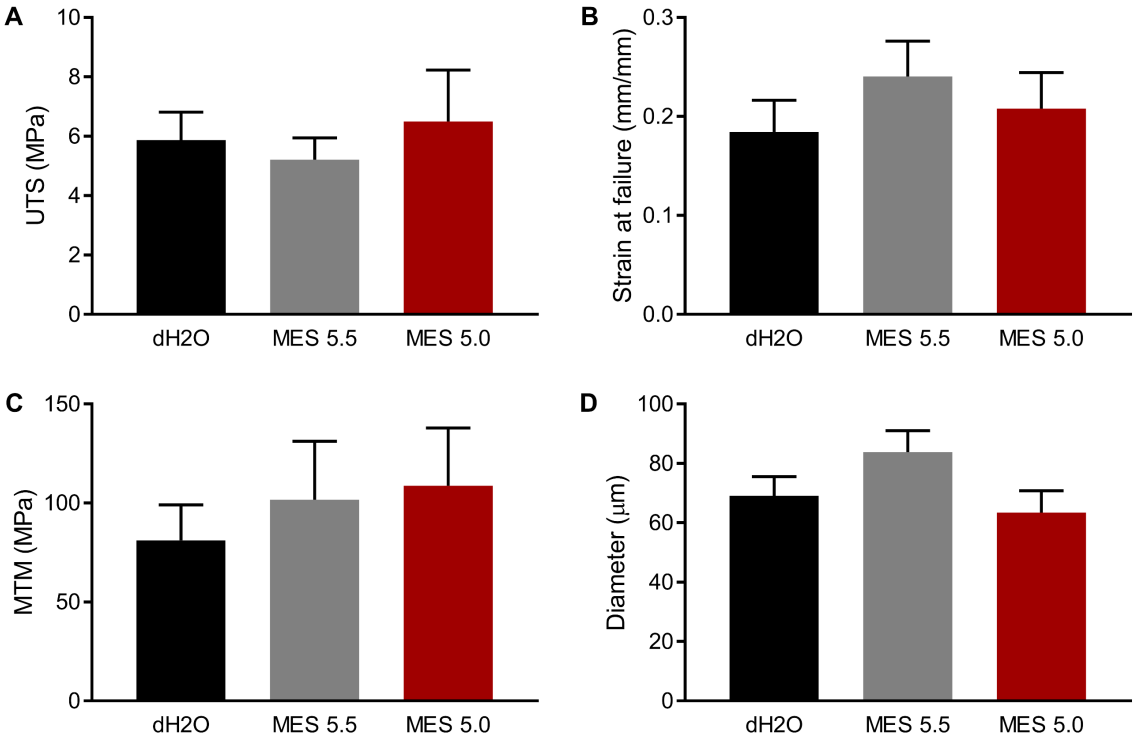

Figure 3.6. Mechanical properties of control and MES etched fibrin microthreads. Uniaxial tensile testing of fibrin microthreads was performed to failure and resulting stress-strain curves were analyzed to evaluate ultimate tensile strength (UTS) of scaffolds (A), strain at failure (SAF) (B), and maximum tangent modulus (MTM) (C). No statistically significant differences in mechanical properties between dH_2O, MES 5.5, and MES 5.0 microthreads were found. No differences in hydrated microthread diameter were noted between control and etched microthreads (D). ($N \geq 5$ experimental replicates, $n \geq 20$ microthreads).

No significant differences were observed in UTS, SAF, or MTM between MES 5.0, MES 5.5, and dH_2O microthreads (**Figure 3.6 A - C**), indicating that the surface etching treatment had no marked effect on bulk microthread mechanical properties.

3.3.3 Myoblasts preferentially align on fibrin microthread scaffolds

To investigate the effect of myoblast alignment on fibrin microthreads with anisotropic surface features, C2C12 myoblasts were seeded on single and bundled microthreads for 24 hours, fixed, and stained with Hoechst to visualize nuclei. Single and bundled microthreads were also stained with phalloidin to visualize F-actin organization of cells seeded on etched microthreads. Myoblasts seeded on MES 5.0 microthread bundles appeared elongated along the long axis of the microthreads, while those seeded on MES 5.5 and dH_2O microthread bundles demonstrated less preferential alignment (**Figure 3.7 A**). Additionally, F-actin stress fiber organization appeared randomly oriented on MES 5.5 and dH_2O microthread bundles, and highly aligned along the long axis of the microthread on MES 5.0 microthread bundles. These results were consistent with what we observed when myoblasts were seeded on individual microthreads (**Figure 3.8**). We also noticed that on all bundled microthread conditions, myoblasts exhibited a high degree of alignment when located in the grooves between adjacent microthreads. Nuclear orientation was evaluated with respect to the long axis of the microthread, where an angle of 0° corresponds to alignment with the long axis of the microthread. Circular histograms showing the distribution of nuclear orientation angle indicate that myoblasts preferentially aligned with the long axis of the microthreads in all experimental conditions (**Figure 3.7 B).** Kurtosis values were calculated for each condition to indicate the sharpness of the peak in the data. The dH_2O condition had a kurtosis value of 0.0654, MES 5.5 was 0.219, and MES 5.0 was 0.683, indicating a trend in increasing peakness of the data where the anisotropic MES 5.0 condition had the greatest degree of peakness. The MES 5.0 condition had the highest percentage of total aligned cells, 57.7 +/- 11.6%, which is defined as cells that align within 15° of the long axis of the microthread (**Figure 3.7 C**). MES 5.0 microthreads had a significantly higher percentage of aligned cells compared to MES 5.5 microthreads (**Figure 3.7 C**). However, anisotropic surface features on MES 5.0 microthreads did not appear to influence total average cell angle (**Figure 3.7 D**).

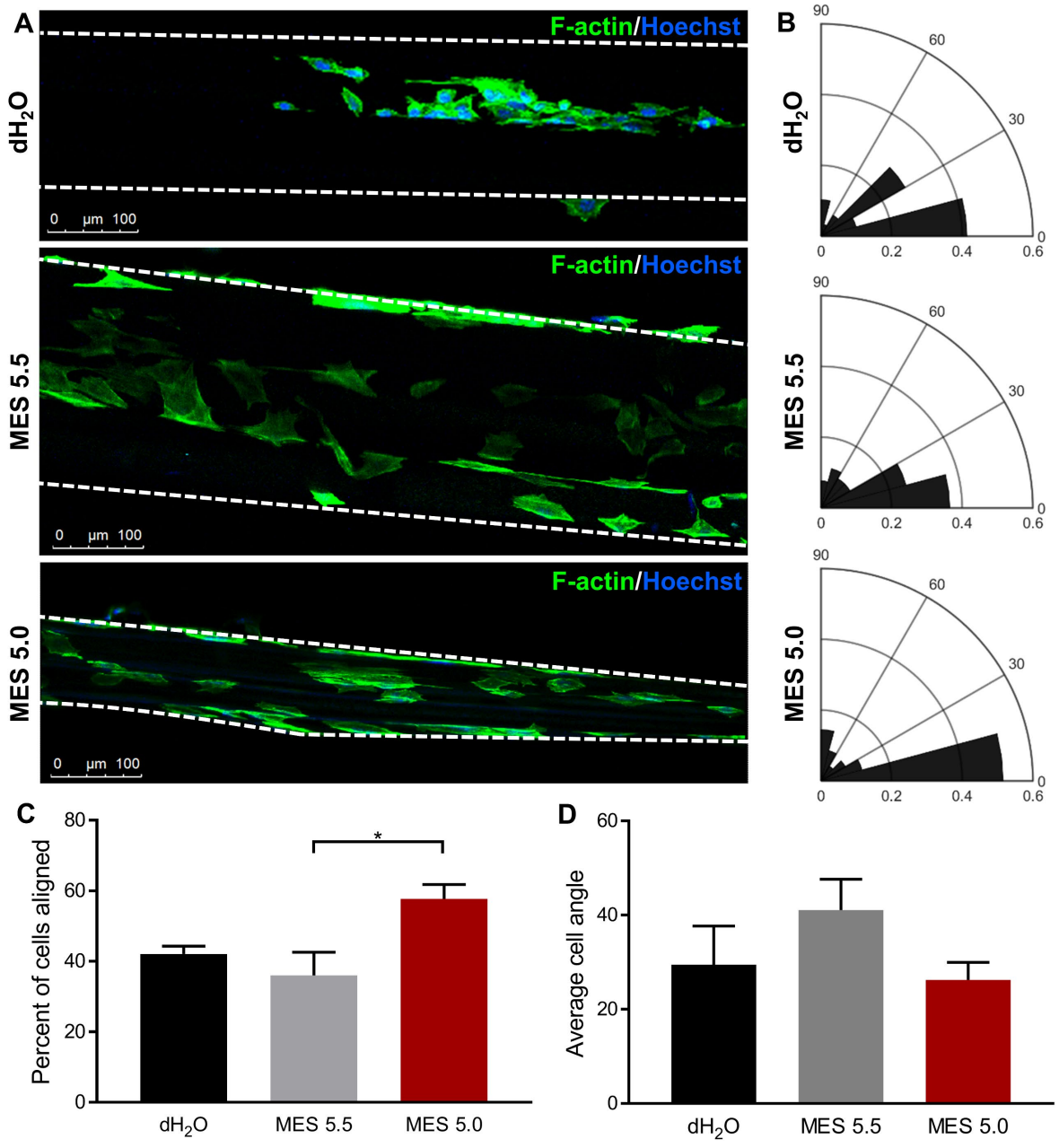

Figure 3.7. Cellular alignment analysis of myoblasts seeded on single and bundled fibrin microthreads. To visualize cellular spreading and F-actin organization, bundles of five microthreads seeded with myoblasts were fixed and stained with phalloidin (green) and Hoechst (blue) to visualize F-actin and nuclei, respectively. White dotted lines represent microthread bundle edges (A). To quantify nuclear orientation of myoblasts on single microthreads, nuclear orientation with respect to the long axis of the fibrin microthread was analyzed using ImageJ software, where the long axis of the microthread is represented as 0°. Circular histograms of nuclear orientation angle show that nuclei demonstrate preferential orientation along the long axis of the microthread in all conditions (B). We also evaluated the percent of total cells on each microthread condition considered to be aligned (0-15°) and note a significant increase in percent aligned cells on MES 5.0 microthreads compared to MES 5.5. (C), Average cell angle on each microthread condition was also evaluated and found no statistically significant differences between conditions (D). ($N \geq 6$ experimental replicates).

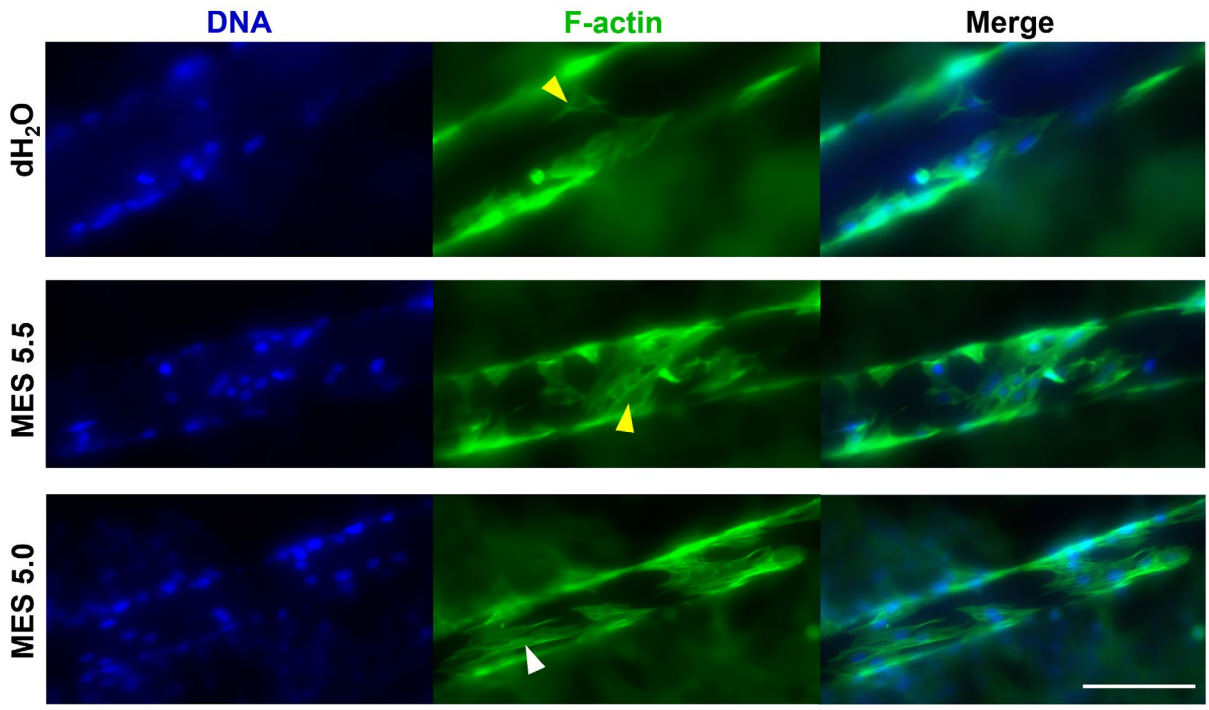

Figure 3.8. Cytoskeletal alignment analysis of myoblasts seeded on single fibrin microthreads. To visualize cellular spreading and F-actin organization, single microthreads were seeded with myoblasts, fixed, and stained with phalloidin (green) and Hoechst (blue) to visualize F-actin and nuclei, respectively. Scale bar is 100 µm. (N ≥ 3 experimental replicates).

3.4 DISCUSSION

To recapitulate native skeletal muscle architecture and facilitate myoblast alignment, the goal of this study was to fabricate and characterize fibrin microthread scaffolds with aligned surface features. Anisotropic surface grooves were created on fibrin microthreads with a simple and easily implemented method of acid etching, where the pH of MES buffer regulated the topography of resulting nanoscale surface features. Addition of surface features did not change surface area or roughness, indicating that changes in myoblast alignment are due specifically to feature architecture. The generation of surface features did not attenuate the tensile properties of the microthreads, demonstrating that scaffold topography can be tuned independent of other important biophysical cues such as scaffold stiffness. Finally, myoblasts preferentially aligned along the long axis of microthreads on MES 5.0 microthreads, suggesting that this surface topography guides myoblast response.

Aligned features were created on the surface of fibrin microthreads with a facile method

of acid etching, where the pH of MES buffer regulated the resulting nanoscale surface topography. Initial studies evaluating a wide range of pH and time in buffer indicated that these surface features were created in as early as 15 minutes, and in buffer with a pH of 5.0. MES buffer with a pH lower than 5.0 resulted in microthread degradation, which would compromise the structural integrity of the scaffold. MES buffer with a pH of 5.5 resulted in surface features that appeared amorphous upon inspection with SEM and AFM. FFT analysis further confirmed that MES 5.5 microthreads had less pronounced anisotropic surface features than MES 5.0 microthreads. We hypothesize that the anisotropic surface features are a result of an interaction between the fibrin microthread surface and acidic buffer environment. One possible mechanism for the generation of more aligned features on MES 5.0 microthreads is that the more acidic MES bath degrades fibrin on the microthread surface, exposing aligned interfibrillar structures within the fibrin microthread. A critical step in fibrin microthread fabrication is uniaxial stretching after initial polymerization. Previous observations in fibrin gel and microthread systems subjected to similar uniaxial strain exhibit a high degree of interfibrillar alignment, with features on the same size scale as those observed on MES 5.0 microthreads.[16, 32, 41-43] Additionally, pH is known to play an important role in regulating fibrin clot formation and fibrillar microstructure.[44] This may also explain why changes in fibrin microthread surface topography were observed as a function of MES buffer pH. Future studies to investigate the role of pH and buffer chemistry will elucidate the mode of action for surface feature generation.

MES surface treatment produces aligned surface features on fibrin microthreads that recapitulate native ECM architecture in skeletal muscle. Skeletal muscle is a highly aligned and hierarchically organized tissue with bundles of parallel multinucleated myotubes that synchronously contract to generate uniaxial force transduction and voluntary locomotion. This aligned tissue structure is essential for generating efficient tissue contraction and force generation. Initial alignment of myoblasts is essential in dictating myotube formation, alignment, and maturation, and is known to be guided in vivo by micron-scale grooves between adjacent muscle fibers. Skeletal muscle ECM surrounding myofibers has a highly aligned and fibrous architecture, which provides these contact guidance cues and plays an important role in dictating muscle tissue structure, function, and repair.[2] During muscle repair, satellite cells are guided by the basement membrane surrounding necrotic myofibers to facilitate aligned cell division,

migration, and fusion into mature myofibers.[45, 46] These mechanisms are driven in part by the topographical cues provided by the basement membrane. Structural evaluation of skeletal muscle basement membrane shows an aligned organization of ECM architecture, including perimysial collagen bundles approximately 0.5-1 μm in diameter that run parallel to muscle fibers.[2] Through AFM characterization, we found that grooves created on MES 5.0 microthreads had an average spacing of 646 +/- 163 nm, which is consistent with the dimensions of hierarchically organized collagen fiber bundles in native tissue. Dimensions of these surface features are also consistent with reported dimensions in literature for nanofibers and grooved nanopatterned substrates that have been effective in eliciting myoblast alignment and myotube formation.[4, 6, 12] Huang et al. noted that although both micropatterned and nanofibrous substrates permitted cytoskeletal alignment and myotube formation, the nanofibrous scaffolds (500 nm in diameter) were more effective in promoting longer and wider myotubes.[4] This study supports our findings which suggest that the addition of sub-micron grooves on microthreads may further promote myoblast alignment. Future work will investigate the effect of fibrin microthread etched surface features on focal adhesion formation and differentiation into mature myotubes. This may elucidate underlying cellular mechanisms of how myoblasts respond to surface topography, which is still not understood. Additionally, AFM characterization indicated that despite marked changes in surface features, there were no significant differences in surface area and roughness between the dH_2O, MES 5.5, and MES 5.0 microthreads. This suggests that it is specifically the aligned features of the surface morphology, not just a change in surface area or roughness that is causing trends in increasing cellular alignment.

Despite significant changes in surface features, fibrin microthreads etched with MES did not exhibit any changes in tensile mechanical properties compared to control dH_2O microthreads. In addition to surface topography, other biophysical cues such as scaffold elasticity play an important role in regulating muscle cell maturation. While substrate stiffness does not affect the propensity for myoblasts to assemble into myotubes, it was shown to have an important role on the formation of myosin/actin striations.[40] Myoblasts cultured on substrates with a modulus of 12 kPa, which matches the elasticity of native muscle tissue, were found to have significantly increased striations, indicating a more functional and mature cellular phenotype.[40] While our scaffolds have a stiffness that exceeds the 12 kPa static stiffness of native muscle tissue, tissue

stiffness has been reported to increase to 11.2 MPa while contracting[47]; this places our scaffolds in the same range as native contracting muscle. Additionally, substrates stiffer than native muscle tissue have previously been shown to promote enhanced myoblast differentiation via upregulation of muscle creatine kinase and myogenin.[48, 49] Furthermore, we report fibrin microthread scaffolds with strains at failure between 23-27%, which closely aligns with the 10-30% strains experienced by native skeletal muscle.

In addition to surface topography, other methods of promoting skeletal muscle maturation such as mechanical and electrical stimulation have demonstrated some success in recapitulating skeletal muscle structure and function.[50] *In vivo*, skeletal muscle receives electric signals from motor neurons via neuromuscular junctions, which initiate muscle contraction. When applied to anisotropically aligned electrospun constructs, electrical stimulation has been shown to further enhance myoblast alignment, contractile protein expression, and contractility.[11, 51] These findings motivate the future incorporation of electrical stimulation to fibrin microthread culture as a method of further enhancing myoblast alignment on these scaffolds. In addition to electrical signals, skeletal muscle experiences mechanical strains during development that are known to play an important role in myogenesis. Researchers demonstrated that a wide range of mechanical strain regimes on tissue engineered skeletal muscle constructs have resulted in enhanced myogenic outcomes.[52] There is promising potential in combining electrical and mechanical stimulation regimes with anisotropically aligned scaffolds towards the goal of further enhancing myoblast maturation, alignment, and differentiation. Preliminary work in our lab is focused on providing these instructive mechanical and electrical cues to fibrin microthread scaffolds and will be an important thrust of our research moving forward.

Fibrin microthreads with aligned topographical surface features have broader applications in tissue engineered systems where alignment of cells is of paramount concern for tissue maturation and functionality. Scaffolds with aligned nanoscale features have been used to promote endothelial cell and cytoskeletal alignment, gap-junction formation, and increased resistance to detachment towards the goal of developing tissue engineered vascular grafts.[53, 54] Scaffolds with aligned topographical features have been explored for the generation of nerve guidance conduits for treatment of peripheral nervous system injuries to facilitate axonal growth.[55] Toward the development of tendon and ligament grafts, microthreads have been

bundled, knitted, braided, and incorporated into composites towards the goal of matching native tendon mechanical properties, tuning scaffold degradation rate, and enhancing cellular response.[18] Finally, aligned scaffolds have also been used to stimulate the generation of mature and contractile cardiomyocytes. Notably, recent work by Chrobak et al. found that incorporating fibrin microthreads into a composite scaffold allowed for the development of a cardiac patch that mechanically matched native myocardium and supported cardiomyocyte maturation, contraction, and alignment.[29] With their tunable biochemical, mechanical, and surface properties, microthread scaffolds have the potential to serve as a platform technology to significantly enhance the restoration of many axially aligned and hierarchically complex tissues.[18]

3.5 CONCLUSIONS

In this study, we presented a new method of creating anisotropic topography on the surface of fibrin microthread scaffolds. Characterization of these surface features with multiple imaging modalities indicated the generation of aligned, sub-micron sized grooves as a function of MES buffer pH. Microthreads etched with surface features had comparable tensile mechanical properties, indicating that this surface treatment does not inhibit the bulk properties of this scaffold. The ability to tune scaffold topography independent of mechanical properties is a useful tool for microthread-based scaffold modifications and has the potential to have an important role in further stimulating desired cellular functions such as alignment and differentiation. Myoblasts preferentially aligned on etched and control microthreads, likely due to the fact that microthread architecture initiates cellular alignment. However, our data suggests that MES 5.0 microthreads may further enhance myoblast alignment on microthread scaffolds. Future work to investigate myotube differentiation will further elucidate the ability of this anisotropic scaffold topography to promote functional skeletal muscle regeneration.

3.6 ACKNOWLEDGEMENTS

We thank Lyra Huynh, Giulio Cataldo, and Matthew Cannata for their assistance with preparing scaffolds and conducting mechanical testing analysis. We also thank Jon Grasman, Ph.D. for his initial investigations of fibrin microthread surface etching. This work was funded in part by NIH R15 HL137145 (GDP) and NSF DGE IGERT 1144804 (MEC).

3.7 REFERENCES

1. Carnes, M. E.; Pins, G. D., Etching anisotropic surface topography onto fibrin microthread scaffolds for guiding myoblast alignment. *J Biomed Mater Res B Appl Biomater* **2020,** *108* (5), 2308-2319.
2. Gillies, A. R.; Lieber, R. L., Structure and function of the skeletal muscle extracellular matrix. *Muscle & nerve* **2011,** *44* (3), 318-31.
3. Huang, N. F.; Lee, R. J.; Li, S., Engineering of aligned skeletal muscle by micropatterning. *Am J Transl Res* **2010,** *2* (1), 43-55.
4. Huang, N. F., Patel, S., Thakar, R.G., Wu, J., Hsiao, B.S., Chu, B., Lee, R.J., and Li, S., Myotube Assembly on Nanofibrous and Micropatterned Polymers. *Nano Letters* **2006,** *6* (3), 537-542.
5. Charest, J. L.; Garcia, A. J.; King, W. P., Myoblast alignment and differentiation on cell culture substrates with microscale topography and model chemistries. *Biomaterials* **2007,** *28* (13), 2202-10.
6. Wang, P. Y.; Yu, H. T.; Tsai, W. B., Modulation of alignment and differentiation of skeletal myoblasts by submicron ridges/grooves surface structure. *Biotechnology and bioengineering* **2010,** *106* (2), 285-94.
7. Monge, C.; Ren, K.; Berton, K.; Guillot, R.; Peyrade, D.; Picart, C., Engineering muscle tissues on microstructured polyelectrolyte multilayer films. *Tissue Eng Part A* **2012,** *18* (15-16), 1664-76.
8. Flemming, R. G., Murphy, C.J., Abrams, G.A., Goodman, S.L., Nealey, P.F, Effects of synthetic micro- and nano-structures surfaces on cell behavior. *Biomaterials* **1999,** *20*, 573-588.
9. Zhao, Y.; Zeng, H.; Nam, J.; Agarwal, S., Fabrication of skeletal muscle constructs by topographic activation of cell alignment. *Biotechnology and bioengineering* **2009,** *102* (2), 624-31.
10. Bian, W.; Liau, B.; Badie, N.; Bursac, N., Mesoscopic hydrogel molding to control the 3D geometry of bioartificial muscle tissues. *Nature protocols* **2009,** *4* (10), 1522-34.
11. Chen, M. C.; Sun, Y. C.; Chen, Y. H., Electrically conductive nanofibers with highly oriented structures and their potential application in skeletal muscle tissue engineering. *Acta Biomater* **2013,** *9* (3), 5562-72.
12. Choi, J. S.; Lee, S. J.; Christ, G. J.; Atala, A.; Yoo, J. J., The influence of electrospun aligned poly(epsilon-caprolactone)/collagen nanofiber meshes on the formation of self-aligned skeletal muscle myotubes. *Biomaterials* **2008,** *29* (19), 2899-906.
13. Ku, S. H.; Lee, S. H.; Park, C. B., Synergic effects of nanofiber alignment and electroactivity on myoblast differentiation. *Biomaterials* **2012,** *33* (26), 6098-104.
14. Li, W., Mauck, R.L., Cooper, J.A., Yuan, X., and Tuan, R.S., Engineering controllable anisotropy in electrospun biodegradable nanofibrous scaffolds for musculoskeletal tissue engineering. *Journal of Biomechanics* **2007,** *40*, 1686-1693.
15. Aviss, K. J.; Gough, J. E.; Downes, S., Aligned electrospun polymer fibres for skeletal muscle regeneration. *European cells & materials* **2010,** *19*, 193-204.
16. Zhang, S.; Liu, X.; Barreto-Ortiz, S. F.; Yu, Y.; Ginn, B. P.; DeSantis, N. A.; Hutton, D. L.; Grayson, W. L.; Cui, F. Z.; Korgel, B. A.; Gerecht, S.; Mao, H. Q., Creating polymer hydrogel microfibres with internal alignment via electrical and mechanical stretching. *Biomaterials* **2014,** *35* (10), 3243-51.
17. Cornwell, K. G.; Pins, G. D., Discrete crosslinked fibrin microthread scaffolds for tissue regeneration. *J Biomed Mater Res A* **2007,** *82* (1), 104-12.
18. O'Brien, M. P.; Carnes, M. E.; Page, R. L.; Gaudette, G. R.; Pins, G. D., Designing Biopolymer Microthreads for Tissue Engineering and Regenerative Medicine. *Curr Stem Cell Rep* **2016,** *2* (2), 147-157.
19. Pins, G. D.; Silver, F. H., A self-assembled collagen scaffold suitable for use in soft and hard tissue replacement. *Materials Science and Engineering: C* **1995,** *3* (2), 101-107.
20. Jana, S.; Cooper, A.; Zhang, M., Chitosan scaffolds with unidirectional microtubular pores for large skeletal myotube generation. *Advanced healthcare materials* **2013,** *2* (4), 557-61.

21. Kroehne, V.; Heschel, I.; Schugner, F.; Lasrich, D.; Bartsch, J. W.; Jockusch, H., Use of a novel collagen matrix with oriented pore structure for muscle cell differentiation in cell culture and in grafts. *J Cell Mol Med* **2008,** *12* (5A), 1640-8.
22. Ma, P. X.; Zhang, R., Microtubular architecture of biodegradable polymer scaffolds. *J Biomed Mater Res* **2001,** *56* (4), 469-77.
23. Huang, Z. M.; Zhang, Y. Z.; Kotaki, M.; Ramakrishna, S., A review on polymer nanofibers by electrospinning and their applications in nanocomposites. *Compos Sci Technol* **2003,** *63* (15), 2223-2253.
24. Deng, M.; James, R.; Laurencin, C. T.; Kumbar, S. G., Nanostructured Polymeric Scaffolds for Orthopaedic Regenerative Engineering. *Ieee T Nanobiosci* **2012,** *11* (1), 3-14.
25. Tamayol, A.; Akbari, M.; Annabi, N.; Paul, A.; Khademhosseini, A.; Juncker, D., Fiber-based tissue engineering: Progress, challenges, and opportunities. *Biotechnol Adv* **2013,** *31* (5), 669-87.
26. Hong, Y.; Takanari, K.; Amoroso, N. J.; Hashizume, R.; Brennan-Pierce, E. P.; Freund, J. M.; Badylak, S. F.; Wagner, W. R., An elastomeric patch electrospun from a blended solution of dermal extracellular matrix and biodegradable polyurethane for rat abdominal wall repair. *Tissue Eng Part C Methods* **2012,** *18* (2), 122-32.
27. Leong, M. F.; Chan, W. Y.; Chian, K. S.; Rasheed, M. Z.; Anderson, J. M., Fabrication and in vitro and in vivo cell infiltration study of a bilayered cryogenic electrospun poly(D,L-lactide) scaffold. *J Biomed Mater Res A* **2010,** *94A* (4), 1141-1149.
28. Shabani, I.; Haddadi-Asl, V.; Seyedjafari, E.; Soleimani, M., Cellular infiltration on nanofibrous scaffolds using a modified electrospinning technique. *Biochem Bioph Res Co* **2012,** *423* (1), 50-54.
29. Chrobak, M. O.; Hansen, K. J.; Gershlak , J. R.; Vratsanos, M.; Kanellias, M.; Gaudette, G. R.; Pins, G. D., Design of a Fibrin Microthread-Based Composite Layer for Use in a Cardiac Patch. *ACS Biomater. Sci. Eng.* **2017,** *3* (7), 1394–1403.
30. Grasman, J. M.; Do, D. M.; Page, R. L.; Pins, G. D., Rapid release of growth factors regenerates force output in volumetric muscle loss injuries. *Biomaterials* **2015,** *72*, 49-60.
31. Page, R. L.; Malcuit, C.; Vilner, L.; Vojtic, I.; Shaw, S.; Hedblom, E.; Hu, J.; Pins, G. D.; Rolle, M. W.; Dominko, T., Restoration of Skeletal Muscle Defects with Adult Human Cells Delivered on Fibrin Microthreads. *Tissue Eng Part A* **2011,** *17* (21), 2629-2640.
32. Grasman, J. M.; Pumphrey, L. M.; Dunphy, M.; Perez-Rogers, J.; Pins, G. D., Static axial stretching enhances the mechanical properties and cellular responses of fibrin microthreads. *Acta Biomater* **2014,** *10* (10), 4367-76.
33. Megelski, S.; Stephens, J. S.; Chase, D. B.; Rabolt, J. F., Micro- and nanostructured surface morphology on electrospun polymer fibers. *Macromolecules* **2002,** *35* (22), 8456-8466.
34. Williamson, M. R.; Adams, E. F.; Coombes, A. G., Gravity spun polycaprolactone fibres for soft tissue engineering: interaction with fibroblasts and myoblasts in cell culture. *Biomaterials* **2006,** *27* (7), 1019-26.
35. Grasman, J. M.; Page, R. L.; Dominko, T.; Pins, G. D., Crosslinking strategies facilitate tunable structural properties of fibrin microthreads. *Acta Biomater* **2012,** *8* (11), 4020-30.
36. Cornwell, K. G.; Pins, G. D., Enhanced proliferation and migration of fibroblasts on the surface of fibroblast growth factor-2-loaded fibrin microthreads. *Tissue Eng Part A* **2010,** *16* (12), 3669-77.
37. Hansen, K. J.; Laflamme, M. A.; Gaudette, G. R., Development of a Contractile Cardiac Fiber From Pluripotent Stem Cell Derived Cardiomyocytes. *Front Cardiovasc Med* **2018,** *5*, 52.
38. Ayres, C. E.; Jha, B. S.; Meredith, H.; Bowman, J. R.; Bowlin, G. L.; Henderson, S. C.; Simpson, D. G., Measuring fiber alignment in electrospun scaffolds: a user's guide to the 2D fast Fourier transform approach. *J Biomater Sci Polym Ed* **2008,** *19* (5), 603-21.
39. Proulx, M. K.; Carey, S. P.; DiTroia, L. M.; Jones, C. M.; Fakharzadeh, M.; Guyette, J. P.; Clement, A. L.; Orr, R. G.; Rolle, M. W.; Pins, G. D.; Gaudette, G. R., Fibrin microthreads support mesenchymal stem cell growth while maintaining differentiation potential. *J Biomed Mater Res A* **2011,** *96A* (2), 301-312.

40. Engler, A. J.; Griffin, M. A.; Sen, S.; Bonnemann, C. G.; Sweeney, H. L.; Discher, D. E., Myotubes differentiate optimally on substrates with tissue-like stiffness: pathological implications for soft or stiff microenvironments. *The Journal of cell biology* **2004,** *166* (6), 877-87.
41. Brown, A. E.; Litvinov, R. I.; Discher, D. E.; Purohit, P. K.; Weisel, J. W., Multiscale mechanics of fibrin polymer: gel stretching with protein unfolding and loss of water. *Science* **2009,** *325* (5941), 741-4.
42. Matsumoto, T.; Sasaki, J.; Alsberg, E.; Egusa, H.; Yatani, H.; Sohmura, T., Three-dimensional cell and tissue patterning in a strained fibrin gel system. *PLOS ONE* **2007,** *2* (11), e1211.
43. Keijdener, H.; Konrad, J.; Hoffmann, B.; Gerardo-Nava, J.; Rutten, S.; Merkel, R.; Vazquez-Jimenez, J.; Brook, G. A.; Jockenhoevel, S.; Mela, P., A bench-top molding method for the production of cell-laden fibrin micro-fibers with longitudinal topography. *J Biomed Mater Res B Appl Biomater* **2019**.
44. Ferry, J. D.; Morrison, P. R., Preparation and properties of serum and plasma proteins; the conversion of human fibrinogen to fibrin under various conditions. *J Am Chem Soc* **1947,** *69* (2), 388-400.
45. Serrano, A. L.; Munoz-Canoves, P., Regulation and dysregulation of fibrosis in skeletal muscle. *Experimental cell research* **2010,** *316* (18), 3050-8.
46. Webster, M. T.; Manor, U.; Lippincott-Schwartz, J.; Fan, C. M., Intravital Imaging Reveals Ghost Fibers as Architectural Units Guiding Myogenic Progenitors during Regeneration. *Cell stem cell* **2016,** *18* (2), 243-52.
47. Caiozzo, V. J., Plasticity of skeletal muscle phenotype: mechanical consequences. *Muscle & nerve* **2002,** *26* (6), 740-68.
48. Boontheekul, T.; Hill, E. E.; Kong, H. J.; Mooney, D. J., Regulating myoblast phenotype through controlled gel stiffness and degradation. *Tissue Eng* **2007,** *13* (7), 1431-42.
49. Gilbert, P. M.; Havenstrite, K. L.; Magnusson, K. E.; Sacco, A.; Leonardi, N. A.; Kraft, P.; Nguyen, N. K.; Thrun, S.; Lutolf, M. P.; Blau, H. M., Substrate elasticity regulates skeletal muscle stem cell self-renewal in culture. *Science* **2010,** *329* (5995), 1078-81.
50. Qazi, T. H.; Mooney, D. J.; Pumberger, M.; Geißler, S.; Duda, G. N., Biomaterials based strategies for skeletal muscle tissue engineering: Existing technologies and future trends. *Biomaterials* **2015,** *53*, 502-521.
51. Liao, I. C.; Liu, J. B.; Bursac, N.; Leong, K. W., Effect of Electromechanical Stimulation on the Maturation of Myotubes on Aligned Electrospun Fibers. *Cellular and molecular bioengineering* **2008,** *1* (2-3), 133-145.
52. Somers, S. M.; Spector, A. A.; DiGirolamo, D. J.; Grayson, W. L., Biophysical Stimulation for Engineering Functional Skeletal Muscle. *Tissue Eng Part B Rev* **2017,** *23* (4), 362-372.
53. Whited, B. M.; Rylander, M. N., The influence of electrospun scaffold topography on endothelial cell morphology, alignment, and adhesion in response to fluid flow. *Biotechnology and bioengineering* **2014,** *111* (1), 184-95.
54. Uttayarat, P.; Toworfe, G. K.; Dietrich, F.; Lelkes, P. I.; Composto, R. J., Topographic guidance of endothelial cells on silicone surfaces with micro- to nanogrooves: orientation of actin filaments and focal adhesions. *J Biomed Mater Res A* **2005,** *75* (3), 668-80.
55. Sarker, M.; Naghieh, S.; McInnes, A. D.; Schreyer, D. J.; Chen, X., Strategic Design and Fabrication of Nerve Guidance Conduits for Peripheral Nerve Regeneration. *Biotechnology journal* **2018,** *13* (7), e1700635.

Chapter 4: Horseradish Peroxidase-Catalyzed Crosslinking of Fibrin Microthread Scaffolds[1]

4.1 INTRODUCTION

Native tissues possess extracellular matrix (ECM) architectural cues that are highly complex and dictate tissue-specific functions. The primary structural components of ECM are fibrillar elements, arranged into hierarchically ordered structures from the nano- to macro-scale. The organization of these fibers varies from tissue to tissue to optimize the mechanical properties, contact guidance cues, and function of specific tissues. In tendon and ligament, type I, II, and V collagen fibrils organize into dense and highly aligned cable-like bundles to facilitate uniaxial force transduction.[2] In skin, type I and III collagen fibers form sheet-like arrays in various orientations, capable of resisting tension in multiple directions.[3] This structure-function relationship has motivated the rational design and development of microfiber scaffolds that mimic this complex, fibrous tissue architecture. Microthreads are discrete, fibrous scaffolds comprised of naturally derived biopolymers including fibrin,[4-8] collagen,[9-12] silk,[13, 14] and chitosan.[15, 16] Their structure is analogous to native ECM fibrils, and they can be similarly arranged to create hierarchically complex scaffolds to recapitulate a variety of tissue architectures.[17] Microfiber scaffolds also provide provisional structural and mechanical support, topographic cues, and biochemical signaling cues to direct cell-mediated tissue regeneration.[17]

Fibrin microthreads are a microfiber scaffold whose cylindrical form mimics native ECM fibrils, promoting cellular alignment and guided tissue regeneration.[4, 5, 7, 8, 18-21] Fibrin, the bioactive provisional matrix protein responsible for blood clotting, recruits cells that direct wound healing and functional tissue regeneration, making it a beneficial scaffold material.[22] Fibrin microthreads are fabricated by extruding solutions of fibrinogen and thrombin, which triggers the polymerization of a fibrin matrix.[4] These scaffolds can be modified to deliver therapeutic proteins such as fibroblast growth factor 2[23] and hepatocyte growth factor[18, 24] to

enhance cellular proliferation and migration. Discrete fibrin microthreads hierarchically organized into bundles or aligned composite patches mimic the organization and mechanical properties of muscle and cardiac tissue, respectively.[5, 8, 18] While fibrin microthreads have robust mechanical properties compared to fibrin hydrogel-based systems, uncrosslinked fibrin scaffolds remain susceptible to rapid degradation by fibrinolytic proteases when implanted *in vivo*, limiting the regenerative capacity of these matrices.[4, 6, 7] This motivated the investigation of production and post-processing modifications to increase the structural stability and persistence of these scaffolds.

Towards this, the mechanical properties of fibrin microthread scaffolds have been modified through both production[7] and post-processing crosslinking techniques.[4, 6] Increasing the degree to which fibrin microthreads are stretched during production yields scaffolds with significantly greater tensile strength and stiffness, but does not decrease the scaffold degradation rate.[7] Fibrin microthreads have also been ultraviolet (UV)[4] and carbodiimide crosslinked[6] via post-processing methods. While the facile method of UV crosslinking produced microthreads with two-fold greater ultimate tensile strength and moduli, UV crosslinked microthreads attenuated fibroblast proliferation.[4] This significantly limits the utility of UV crosslinking for implantable tissue engineering scaffolds. Carbodiimide crosslinking of fibrin microthreads also resulted in tunable scaffold mechanics.[6] However, when carbodiimide crosslinked microthreads were implanted into a murine muscle injury, scaffolds demonstrated minimal signs of degradation, even 60 days after implantation.[18] The results of this study suggest that the high degree of crosslinking limited scaffold degradation and cell mediated scaffold remodeling. Thus, there is a significant unmet need for a crosslinking strategy that tunes fibrin microthread mechanical properties and degradation while maintaining cell viability.

One alternative method of crosslinking biomaterial scaffolds is through dityrosine crosslinking.[25, 26] Dityrosine crosslinks are responsible for stabilizing biopolymers *in vivo*[27, 28] by exploiting naturally occurring tyrosine residues within biomaterial scaffolds.[25] Fibrin has the requisite phenol groups, containing approximately 3.3 mol% tyrosine, to enable utilization of this crosslinking method.[29, 30] Formation of dityrosine bonds can be facilitated by fenton-like, photo-initiated, and enzymatic reactions.[25] Researchers investigated the use of both fenton and photo-initiated reactions to dityrosine crosslink fibrin.[30-33] Fibrinogen was crosslinked through a fenton

reaction by exposure to hematin and non-thermal plasma treatment, which generates hydrogen peroxide (H_2O_2).[33] H_2O_2 and the ferrous ion in hematin are requisites for fenton-like dityrosine crosslinking, and resulted in the formation of dityrosine bonds in fibrinogen.[33] Photo-initiated reactions to dityrosine crosslink fibrin with ruthenium sodium persulfate have also been investigated as a means of enhancing structural stability and limiting cellular remodeling and degradation.[30-32] Finally, enzymatic reactions to dityrosine crosslink scaffolds take place in aqueous solutions and at neutral pH, making this method amenable to biopolymer scaffold modifications. Additionally, enzymes have high specificity, limiting deleterious side chain reactions common with other dityrosine crosslinking methods such as photo-initiated reactions.

Horseradish peroxidase (HRP) is one of the most commonly used enzymes, with H_2O_2 frequently used as the substrate. H_2O_2 interacts with the Fe(III) core of HRP, generating a high oxidation state intermediate compound. This intermediary consists of an Fe(IV) oxyferryl center and porphyrin-based cation radial.[34] In the presence of a phenol that acts as a reducing substrate, the intermediate compound undergoes two consecutive reduction steps to return HRP to its resting state. Resulting phenol radicals create a covalent dityrosine bond between polymer-phenol conjugates. Because the catalytic cycle of HRP consumes one H_2O_2 molecule and generates two phenolic radicals (and thus one crosslink), varying H_2O_2 concentration has been utilized to easily tune polymer scaffold mechanical properties, swelling ratio, gelation time, and degradation rate in a variety of phenol-containing biomaterial scaffolds.[35-46] Additionally, biomaterials crosslinked with HRP are biocompatible, and have demonstrated desired cellular responses in applications such as cartilage regeneration, wound healing, and stem cell differentiation and delivery.[39, 42, 44, 47-53] While enzymatic dityrosine crosslinking has been used for many biomaterials, to our knowledge it has yet to be used to crosslink fibrin.

Here we report the results of the first study to investigate the HRP-catalyzed dityrosine crosslinking of a fibrin scaffold. We examined the effect of varying HRP and H_2O_2 incorporation approaches on the resulting crosslink density and structural properties of fibrin microthreads. We evaluated both primary and secondary scaffold modification techniques to crosslink fibrin microthreads. The incorporation of crosslinking agents into the precursor solutions during microthread extrusion was considered a primary method, while soaking microthreads in a post-processing crosslinker bath was considered a secondary method of scaffold modification. Fibrin

microthreads were enzymatically crosslinked through primary, secondary, or both approaches. Resulting microthreads were evaluated for crosslink density, mechanical properties, resistance to proteolytic degradation, and their ability to support cell viability. We hypothesized that strategically varying the incorporation strategy of HRP and H_2O_2 through extrusion or post-processing modifications would yield scaffolds with tunable crosslink densities, tensile mechanical properties, and degradation rates. The purpose of this work was to enable the rational design of enzymatically crosslinked fibrin microthreads with tunable structural properties, facilitating their use for tissue engineering applications that target a broad range of tissues with varying mechanical and structural properties.

4.2 MATERIALS and METHODS

4.2.1 Fibrin Microthread Extrusion

Fibrin microthreads were generated by co-extruding fibrinogen and thrombin as previously described.[4] Briefly, fibrinogen isolated from bovine plasma (MP Biomedicals, Irvine, CA) was dissolved in HEPES (N-[2-Hydroxyethyl]piperazine-N'-[2-ethanesulfonic acid]) buffered saline (HBS, 20 mM HEPES, 0.9% NaCl, pH 7.4) to a concentration of 70 mg/mL and stored at -20°C until use. Thrombin isolated from bovine plasma (Sigma Aldrich, St. Louis, MO) was dissolved in HBS at 40 U/mL and stored at -20°C until use. To produce uncrosslinked (UNX) control microthreads, fibrinogen and thrombin solutions were thawed to room temperature, and thrombin was mixed with a 40 mM $CaCl_2$ solution to form a working solution of 6 U/mL thrombin and 34 mM $CaCl_2$. Equal volumes of fibrinogen and thrombin solutions were aspirated into separate 1 mL syringes and inserted into the end of a blending applicator (Micromedics Inc., St. Paul, MN; SA-3670). The solutions were mixed in the blending applicator and extruded through 0.86 mm inner diameter polyethylene tubing (Becton Dickinson, Sparks, MD) into a 10 mM HEPES buffer bath (pH 7.4) in a Teflon coated pan. Threads were extruded at 0.225 mL/m using a dual syringe pump. After 15 m incubation to allow for polymerization, the microthread scaffolds were removed and stretched to 300% of their initial drawn length and hung overnight to dry under the tension of their own weight. Previous work demonstrated that stretching microthreads enhances mechanical properties compared to unstretched microthreads.[7]

UNX control microthreads are defined as microthreads that were not subject to additional processing or crosslinking beyond thrombin-mediated polymerization.

4.2.2 Preparation of HRP crosslinked microthreads

Three different crosslinking methods were developed to evaluate the effect of scaffold crosslinking techniques on fibrin microthread crosslink densities, mechanical properties, and degradation rates. Primary extrusion and secondary post-processing scaffold modification techniques were utilized to crosslink fibrin microthreads. HRP and H_2O_2 were either included in precursor solutions prior to microthread extrusion, referred to as a primary (1º) incorporation method, included in a post-processing bath, referred to as a secondary (2º) method, or a combination of both approaches (1º/2º) (**Figure 4.1 B**). A 1000 U/mL HRP stock solution was prepared by reconstituting type VI lyophilized HRP powder (Sigma Aldrich) in deionized (DI) water and stored at -20°C until use. A stock solution of 0.165 M H_2O_2 was made by diluting H_2O_2 (Sigma Aldrich) in DI water and stored at 4°C until use.

For the first crosslinking method, 2º HRP crosslinking, fibrin microthreads were extruded and then crosslinked through a post-processing bath. Fibrin microthreads were extruded into a bath of HBS, stretched, and dried overnight as described earlier to generate UNX microthreads. These microthreads were secured in 1-well plates (Nunc, Thermo Fisher Scientific) by suspending them taught between two slatted polydimethylsiloxane (PDMS) columns placed on the edges of the 1-well plates, as described previously.[54] Approximately thirteen (13) 5 cm long microthreads were suspended in each 1-well plate. Microthreads then underwent post-processing by first hydrating with 30 mL of DI water for 30 m, then replacing DI water with 30 mL of HRP (0.02 U/mL) and H_2O_2 (4.83 μM) solution and incubating at 37ºC on a shaker plate for 4 h. After 4 h, threads were rinsed three times with DI water and dried under tension. An additional control was included, UNX 2º H_2O_2, where microthreads were incubated in a bath containing only H_2O_2 (4.83 μM) solution with no HRP. Without the addition of HRP to catalyze the reaction, these UNX 2º H_2O_2 microthreads are considered uncrosslinked.

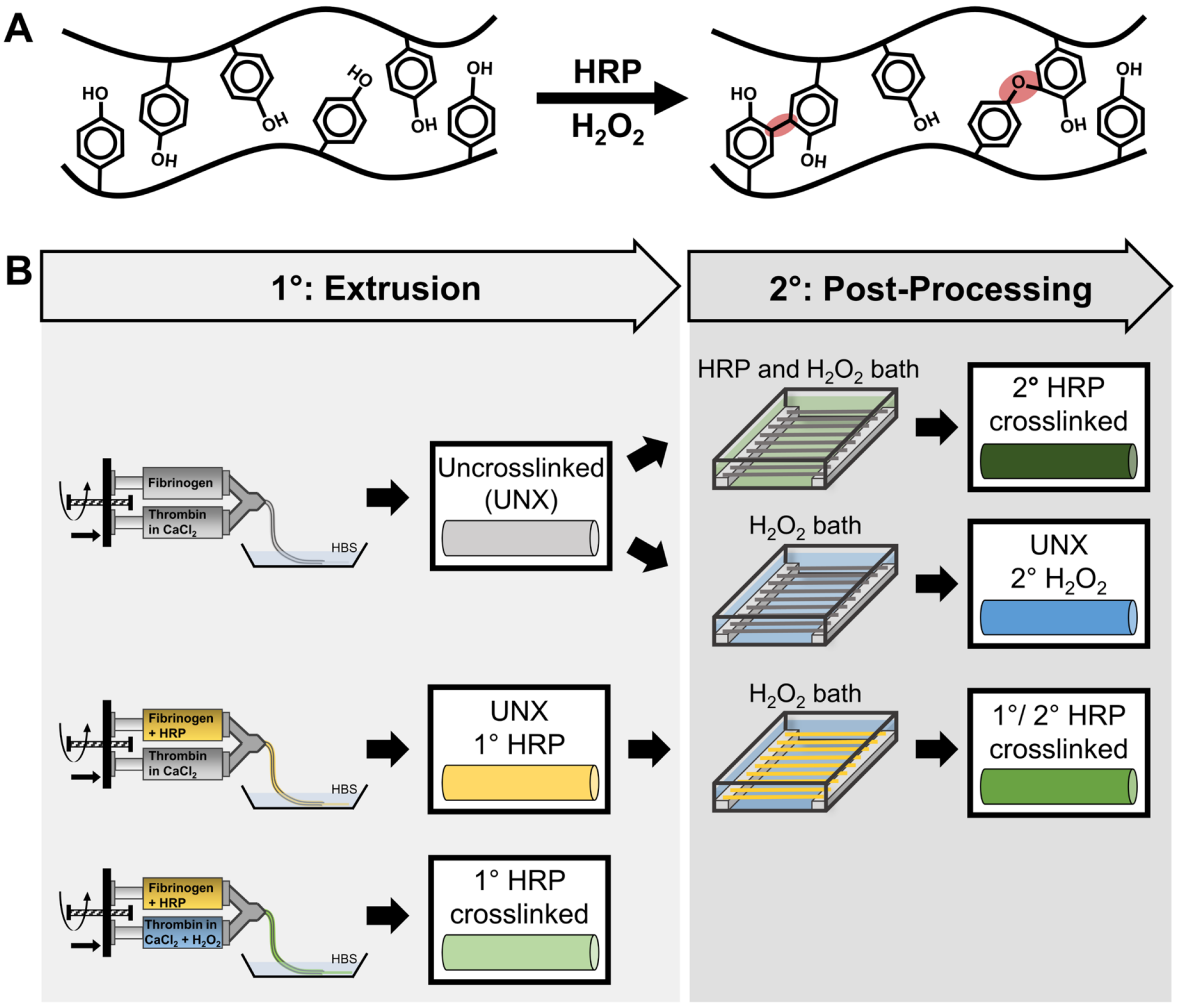

Figure 4.1. Method of HRP-catalyzed dityrosine crosslinking. (A) Schematic of HRP-catalyzed oxidation reaction of tyrosine residues on fibrin, yielding the formation of dityrosine and isodityrosine bonds. (B) Incorporation strategies utilized to crosslink fibrin microthreads. HRP and H2O2 were either included in precursor solutions prior to microthread extrusion, referred to as a primary (1º) incorporation method, or included in a post-processing bath, referred to as a secondary (2º) method.

For the second crosslinking method, 1º/ 2º HRP crosslinking, HRP was added to the fibrinogen solution prior to extrusion (1º), and H_2O_2 was introduced via a post-processing bath (2º). We chose to incorporate HRP into the fibrinogen precursor solution based on previous work crosslinking fibrinogen with hematin, a molecule of similar size and structure to HRP, which showed that fibrinogen maintained its activity with this molecule incorporated.[33] A solution of fibrinogen (70 mg/mL) and HRP (0.22 U/mL) was coextruded with thrombin (6 U/mL) into

HBS. Microthreads were stretched, dried, and affixed within a 1-well plate suspended between PDMS columns. Microthreads were then post-processed by incubation in a H_2O_2 (4.83 μM) bath at 37ºC on a shaker plate for 4 h. After 4 h, threads were rinsed three times with DI water and dried in tension. The intermediary product of fibrin microthreads extruded with HRP (UNX 1º HRP) served as an additional uncrosslinked control for this study.

For the third crosslinking method, 1º HRP crosslinking, both HRP and H_2O_2 were mixed into precursor fibrinogen and thrombin solutions, respectively, immediately prior to microthread extrusion. A fibrinogen (70 mg/mL) and HRP (0.22 U/mL) solution was coextruded with a thrombin (6 U/mL) and H_2O_2 (52.5 μM) solution into HBS. Prior to stretching, threads were incubated at 37ºC in HBS for 4 h, then stretched and dried.

For all methods, the concentration of H_2O_2 in the preparations was calculated to be 10x greater than the theoretical amount required to react with all the tyrosine groups in the fibrin microthreads. The HRP concentration was determined by holding the ratio of H_2O_2: HRP constant, 240 μM H_2O_2: 1 U/mL HRP, based on previously published literature which sought to optimize HRP crosslinking parameters.[36]

4.2.3 Fluorescence spectroscopy

Ultraviolet (UV) fluorescence microscopy using a Zeiss Axiovert 200M microscope (Carl Zeiss, Germany) was performed with uniform exposure time to assess the fluorescence of dityrosine crosslinked scaffolds, where excitation of a dityrosine crosslinked material at 315 nm results in an emission centered at 400 nm.[55] To quantify changes in fluorescence between microthread conditions, pixel intensities of images from randomly selected regions were quantified using ImageJ by converting the blue channel to 8-bit gray scale and determining the mean grey value from 3 regions on the microthread. Mean grey values of the image background were subtracted to normalize data ($n \geq 9$).

4.2.4 Fourier transform infrared spectroscopy

To further characterize HRP mediated isodityrosine bonds in fibrin microthreads, analyses of samples were conducted with Fourier transform infrared spectroscopy (FTIR). Twelve (12) - 2 cm long microthread samples were positioned onto the attenuated total

reflectance (ATR) crystal of a Bruker Vertex 70 instrument (Bruker, Billerica, MA) with a Golden Gate ATC accessory (Specac, Swedesboro, NJ). FTIR absorbance spectra data were collected in the mid-IR range, 4500-800 cm^{-1}, and obtained by averaging 1024 scans. Backgrounds were subtracted from each spectrum. Three batches of microthreads for each condition were analyzed and averaged to obtain a representative spectrum for comparison to other conditions. Baseline correction of absorbance was performed by normalizing data at 4200 cm^{-1}, a region of the spectra with no characteristic peaks. For quantitative comparison of isodityrosine peaks, ratio of the 1040 cm^{-1} characteristic peak to C-H stretch (2955 cm^{-1}) for each sample were compared and statistically evaluated ($n \geq 3$).

4.2.5 Mechanical characterization

Mechanical analysis of HRP crosslinked fibrin microthreads was performed using methods described by our laboratory previously.[6, 56] Briefly, individual microthreads were attached with medical grade silicone adhesive (Factor II, Lakeside, AZ) to vellum paper frames with precut windows of 2.0 cm, which defined the region of loading. The 2.0 cm distance was the space between the adhesive spots on the two edges of the vellum frame window and was used as the initial gauge length for testing. The microthreads adhered to vellum frames were hydrated in phosphate buffered saline (PBS) (pH 7.4, room temperature) for 1 h prior to testing. Th hydrated microthread diameters were measured using a calibrated reticule with a 10x objective on a Nikon Eclipse E600 upright microscope (Nikon, Melville, NY). To define the cross-sectional area, the microthreads were assumed to be cylindrical. Three measurements were taken along the length of each microthread and averaged. The hydrated microthreads within the vellum frame were mounted in the grips of an ElectroPuls E1000 uniaxial testing machine (Instron, Norwood, MA) with a 1 N load cell. Once secured, the two edges of each vellum frame were cut, and the microthreads were uniaxially loaded until failure at 10 mm/min. Force and displacement data were recorded every 0.1 s through each test.

The engineering stress was calculated as the recorded force divided by the initial cross-sectional area of the microthread. The strain was calculated as the increased extension from the initial 2.0 cm gauge length. A MATLAB (MathWorks, Natick, MA) script was written to analyze the ultimate tensile strength, maximum tangent modulus (MTM), strain at failure, and

load at failure for each sample. The MTM was defined as the highest linear region of the stress-strain curve for each sample that corresponds to at least 20% of the total length of each test. Outliers were identified as datum that fell outside the mean ± two standard deviations within each data set and were subsequently removed from further analysis ($n \geq 23$).

4.2.6 Degradation assay

To assess proteolytic degradation of HRP crosslinked microthreads, an *in vitro* plasmin degradation assay was performed, as described previously.[6] Single crosslinked microthreads were cut to 1 cm in length and secured to the bottom of 48-well plates with medical grade silicone adhesive. Each experimental condition was run in triplicate. Brightfield images of microthreads were taken on a Nikon Eclipse TS100 inverted microscope before and after hydration (d_0) in 0.5 mL tris buffered saline (TBS, 25 mM Tris-HCl, 0.9% NaCl, pH 7.5). After 1 h hydration, TBS was replaced with 0.5 mL of 0.5 U/mL human plasmin (EMD Biosciences, San Diego, CA) in TBS and incubated at 37°C. The microthreads were imaged at 0 h, 1 h, 3 h, 6 h, 9 h, 1 d, 2 d, 3 d, and 4 d after addition of plasmin. Each image was analyzed with ImageJ to measure microthread diameter at three different positions along the length of the microthread. Data were plotted as a ratio to the initial diameter (d/d_0) ($n \geq 9$).

4.2.7 Swelling ratio

Fibrin microthread swelling ratios were determined by measuring microthread diameter measurements before and after hydration, using a well characterized tool for evaluating microthread swelling ratio.[4, 6, 7, 10, 57] Microthread diameter measurements made before and after 1 h hydration in TBS (prior to addition of plasmin) in the degradation assay were used to calculate swelling ratio, based on previous work.[6] In a preliminary experiment we observed no appreciable changes in diameter beyond 1 h, and therefore, this was deemed adequate to fully hydrate the microthreads. The three measured diameters for each microthread were averaged. Swelling ratio was defined as the ratio of the wet diameter of a microthreads to its dry diameter (wet/dry diameter) ($n \geq 9$).

4.2.8 Cell culture

C2C12 immortalized mouse myoblasts (ATCC CRL-1772, Manassas, VA) were cultured in complete medium, consisting of a 1:1 (v/v) ratio of high glucose Dulbecco's modified Eagle Medium (DMEM, Gibco, Thermo Fisher Scientific) and Ham's F12 (Gibco), supplemented with 4 mM L-glutamine, 10% fetal bovine serum (FBS, HyClone, Logan, UT), 100 U/mL penicillin, 100 µg/mL streptomycin (Thermo Fisher Scientific, Waltham, MA), and 2.5 µg/mL amphotericin-B (Thermo Fisher Scientific), as described previously.[6] Cells were incubated at 37°C with 5% CO_2 and maintained at a density below 70% confluence using standard cell culture techniques. Cell passage was carried out using 0.25% trypsin-EDTA (Corning, Corning, NY).

4.2.9 Myoblast viability

To facilitate cell attachment, five microthreads were bundled together by hydrating scaffolds dropwise with PBS until microthreads adhered together, as previously described.[58] The microthread bundles were adhered with medical grade silicone adhesive to Thermanox™ coverslips (Thermo Fisher Scientific, Waltham, MA) cut to 2.5 cm by 2.5 cm. Individual coverslips with adhered microthread bundles were placed in 6-well plates, sterilized with ethylene oxide (EtO), and allowed to aerate for at least 24 h to remove residual EtO. Immediately prior to seeding, the microthread bundles were rehydrated with 1 mL of PBS for 1 h. After 1 h, PBS was aspirated and 500 µL of a 250,000 cells/mL cell suspension in complete medium supplemented with 50 µg/mL aprotinin was added to the top of the coverslip. After 4 h of incubation, medium and unattached cells were aspirated from each well immediately followed by replacing with 2 mL of fresh medium to completely submerge the microthread bundles. Seeded microthreads were cultured for 3 d. Cell viability was qualitatively assessed with a LIVE/DEAD staining kit (Molecular Probes, Eugene, OR) according to manufacturer's protocol. After staining, microthreads bundles were removed from the culture coverslips and placed on glass slides for fluorescence imaging, to ensure that only cells that are directly attached to the microthread bundles are imaged. The microthreads were imaged using a fluorescence microscope (Zeiss Axiovert 200M microscope, Carl Zeiss, Germany) ($n \geq 6$).

4.2.10 Statistical analyses

Statistical analyses were performed using Graphpad Prism 7 software (Graphpad, Software, La Jolla, CA). Statistical differences between means of the fluorescence pixel intensity and normalized FTIR peak intensity were determined by one-way ANOVA ($p < 0.05$) with Tukey's multiple comparisons post hoc analysis. When ANOVA assumptions were not met, a non-parametric equivalent Kruskal Wallis test was run with Tukey's multiple comparison post hoc analysis; this was performed to analyze statistical differences between the medians for swelling ratio and mechanical data. Two-way ANOVA ($p < 0.05$) with Tukey's multiple comparisons post hoc analysis was used to evaluate degradation. Values reported are means ± standard error of the mean (SEM) unless otherwise stated. Significance is indicated as * $p \leq 0.05$, ** $p \leq 0.01$, *** $p \leq 0.001$, and **** $p \leq 0.0001$. Additionally, γ indicates significance ($p \leq 0.05$) from all other groups.

4.3 RESULTS

4.3.1 Altering HRP incorporation strategy yields microthreads with varying crosslink density

Three methods of crosslinking fibrin microthreads were investigated by varying the incorporation strategy of crosslinking reagents HRP and H_2O_2. Crosslinking reagents were either 1) incorporated with fibrinogen and thrombin precursor solutions prior to microthread extrusion (1º HRP crosslinking), 2) mixed into a post-processing bath (2º HRP crosslinking), or 3) combined using both extrusion and post-processing strategies (1º/2º HRP crosslinking) (**Figure 4.1 B**). The addition of HRP and H_2O_2 to fibrin microthread extrusion and/or post-processing resulted in the formation of covalent bonds between tyrosine residues of fibrin (**Figure 4.1 A**), which was confirmed by quantitative fluorescence microscopy and FTIR (**Figure 4.2**). UV fluorescence microscopy and subsequent pixel intensity quantification was performed to assess the fluorescence properties of dityrosine crosslinked scaffolds. All fibrin microthread scaffolds crosslinked with HRP and H_2O_2 via primary and/or secondary methods exhibited increased fluorescence compared to UNX controls, indicating an increase in dityrosine crosslink density (**Figure 4.2 A**). Pixel intensity analyses of fluorescence images was performed to further quantify this finding (**Figure 4.2 B**). Pixel intensity quantification suggests increasing dityrosine bond formation in all HRP crosslinked fibrin microthreads compared to UNX microthreads.

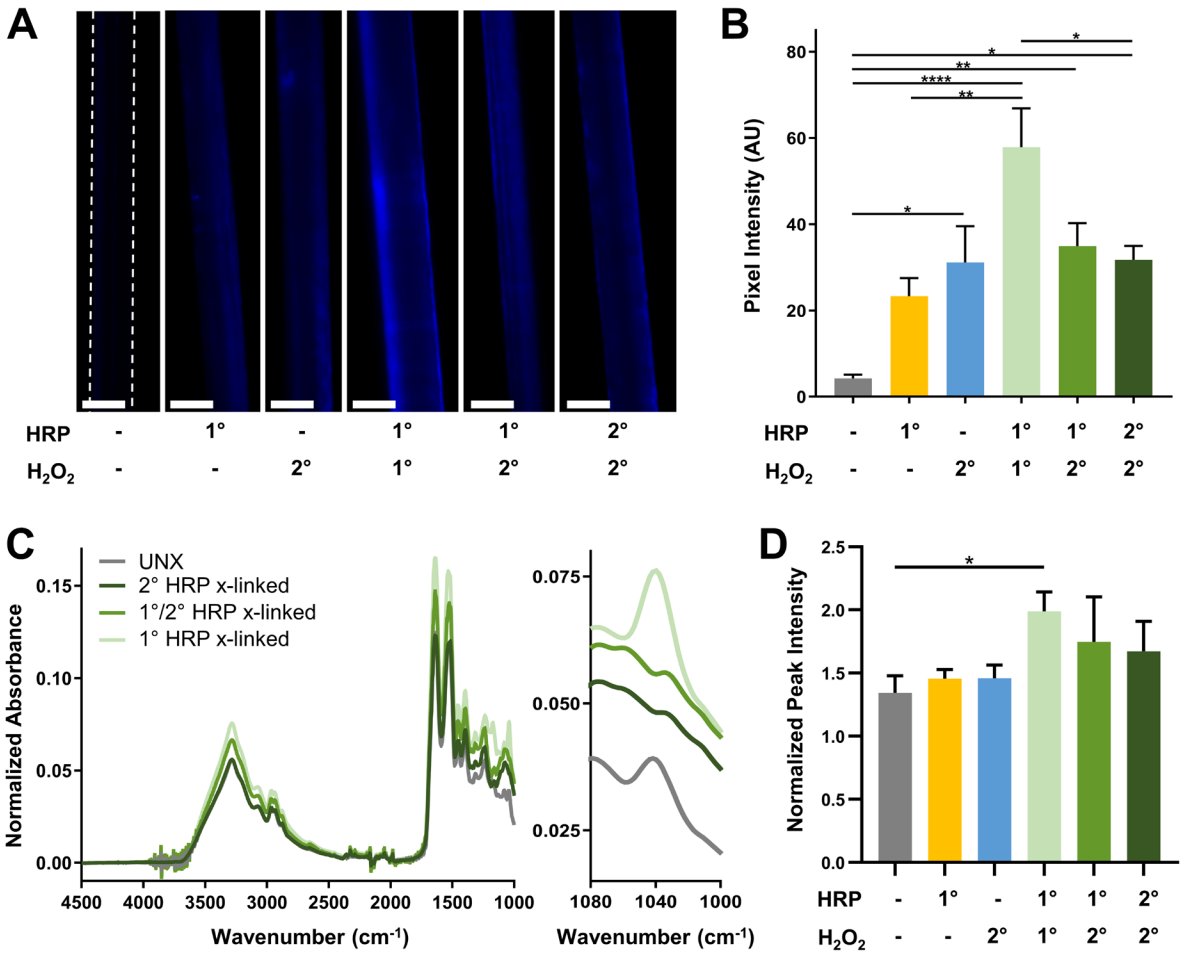

Figure 4.2. Analyses of crosslink density for HRP crosslinked fibrin microthreads. (A) Representative images of microthread fluorescence indicate dityrosine bond formation. (B) Pixel intensity quantification of microthread fluorescence suggests increasing dityrosine bond formation in HRP crosslinked fibrin microthreads. (C) Average normalized FTIR spectrum of control and HRP crosslinked microthreads. The peak at 1040 cm-1, indicative of an ether bond, indicates the addition of isodityrosine bonds in 1º HRP crosslinked microthreads. (D) Peak normalization indicates a significant increase in isodityrosine bonds in 1º HRP crosslinked microthreads. Scale bars are 50 µm.

To further characterize the effect of HRP-catalyzed crosslinking on fibrin microthread secondary structure, FTIR was performed (**Figure 4.2 C**). In addition to dityrosine bonds, HRP-catalyzed crosslinking can yield the formation of isodityrosine, a diphenyl ether bond.[59] Isodityrosine bonds were characterized by the formation of peaks in FTIR spectra centered at 1040 cm^{-1}, indicative of ether bonds. Only 1º HRP crosslinked microthreads exhibited a peak in the FTIR spectra at 1040 cm^{-1} (**Figure 4.2 C**). A significant increase in the relative amount of

this bond compared to C-H stretch (2955 cm^{-1}) was observed in 1º HRP crosslinked microthreads compared to UNX controls, suggesting that only this method of crosslinking microthreads yielded the formation of isodityrosine bonds (**Figure 4.2 D**).

4.3.2 HRP-mediated crosslinking modulates the tensile mechanical properties of fibrin microthreads

Uniaxial tensile testing was performed on HRP crosslinked microthreads to characterize the effect of crosslink density on scaffold mechanical properties. After crosslinking, fibrin microthreads were mounted onto vellum frames, hydrated, and uniaxially loaded until failure to determine their tensile mechanical properties. Characteristic stress-strain curves of UNX microthreads revealed initial toe regions where there was small increase in stress with increasing elongation, similar to previous work evaluating fibrin microthread tensile properties (**Figure 4.3 A**).[7] HRP crosslinked microthreads displayed shorter toe regions with more rapid increase in stress until failure than UNX microthreads (**Figure 4.3 A**). Regardless of whether HRP and H_2O_2 were incorporated during extrusion (1º), post-processing (2º), or a combination of both methods (1º/2º), all crosslinked microthreads exhibited significantly greater ultimate tensile strengths compared to UNX controls ($p < 0.01$) (**Figure 4.3 B**). Ultimate tensile strengths of HRP crosslinked microthreads ranged between 6 and 9.5 MPa. HRP crosslinking yielded varying MTM values depending on HRP and H_2O_2 incorporation strategy (**Figure 4.3 C**). The MTM of 1º/2º HRP crosslinked microthreads was approximately 4.5-fold greater than UNX control threads ($p < 0.0001$) (**Figure 4.3 C**). However, no significant increase in MTM was observed for both 1º and 2º HRP crosslinked microthreads compared to UNX controls. The significant differences between tangent moduli for each HRP crosslinking method suggests the dependence of scaffold mechanical properties on crosslinker incorporation strategy. While all HRP crosslinked microthreads displayed trends in lower strain at failure, 1º/2º HRP crosslinked microthreads was the only crosslinked condition with significantly reduced strain at failure compared to UNX controls ($p<0.001$) (**Figure 4.3 D**).

Moreover, the addition of either HRP or H_2O_2 alone to fibrin microthreads affected scaffold mechanical properties. Both UNX 1º HRP and UNX 2º H_2O_2 microthreads exhibited significantly higher ultimate tensile strength and MTM compared to UNX microthreads (**Figure**

4.3 B-C). Additionally, UNX 1º HRP microthreads possessed significantly reduced strain at failure compared to UNX control microthreads (**Figure 4.3 D**). All mechanical data are summarized in **Table 4.1**.

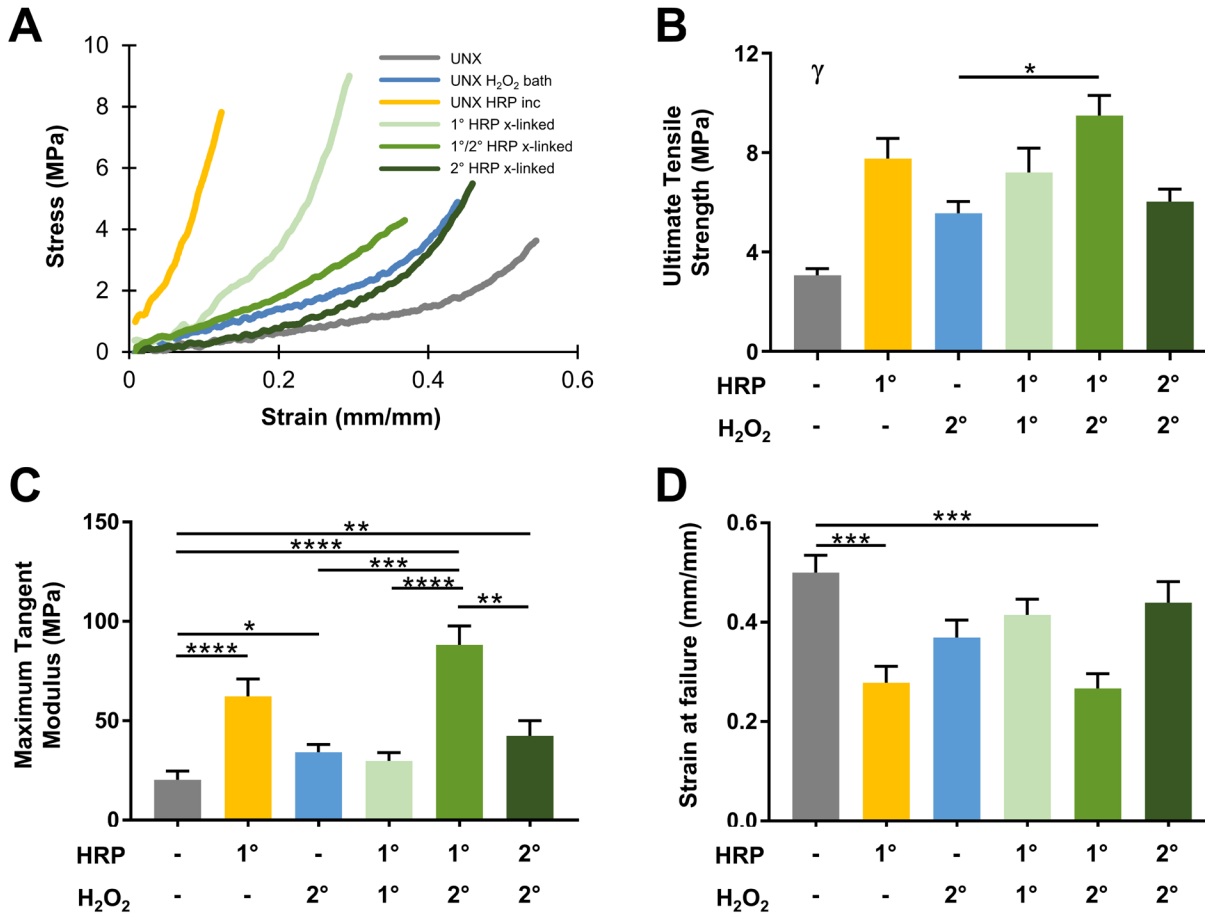

Figure 4.3. Tensile mechanical properties of HRP crosslinked microthreads. (A) Representative stress strain curves from uniaxial tensile testing of fibrin microthreads to failure show that crosslinked microthreads exhibit shorter toe regions with more rapid increase in stress until failure than UNX control microthreads. (B) Ultimate tensile strength of all HRP crosslinked scaffolds regardless of incorporation strategy was increased compared to control UNX microthreads. (C) Strain at failure is significantly decreased in 1º/2º HRP crosslinked microthreads compared to control microthreads. (D) MTM is significantly higher in 1º/2º and 2º HRP crosslinked microthreads compared to control. γ indicates significance ($p \leq 0.05$) from all other groups.

Table 4.1. The mechanical and structural properties of fibrin microthreads crosslinked with HRP. Data presented as mean ± SEM (n #).

	Diameter (μm)		Swelling Ratio	UTS (MPa)	MTM (MPa)	SAF (mm/mm)	Load (mN)
	Dry	Hydrated					
UNX	56.5 ± 9.1 (9)	117.1 ± 18.2 (9)	2.08 ± 0.12 (18)	3.1 ± 1.7 (40)	20.3 ± 28.3 (41)	0.50 ± 0.22 (40)	15.0 ± 3.4 (41)
UNX HRP inc	50.0 ± 10.1 (9)	96.6 ± 23.7 (9)	1.92 ± 0.18 (9)	7.8 ± 4.5 (30)	62.3 ± 46.9 (29)	0.28 ± 0.18 (29)	12.9 ± 6.7 (29)
UNX H_2O_2 bath	48.1 ± 15.8 (9)	86.6 ± 33.5 (9)	1.78 ± 0.13 (9)	5.6 ± 2.7 (34)	34.1 ± 22.3 (33)	0.37 ± 0.21 (36)	16.9 ± 5.9 (34)
1° HRP x-linked	57.5 ± 13.0 (9)	115.7 ± 32.9 (9)	1.99 ± 0.18 (9)	7.2 ± 5.4 (30)	29.9 ± 22.3 (29)	0.41 ± 0.18 (32)	25.8 ± 8.5 (30)
1°/2° HRP x-linked	49.9 ± 10.5 (9)	94.1 ± 22.5 (9)	1.88 ± 0.19 (9)	9.5 ± 4.0 (24)	88.2 ± 45.6 (23)	0.27 ± 0.15 (25)	13.1 ± 4.9 (24)
2° HRP x-linked	44.5 ± 9.7 (9)	82.1 ± 21.9 (9)	1.83 ± 0.14 (9)	6.0 ± 2.7 (30)	42.4 ± 41.6 (30)	0.44 ± 0.24 (32)	19.8 ± 7.0 (31)

4.3.3 Microthread swelling ratio is influenced by HRP incorporation strategy

To further elucidate the effect of HRP-catalyzed crosslinking on microthread crosslink density, the swelling ratios of the scaffolds were analyzed. Microthreads were hydrated in TBS for 1 h and imaged on an inverted microscope before and after hydration to measure microthread diameters. These measurements were used to calculate swelling ratios.[6, 10, 60] A trend of decreased swelling ratios relative to UNX microthreads was observed for all microthread scaffolds processed with HRP and/or H_2O_2, although not all swelling ratios showed significant reductions (**Figure 4.4**). Scaffolds crosslinked by means of post-processing (2º HRP crosslinked microthreads), as well as UNX 2º H_2O_2 microthreads, swelled significantly less than UNX microthreads (**Figure 4.4**). All microthread diameters and swelling ratios are summarized in **Table 4.1**.

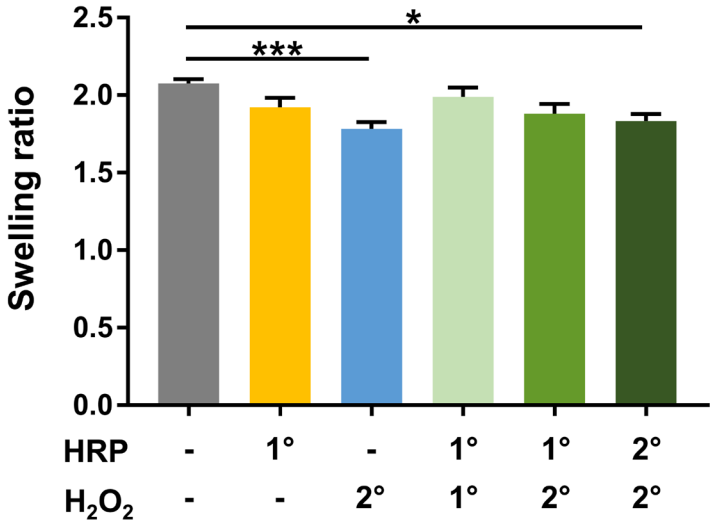

Figure 4.4. Swelling ratios of fibrin microthreads as a function of HRP and H2O2 incorporation strategy. UNX 2º H2O2 and 2º HRP crosslinked microthreads both had significantly lower swelling ratios compared to UNX microthreads, suggesting an increase in crosslink density.

4.3.4 Prolonged degradation of 1º HRP crosslinked fibrin microthreads

The structural integrity of HRP crosslinked microthreads was evaluated by performing an *in vitro* plasmin degradation assay. Plasmin is the primary enzyme responsible for fibrinolysis *in vivo*.[61] Hydrated fibrin microthread diameters were measured before (d_0) and after the addition of

plasmin (d). Diameter measurements of degrading microthreads were made up to 4 d after the addition of plasmin and used to calculate the ratio d/d_0. Degradation profiles of all plasmin-treated microthreads over time exhibited an initial rapid decrease in diameter within the first 24 h, followed by slower degradation through day 4 (**Figure 4.5 A**). In contrast, UNX microthreads not exposed to plasmin (negative control) did not decrease in diameter over time, validating that observed degradation is solely plasmin-mediated (**Figure 4.5 A**).

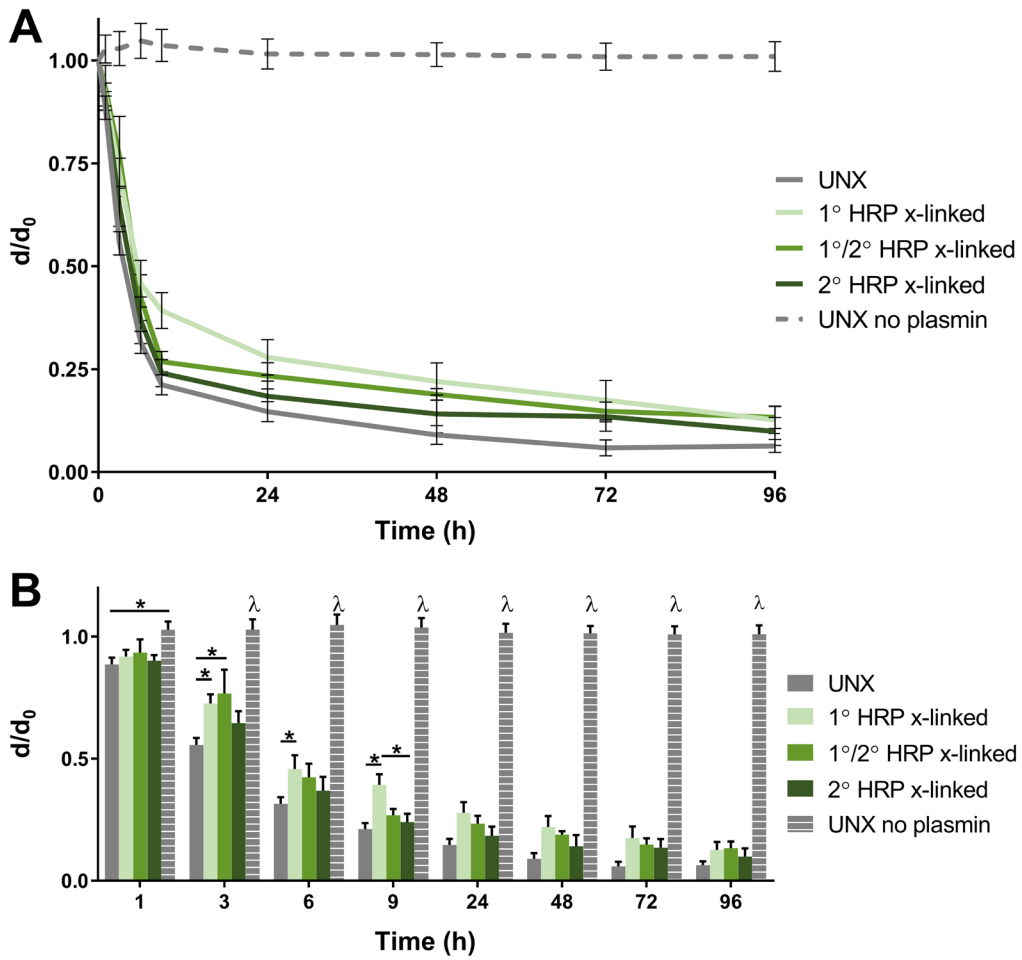

Figure 4.5. *In vitro* plasmin degradation assay. The structural integrity of HRP crosslinked microthreads was evaluated as a function of time by measuring the diameters of degrading microthreads (d) relative to their initial hydrated diameters prior to the addition of plasmin (d0) by calculating the ratio d/d0. (A) Degradation profiles of all plasmin-treated microthreads indicate an initial rapid decrease in diameter. (B) The same data was plotted as a column graph to compare differences between conditions at discrete time points. At all time points after 1 h, UNX microthreads with no plasmin exposure had significantly less degradation than all plasmin-treated conditions. Additionally, 1º HRP crosslinked microthreads had significantly lower degradation than UNX microthreads at early time points before 24 h, suggesting that incorporating crosslinkers during extrusion yields scaffolds with increased resistance to proteolytic plasmin degradation.

To further elucidate differences in degradation between control and crosslinking conditions at discrete time points, the data were also plotted as a column graph (**Figure 4.5 B**). At all time points beyond 1 h, UNX microthreads with no plasmin exposure had significantly less degradation than all other plasmin-treated conditions at that time point (**Figure 4.5 B**). Notably, at 3, 6, and 9 h after the addition of plasmin, 1º HRP crosslinked microthreads had significantly less degradation than UNX microthreads. This suggests that incorporating crosslinkers during microthread extrusion yields scaffolds with increased resistance to proteolytic degradation (**Figure 4.5 B**).

4.3.5 Cellular viability is retained on crosslinked scaffolds

To verify that HRP crosslinked fibrin microthreads were suitable to support extended cell viability, C2C12 murine myoblasts were seeded on the surface of crosslinked microthread bundles. Seeded microthread bundles were cultured for 3 days before Live/dead staining and fluorescence imaging was performed to qualitatively evaluate cell viability. Cells grown on tissue culture plastic (TCP) served as a positive control, and cell growth on TCP and exposed to 70% ethanol for 1 h immediately prior to staining served as a negative control. One hundred percent viability was observed for the live cell TCP positive controls, and no living cells were observed for the negative controls (**Figure 4.6**). To account for fibrin microthread autofluorescence, an unseeded thread bundle also served as a negative control to denote the diffuse background fluorescence observed in several seeded conditions, such as the 1º HRP crosslinked condition (**Figure 4.6**). While it is possible that this background fluorescence may attenuate the ability to visually quantify dead cells, a high degree of cell viability was observed for all control and HRP crosslinked microthread bundles (**Figure 4.6**).

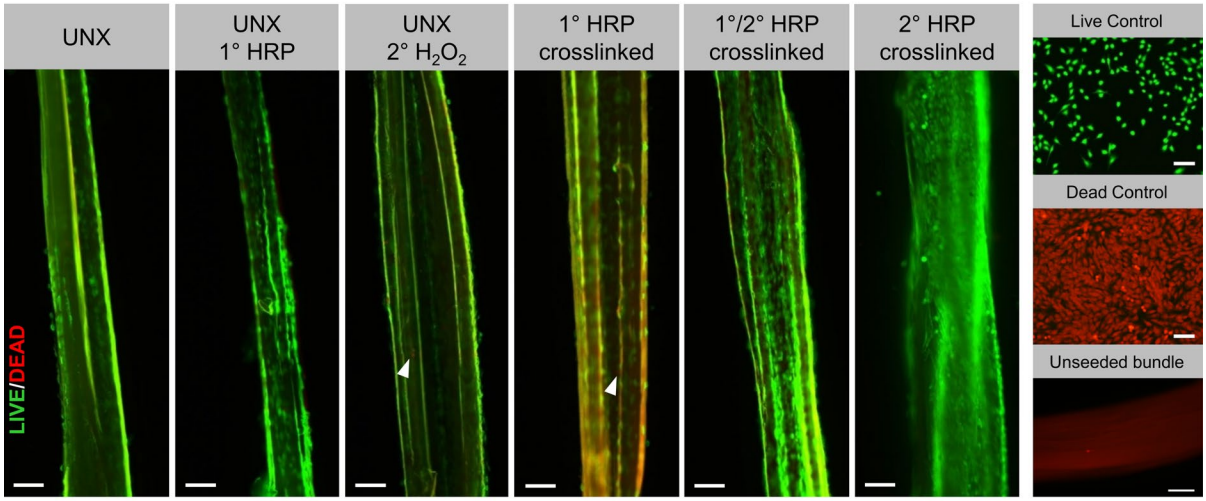

Figure 4.6. Cellular viability on HRP crosslinked fibrin microthreads. C2C12 murine myoblasts demonstrate high viability after 3 d on control and HRP crosslinked fibrin microthread bundles, as demonstrated by fluorescence imaging of live/dead staining. Only a few dead cells could be identified on the surface of microthreads bundles (white arrows). Scale bars are 100 µm.

4.4 DISCUSSION

The goal of the present study was to dityrosine crosslink fibrin microthreads to facilitate tunable scaffold crosslink density, mechanical properties, and degradation rates. While dityrosine crosslinking of fibrin has been achieved by photochemical[30-32] and fenton-like reactions,[33] the use of HRP-catalyzed dityrosine crosslinking had never been investigated for crosslinking fibrin scaffolds. HRP and H_2O_2 mediated crosslinking strategies were varied through primary and/or secondary scaffold modification techniques by mixing reagents with precursor solutions prior to extrusion (1º), by adding reagents into a post-processing bath (2º), or through a combination of both methods (1º/2º). Utilization of primary and/or secondary incorporation strategies yielded microthreads with a range of crosslink densities, evaluated by FTIR and dityrosine fluorescence analyses. Characterization of tensile mechanical properties revealed that all HRP crosslinked microthreads were significantly stronger than UNX control microthreads and exhibited a range of MTM and strain at failure values. Additionally, 1º HRP crosslinked microthreads demonstrated significantly slower plasmin degradation rates than UNX microthreads, suggesting that incorporating HRP and H_2O_2 during extrusion yields scaffolds with increased resistance to proteolytic degradation. Finally, cells seeded on all crosslinked microthreads exhibited a high

degree of viability, demonstrating that HRP crosslinking yields biocompatible scaffolds suitable for tissue engineering applications. Taken together, these findings support the strategic design of engineered fibrin microthreads with a range of biophysical properties, using a facile method of varying crosslinker incorporation strategy. Tunable scaffold mechanics and degradation rates enable the application of fibrin microthreads to a diverse array of target tissues with varying structure, mechanical properties, and functions, such as skeletal or cardiac muscle, tendon, ligament or skin.

Most notably, altering HRP incorporation strategy resulted in fibrin microthreads with varying degrees of crosslink density. In both primary and secondary crosslinking methods, important parameters that govern this reaction including temperature, pH, protein concentration, reaction time, and HRP:H_2O_2 ratio were held constant.[36, 38] To account for differences between the crosslinking methods, concentrations of H_2O_2 were normalized for each method by calculating the concentration needed to react 10 times the theoretical amount of tyrosine in the fibrin microthreads. Quantification of dityrosine fluorescence within fibrin microthreads indicated that 1º HRP crosslinked microthreads had the highest degree of dityrosine crosslinking. We believe the fluorescence gradient observed in 1º HRP crosslinked can be attributed to fibrin autofluorescence and imaging inhomogeneities related to the cylindrical geometries of the scaffolds, rather than an uneven distribution of crosslinking throughout the microthread. The initiation of crosslinking was further substantiated by FTIR analyses, which confirmed the formation of isodityrosine chemical bonds on 1º HRP crosslinked microthreads, which occur between phenol groups of fibrin.[59, 62, 63] Interestingly, 2º and 1º/2º HRP crosslinked microthreads did not appear to contain detectable levels of isodityrosine bonds. Isodityrosine bonds are a less common reaction product of this enzymatic reaction, and may be dependent on factors such as reaction pH, steric hinderance of tyrosine residues within fibrin, and the degree of surface exposure of tyrosines.[64] Taken together, these results confirm that HRP-catalyzed crosslinking of fibrin occurs as hypothesized, and that the crosslinking is dependent on whether HRP and H_2O_2 are incorporated during extrusion or post-processing steps. Future analyses of crosslink density with liquid chromatography and/or mass spectroscopy may provide additional information about this reaction, including the percentage of tyrosines participating in the crosslinking reaction.[25, 65] This data would enable further tuning of this system to optimize crosslink density toward the

precise engineering of an instructive biomaterial scaffold.

Differences in the extent of crosslinking observed between HRP incorporation strategies may likely be explained by the distribution of HRP and H_2O_2 within the microthreads. When crosslinked through primary means, HRP and H_2O_2 were mixed with fibrinogen and thrombin precursor solutions, respectively, immediately prior to extrusion. This ensured a uniform distribution of enzyme and substrate within the fibrin during polymerization, which may facilitate the generation of more phenol radicals. Additionally, this crosslinking method took place during polymerization when we anticipate a higher degree of polymer chain mobility, which is important for permitting radical collisions that result in covalent crosslinks.[36] In contrast, the secondary crosslinking strategy of soaking microthreads in a post-processing bath relied on diffusion of HRP and H_2O_2 from the surface of the material into the microthreads. Fibrin microthreads are dense structures made with markedly higher concentrations of fibrinogen than fibrin hydrogels, which may limit the diffusion of HRP into the microthreads. We hypothesize that this limited diffusion may result in crosslinking occurring predominantly on the surface of the microthreads where it comes in direct contact with the crosslinking bath, significantly reducing the generation of phenolic radicals and thus crosslinks. Additionally, this post-processing technique took place after microthreads underwent polymerization and likely exhibit lower polymer chain mobility, which may also limit radical collisions. This hypothesis has previously been proposed by researchers who crosslinked electrospun gelatin and collagen fibers with glutaraldehyde.[66, 67] They speculated that a lack of glutaraldehyde diffusion into the collagen and gelatin fibers resulted in uneven crosslinking and the generation of a highly crosslinked outer shell on the fiber scaffolds.[66, 67] This hypothesis may explain the discrepancies observed between crosslink density and the swelling ratio of microthreads. Secondary (2º) HRP crosslinked microthreads were the only crosslinked scaffold that had significantly lower swelling ratio than UNX microthreads. This may be due to a high degree of crosslinking along the periphery of the microthread, preventing diffusion of buffer into the scaffold and limiting swelling.[66, 67] While 1º HRP crosslinking generated the most dityrosine and isodityrosine crosslinks, we did not observe a significant decrease in the swelling ratio of 1º HRP crosslinked microthreads compared to UNX controls. This may be a result of the uniform distribution of crosslinks throughout the microthread, allowing buffer to diffuse into the microthread.

HRP crosslinking of fibrin microthreads yielded enhanced biophysical properties, including increased tensile strength and stiffness. HRP crosslinking produced ultimate tensile strengths approximately 2 - 3 times greater than UNX microthreads, depending on crosslinking strategy. These results are consistent with previous literature performing photochemical dityrosine crosslinking on fibrin hydrogel scaffolds. Work by Elvin and colleagues irradiated fibrinogen in the presence of ruthenium trisbipyridyl chloride and sodium persulfate to generate covalent dityrosine crosslinks.[30] They found that crosslinked fibrinogen reached an ultimate tensile strength of 45 kPa, representing a 60% increase compared to their previously reported fibrin hydrogel crosslinked with thrombin and factor XIII.[30, 68] Ultimate tensile strengths of HRP crosslinked microthreads are comparable to UV and carbodiimide crosslinked fibrin microthreads, which ranged from 1.2 - 3.8 times greater than UNX microthreads.[4, 6] Additionally, we found that the MTM values of fibrin microthreads increased by approximately 1.5 - 3.5 times by utilizing varying HRP crosslinking strategies. This is similar to UV crosslinked microthreads, which had MTM values approximately 1.3 – 1.9 times greater than UNX microthreads.[4] Other researchers reported a two-fold increase in fibrin hydrogel compressive stiffness after photochemical crosslinking to initiate dityrosine bond formation.[32] Finally, the conservation of the 1º HRP crosslinked and UNX 1º HRP microthreads structural and mechanical properties suggests that the addition of H_2O_2 to thrombin prior to extrusion did not inhibit the enzyme's functional activity.

Interestingly, the addition of HRP or H_2O_2 alone to fibrin microthreads enhanced the mechanical properties of the scaffolds. UNX 1º HRP microthreads and UNX 2º H_2O_2 microthreads both had significantly increased ultimate tensile strength and MTM values, relative to control UNX microthreads. We hypothesize that trace quantities of native reactive oxygen species (ROS) from serum are among the non-specific molecules within the fibrinogen preparation, and they are activated by the HRP in UNX 1º HRP microthreads to initiate crosslinking.[69] The enhanced mechanical properties of UNX 2º H_2O_2 microthreads may be explained by the peroxide generating free radical side groups in the fibrin, which can trigger non-specific crosslinking events.[70] Alternatively, trace quantities of native serum heme peroxidases such as myeloperoxidase may also be present in the fibrinogen preparation.[71] Myeloperoxidase is present in serum and has been shown to crosslink tyrosine residues in the presence of H_2O_2.[72, 73]

Additional native serum peroxidases may activate H_2O_2 in the UNX 2º H_2O_2 microthreads and initiate dityrosine crosslinking. These hypotheses of crosslinking within UNX 2º H_2O_2 microthreads are further strengthened by observations of a significant increase in dityrosine autofluorescence, as well as a significant decrease in swelling ratio compared to control UNX microthreads. Future work will seek to elucidate the mechanisms by which these HRP and H_2O_2 control microthreads are able to seemingly undergo crosslinking and yield enhanced tensile mechanical properties.

The range of microthread ultimate tensile strengths and moduli permitted by utilizing primary and/or secondary HRP crosslinking strategies enables the application of these scaffolds to an array of target tissues that possess varying structures, mechanical demands, and functions. Tunable mechanical stiffnesses of biomaterial scaffolds can regulate an array of cellular processes including adhesion, proliferation, migration, and differentiation.[74] To further exploit this, we plan on conducting future studies that systematically vary fibrinogen, HRP, and H_2O_2 concentrations; it is well recognized that modifying these concentrations yields scaffolds with a range of mechanical properties including modulus and strength.[35-41] However, an excessive increase of H_2O_2 concentration inhibits the enzymatic activity of HRP, so these modifications must be done with discretion.[36, 38] Additionally, future work to hierarchically assemble these microthreads into complex 3D scaffolds such as composites, braids, and bundles will allow us to further optimize bulk scaffold mechanics and mimic tissue-specific ECM architecture such as skeletal muscle, ventricular myocardium, tendon, ligament, or skin.[17]

HRP-catalyzed crosslinking further mediated the resistance of fibrin microthreads to proteolytic degradation. While fibrin microthreads have robust mechanical properties compared to fibrin hydrogels, fibrin remains susceptible to cell-mediated compaction and rapid degradation by proteinases when implanted *in vivo*.[4, 6, 7, 32] Despite significant increases in crosslink density and tensile mechanical properties, both 1º/2º and 2º HRP crosslinked microthreads did not exhibit increased resistance to proteolytic degradation compared to UNX control microthreads. In contrast, 1º HRP crosslinked microthreads, which exhibited the highest degree of crosslink density, demonstrated prolonged degradation at early time points compared to control microthreads. One possible explanation may be that the increased crosslink density inhibits plasmin from accessing its cleavage sites, which was previously hypothesized for carbodiimide

crosslinked microthreads.[6] This may be a result of the location of dityrosine crosslinks between and within monomer units. Tyrosine residues are most abundant on fibrinogen's β-chain (4.9%) and γ-chain (5.6%), which are both cleaved by plasmin to form fibrin degradation products.[29] HRP-mediated crosslinking appears to have a less pronounced effect on fibrin microthread degradation than carbodiimide crosslinking.[6] This result is desired, as carbodiimide crosslinked microthreads implanted into a murine muscle defects showed minimal signs of degradation at the 60 day terminal time point, suggesting that the high crosslink density limited cell mediated tissue remodeling.[18] For applications in tissue regeneration, scaffold degradation should match the rate of new tissue ingrowth and ECM deposition.[75] HRP-catalyzed crosslinking has been previously shown to prolong the enzyme-mediated degradation of hyaluronic acid (HA)-tyramine and silk-HA composite hydrogels.[37, 41, 42] Tunable scaffold degradation was achieved by altering H_2O_2 concentration,[37] percent concentration of composite components,[41] and delivery method.[42] Future work varying fibrinogen, HRP, and H_2O_2 concentrations within our crosslinked microthreads will allow us to develop more robust changes in scaffold degradation kinetics.

In addition to controlled degradation, tissue engineered scaffolds must support cellular viability and not elicit an immunological response. We qualitatively observed robust myoblast viability after three days of culture on all HRP crosslinked fibrin microthreads. C2C12 myoblasts were chosen as an immortalized musculoskeletal cell line to perform initial cellular viability assessments. These results are consistent with previous literature supporting extended viability and proliferation of cells seeded on or encapsulated within HRP crosslinked scaffolds fabricated from a large range of biomaterials including silk,[35, 41] HA,[50, 53] silk-HA composites,[41] alginate,[44] chitosan,[48] gelatin,[49, 51, 52, 76] and dextran.[47] Future studies to further characterize myoblast seeding efficiency, proliferation, and metabolic activity may better elucidate their interaction with HRP crosslinked fibrin microthreads.

Despite this, concerns remain regarding the *in vivo* immunological response to plant-derived HRP, which could potentially hinder its efficacy as a crosslinker for implantable biomaterial scaffolds.[38, 77, 78] In two *in vivo* rodent models, HRP immunization with subsequent boosters containing Freund's adjuvant elicited the production of antibodies against HRP.[77, 78] While immunization with Freund's adjuvants likely heighted this immune response, the efficacy of HRP-based treatments still must be rigorously evaluated before its clinical application can be

realized. Some groups have addressed this limitation by generating enzyme-free scaffolds whereby HRP is immobilized to magnetic or silica beads.[79, 80] By passing the hydrogel solutions through a syringe filled with beads, immobilized HRP is able to catalyze the crosslinking reaction and subsequently be contained within the syringe, eliminating it from the final crosslinked hydrogel.[79, 80]Alternatively, the use of human peroxidases or oxidoreductases capable of catalyzing phenolic coupling could alleviate the aforementioned concerns with immunogenicity and clinical translation.[38, 81-83] One example is myeloperoxidase, which has been shown to crosslink tyrosine residues in the presence of H_2O_2.[72] Alternative human-derived catalysts such as hematin, obtained through decomposition of hemoglobin, have been evaluated for their ability to catalyze dityrosine crosslinking.[33, 84, 85]

In addition to HRP's immunogenicity, additional concerns regarding cytocompatibility of H_2O_2 have also been raised.[38, 40, 86, 87] Both Gardner et al. and Gulden et al. determined that increasing concentration of and/or exposure time to H_2O_2 *in vitro* resulted in increasing cytotoxicity in murine fibroblasts and C6 glioma cells, respectively.[87] Others demonstrated senescence-like growth arrest upon exposure of human diploid fibroblasts to low concentrations (200 μM) of H_2O_2.[88] We anticipate cytotoxicity resulting from H_2O_2 to be minimal in our HRP crosslinked fibrin microthreads because these scaffolds are crosslinked and subsequently rinsed thoroughly prior to being seeded with cells, removing residual H_2O_2. This is unlike many HRP crosslinked hydrogel scaffolds that encapsulate cells during the crosslinking process, where cells are directly exposed to H_2O_2. Nonetheless, the immunological and cytotoxicity concerns of HRP and H_2O_2 emphasize the importance of thoughtful scaffold design in order to minimize deleterious effects from crosslinking and warrants further investigation. Future scaffold modifications could include careful consideration of HRP and H_2O_2 concentrations and exposure times, the development of enzyme-free systems, and use of human peroxidases or HRP-mimetics.

4.5 CONCLUSIONS

In the present study we demonstrated that fibrin microthread scaffolds can be dityrosine crosslinked using HRP as a catalyst. To our knowledge, this is the first investigation to apply HRP-catalyzed dityrosine crosslinking to fibrin-based scaffolds. We investigated the effect of

varying HRP and H_2O_2 incorporation strategy through primary extrusion and/or secondary post-processing scaffold modification techniques to facilitate the generation of tunable scaffold crosslink density, mechanical properties, and degradation rate. HRP crosslinking of fibrin microthreads resulted in the generation of dityrosine bonds and increased crosslink density. Characterization of tensile mechanical properties revealed that all HRP crosslinked microthreads were significantly stronger than control microthreads and demonstrated a range of moduli and strain at failure values. Scaffolds crosslinked by primary processing demonstrated significantly slower degradation rates than control microthreads, suggesting that incorporating HRP and H_2O_2 during microthread extrusion yields scaffolds with increased resistance to proteolytic degradation. Lastly, cells seeded on HRP crosslinked microthreads retained a high degree of viability. Together, these findings demonstrate that HRP crosslinking yields biocompatible scaffolds suitable for tissue engineering applications. Furthermore, these results demonstrate the strategic engineering of fibrin microthread scaffolds with a tunable range of microthread biophysical properties by a facile method of varying crosslinker incorporation strategy. The ability to generate tunable scaffold mechanics and degradation rates will enable the application of fibrin microthreads for the biomimetic design of engineered tissues with varying tissue architectures, mechanical properties, and functional requirements.

4.6 ACKNOWLEDGMENTS

This work was funded in part by NIH R15 HL137145 (GDP), NSF DGE IGERT 1144804 (MEC), and NSF EEC REU 1559819 (RGM and JWN).

4.7 REFERENCES

1. Carnes, M. E.; Gonyea, C. R.; Mooney, R. G.; Njihia, J. W.; Coburn, J. M.; Pins, G. D., Horseradish Peroxidase-Catalyzed Crosslinking of Fibrin Microthread Scaffolds. *Tissue Eng Part C Methods* **2020,** *26* (6), 317-331.
2. Franchi, M.; Trire, A.; Quaranta, M.; Orsini, E.; Ottani, V., Collagen structure of tendon relates to function. *ScientificWorldJournal* **2007,** *7*, 404-420.
3. Smith, L. T.; Holbrook, K. A.; Byers, P. H., Structure of the dermal matrix during development and in the adult. *J Invest Dermatol* **1982,** *79* (1), 93-104.
4. Cornwell, K. G.; Pins, G. D., Discrete crosslinked fibrin microthread scaffolds for tissue regeneration. *J Biomed Mater Res A* **2007,** *82* (1), 104-12.

5. Chrobak, M. O.; Hansen, K. J.; Gershlak , J. R.; Vratsanos, M.; Kanellias, M.; Gaudette, G. R.; Pins, G. D., Design of a Fibrin Microthread-Based Composite Layer for Use in a Cardiac Patch. *ACS Biomater. Sci. Eng.* **2017,** *3* (7), 1394–1403.
6. Grasman, J. M.; Page, R. L.; Dominko, T.; Pins, G. D., Crosslinking strategies facilitate tunable structural properties of fibrin microthreads. *Acta Biomater* **2012,** *8* (11), 4020-30.
7. Grasman, J. M.; Pumphrey, L. M.; Dunphy, M.; Perez-Rogers, J.; Pins, G. D., Static axial stretching enhances the mechanical properties and cellular responses of fibrin microthreads. *Acta Biomater* **2014,** *10* (10), 4367-76.
8. Page, R. L.; Malcuit, C.; Vilner, L.; Vojtic, I.; Shaw, S.; Hedblom, E.; Hu, J.; Pins, G. D.; Rolle, M. W.; Dominko, T., Restoration of Skeletal Muscle Defects with Adult Human Cells Delivered on Fibrin Microthreads. *Tissue Eng Part A* **2011,** *17* (21), 2629-2640.
9. Cornwell, K. G.; Lei, P.; Andreadis, S. T.; Pins, G. D., Crosslinking of discrete self-assembled collagen threads: Effects on mechanical strength and cell-matrix interactions. *J Biomed Mater Res A* **2007,** *80* (2), 362-71.
10. Pins, G. D., Christiansen, D.L., Patel, R., and Silver, F. H., Self-assembly of Collagen Fibers. Influence of Fibrillar Alignment and Decorin on Mechanical Properties. *Biophys J* **1997,** *73*, 2164-2172.
11. Dunn, M. G., Avasarala, P. N., and Zawadsky, J. P., Optimization of extruded collagen fibers for ACL reconstruction. *J Biomed Mat Res* **1993,** *27*, 1545-1552.
12. Zeugolis, D. I.; Paul, R. G.; Attenburrow, G., Engineering extruded collagen fibers for biomedical applications. *J Appl Polym Sci* **2008,** *108* (5), 2886-2894.
13. Altman, G. H.; Horan, R. L.; Lu, H. H.; Moreau, J.; Martin, I.; Richmond, J. C.; Kaplan, D. L., Silk matrix for tissue engineered anterior cruciate ligaments. *Biomaterials* **2002,** *23*, 4131-4141.
14. Kinahan, M. E.; Filippidi, E.; Koster, S.; Hu, X.; Evans, H. M.; Pfohl, T.; Kaplan, D. L.; Wong, J., Tunable silk: using microfluidics to fabricate silk fibers with controllable properties. *Biomacromolecules* **2011,** *12* (5), 1504-11.
15. Funakoshi, T.; Majima, T.; Iwasaki, N.; Yamane, S.; Masuko, T.; Minami, A.; Harada, K.; Tamura, H.; Tokura, S.; Nishimura, S., Novel chitosan-based hyaluronan hybrid polymer fibers as a scaffold in ligament tissue engineering. *J Biomed Mater Res A* **2005,** *74* (3), 338-46.
16. Funakoshi, T.; Majima, T.; Iwasaki, N.; Suenaga, N.; Sawaguchi, N.; Shimode, K.; Minami, A.; Harada, K.; Nishimura, S., Application of tissue engineering techniques for rotator cuff regeneration using a chitosan-based hyaluronan hybrid fiber scaffold. *Am J Sports Med* **2005,** *33* (8), 1193-201.
17. O'Brien, M. P.; Carnes, M. E.; Page, R. L.; Gaudette, G. R.; Pins, G. D., Designing Biopolymer Microthreads for Tissue Engineering and Regenerative Medicine. *Curr Stem Cell Rep* **2016,** *2* (2), 147-157.
18. Grasman, J. M.; Do, D. M.; Page, R. L.; Pins, G. D., Rapid release of growth factors regenerates force output in volumetric muscle loss injuries. *Biomaterials* **2015,** *72*, 49-60.
19. Hansen, K. J.; Laflamme, M. A.; Gaudette, G. R., Development of a Contractile Cardiac Fiber From Pluripotent Stem Cell Derived Cardiomyocytes. *Front Cardiovasc Med* **2018,** *5*, 52.
20. Zhang, S.; Liu, X.; Barreto-Ortiz, S. F.; Yu, Y.; Ginn, B. P.; DeSantis, N. A.; Hutton, D. L.; Grayson, W. L.; Cui, F. Z.; Korgel, B. A.; Gerecht, S.; Mao, H. Q., Creating polymer hydrogel microfibres with internal alignment via electrical and mechanical stretching. *Biomaterials* **2014,** *35* (10), 3243-51.
21. Somers, S. M.; Zhang, N. Y.; Morrissette-McAlmon, J. B. F.; Tran, K.; Mao, H. Q.; Grayson, W. L., Myoblast maturity on aligned microfiber bundles at the onset of strain application impacts myogenic outcomes. *Acta Biomater* **2019,** *94*, 232-242.
22. Clark, R. A. F., Fibrin and Wound Healing. *Ann N Y Acad Sci*, 355-367.
23. Cornwell, K. G.; Pins, G. D., Enhanced proliferation and migration of fibroblasts on the surface of fibroblast growth factor-2-loaded fibrin microthreads. *Tissue Eng Part A* **2010,** *16* (12), 3669-77.

24. Grasman, J. M., Page, R. L., and Pins, G. D., Design of an In Vitro Model of Cell Recruitment for Skeletal Muscle Regeneration Using Hepatocyte Growth Factor-Loaded Fibrin Microthreads. *Tissue Eng Part A* **2017,** *23* (15-16), 773-783.
25. Partlow, B. P.; Applegate, M. B.; Omenetto, F. G.; Kaplan, D. L., Dityrosine Cross-Linking in Designing Biomaterials. *Acs Biomater Sci Eng* **2016,** *2* (12), 2108-2121.
26. Aeschbach, R.; Amado, R.; Neukom, H., Formation of Dityrosine Cross-Links in Proteins by Oxidation of Tyrosine Residues. *Biochim Biophys Acta* **1976,** *439* (2), 292-301.
27. Raven, D. J.; Earland, C.; Little, M., Occurrence of dityrosine in Tussah silk fibroin and keratin. *Biochim Biophys Acta* **1971,** *251* (1), 96-9.
28. Andersen, S. O., The Cross-Links in Resilin Identified as Dityrosine and Trityrosine. *Biochim Biophys Acta* **1964,** *93*, 213-5.
29. Henschen, A.; Lottspeich, F.; Kehl, M.; Southan, C., Covalent structure of fibrinogen. *Ann N Y Acad Sci* **1983,** *408*, 28-43.
30. Elvin, C. M.; Brownlee, A. G.; Huson, M. G.; Tebb, T. A.; Kim, M.; Lyons, R. E.; Vuocolo, T.; Liyou, N. E.; Hughes, T. C.; Ramshaw, J. A.; Werkmeister, J. A., The development of photochemically crosslinked native fibrinogen as a rapidly formed and mechanically strong surgical tissue sealant. *Biomaterials* **2009,** *30* (11), 2059-65.
31. Bjork, J. W.; Johnson, S. L.; Tranquillo, R. T., Ruthenium-catalyzed photo cross-linking of fibrin-based engineered tissue. *Biomaterials* **2011,** *32* (10), 2479-88.
32. Syedain, Z. H.; Bjork, J.; Sando, L.; Tranquillo, R. T., Controlled compaction with ruthenium-catalyzed photochemical cross-linking of fibrin-based engineered connective tissue. *Biomaterials* **2009,** *30* (35), 6695-701.
33. Ke, Z.; Huang, Q., Haem-assisted dityrosine-cross-linking of fibrinogen under non-thermal plasma exposure: one important mechanism of facilitated blood coagulation. *Sci Rep* **2016,** *6*, 26982.
34. Rodriguez-Lopez, J. N.; Lowe, D. J.; Hernandez-Ruiz, J.; Hiner, A. N.; Garcia-Canovas, F.; Thorneley, R. N., Mechanism of reaction of hydrogen peroxide with horseradish peroxidase: identification of intermediates in the catalytic cycle. *J Am Chem Soc* **2001,** *123* (48), 11838-47.
35. Partlow, B. P.; Hanna, C. W.; Rnjak-Kovacina, J.; Moreau, J. E.; Applegate, M. B.; Burke, K. A.; Marelli, B.; Mitropoulos, A. N.; Omenetto, F. G.; Kaplan, D. L., Highly tunable elastomeric silk biomaterials. *Adv Funct Mater* **2014,** *24* (29), 4615-4624.
36. McGill, M.; Coburn, J. M.; Partlow, B. P.; Mu, X.; Kaplan, D. L., Molecular and macro-scale analysis of enzyme-crosslinked silk hydrogels for rational biomaterial design. *Acta Biomater* **2017,** *63*, 76-84.
37. Lee, F.; Chung, J. E.; Kurisawa, M., An injectable enzymatically crosslinked hyaluronic acid-tyramine hydrogel system with independent tuning of mechanical strength and gelation rate. *Soft Matter* **2008,** *4* (4), 880-887.
38. Lee, F.; Bae, K. H.; Kurisawa, M., Injectable hydrogel systems crosslinked by horseradish peroxidase. *Biomed Mater* **2016,** *11* (1), 014101.
39. Bae, J. W.; Choi, J. H.; Lee, Y.; Park, K. D., Horseradish peroxidase-catalysed in situ-forming hydrogels for tissue-engineering applications. *J Tissue Eng Regen Med* **2015,** *9* (11), 1225-32.
40. Khanmohammadi, M.; Dastjerdi, M. B.; Ai, A.; Ahmadi, A.; Godarzi, A.; Rahimi, A.; Ai, J., Horseradish peroxidase-catalyzed hydrogelation for biomedical applications. *Biomater Sci* **2018,** *6* (6), 1286-1298.
41. Raia, N. R.; Partlow, B. P.; McGill, M.; Kimmerling, E. P.; Ghezzi, C. E.; Kaplan, D. L., Enzymatically crosslinked silk-hyaluronic acid hydrogels. *Biomaterials* **2017,** *131*, 58-67.
42. Kurisawa, M.; Chung, J. E.; Yang, Y. Y.; Gao, S. J.; Uyama, H., Injectable biodegradable hydrogels composed of hyaluronic acid-tyramine conjugates for drug delivery and tissue engineering. *ChemComm* **2005,** (34), 4312-4314.

43. Sakai, S.; Kawakami, K., Synthesis and characterization of both ionically and enzymatically cross-linkable alginate. *Acta Biomater* **2007,** *3* (4), 495-501.
44. Sakai, S.; Hirose, K.; Moriyama, K.; Kawakami, K., Control of cellular adhesiveness in an alginate-based hydrogel by varying peroxidase and H(2)O(2) concentrations during gelation. *Acta Biomater* **2010,** *6* (4), 1446-52.
45. Sakai, S.; Moriyama, K.; Kawakami, K., Controlling Thermo-Reversibility of Gelatin Gels through a Peroxidase-Catalyzed Reaction under Mild Conditions for Mammalian Cells. *J Biomat Sci-Polym E* **2011,** *22* (9), 1147-1156.
46. LaBella, F.; Waykole, P.; Queen, G., Formation of insoluble gels and dityrosine by the action of peroxidase on soluble collagens. *Biochem Biophys Res Commun* **1968,** *30* (4), 333-8.
47. Jin, R.; Moreira Teixeira, L. S.; Dijkstra, P. J.; Zhong, Z.; van Blitterswijk, C. A.; Karperien, M.; Feijen, J., Enzymatically crosslinked dextran-tyramine hydrogels as injectable scaffolds for cartilage tissue engineering. *Tissue Eng Part A* **2010,** *16* (8), 2429-40.
48. Jin, R.; Moreira Teixeira, L. S.; Dijkstra, P. J.; Karperien, M.; van Blitterswijk, C. A.; Zhong, Z. Y.; Feijen, J., Injectable chitosan-based hydrogels for cartilage tissue engineering. *Biomaterials* **2009,** *30* (13), 2544-51.
49. Sakai, S.; Hirose, K.; Taguchi, K.; Ogushi, Y.; Kawakami, K., An injectable, in situ enzymatically gellable, gelatin derivative for drug delivery and tissue engineering. *Biomaterials* **2009,** *30* (20), 3371-7.
50. Toh, W. S.; Lim, T. C.; Kurisawa, M.; Spector, M., Modulation of mesenchymal stem cell chondrogenesis in a tunable hyaluronic acid hydrogel microenvironment. *Biomaterials* **2012,** *33* (15), 3835-45.
51. Wang, L. S.; Chung, J. E.; Chan, P. P.; Kurisawa, M., Injectable biodegradable hydrogels with tunable mechanical properties for the stimulation of neurogenesic differentiation of human mesenchymal stem cells in 3D culture. *Biomaterials* **2010,** *31* (6), 1148-57.
52. Wang, L. S.; Du, C.; Toh, W. S.; Wan, A. C.; Gao, S. J.; Kurisawa, M., Modulation of chondrocyte functions and stiffness-dependent cartilage repair using an injectable enzymatically crosslinked hydrogel with tunable mechanical properties. *Biomaterials* **2014,** *35* (7), 2207-17.
53. Wang, L. S.; Lee, F.; Lim, J.; Du, C.; Wan, A. C. A.; Lee, S. S.; Kurisawa, M., Enzymatic conjugation of a bioactive peptide into an injectable hyaluronic acid-tyramine hydrogel system to promote the formation of functional vasculature. *Acta Biomater* **2014,** *10* (6), 2539-2550.
54. Carnes, M. E.; Pins, G. D., Etching anisotropic surface topography onto fibrin microthread scaffolds for guiding myoblast alignment. *J Biomed Mater Res B Appl Biomater* **2020,** *108* (5), 2308-2319.
55. Harms, G. S., Pauls, S. W., Hedstrom, J. F., & Johnson, C. K. , Fluorescence and rotational dynamics of dityrosine. *J Fluoresc* **1997,** *7* (4), 283-292.
56. Grasman, J. M.; O'Brien, M. P.; Ackerman, K.; Gagnon, K. A.; Wong, G. M.; Pins, G. D., The Effect of Sterilization Methods on the Structural and Chemical Properties of Fibrin Microthread Scaffolds. *Macromol Biosci* **2016,** *16* (6), 836-46.
57. Zeugolis, D. I.; Paul, G. R.; Attenburrow, G., Cross-linking of extruded collagen fibers-A biomimetic three-dimensional scaffold for tissue engineering applications. *J Biomed Mater Res A* **2009,** *89a* (4), 895-908.
58. Proulx, M. K.; Carey, S. P.; DiTroia, L. M.; Jones, C. M.; Fakharzadeh, M.; Guyette, J. P.; Clement, A. L.; Orr, R. G.; Rolle, M. W.; Pins, G. D.; Gaudette, G. R., Fibrin microthreads support mesenchymal stem cell growth while maintaining differentiation potential. *J Biomed Mater Res A* **2011,** *96A* (2), 301-312.
59. Michon, T.; Chenu, M.; Kellershon, N.; Desmadril, M.; Gueguen, J., Horseradish peroxidase oxidation of tyrosine-containing peptides and their subsequent polymerization: A kinetic study. *Biochemistry* **1997,** *36* (28), 8504-8513.

60. Zeugolis, D. I.; Paul, G. R.; Attenburrow, G., Cross-linking of extruded collagen fibers--a biomimetic three-dimensional scaffold for tissue engineering applications. *J Biomed Mater Res A* **2009,** *89* (4), 895-908.
61. Mosesson, M. W., Fibrinogen and fibrin structure and functions. *J Thromb Haemost* **2005,** *3* (8), 1894-904.
62. Gross, A. J.; Sizer, I. W., The oxidation of tyramine, tyrosine, and related compounds by peroxidase. *J Biol Chem* **1959,** *234* (6), 1611-4.
63. Oudgenoeg, G.; Hilhorst, R.; Piersma, S. R.; Boeriu, C. G.; Gruppen, H.; Hessing, M.; Voragen, A. G.; Laane, C., Peroxidase-mediated cross-linking of a tyrosine-containing peptide with ferulic acid. *J Agric Food Chem* **2001,** *49* (5), 2503-10.
64. Fry, S. C., Formation of Isodityrosine by Peroxidase Isozymes. *J Exp Bot* **1987,** *38* (190), 853-862.
65. Malencik, D. A.; Sprouse, J. F.; Swanson, C. A.; Anderson, S. R., Dityrosine: preparation, isolation, and analysis. *Anal Biochem* **1996,** *242* (2), 202-13.
66. Newton, D.; Mahajan, R.; Ayres, C.; Bowman, J. R.; Bowlin, G. L.; Simpson, D. G., Regulation of material properties in electrospun scaffolds: Role of cross-linking and fiber tertiary structure. *Acta Biomater* **2009,** *5* (1), 518-29.
67. Lin, W. H.; Tsai, W. B., In situ UV-crosslinking gelatin electrospun fibers for tissue engineering applications. *Biofabrication* **2013,** *5* (3), 035008.
68. Sierra, D. H.; Eberhardt, A. W.; Lemons, J. E., Failure characteristics of multiple-component fibrin-based adhesives. *J Biomed Mater Res* **2002,** *59* (1), 1-11.
69. Hayashi, I.; Morishita, Y.; Imai, K.; Nakamura, M.; Nakachi, K.; Hayashi, T., High-throughput spectrophotometric assay of reactive oxygen species in serum. *Mutat Res-Gen Tox En* **2007,** *631* (1), 55-61.
70. Kim, J. R.; Yoon, H. W.; Kwon, K. S.; Lee, S. R.; Rhee, S. G., Identification of proteins containing cysteine residues that are sensitive to oxidation by hydrogen peroxide at neutral pH. *Anal Biochem* **2000,** *283* (2), 214-221.
71. Psychogios, N.; Hau, D. D.; Peng, J.; Guo, A. C.; Mandal, R.; Bouatra, S.; Sinelnikov, I.; Krishnamurthy, R.; Eisner, R.; Gautam, B.; Young, N.; Xia, J.; Knox, C.; Dong, E.; Huang, P.; Hollander, Z.; Pedersen, T. L.; Smith, S. R.; Bamforth, F.; Greiner, R.; McManus, B.; Newman, J. W.; Goodfriend, T.; Wishart, D. S., The human serum metabolome. *PLOS ONE* **2011,** *6* (2), e16957.
72. Heinecke, J. W.; Li, W.; Francis, G. A.; Goldstein, J. A., Tyrosyl radical generated by myeloperoxidase catalyzes the oxidative cross-linking of proteins. *J Clin Invest* **1993,** *91* (6), 2866-72.
73. Heinecke, J. W., Tyrosyl radical production by myeloperoxidase: a phagocyte pathway for lipid peroxidation and dityrosine cross-linking of proteins. *Toxicology* **2002,** *177* (1), 11-22.
74. Handorf, A. M.; Zhou, Y.; Halanski, M. A.; Li, W. J., Tissue stiffness dictates development, homeostasis, and disease progression. *Organogenesis* **2015,** *11* (1), 1-15.
75. Nicodemus, G. D.; Bryant, S. J., Cell encapsulation in biodegradable hydrogels for tissue engineering applications. *Tissue Eng Part B Rev* **2008,** *14* (2), 149-65.
76. Lim, T. C.; Toh, W. S.; Wang, L. S.; Kurisawa, M.; Spector, M., The effect of injectable gelatin-hydroxyphenylpropionic acid hydrogel matrices on the proliferation, migration, differentiation and oxidative stress resistance of adult neural stem cells. *Biomaterials* **2012,** *33* (12), 3446-55.
77. Sminia, T.; Delemarre, F.; Janse, E. M., Histological observations on the intestinal immune response towards horseradish peroxidase in rats. *Immunology* **1983,** *50* (1), 53-6.
78. Bardor, M.; Faveeuw, C.; Fitchette, A. C.; Gilbert, D.; Galas, L.; Trottein, F.; Faye, L.; Lerouge, P., Immunoreactivity in mammals of two typical plant glyco-epitopes, core alpha(1,3)-fucose and core xylose. *Glycobiology* **2003,** *13* (6), 427-34.

79. Bae, J. W.; Kim, B. Y.; Lih, E.; Choi, J. H.; Lee, Y.; Park, K. D., In situ formation of enzyme-free hydrogels via ferromagnetic microbead-assisted enzymatic cross-linking. *ChemComm* **2014,** *50* (89), 13710-3.
80. Li, L.; Bae, K. H.; Ng, S.; Yamashita, A.; Kurisawa, M., Peroxidase-immobilized porous silica particles for in situ formation of peroxidase-free hydrogels with attenuated immune responses. *Acta Biomater* **2018,** *81*, 103-114.
81. Claus, H., Laccases: structure, reactions, distribution. *Micron* **2004,** *35* (1-2), 93-6.
82. Jee, J. G.; Park, S. J.; Kim, H. J., Tyrosinase-induced cross-linking of tyrosine-containing peptides investigated by matrix-assisted laser desorption/ionization time-of-flight mass spectrometry. *Rapid Commun Mass Spectrom* **2000,** *14* (16), 1563-7.
83. Kim, Y. J.; Uyama, H., Tyrosinase inhibitors from natural and synthetic sources: structure, inhibition mechanism and perspective for the future. *Cell Mol Life Sci* **2005,** *62* (15), 1707-23.
84. Sakai, S.; Moriyama, K.; Taguchi, K.; Kawakami, K., Hematin is an Alternative Catalyst to Horseradish Peroxidase for In Situ Hydrogelation of Polymers with Phenolic Hydroxyl Groups In Vivo. *Biomacromolecules* **2010,** *11* (8), 2179-2183.
85. Akkara, J. A.; Wang, J. Z.; Yang, D. P.; Gonsalves, K. E., Hematin-catalyzed polymerization of phenol compounds. *Macromolecules* **2000,** *33* (7), 2377-2382.
86. Gulden, M.; Jess, A.; Kammann, J.; Maser, E.; Seibert, H., Cytotoxic potency of H2O2 in cell cultures: impact of cell concentration and exposure time. *Free Radic Biol Med* **2010,** *49* (8), 1298-305.
87. Gardner, A. M.; Xu, F. H.; Fady, C.; Jacoby, F. J.; Duffey, D. C.; Tu, Y.; Lichtenstein, A., Apoptotic vs. nonapoptotic cytotoxicity induced by hydrogen peroxide. *Free Radic Biol Med* **1997,** *22* (1-2), 73-83.
88. Chen, Q.; Ames, B. N., Senescence-like growth arrest induced by hydrogen peroxide in human diploid fibroblast F65 cells. *Proc Natl Acad Sci U S A* **1994,** *91* (10), 4130-4.

Chapter 5: Sustained release of fibroblast growth factor 2 from fibrin microthread scaffolds for skeletal muscle tissue engineering

5.1 INTRODUCTION

A total of 65.8 million Americans suffer from musculoskeletal injuries annually, costing approximately 176 billion dollars to treat.[1-5] Although these injuries are not commonly life threatening, they profoundly impact the quality of life of patients. These traumatic injuries known as volumetric muscle loss (VML) are characterized by a large-scale injury that results in limited functional recovery. Skeletal muscle is capable of endogenous regeneration through activation of resident progenitor cells known as satellite cells, but this ability is greatly reduced in VML. These large-scale injuries destroy native signaling cues and growth factor reservoirs such as the basement membrane and connective tissue, hindering the damaged tissue's ability to direct regeneration. Instead of regenerating functional, contractile muscle, non-functional scar tissue is deposited to fill the void. Current standard of care for VML injuries is autologous tissue transfer, where a muscle flap is excised from an undamaged muscle and grafted into the injury.[6] This procedure is complicated, time consuming, and has exhibited limited ability to restore function.[7, 8] Additionally, approximately 10% of muscle flap procedures result in complications such as infection or donor site morbidity due to tissue necrosis.[6] As such, there is a need for an alternative treatment for VML capable of enhancing functional muscle regeneration.

Growth factors serve to guide regeneration *in vivo* and have been shown to promote functional muscle regeneration when delivered to an injury, thus representing a promising therapeutic strategy for treating VML.[9-19] Fibroblast growth factor 2 (FGF2) is an ideal growth factor for treating skeletal muscle injuries due to its pleiotropic effects on myogenesis, angiogenesis, and innervation.[20] After injury, the basement membrane releases heparan sulfate proteoglycan-bound growth factors such as FGF2.[21-25] FGF2 is responsible for stimulating the proliferation and migration of activated satellite cells,[26-29] and is present in injured muscle tissue

2-8 days after injury and peaks at 6-8 days.[30] FGF2 has also been shown to stimulate endothelial migration and sprouting, as well as pericyte and smooth muscle cell migration.[31] *In vivo*, FGF2 stimulates the formation of more mature vessels than other proangiogenic growth factors such as vascular endothelial growth factor (VEGF).[32] Additionally, FGF2 has been shown to have neurotrophic activity, stimulating the synthesis and secretion of nerve growth factor (NGF) and promoting neuronal survival and outgrowth.[20, 33-36] Taken together, FGF2 is a promising growth factor for treating complex, multi-tissue VML injuries.

Initially, FGF2 was investigated for treating cardiovascular disease, with the goal of stimulating revascularization in ischemic heart regions.[37] However, early Phase II clinical trials delivering FGF2 via bolus intra-coronary or intra-arterial infusion did not demonstrate therapeutic effectiveness at trial end points.[38, 39] This was due to the inability to sustain physiologically relevant levels of FGF2 for the necessary time frame, due to its short *in vivo* half-life on the order of minutes.[37, 40] To mitigate these issues, biomaterial-based strategies have been employed that either chemically immobilize or physically encapsulate growth factors within a polymer matrix, sustaining their release over a clinically-relevant time frame and preventing their denaturation.[41] One method of chemical immobilization uses heparin, a glycosaminoglycan that binds with high affinity to certain growth factors including FGF2.[21, 22, 42, 43] Heparin sulfate is a proteoglycan found in the basement membrane that acts as a reservoir for growth factors essential for myogenesis, including FGF2.[21, 23, 44] Heparan sulfate also significantly enhances FGF2 signaling, binding to both the growth factor and its receptor, forming a ternary complex.[45, 46] Heparin-conjugated scaffolds provide controlled release of growth factors and mimic the presentation of growth factors in the extracellular matrix.[21, 22, 32, 35, 43, 47] A Phase I clinical trial delivered sustained release of FGF2 via heparin-alginate microcapsules implanted in ischemic myocardial regions of patients.[48] Significant improvement in perfusion after 90 days was demonstrated in the high dose FGF2 group compared with controls. A three year follow-up study found patients treated with heparin-delivered FGF2 had significantly lower symptom recurrence, indicating a prolonged revascularization due to sustained heparin-mediated FGF2 release.[49]

More recently, the therapeutic effects of sustained FGF2 release have been applied in early clinical trials to treat ischemic skeletal muscle tissue.[50-52] Two phase I-IIa studies investigating the safety and efficacy of FGF2-incorporated gelatin hydrogel microspheres delivered via

intramuscular (IM) injection to patients with critical limb ischemia (CLI) demonstrated significant improvements in primary endpoints compared to pretreatment.[50, 52] Another pilot clinical study tested the safety and efficacy of IM injection of FGF2-incorporated hydrogels on patients with CLI, and found no adverse events and improved ischemic symptoms compared to pretreatment at the trial end point.[51] While sustained release of FGF2 shows promise in treating ischemic skeletal muscle injuries, its use in treating the more complex, multi-tissue injuries incurred in VML is still actively under investigation.

Several groups have investigated delivering FGF2 to VML defects in preclinical animal models. Multiple biomaterial scaffold strategies to deliver FGF2 to these injuries have been investigated, including delivering FGF2 alone,[11, 12, 17, 53] FGF2 in tandem with cells,[11, 12, 53-55] FGF2 transgenes,[56] and myoblasts overexpressing FGF2.[57] When plasmid and adenoviral vectors encoding FGF2 immobilized in a collagen-gelatin hydrogel were delivered to rat quadriceps injuries, FGF2 gene delivery enhanced the number of CD31+ endothelial cells and CD56+ myotubes compared to matrix alone, indicating enhanced angiogenesis and myogenesis in FGF2-treated wounds.[56] Another study evaluated delivery of FGF2-overexpressing myoblasts encapsulated within alginate spheres to a soleus muscle crush injury in a rat.[57] They found that delivery of FGF2 overexpressing myoblasts increased microvessel density and skeletal muscle cell proliferation at 4 days after injury. Other studies have utilized FGF2 delivery to enhance transplanted myoblast or stem cell survival and proliferation.[53, 55] Co-delivery of FGF2 and human adipose-derived stem cells resulted in functional recovery, revascularization, reinnervation, and minimal fibrosis in a murine VML laceration injury.[53] Co-delivery of FGF2 and myoblasts in gelatin microspheres to a rat muscle injury found significantly enhanced relative gene expression levels of CD31 and myogenin in FGF2/myoblast scaffolds compared to myoblasts alone or unloaded gelatin microspheres.[55] Similarly, polymeric delivery of FGF2 alone to rat VML defects has demonstrated enhanced host cell infiltration and myofiber regeneration,[17] as well as functional recovery.[12] Taken together, FGF2 has shown marked enhancement of myogenesis, revascularization, and reinnervation when delivered alone or in tandem with cells to a VML injury. While this work demonstrates the therapeutic potential of sustained FGF2 delivery from polymer scaffolds, it has primarily utilized hydrogel scaffolds, which lack the mechanical support and aligned contact guidance cues of fiber-based scaffolds.[9, 58, 59] The delivery of FGF2 from polymer

scaffolds with robust mechanical properties and topographic alignment cues has yet to be explored for treating VML injuries.

The goal of the present study is to develop an instructive fibrin microthread scaffold, with inherent topographic alignment cues, to provide a physiologically-relevant sustained release of FGF2. To accomplish this, we passively adsorbed or covalently conjugated heparin to the surface of fibrin microthreads, creating a biomimetic conjugation strategy mimicking FGF2 sequestration in the basement membrane. Fibrin is an ideal scaffold material for incorporating FGF2, as it binds with high affinity to FGF2 and protects it from proteolytic degradation.[60] As such, we also evaluated whether co-incorporation of FGF2 within the fibrin microthread scaffolds by mixing prior to extrusion would promote sustained release of FGF2. We evaluated the effect of both FGF2 incorporation techniques on release kinetics as well as myoblast proliferation and outgrowth. We hypothesized that heparin conjugated and co-incorporated fibrin microthreads would facilitate a sustained physiologic release of FGF2 from the scaffold and enhance *in vitro* myoblast proliferation and outgrowth.

5.2 MATERIALS and METHODS

5.2.1 Fibrin microthread extrusion

Fibrin microthreads were formed by co-extruding fibrinogen and thrombin solutions as described previoulsy.[61] Briefly, fibrinogen isolated from bovine plasma (MP Biomedicals) was dissolved in HEPES (N-[2-Hydroxyethyl]piperazine-N'-[2-ethanesulfonic acid]) buffered saline (HBS, 20 mM HEPES, 0.9% NaCl, pH 7.4) to a concentration of 70 mg/mL and stored at -20°C until use. Thrombin isolated from bovine plasma (Sigma Aldrich) was dissolved in HBS at 40 U/mL and stored at -20°C until use. To create microthreads, fibrinogen and thrombin solutions were thawed to room temperature, and thrombin was mixed with a 40 mM $CaCl_2$ solution to form a 6 U/mL working solution. Equal volumes of fibrinogen and thrombin solutions were taken up separately into 1 mL syringes and inserted into the tip of a blending applicator (Micromedics Inc., St. Paul, MN; SA-3670). The solutions were mixed in the blending applicator and extruded through polyethylene tubing (BD, Sparks, MD) with an inner diameter of 0.86 mm into a 10 mM HEPES buffer bath (pH 7.4) in a Teflon coated pan. Threads were extruded at 0.225 mL/min using a dual syringe pump. After microthreads were incubated for 10-15 min to allow for polymerization, the

scaffolds were removed and stretched to approximately 300% of their initial drawn length and hung overnight to dry under the tension of their own weight.

Fibrin microthreads co-incorporated with FGF2 (co-inc) were created as previously described.[62] Recombinant human FGF2 (Peprotech, Rocky Hill, NJ) stock solution was mixed with 70 mg/mL fibrinogen precursor solution to reach a final FGF2 concentration of 1 μg/mL prior to co-extrusion with thrombin. Microthread extrusion, polymerization, and stretching followed the same procedure as described above for uncrosslinked (UNX) microthreads.

5.2.2. Fibrin film generation

Fibrin films were used to evaluate heparin binding due to their ease of production and analysis. Fibrin films are generated by mixing 1:1 (v:v) 70 mg/mL fibrinogen with 6 U/mL thrombin, the same components coextruded 1:1 through a blending applicator to make fibrin microthreads. A non-adhesive casting surface was created by coating a PDMS sheet with 1% Pluronic-F127 (Sigma Aldrich) in deionized water (dH_2O) for 30 min. Immediately after mixing fibrinogen and thrombin solutions together, 150 μL was cast on top of square vellum frames (1.2 x 1.2 cm), which were placed on top of Pluronic-coated PDMS. After 30 minutes of polymerization gels were carefully peeled off PDMS, rinsed three times for 5 min in dH_2O to de-salt, and dried overnight to form a film.

5.2.3 Heparin conjugation to fibrin microthreads and films

To create a bioinspired conjugation strategy to tether FGF2 to fibrin microthreads, heparin was immobilized to the fibrin microthread surface with or without carbodiimide crosslinking. UNX fibrin microthreads were suspended in 1-well dishes by inserting them between two slatted polydimethylsiloxane (PDMS) bars located on the edges of the dish. Approximately 13 - 5 cm long microthreads were suspended in each 1-well dish. Microthreads to be crosslinked were hydrated in 30 mL of 100 mM sodium phosphate buffer (NaH_2PO_4, pH 7.4, Sigma Aldrich) for 30 min at RT. After 30 min, hydrating buffers were removed and replaced with 100 mM sodium phosphate buffer containing 28 mM 1-ethyl-3-(3-dimethyl aminopropyl) carbodiimide (EDC; Sigma Aldrich), 16 mM N-hydroxysuccinimide (NHS; Sigma Aldrich), and heparin sodium salt derived from porcine submucosa (Calbiochem, Gibbstown, NJ) at a final concentration of 0

(EDC), 10 (EDC HEP 10), 100 (EDC HEP 100), or 1000 µg/mL (EDC HEP 1000). After 2 hrs in crosslinking solution, the EDC/NHS solution was aspirated and microthreads were rinsed three times for 5 min with deionized water (dH_2O). Next, a 0.5% glycine in PBS solution was added to microthreads for 1 hr to extract the NHS reaction product and quench any residual activated carboxylic acid groups.[63, 64] After 1 hr, the glycine solution was removed and two 5 min rinses with dH_2O. Suspended microthreads were allowed to dry overnight in tension.

Control microthreads that remained uncrosslinked were hydrated with phosphate buffered saline (PBS) for 30 min at RT. After 30 min, PBS was removed and replaced with 30 mL of 10 (UNX HEP 10), or 1000 µg/mL (UNX HEP 1000) heparin sodium salt in PBS. After 2 hrs, the heparin solution was aspirated and microthreads were rinsed three times for 5 min with deionized water (dH_2O). Next, a 0.5% glycine in PBS solution was added to microthreads for 1 hr, then removed and two 5 min rinses with dH_2O were performed. Suspended microthreads dried overnight under the tension of their own weight.

A final condition evaluated fibrin microthreads that were first EDC crosslinked and subsequently adsorbed with heparin (EDC then HEP 1000). Microthreads were hydrated in 30 mL of 100 mM sodium phosphate buffer (NaH_2PO_4, pH 7.4, Sigma Aldrich) for 30 min at RT. After 30 min, hydrating buffers were removed and replaced with 100 mM sodium phosphate buffer containing 28 mM EDC and 16 mM NHS for 2 hrs. Next, EDC/NHS solution was aspirated and microthreads were rinsed three times for 5 min with dH_2O. After rinses, a 0.5% glycine in PBS solution was added to microthreads for 1 hr, then removed and two 5 min rinses with dH_2O were performed. Next, 30 mL of 1,000 µg/mL heparin sodium salt in PBS was added to microthreads for 2 hrs, followed by two 5 in rinses with dH_2O. Suspended microthreads dried overnight under the tension of their own weight. Fibrin films underwent the same heparin conjugation method with or without crosslinking described above for the fibrin microthreads.

5.2.4 Toluidine blue staining of heparin conjugated scaffolds

Toluidine blue staining was performed to assess the degree of heparin conjugation to fibrin films. Toluidine blue binds with high affinity to heparin via electrostatic interactions, and is a commonly employed method of assessing heparin incorporation in scaffolds.[43, 65-67] To perform staining, heparin conjugated fibrin films were placed in toluidine blue stain (0.1 M HCl, 2 mg/mL

NaCl, 0.4 mg/mL toluidine blue) for 4 hrs at RT, as previously described.[66] After 4 hrs, films were then rinsed two times with dH_2O and allowed to dry. Dried films were placed on a white backdrop and imaged on a Nikon SMZ-U stereo microscope. To quantify changes in dye uptake between microthread conditions, pixel intensity of the images was quantified using ImageJ by converting images to 8-bit gray scale and determining the mean grey value from three 144 x 144 square pixel regions on the film. Mean grey values of the image background from three 144 x 144 square pixel regions were subtracted to normalize data. All conditions were run in duplicate for each experimental replicate, and a total of three experimental replicates were performed.

5.2.5 Fourier transform infrared spectroscopy

Fourier transform infrared spectroscopy (FTIR) was utilized as an additional method to identify heparin conjugation to fibrin film scaffolds by determining that the carboxyl groups of heparin reacted with the amine groups of fibrin.[43, 65, 68, 69] Dried fibrin film samples were positioned onto the attenuated total reflectance (ATR) crystal of a Bruker Vertex 70 instrument (Bruker, Billerica, MA) with a Golden Gate ATC accessory (Specac, Swedesboro, NJ). FTIR absorbance spectra data were collected in the mid-IR range, 4500-800 cm^{-1}, and obtained by averaging 1024 scans. Backgrounds were subtracted from each spectrum. Three batches of films for each condition were analyzed and averaged to obtain a representative spectrum for comparison to other conditions. Baseline correction of absorbance was performed by normalizing data at 4200 cm^{-1}, a region of the spectra with no characteristic peaks. To assess whether an amide link was formed through heparin conjugation, amide I, II, and III bands were evaluated.[43, 65, 68, 69] Amide I (≈1630 cm^{-1}) peaks are primarily a result of C=O stretching, while the amide II (≈1520 cm^{-1}) peak is a result of N-H bending and C-N stretching.[65, 68, 69] Sulfonated groups and amide III are characterized by a peak at 1240 cm^{-1}.[43, 65, 68, 69]

5.2.6 Determine FGF2 release from fibrin microthreads

To quantify FGF2 release from fibrin microthreads over time, an FGF2-specific enzyme-linked immunosorbent assay (ELISA) was performed. Microthread samples were prepared by gluing ten 1.8 cm-long microthreads of the same condition side-by-side onto a medical grade stainless steel ring (1.8 cm inner diameter) with medical grade silicone adhesive. Each ring was

placed in a separate well of a 6-well dish, where it was blocked in 0.25% bovine serum albumin (BSA) in PBS for 1 hr, then replaced with 1 mL of a 3.5 µg/mL solution of human FGF2 (Peprotech) in sterile PBS. Microthread rings were incubated in FGF2 solution for 16 hrs at RT, then the solution was aspirated from wells and excess FGF2 was carefully dabbed off stainless steel rings. Immediately after removing excess FGF2, 1 mL of sterile PBS was added to samples, each remaining in its own well of a 6-well dish. Plates were wrapped with parafilm and placed in a 37°C oven on a shaker plate for continuous agitation. This marked the beginning of the release assay. To evaluate release of FGF2 over time, PBS from samples was collected at 1hr, 4 hr, 8 hr, 1 day, 2 days, 3 days, 4 days, 5 days, 6 days, and 7 days after initiation of the release study, and stored at -20°C in low-bind microcentrifuge tubes.

After all samples were collected, an FGF2-specific ELISA (Peprotech) was performed in accordance with the manufacturer's instructions. Briefly, ELISA plates were coated with capture antibody overnight, blocked in blocking buffer for 1 hr, and then incubated with appropriately diluted samples for 2 hrs. After specific binding of sample antigens, a detection antibody was added to plates for 2 hrs, followed by enzyme-linked avidin-horseradish peroxidase (HRP) which reacted for 30 minutes. Finally, ABTS substrate was added to produce a soluble, colored product. Plates were read at 405 and 650 nm on a spectrophotometer (SpectraMax 250, Molecular Devices, San Jose, CA) so a wavelength subtraction of 405-650 could be performed before converting optical density readings to FGF2 concentration. Finally, the cumulative release of two control samples were subtracted from other samples; these controls were UNX microthreads that did not receive FGF2 and a stainless-steel ring with silicone glue and no microthreads that was passively adsorbed with FGF2.

5.2.7 Cell Culture

C2C12 immortalized mouse myoblasts (ATCC CRL-1772, Manassas, VA) were cultured in complete medium, consisting of a 1:1 (v/v) ratio of high glucose Dulbecco's modified Eagle Medium (DMEM, Gibco) and Ham's F12 (Gibco), supplemented with 4 mM L-glutamine, 10% fetal bovine serum (FBS, HyClone, Logan, UT), 100 U/mL penicillin, 100 µg/mL streptomycin (Thermo Fisher Scientific, Waltham, MA), and 2.5 µg/mL amphotericin-B (Thermo Fisher Scientific) as described previously.[70] Cells were incubated at 37°C with 5% CO_2 and maintained

at a density below 70% confluence using standard cell culture techniques. Cell passage was carried out using 0.25% trypsin-EDTA (Corning, Corning, NY).

5.2.8 Transwell®-based bioactivity and proliferation assay

To determine the bioactivity of FGF2 released from fibrin microthreads, a Transwell®-based myoblast proliferation assay was developed (**Figure 5.1**). Five 1.5-cm long fibrin microthreads of the same condition were attached to PDMS rings, hydrated in PBS for 1 hr, and sterilized for 2 hrs in 70% ethanol. After sterilization microthread constructs were rinsed three times for 5 min with dH_2O and left to dry in the biosafety cabinet overnight. Sterile microthread constructs were then blocked with 0.25% BSA for 1 hr, then loaded with 1 μg/mL sterile FGF2 in PBS for 16 hrs. Then, FGF2 solution was aspirated and excess solution on microthread constructs was carefully blotted off. Microthread constructs were then placed into 6-well Transwell® inserts. 50,000 C2C12 myoblasts were seeded onto the bottom of 6-well dishes in complete medium for 20 hrs. Then, the medium was removed and replaced with serum free medium (SFM; 1:1 DMEM:F12, 100 I.U. penicillin, 100 μg/mL streptomycin, and 2.5 μg/mL amphotericin B) 4 hrs prior to adding the Transwell® insert to the well. Once the Transwell® insert was placed into the well, an additional 1 mL of SFM was added on top of the microthread construct to ensure it was fully submerged.

After the Transwell® was in the plate for 24 hours, it was then moved to a new 6-well dish, which was seeded 24 hrs prior following the same method as the previous plate. The original 6-well dish was then fixed with ice cold methanol. This was continued for 4 days in culture to evaluate the effect of FGF2 release from microthreads on C2C12 proliferation as a function of time. Controls included cells that remained in complete medium or in SFM, PDMS rings (no microthreads) adsorbed with FGF2, and UNX microthreads with and without adsorbed FGF2. At the end of the experiment, plates from all timepoints were permeabilized, blocked, and stained with Hoechst and a primary antibody against Ki67. Microthreads were imaged using a fluorescent microscope (Zeiss Axiovert 200M microscope, Carl Zeiss, Germany). Nuclei were counted with ImageJ software to evaluate the percent of proliferating cells ($Ki67^+$ count/Hoechst count) × 100). Normalized cell number relative to the SFM negative control was also determined by taking the Hoechst count of each condition and dividing by the SFM Hoechst count at each timepoint.

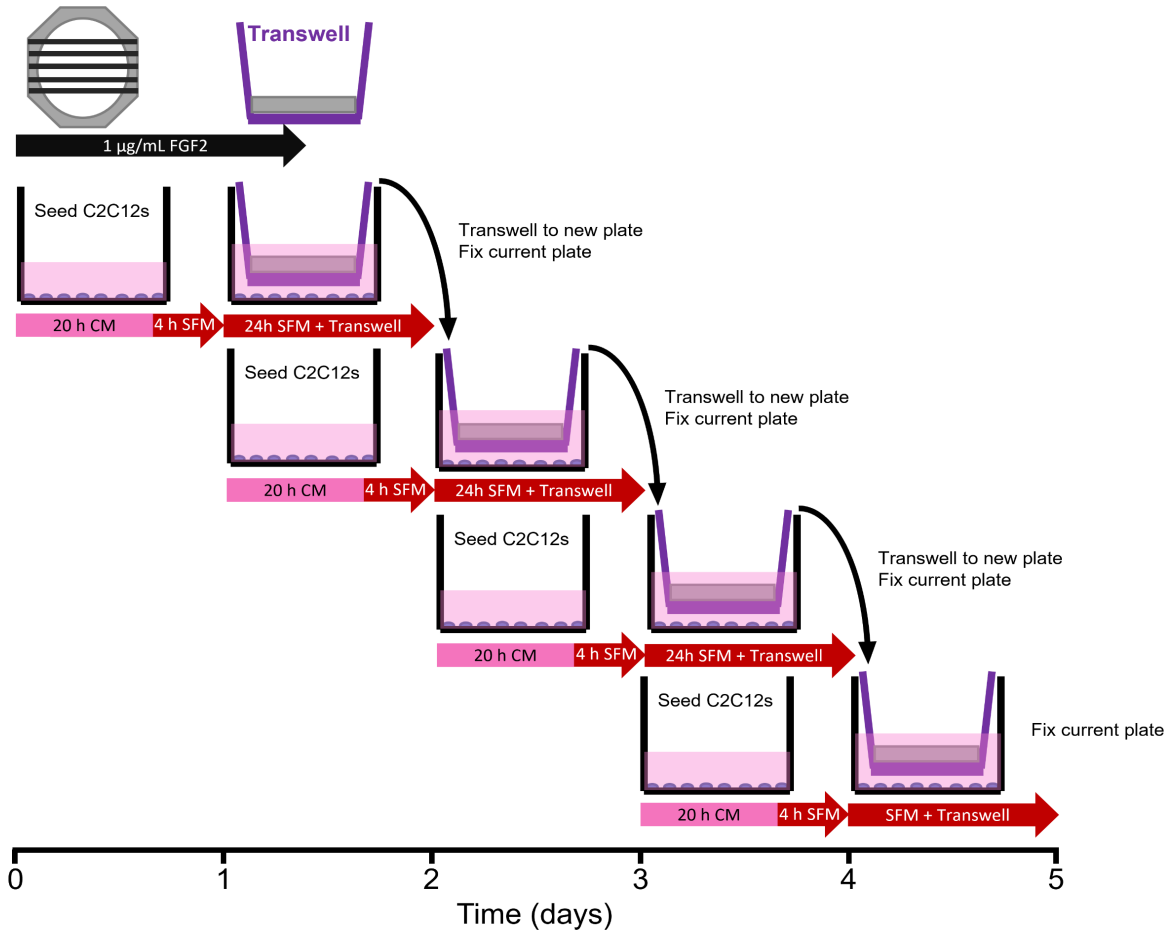

Figure 5.1. Transwell®-based proliferation assay. Myoblasts were seeded in 6-wells 24 hrs prior to addition of the Transwell® insert, which contained the microthread constructs. Medium was switched from complete medium (CM) to serum free medium (SFM) 4 hours prior to the addition of the Transwell®. After 24 hrs in a specific well, the Transwell® insert was moved to a new well, which was seeded 24 hrs prior. The well from which Transwell® was moved from was immediately fixed with ice cold methanol until assay completion, when all wells were stained.

5.2.9 3D myoblast outgrowth assay

A three dimensional (3D) cellular outgrowth assay was performed over a period of 4 days to evaluate myoblast proliferation and migration onto fibrin microthreads, as previously described (**Figure 5.2**).[71, 72] Briefly, rectangular Thermanox™ platforms (3 x 13 mm) were elevated 2 mm above the bottom of a 6-well with PDMS plugs (2 mm diameter) glued with medical grade silicone adhesive. These custom plates were sterilized in 70% ethanol for 2 hrs, rinsed three times for 5 min with dH_2O, and left to dry in a laminar flow hood overnight. Three 1.5 cm long microthreads of the same condition were attached to PDMS rings, hydrated in dH_2O for 1 hr, sterilized in 70%

ethanol for 2 hr, rinsed 3 times for 5 min with dH_2O, and left to dry in a laminar flow hood overnight. Microthreads were blocked with sterile 0.25% BSA in PBS for 1 hr, then passively adsorbed with 1 mL of 0 or 1 µg/mL sterile FGF2 in PBS for 16 hrs. FGF2 was aspirated and ring constructs were carefully blotted off to remove excess FGF2 solution, then transferred to the sterile 6-well dishes containing the elevated Thermanox™ platforms, so microthreads laid centered and flush against the platforms. To ensure they maintained this position, rings were affixed to the bottom of 6-well plates with sterile vacuum grease.

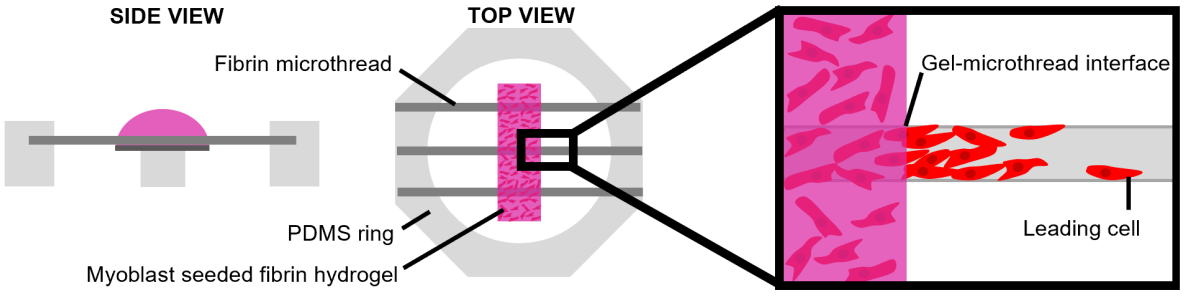

Figure 5.2. Three-dimensional myoblast outgrowth assay. Side and top view of myoblast outgrowth assay, where PDMS rings holding three fibrin microthreads are placed on top of an elevated Thermanox coverslip, onto which a myoblast-seeded fibrin hydrogel is cast. The distance of the leading cell from the gel-microthread interface is measured over the course of four days.

Next, 80 µL of a myoblast-seeded fibrin gel was cast on top of each Thermanox™ platform. These gels were produced by mixing fibrinogen (5.22 mg/mL), calcium chloride (31.25 mM), thrombin (3.25 U/mL), and cell solution (1,500,000 cells/mL) in an 8:1:1:2 ratio. This produced a fibrin gel with a final concentration of 3.5 mg/mL fibrinogen and a final cell concentration of 250,000 cells/mL. Prior to mixing the fibrin gel components, C2C12 myoblasts were loaded with DiI lipophilic tracer (Thermo Fisher Scientific) following manufacturer's instructions to facilitate tracking cellular outgrowth throughout culture. Myoblast-populated fibrin gels were incubated at 37°C for 1 hr to facilitate gel formation, then wells were flooded with 4 mL of SFM supplemented with 20 µg/mL of aprotinin to submerge the entire gel. Each condition was run in duplicate, where each replicate was considered one PDMS ring containing three microthreads of the same condition, with 6 microthread-coverslip interfaces.

To analyze cell outgrowth on the fibrin microthreads, the microthread–coverslip interfaces were imaged daily on a Zeiss Axiovert 200M fluorescent microscope, and the position of the

leading cell was determined based on its distance from the edge of the thread/gel interface, as previously described (**Figure 5.2**).[72] Medium was exchanged every 2 days. After 2 days, C2C12s were reloaded with DiI, as described previously.[72] To quantify the effect of FGF2-loaded microthreads on myoblast outgrowth, we evaluated outgrowth distance and outgrowth rate. Due to regional variations in myoblast concentration throughout the fibrin hydrogel, the microthread-coverslip interfaces at day 1 were evaluated to determine if cell density was too low in that region. All microthreads with low initial cell density in the hydrogel surrounding them were eliminated from further analysis. The outgrowth rate was calculated as the slope of the linear regression curve. After imaging the final day 4 timepoint, microthread constructs were fixed in 4% paraformaldehyde, permeabilized in 0.1% Triton X-100, blocked with 5% BSA in PBS, and stained with Hoechst and a primary antibody against Ki67 (1:400, D3B5; Cell Signaling Technologies, Danvers, MA). Microthreads were imaged using a Zeiss Axiovert 200M fluorescent microscope.

5.2.10 Statistical Analyses

Statistical analyses were performed using Graphpad Prism 7 software (Graphpad, Software, La Jolla, CA). Data was tested for normal distribution using a Shapiro-Wilk test and equal variance using a Bartlett's test. When these assumptions were met, statistical differences between conditions were determined by one-way ANOVA ($p < 0.05$) with Tukey's multiple comparisons post hoc analysis for toluidine blue, ELISA, and outgrowth data. For the Transwell® proliferation assay data, a two-way ANOVA ($p < 0.05$) was performed with Tukey's multiple comparisons post hoc analysis. Values reported are means ± standard error of the mean (SEM) unless otherwise stated. Significance is indicated as * $p \leq 0.05$, ** $p \leq 0.01$, *** $p \leq 0.001$, and **** $p \leq 0.0001$.

5.3 RESULTS

5.3.1 Heparin can be covalently coupled to fibrin microthreads in a dose dependent manner

To create a conjugation strategy that mimics the native sequestration of FGF2 by heparan sulfate proteoglycans in the basement membrane, we covalently conjugated heparin to the surface of fibrin microthread and film-based scaffolds. This was done by employing carbodiimide chemistry, which covalently reacted the free amine groups of fibrin with the activated carboxylic

acid groups on heparin. The dose-dependent conjugation of heparin to fibrin microthreads was evaluated with toluidine blue staining (**Figure 5.3**) and FTIR (**Figure 5.4**). Toluidine blue staining of fibrin films showed an increase in dye uptake with increasing heparin concentration, as anticipated (**Figure 5.3 B**). The same trend was observed when toluidine blue staining was performed on heparin conjugated fibrin microthreads (data not shown). Pixel intensity analyses of images was performed to further quantify this finding on fibrin films (**Figure 5.3 A**). Pixel intensity quantification demonstrates increasing dye uptake with increasing heparin concentration. The highest concentration of heparin evaluated, EDC HEP 1000 films, had significantly higher pixel intensity compared to UNX ($p \leq 0.01$) and EDC ($p \leq 0.05$) films. No statistically significant differences were observed between UNX and EDC films with the same heparin concentrations, indicating that the EDC crosslinking reaction did not increase heparin binding to fibrin microthreads compared to corresponding passively adsorbed UNX conditions.

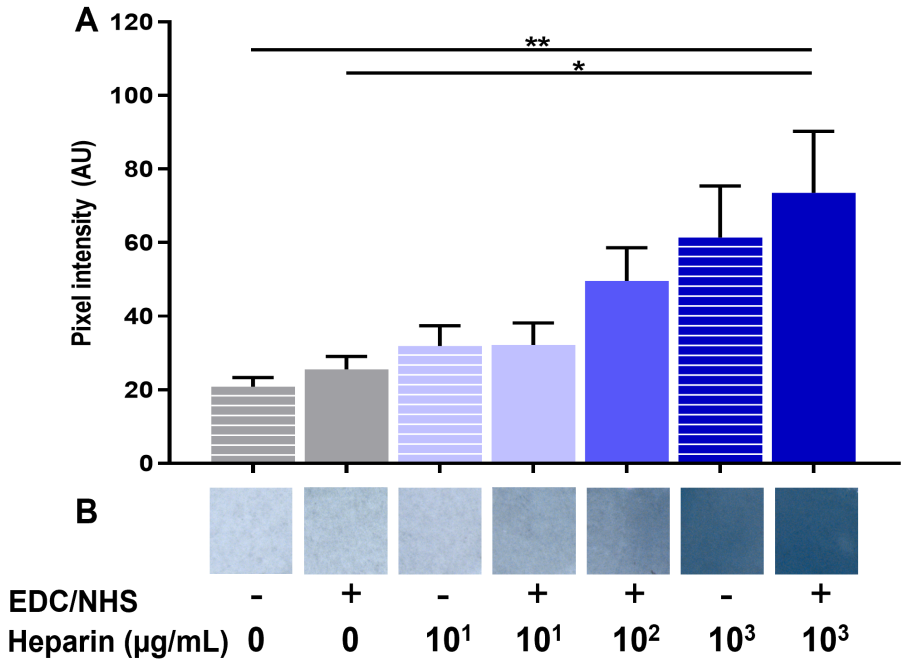

Figure 5.3. Toluidine blue analysis of heparin-conjugated fibrin films. (A) Pixel intensity analysis of UNX passively adsorbed (EDC -) and covalently conjugated (EDC +) fibrin films with varying heparin concentrations stained with toluidine blue. (B) Stereo microscope images of toluidine blue dyed fibrin films, where the blue dye uptake increases with increasing heparin concentration. Statistical significance is indicated by * ($p < 0.05$) and ** ($p < 0.01$) between corresponding groups determined by one-way ANOVA with Tukey's multiple comparisons post hoc analysis ($N \geq 3$ experimental replicates).

To further analyze the binding of heparin to fibrin scaffolds, FTIR analysis was performed to analyze changes in secondary structure as a result of heparin incorporation (**Figure 5.4 A**). Heparin adsorption was characterized by the formation of amide bonds and analyzed by amide I, II, and III peaks centered at 1630 cm^{-1}, 1520 cm^{-1}, and 1240 cm^{-1}, respectively. All scaffold conditions covalently coupled with heparin appeared to have higher amide peaks than UNX scaffolds (**Figure 5.4 B-C**). The adsorption band at 1240 cm^{-1} is also indicative of the presence of sulfonated groups (-SO_3 stretching), which suggests the presence of heparin as it is a sulfated polysaccharide (**Figure 5.4 C**).[69] Taken together, these data may suggest the incorporation of heparin on fibrin films, despite challenges in differentiating variations in overlapping peaks.

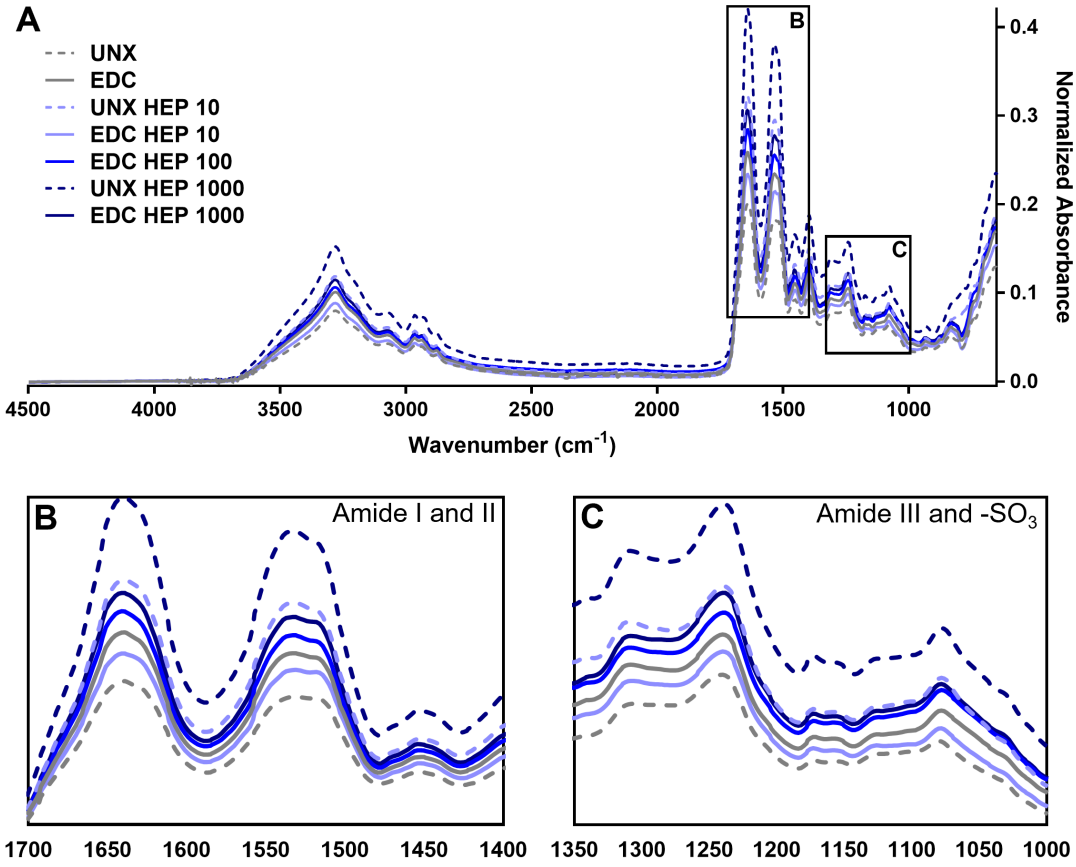

Figure 5.4. FTIR analysis of heparin-conjugated fibrin films. (A) Representative FTIR spectra of fibrin films passively adsorbed or covalently conjugated with heparin. Spectral regions of interest representing (B) Amide I and II, and (C) Amide III and sulfonated groups (-SO_3) (N ≥ 3 experimental replicates).

5.3.2 Sustained release of FGF2 from heparin conjugated and co-incorporated microthreads

Cumulative release kinetics of FGF2 from heparin conjugated and co-incorporated fibrin microthreads were evaluated over a period of 7 days with an ELISA. Co-inc fibrin microthreads demonstrated sustained release of FGF2 over the course of five days, at which point the scaffolds were largely degraded and FGF2 release diminished (**Figure 5.5 A, B**). A linear regression analysis of co-inc microthread release kinetics through 5 days, constrained through the origin, showed that co-inc scaffolds achieved zero-order release kinetics of FGF2 ($R^2 = 0.94$) (**Figure 5.5 B**). Co-inc microthreads had the lowest total quantity of FGF2 release compared to passively adsorbed microthread conditions (**Figure 5.5 C**).

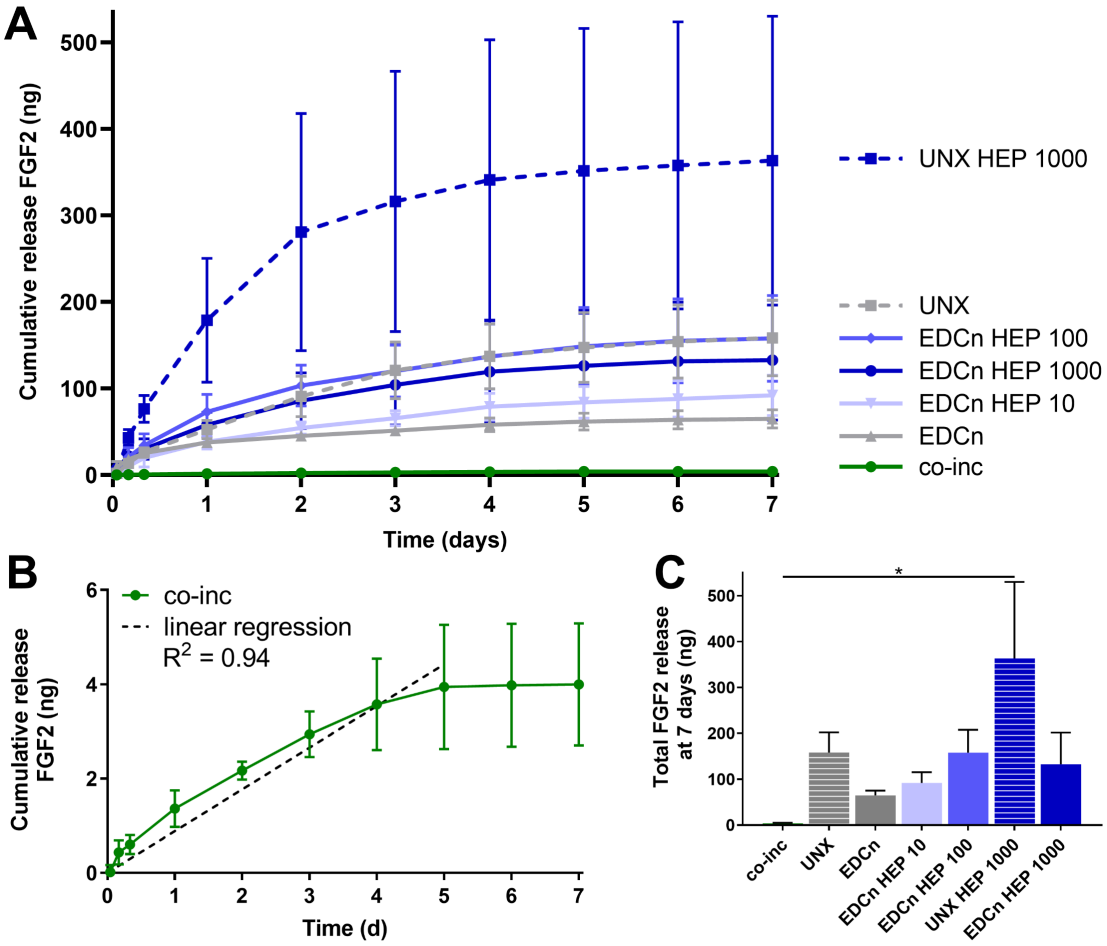

Figure 5.5. FGF2 release kinetics from fibrin microthreads. (A) Cumulative sustained release of FGF2 over one week from heparin conjugated and co-incorporated fibrin microthreads. (B) A linear regression of FGF2 release from co-inc microthreads through day five (dashed line) showed that co-inc scaffolds achieved zero-order release kinetics of FGF2 ($R^2 = 0.94$). (C) Total FGF2 released from fibrin microthreads after one week reveals that UNX HEP 1000 microthreads had the highest total FGF2 release at seven days. Statistical significance is indicated by * ($p < 0.05$) between corresponding groups determined by one-way ANOVA with Tukey's multiple comparisons post hoc analysis ($N \geq 3$ experimental replicates).

Fibrin microthreads passively adsorbed with FGF2 also yielded sustained release of FGF2 over the course of one week (**Figure 5.5 A**). Fibrin microthreads covalently conjugated with heparin via EDC crosslinking appeared to have a higher cumulative release compared to EDC crosslinked threads, although this finding is not significant (**Figure 5.5 C**). EDC HEP 100 and EDC HEP 1000 had similar release profiles, with similar total FGF2 release. Interestingly, UNX microthreads also yielded sustained release of FGF2 over the course of one week, with an average total release comparable to EDC HEP 100 and EDC HEP 1000 microthreads (**Figure 5.5 A, C**). Microthreads passively adsorbed with heparin appeared to have higher total FGF2 release compared to microthreads carbodiimide conjugated with heparin at the same concentration. UNX HEP 1000 microthreads released 2.75-fold more FGF2 than EDC HEP 1000 microthreads. UNX HEP 1000 released a total of 363 ± 289 ng FGF2, while EDC HEP 1000 microthreads released 133 ± 120 ng FGF2. UNX HEP 1000 microthreads also appeared to have a higher initial burst release, where 77% of total FGF2 was released within the first two days, compared to 65% and 64% released from EDC HEP 100 and EDC HEP 1000 microthreads at two days, respectively.

5.3.3 FGF2 released from fibrin microthreads remains bioactive and stimulates myoblast proliferation

A Transwell®-based proliferation assay was performed to determine the bioactivity of FGF2 released from fibrin microthreads over the course of four days. Fibrin microthread constructs in Transwell® inserts were placed in 6-well plates seeded with myoblasts cultured in SFM for 24 hrs before moved to a new myoblast-seeded well (**Figure 5.1**). Plates for each timepoint were fixed and stained with proliferation marker Ki67 to evaluate the effect of FGF2 released from fibrin microthreads on myoblast proliferation over time. At each timepoint, there was no statistically significant difference in the percent of $Ki67^+$ myoblasts between FGF2-loaded fibrin microthread conditions (**Figure 5.6 A**). FGF2-loaded fibrin microthreads appeared to stimulate higher percent $Ki67^+$ myoblasts on days 2-4 compared to SFM and UNX no FGF2 control conditions, although this trend was not statistically significant (**Figure 5.6 A**). We also analyzed proliferation data by looking at each condition as a function of time (**Figure 5.6 B**). The percent of $Ki67^+$ myoblasts significantly increased from day 1 to day 4 in all microthread conditions passively adsorbed with FGF2, including UNX, EDC, and EDC HEP 10, 100, and 1000 microthreads (**Figure 5.6 B**).

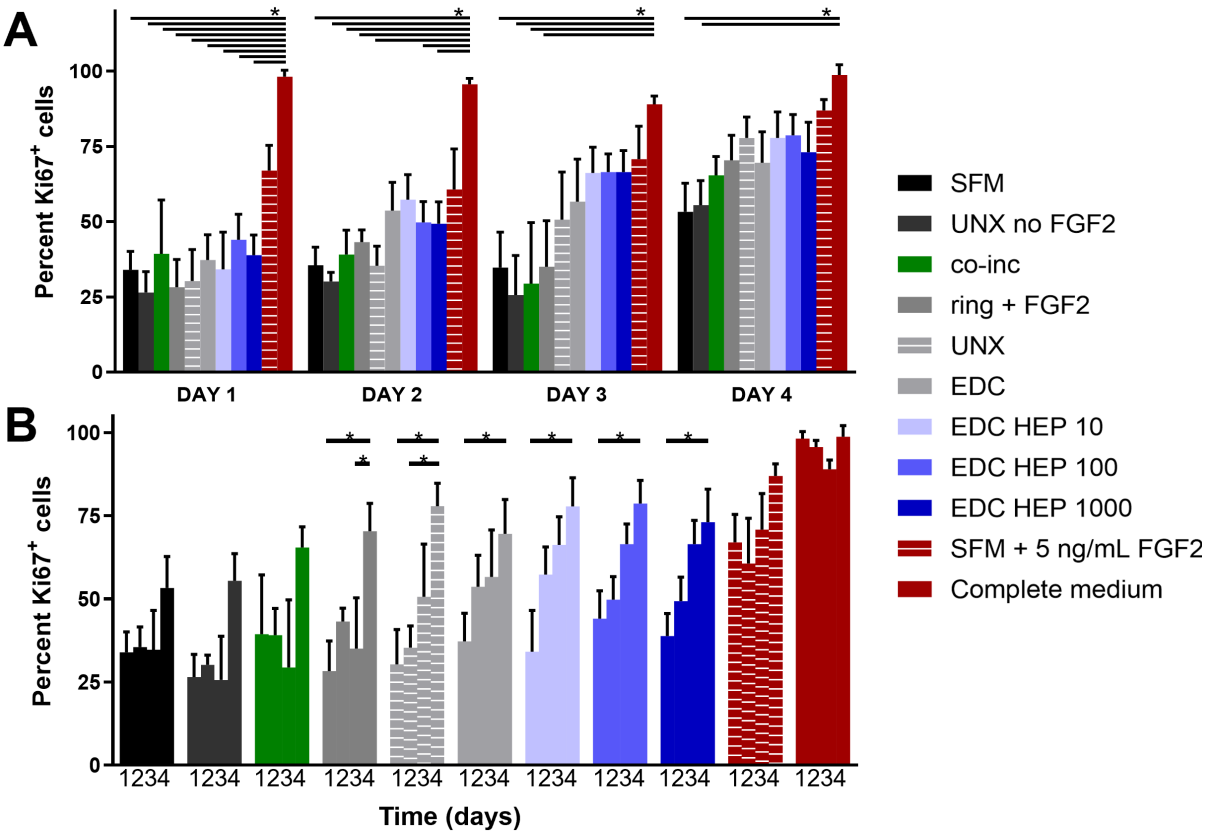

Figure 5.6. Transwell®-based proliferation assay to determine FGF2 bioactivity and its effect on *in vitro* percent Ki67$^+$ myoblasts. (A) Percentage of Ki67$^+$ cells are presented as a function of time and demonstrates trends in increasing percent Ki67$^+$ cells with fibrin microthreads passively adsorbed with FGF2. (B) The same data presented as a function of FGF2 incorporation strategy demonstrates that the percent Ki67$^+$ myoblasts significantly increase with time for all conditions passively adsorbed with FGF2. Statistical significance is indicated by * ($p < 0.05$) between corresponding groups determined by two-way ANOVA with Tukey's multiple comparisons post hoc analysis ($N \geq 3$ experimental replicates).

Further analyses were conducted to evaluate myoblast number normalized to the SFM negative control (**Figure 5.7**). At each timepoint, all microthreads loaded with FGF2, including co-inc and EDC HEP microthreads, had elevated cell numbers relative to the SFM negative control condition (**Figure 5.7 A**). Additionally, normalized myoblast cell numbers remained elevated over the course of four days for FGF2 co-inc and EDC HEP microthreads (**Figure 5.7 B**). Taken together with the Ki67 data, these data demonstrate that FGF2 co-incorporated within or passively adsorbed to fibrin microthreads is released from the scaffolds over time and acts as a mitogen to stimulate myoblast proliferation.

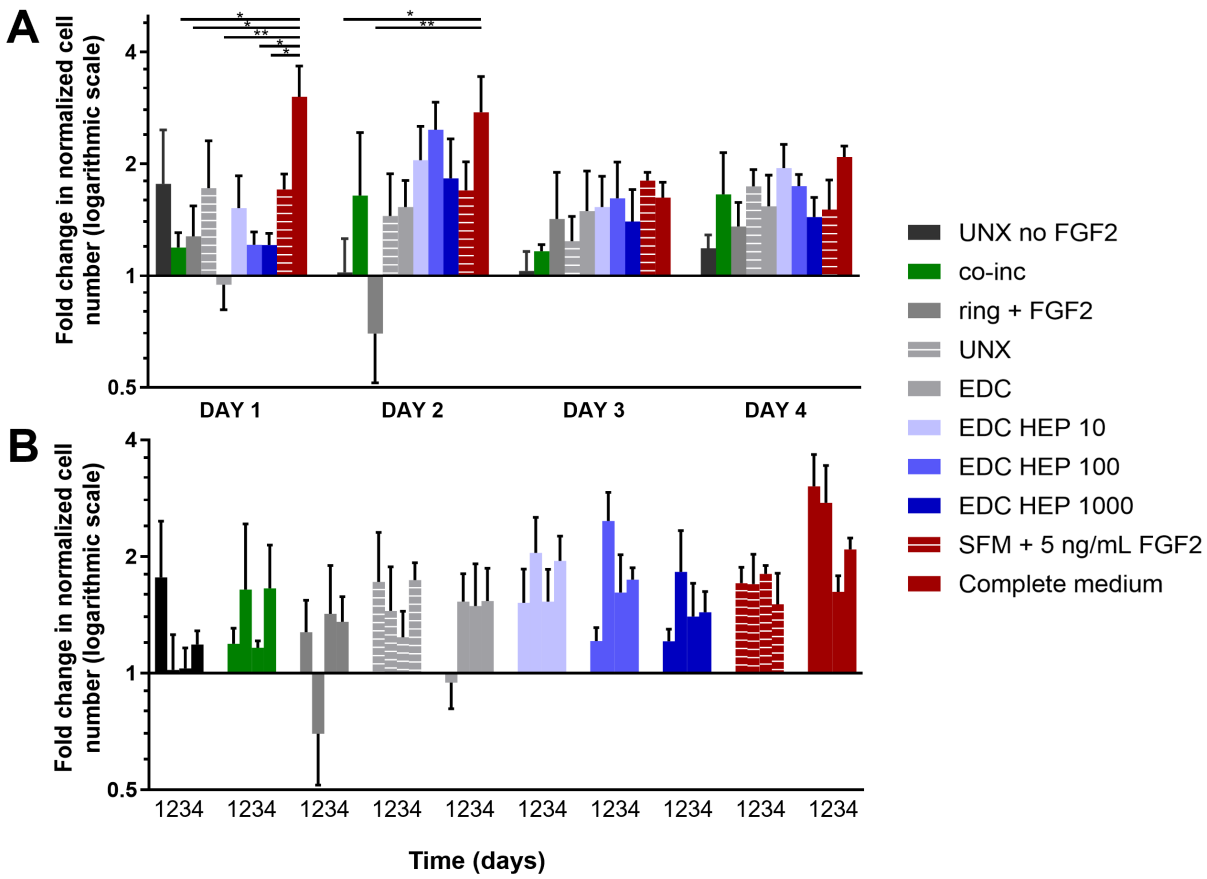

Figure 5.7. Transwell®-based proliferation assay to determine FGF2 bioactivity and its effect on *in vitro* myoblast normalized cell number. (A) Fold change in cell number normalized to serum free media (SFM) cell number as a function of time and (B) the same data presented as a function of FGF2 incorporation strategy indicate increased cell numbers in all FGF2 loaded microthreads. Statistical significance is indicated by * ($p < 0.05$) between corresponding groups determined by two-way ANOVA with Tukey's multiple comparisons post hoc analysis ($N \geq 3$ experimental replicates).

5.3.4 Myoblast outgrowth on FGF2-loaded fibrin microthreads

A cellular outgrowth assay was performed to determine the effect of FGF2-loaded fibrin microthreads on myoblast proliferation and migration over the course of four days. A 3D outgrowth assay developed by our lab was used, where a myoblast seeded fibrin hydrogel is cast over suspended fibrin microthreads so myoblasts can proliferate and migrate onto the microthreads over several days (**Figure 5.2**). For most conditions, outgrowth was observed as several "leading" myoblasts on the microthread, which was followed by a more confluent layer of cells (**Figure 5.8**).

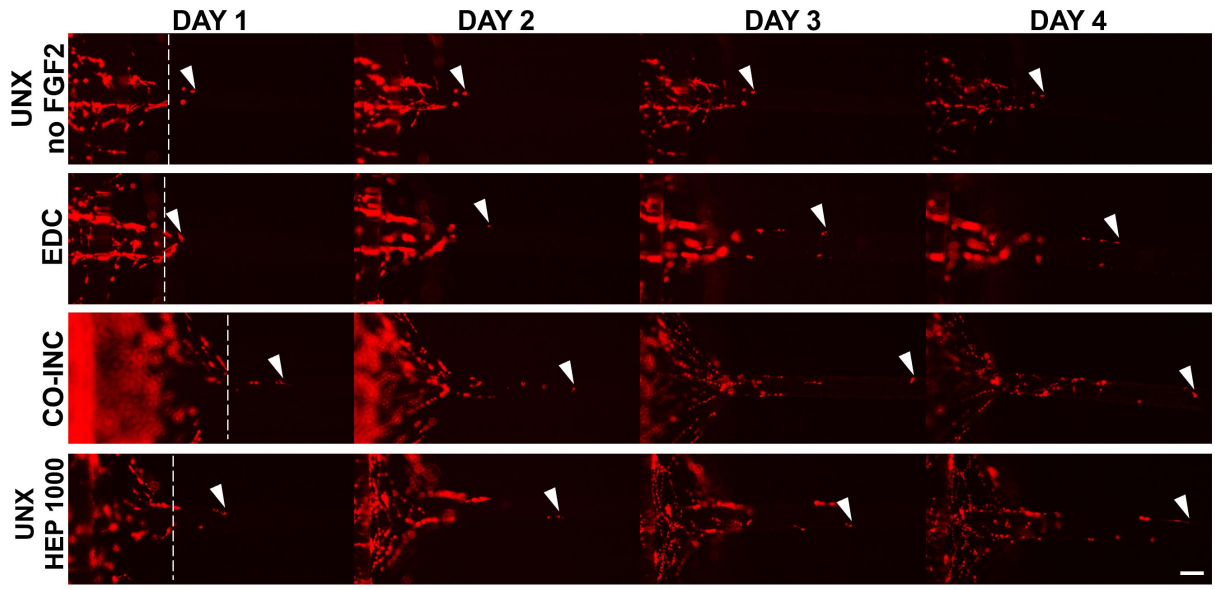

Figure 5.8. Representative images of myoblast outgrowth on fibrin microthreads. Outgrowth on fibrin microthreads with no FGF2 (UNX no FGF2), co-incorporated with FGF2 (co-inc), or passively adsorbed with FGF2 (EDC, UNX HEP 1000). Myoblast outgrowth (visualized with DiI staining) was observed as several "leading" myoblasts furthest out on the microthread, which was followed by a more confluent layer of cells. White dotted lines show the microthread-gel interface at day one. White arrows indicate the leading cell position. Scale bar is 100 µm.

All fibrin microthread conditions evaluated demonstrated a linear outgrowth rate, where outgrowth increased over time (**Figure 5.9 A**). A linear regression analysis of myoblast outgrowth kinetics through day four constrained through the origin, demonstrated that myoblast outgrowth rate was linear on all microthread conditions ($0.92 < R^2 < 0.99$). Myoblast outgrowth rate was highest on co-inc and UNX HEP 1000 microthreads, which both had a rate of 145 µm/day (**Figure 5.9 B**). This is approximately 1.5-fold higher than the rate of myoblast outgrowth observed on UNX microthreads with no FGF2. When comparing microthread conditions loaded with 1000 µg/mL of heparin, UNX HEP 1000 microthreads had the highest outgrowth rate, followed by EDC HEP 1000, and finally EDC then HEP 1000. Similar trends between conditions were observed when evaluating distance of the leading cell at day four (**Figure 5.9 C**). Myoblasts traveled an average of 273 – 614 µm over the course of four days in culture, depending on microthread condition.

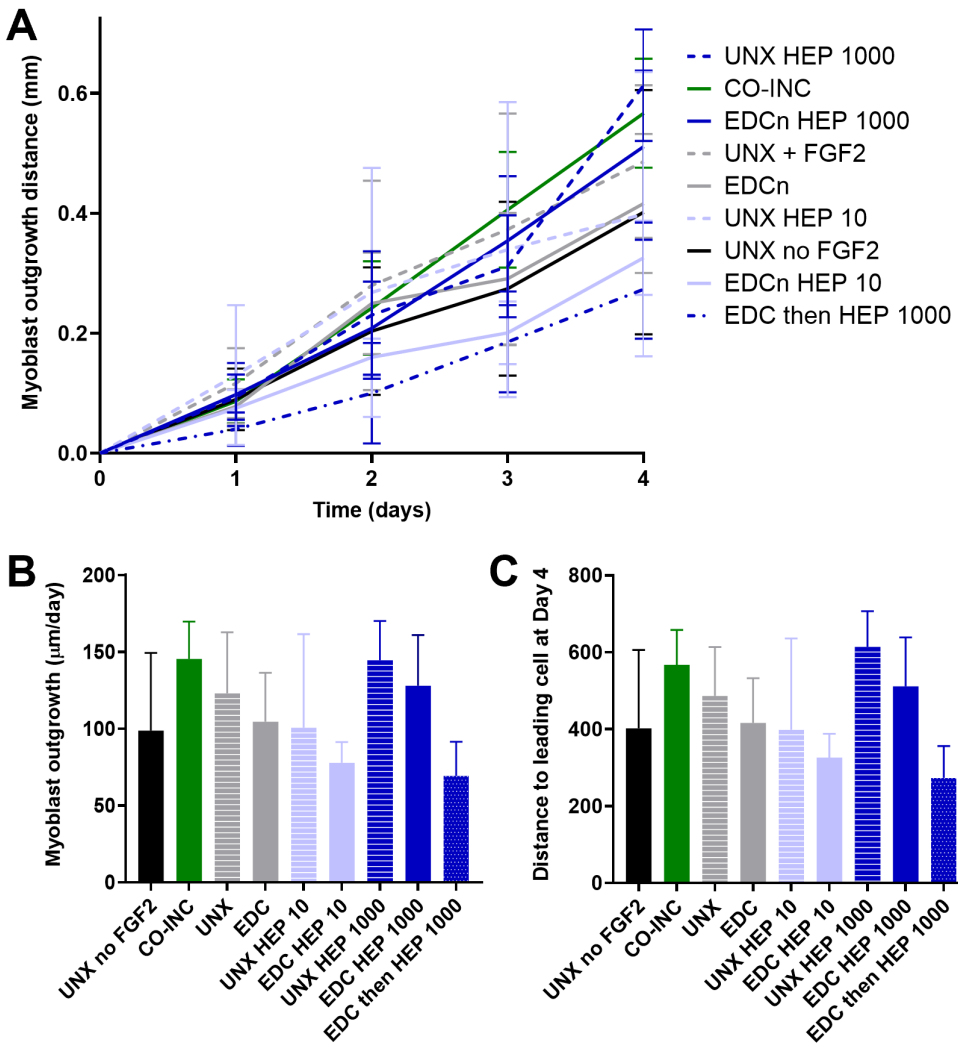

Figure 5.9. Myoblast outgrowth on FGF2-loaded fibrin microthreads. (A) C2C12 myoblast outgrowth distance on fibrin microthreads as a function of time. Linear regression analysis constrained through the origin revealed that myoblast outgrowth rate was linear on all microthread conditions ($0.92 < R^2 < 0.99$). (B) Myoblast outgrowth was calculated as the linear slope over a period of four days and indicates that myoblasts on co-inc and UNX HEP 1000 microthreads had the highest rate of outgrowth. (C) Similar trends were observed when evaluating total distance traveled of the leading cell at day four ($N \geq 3$ experimental replicates).

Myoblast outgrowth is known to be a function of both proliferation and migration.[71, 72] To uncouple the cellular mechanism primarily contributing to the myoblast outgrowth observed on FGF2-loaded fibrin microthreads, we performed Ki67 staining of fibrin microthreads from the 3D myoblast outgrowth assay at the terminal day four timepoint by fixing and removing microthreads from the assay to stain and image (**Figure 5.10 A**). Representative images of Ki67-stained fibrin microthreads display minimal Ki67 staining at four days in conditions with no FGF2, co-

incorporated with FGF2, and passively adsorbed with FGF2 (**Figure 5.10 B-K**). Due to low staining, this result could not be further quantified.

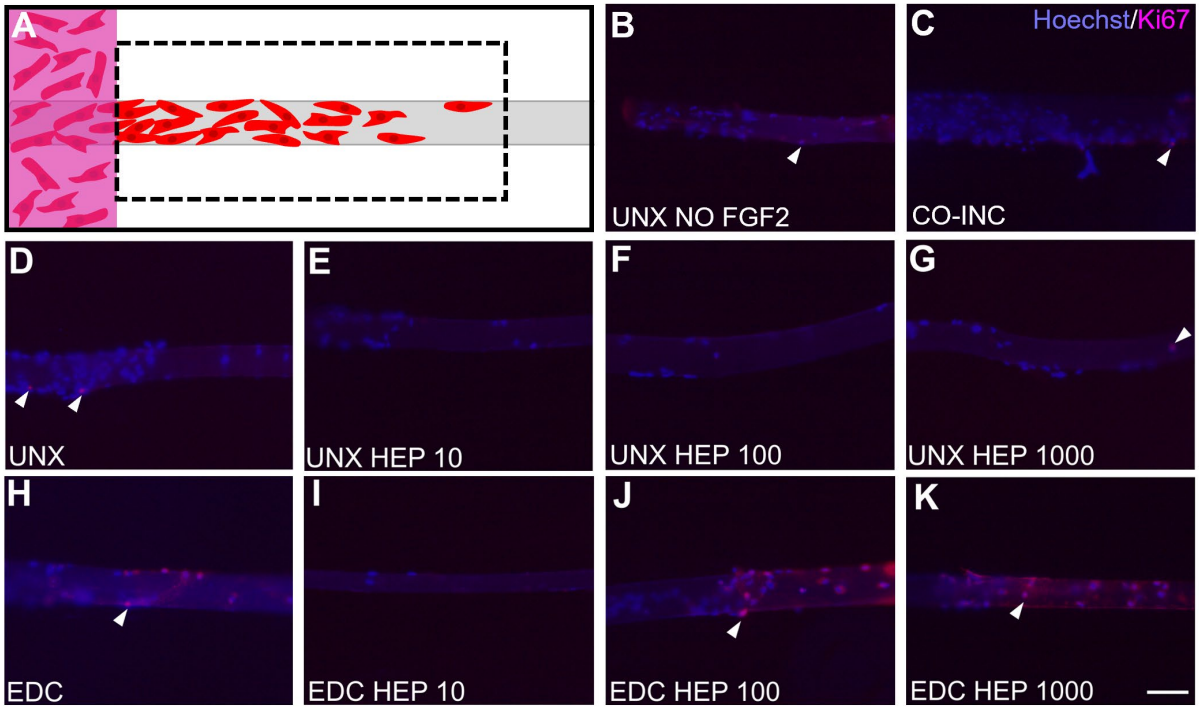

Figure 5.10. Evaluating myoblast proliferation on fibrin microthreads from the 3D outgrowth assay. (A) At the terminal day four timepoint of the myoblast outgrowth assay, microthreads were fixed, removed from outgrowth assays, and stained with Hoechst and Ki67 to determine the extent of myoblast proliferation. (B-K) Representative images of Ki67 stained microthreads, including (B) uncrosslinked microthreads with no FGF2, (C) microthreads co-incorporated with 1 ug/mL FGF2, and (D-K) UNX or EDC crosslinked microthreads with 0 (D, H), 10 (E, I), 100 (F, J), and 1000 µg/mL (G, K) heparin and passively adsorbed with 1 ug/mL FGF2. White arrows indicate sparse $Ki67^{+}$ nuclei microthreads. Scale bar is 100 µm.

5.4 DISCUSSION

The goal of this study was to develop fibrin microthread scaffolds with sustained, physiologically relevant release of FGF2, towards the goal of developing an implantable scaffold to treat VML injuries. To generate fibrin microthreads with sustained release of FGF2, we evaluated two strategies to incorporate the growth factor. First, we covalently conjugated heparin to fibrin microthreads via carbodiimide coupling, creating a biomimetic strategy mimicking FGF2 sequestration in native skeletal muscle ECM (EDC HEP). A second strategy incorporated FGF2 within fibrin microthreads by mixing FGF2 with fibrinogen prior to co-extrusion (Co-inc). Fibrin is ideally suited for incorporating FGF2 because it binds with high affinity to FGF2 and protects

it from proteolytic degradation.[60] Toluidine blue staining and FTIR confirmed heparin conjugation to fibrin microthreads by demonstrating increasing dye uptake and amide bond peaks, respectively. FGF2 release kinetics revealed that fibrin microthreads conjugated with heparin had sustained release over one week and may deliver a higher total amount of FGF2 than EDC microthreads without heparin. Additionally, microthreads co-incorporated with FGF2 achieved zero-order release kinetics over five days. UNX HEP 1000 microthreads had the highest total FGF2 release but appeared to have a greater initial burst release compared to EDC HEP 1000 microthreads, which may be due to the non-covalent attachment of heparin. A Transwell®-based proliferation assay demonstrated that FGF2 released from fibrin microthread scaffolds was bioactive, stimulating myoblast proliferation over a period of four days *in vitro*. Finally, a 3D outgrowth assay demonstrated that co-inc and heparin conjugated microthreads may enhance myoblast outgrowth. Minimal $Ki67^{+}$ myoblasts on these microthreads suggest that outgrowth may be primarily driven by cellular migration. Taken together, these results suggest that heparin conjugated fibrin microthreads create a biomimetic delivery strategy for FGF2 with the added benefit of mechanical strength and alignment cues from a fiber-based scaffold. This work addresses limitations in the field to develop a scaffold that synergistically provides biochemical and biophysical cues simultaneously. The combined effect of fibrin microthread mechanical properties, topographic alignment cues, and FGF2 may be an effective scaffold for treating VML injuries in the future.

We implemented a biomimetic FGF2 delivery strategy by passively adsorbing or chemically immobilizing heparin sodium salt to fibrin microthreads. In passively adsorbed conditions, heparin likely binds to fibrin primarily through electrostatic interactions, as well as the hydrophobic effect and hydrogen bonding.[73] Carbodiimide crosslinking was employed to create a covalent amide bond between the carboxyl groups of heparin and the amine groups of fibrin. We chose to utilize carbodiimide crosslinking because it creates a stable covalent bond and is a "zero length" crosslinker, meaning that no residues from the crosslinking reaction become a part of the bond structure.[74] Previous studies have demonstrated that EDC crosslinking chemistry can be used to covalently couple heparin to polymer scaffolds with free amine groups, including collagen[32, 74-76], fibrin[43, 77], poly-lactic-co-glycolic acid (PLGA)[78] , and poly(ε-caprolactone) (PCL).[65] Toluidine blue staining and FTIR confirmed that heparin was successfully conjugated to fibrin microthreads

in a dose-dependent manner. Both passively adsorbed (UNX HEP) and covalently conjugated (EDC HEP) conditions demonstrated increasing toluidine blue dye uptake and amide bond peaks with increasing concentrations of heparin from 0 to 1000 μg/mL. Other researchers demonstrated an increasing amount of conjugated heparin on collagen scaffolds by increasing the concentration of heparin within the crosslinking solution, which were determined by a toluidine blue or dimethylmethylene blue assay.[74, 76]

In the future, additional methods to modify the degree of heparin conjugation to fibrin microthreads could be investigated. This could include altering the EDC crosslinking reaction time and pH, which have both been shown to effect the degree of heparin conjugation to polymer scaffolds.[65, 74] Despite being an effective conjugation strategy, EDC crosslinking can yield scaffolds that are largely resistant to proteolytic degradation.[18] Upon implantation into a hind limb murine VML defect, EDC crosslinked fibrin microthreads persisted through 60 days post implantation.[18] Ideally, we want these scaffolds to degrade at the same rate of new tissue infiltration, so it can provide provisional structural support yet ultimately be replaced by functional tissue. Alternative, more sophisticated heparin conjugation strategies have also been investigated.[35, 79-82] Sakiyama-Elbert et al. covalently immobilized a bi-domain peptide to fibrin through transglutaminase activity, and then bound heparin to this peptide through non-covalent, electrostatic interactions.[35] This release system was able to sustain the release of FGF2 from heparinized fibrin matrices, improving dorsal root ganglia neurite extension *in vitro*.[81] Finally, the development of synthetic heparin mimetics eliminate concerns with heparin's inherent heterogeneity and allows for the precise control over structure and binding affinity.[73] Maynard et al. developed a tetra-peptide of sulfated amino acids, which bound VEGF with high affinity.[82] Freeman et al. mimicked heparin binding by sulfating the uronic acid groups in alginate and hyaluronan (HA),[83] based on the knowledge that the degree of heparin sulfation influences growth factor binding.[84, 85] They found that sulfated alginate and HA provided strong binding and sustained release of heparin-binding growth factors such as FGF2.[83] Ultimately, tuning of the EDC covalent crosslinking conjugation strategy, or development of more sophisticated linker peptides or heparin mimetics may allow for further tuning of heparin conjugation to fibrin microthread scaffolds.

Co-inc fibrin microthreads yielded sustained release of FGF2 over the course of five days. After a muscle crush injury, FGF2 is detected in wound fluid 2-8 days after injury and peaks at 6-8 days.[30] This emphasizes the need for sustained release of FGF2 over the course of one week to mimic its *in vivo* temporal release. Previous work in our laboratory initially developed this co-incorporation strategy and found that FGF2 was well distributed throughout the fibrin microthreads, but did not evaluate its release kinetics from the scaffold.[62] We found that co-inc microthreads had sustained release of FGF2 over five days, at which point the scaffolds were largely degraded and FGF2 release tapered off. FGF2 binds with high affinity to fibrin and protects it from proteolytic degradation,[60] which we hypothesize is why we these scaffolds achieved sustained release. A linear regression analysis of release kinetics through day five revealed that co-inc scaffolds achieved zero-order release kinetics of FGF2 ($R^2 = 0.94$). Jeon et al. also achieved zero-order release of FGF2 from heparin conjugated PLGA microspheres encapsulated within a fibrin hydrogel.[78] They found that zero-order release kinetics of FGF2 were achieved over four weeks by increasing the fibrinogen concentration to 94 mg/mL or higher. Fibrin microthread scaffolds are analogous to dense hydrogels as they also have a high fibrinogen concentration (35 mg/mL), which may explain how they mediate the controlled release we observed. Because these scaffolds were not crosslinked, we hypothesize that release was mediated by a combination of hydrolysis, bulk degradation, dissociation of FGF2 from fibrin, and diffusion through the microthread. Co-inc microthreads also had the smallest total quantity of FGF2 release which is likely explained by differences in loading strategy.

Fibrin microthreads covalently conjugated with heparin yielded sustained release of FGF2 over the course of one week, where higher heparin conjugation resulted in a more sustained release and a higher total amount of FGF2 released. This result is similar to work by other researchers who conjugated heparin to polymer scaffolds to mediate the release of FGF2[43, 78, 86] and other heparin-binding growth factors.[76, 77, 87, 88] Younesi et al. also showed that increasing the concentration of heparin in the EDC crosslinker bath from 0 to 10 mg/mL created a more sustained release of platelet-derived growth factor (PDGF) from collagen microthreads over the course of 15 days, with the majority of release taking place in the first week.[76] Yang et al. observed similar sustained release of FGF2 from a fibrinogen scaffold conjugated with heparin via EDC crosslinking.[43] They found only 40% of FGF2 released from their scaffold by one week, and

sustained release of FGF2 continued up to three weeks. Because this study utilized the same scaffold biomaterial (fibrin), heparin conjugation strategy (EDC), and growth factor (FGF2) as this work, we hypothesize it is very likely that FGF2 remains bound to heparin conjugated fibrin microthreads after one week. This would be expected, as the electrostatic interaction between FGF2 and heparin is a strong noncovalent bond.[73] We performed a glycine rinse to prevent any residual activated carboxylic acid groups from the EDC reaction to covalently bind FGF2 to fibrin.[63, 64] FGF2 release from heparin conjugated fibrin microthreads likely occurs through different mechanisms, including FGF2 dissociation from heparin and degradation of fibrin.[35, 86] *In vivo*, additional factors would influence FGF2 release including proteolytic degradation of fibrin via plasmin and enzymatic degradation of heparin via heparinase,[35] which may likely lead to faster release of FGF2 than what we observed *in vitro*. Future analyses to evaluate extended release of FGF2 over several weeks and to quantify FGF2 remaining on our scaffolds will provide more information about how heparin-conjugated fibrin microthreads mediate FGF2 binding, sequestration, and release.

Interestingly, UNX and UNX HEP 1000 microthreads both yielded higher total FGF2 release compared to EDC microthreads crosslinked with the same corresponding heparin concentration (EDC and EDC HEP 1000, respectively). UNX HEP 1000 microthreads also exhibited a higher initial burst release, where 77% of total FGF2 was released within the first two days, compared to 65% and 64% of total FGF2 released from EDC HEP 100 and EDC HEP 1000 microthreads at two days, respectively. This is a similar finding to work by Yang et al., who compared FGF2 release from fibrin hydrogels containing free and EDC conjugated heparin.[43] They found that fibrin hydrogels containing free heparin had less sustained release than heparin conjugated fibrinogen, and exhibited a much higher initial burst release within the first few days.[43] This is likely because electrostatic attraction forces in fibrin with free heparin are weaker than the covalent bond formed when heparin is carbodiimide crosslinked to fibrin. The high sustained release from UNX microthreads may be due to the high binding affinity FGF2 has for fibrin, with reported equilibrium dissociation constant (K_d) ranging from 0.8 – 261 nM.[60] Thus, we hypothesize that FGF2 binds with specificity to saturate UNX microthreads, which mediates its sustained release from the scaffold. Visual inspection indicated that UNX and UNX HEP 1000 microthreads were largely degraded after the one week release assay, so it is likely that that total

FGF2 release reported is close to the total amount of FGF2 initially loaded on these scaffolds. In contrast, EDC microthreads had not noticeably degraded at the terminal one week timepoint of the release assay.

A limitation of this work is that we were unable to accurately quantify the amount of FGF2 initially bound to fibrin microthreads with an ELISA. We hypothesize that differences in cumulative release between fibrin microthread conditions is likely a result of differences in initial FGF2 binding as well as the release mechanisms. Researchers demonstrated that increasing concentrations of heparin when EDC crosslinked to collagen scaffolds is correlated with an increase in FGF2 binding.[66, 89, 90] A 2 to 3.4-fold increase in the amount of bound FGF2 was observed on heparinized collagen matrices compared to unmodified collagen scaffolds, as determined by measuring the radioactivity of ^{125}I-FGF2.[66, 89, 90] Higher FGF2 binding was also observed on heparinized, EDC crosslinked PLGA nanofibers compared to unmodified nanofibers.[80] Based on these studies, we hypothesize that with increasing concentrations of heparin, we are increasing the amount of FGF2 binding to fibrin microthreads. It is not clear whether the effect of passively adsorbing vs. chemically conjugating heparin would influence the efficiency of FGF2 binding. Quantification of toluidine blue staining did not reveal any significant differences in heparin incorporation on passively adsorbed vs. chemically conjugated scaffolds with the same heparin concentration. Because of this, we hypothesize that FGF2 binding is comparable on passively adsorbed and EDC coupled scaffolds when heparin concentration is held constant. This should be investigated in future studies by quantifying the amount of bound FGF2 with a Western blot, fluorescently conjugated FGF2, or radioactive ^{125}I-FGF2, following complete scaffold digestion.

FGF2 incorporated onto or within fibrin microthreads remained bioactive, as it was able to stimulate myoblast proliferation in a Transwell®-based assay. FGF2 is a known mitogen for myoblasts.[26-29, 91, 92] FGF2-loaded microthreads stimulated myoblast proliferation comparable to 5 ng/mL FGF2 supplemented SFM. Additionally, the percent of Ki67^{+} myoblasts increased significantly from day 1 to 4 in all microthread conditions passively adsorbed with FGF2. These results further confirmed that (1) co-inc and heparin-mediated FGF2 incorporation strategies did not inhibit the bioactivity of FGF2, and (2) FGF2 released from heparin-conjugated microthreads is able to act on myoblasts over a prolonged time. Other researchers performed similar bioactivity

assays by placing FGF2-loaded scaffolds into Transwell® culture inserts and evaluating the effect of FGF2 release on fibroblast[78, 86] or endothelial cell[43] number over time.[43, 78] These studies also found that released FGF2 remained bioactive, as it was able to stimulate proliferation to the same degree as FGF2 supplemented medium. The Transwell®-based proliferation assay relies on bound FGF2 releasing from fibrin microthreads and diffusing through the Transwell® membrane to stimulate myoblast proliferation. To assess the ability of bound FGF2 on fibrin microthreads to stimulate myoblast proliferation and migration, we performed a 3D cellular outgrowth assay.

Our lab developed a 3D cellular outgrowth assay, an *in vitro* model system that examines the combined effect of cellular proliferation and migration, termed outgrowth, onto fibrin microthreads from a myoblast-populated hydrogel.[71, 72] This assay more accurately recapitulates myoblast outgrowth from a wound margin compared to other commonly used migration assays including Transwell® inserts and scratch assays.[93] The outgrowth assay allows for evaluation of proliferation and migration of myoblasts directly attached to the microthreads; this allows us to measure the influence of the bound heparin and FGF2 complex, where other migration assays rely of FGF2 being released from the scaffold. This is particularly important for analyzing heparin-conjugated scaffolds because they likely sequester more FGF2, and bound heparin facilitates FGF2 binding with its receptor.[45, 46, 94]

FGF2-loaded fibrin microthreads appeared to influence myoblast outgrowth as a function of growth factor incorporation strategy. Outgrowth rates were highest on co-inc and UNX HEP 1000 microthreads, which were both approximately 1.5-fold higher than the rate of myoblast outgrowth observed on UNX microthreads with no FGF2. Similarly, Cornwell et al. saw an approximately 2-fold increase in fibroblast outgrowth on fibrin microthreads co-incorporated with 200 ng/mL FGF2.[62] However, this assay was carried out in proliferation media with 2% FBS, which is more conducive to cellular proliferation and migration than the SFM used in the present study. Although not significant, there appeared to be a trend where EDC crosslinked microthreads directed lower myoblast outgrowth rates and distances compared to UNX microthreads with corresponding heparin concentrations. Researchers demonstrated that EDC crosslinking of collagen films reduced C2C12 binding and spreading, which they hypothesize was caused by a reduction in the number of available cell binding sites.[95] Bax et al. demonstrated that with an increasing degree of EDC crosslinking of collagen, β_1 integrin-mediated cell spreading, apoptosis,

and proliferation were reduced in HT1080 fibrosarcoma and C2C12 cell lines.[96] This study suggests that EDC crosslinking utilizes the same carboxylic side chain chemistry that is necessary for integrin-mediated cell interactions. This is further substantiated by work confirming that C2C12s highly express β_1 integrin subunits.[97] Thus, we hypothesize EDC crosslinking of fibrin microthreads may utilize and subsequently block the functional groups necessary for integrin-mediated cellular attachment.

To uncouple which cellular mechanism, proliferation or migration, is primarily responsible for myoblast outgrowth, Ki67 staining was performed on myoblast-seeded fibrin microthreads from the outgrowth assay. All conditions, regardless of the presence of FGF2 or its incorporation strategy, revealed minimal expression of $Ki67^+$ nuclei. Thus, it is likely that the outgrowth observed on fibrin microthreads is driven by myoblast migration, rather than proliferation. Ki67 staining of myoblasts on fibrin microthreads at earlier timepoints during the outgrowth assay would further elucidate the role of cellular proliferation at earlier stages during outgrowth. We hypothesize that minimal $Ki67^+$ nuclei were observed because the outgrowth assay was conducted in SFM. There are conflicting reports in the literature regarding whether FGF2 is able to stimulate myoblast proliferation in the absence of serum.[91, 98] Performing this assay in the presence of serum may allow for more robust myoblast outgrowth, as was demonstrated on fibrin microthreads passively adsorbed with hepatocyte growth factor (HGF), another well-known mitogen.[72] In the future, optimization of FGF2 concentration may allow for a more pronounced effect on myoblast proliferation and migration. A dose-dependent effect of FGF2 concentration on C2C12 proliferation has been previously observed.[99]

In the future, FGF2-loaded fibrin microthreads could also be investigated for their ability to promote angiogenesis, re-innervation, and fibrosis, which are essential elements of VML regeneration in addition to myogenesis. FGF2 has been shown to stimulate endothelial sprouting, and pericyte and smooth muscle cell migration, allowing FGF2 to stimulate the formation of more mature vessels than other proangiogenic growth factors such as VEGF.[32] Researchers found that heparin conjugated collagen scaffolds crosslinked with EDC and loaded with FGF2 promoted angiogenesis upon subcutaneous implantation in rats.[32, 66, 90] Fibrin-based scaffolds are also ideal for delivering FGF2 for angiogenesis, as it potentiates FGF2 mediated endothelial cell proliferation.[100] Researchers delivered EDC crosslinked, heparinized, FGF2-loaded fibrin

hydrogels to treat murine ischemic hind limb injuries.[43] Injuries treated with FGF2-loaded heparinized fibrin had significantly lower fibrosis and enhanced vascularization compared to controls. Additionally, FGF2 has neurotrophic activity, stimulating NGF synthesis and secretion and promoting neuronal survival and outgrowth.[20, 33-36] Heparinized fibrin hydrogels loaded with FGF2 significantly enhanced neurite length *in vitro* compared to fibrin hydrogels alone.[35] Patel et al. developed aligned poly(L-lactide) (PLLA) nanofibers conjugated with heparin to provide sustained release of FGF2, and found these scaffolds stimulated a significantly higher rate of neurite outgrowth compared to unloaded scaffolds.[80] Neurite outgrowth was also enhanced in part due to the aligned, fibrous architecture of this scaffold. This further motivates the use of biopolymer microthread scaffolds with both topographic alignment cues and biomimetic growth factor delivery strategies.[101] Future work should also investigate FGF2 signaling, as many intracellular signaling pathways are known to be activated by FGF2 including mitogen-activated protein kinases (MAPKs), mTOR, STAT, and PLCγ.[102] Variations in FGF2 signal transduction pathways explains its pleiotropic nature and may better elucidate its role in a variety of regenerative processes including fibrosis, myogenesis, angiogenesis, and innervation. Additionally, this heparin conjugation strategy can also be used to deliver other heparin-binding growth factors, including PDGF, VEGF, bone morphogenetic protein-2 (BMP-2), and HGF, and combinations therein.[103]

5.5 CONCLUSIONS

In the present study we developed fibrin microthread scaffolds to provide physiologically relevant, sustained release of FGF2 by evaluating two incorporation strategies. The first strategy coupled heparin to microthreads through either passive adsorption or covalent carbodiimide coupling, mimicking the presentation of heparan sulfate bound FGF2 in native ECM. Second, we co-incorporated FGF2 by mixing with fibrinogen prior to co-extrusion of microthreads. This strategy sought to leverage fibrin's high binding affinity to FGF2, which also protects FGF2 from proteolytic degradation. To validate heparin conjugation to microthreads, toluidine blue staining and FTIR were performed, and demonstrated increasing dye uptake and amide bond peaks with increasing concentrations of heparin, respectively. Release kinetics of FGF2 from fibrin microthreads indicated that microthreads passively adsorbed and covalently coupled with heparin

had sustained release of FGF2 over one week. Co-incorporated microthreads achieved zero-order release of FGF2 over five days. An *in vitro* Transwell®-based proliferation assay confirmed that FGF2 released from fibrin microthreads with both incorporation strategies remained bioactive, as it was able to stimulate myoblast proliferation over four days. A 3D outgrowth assay demonstrated that co-inc and heparin conjugated microthreads may enhance myoblast outgrowth. Overall, we demonstrated that both FGF2 incorporation strategies achieved sustained growth factor release and were able to stimulate myoblasts *in vitro*. This scaffold addresses limitations of current FGF2 delivery strategies, which primarily use hydrogels that often lack the mechanical strength and alignment cues of microthread scaffolds. Fibrin microthreads that provide mechanical support, topographical alignment cues, and sustained release of FGF2 are a promising scaffold for treating VML injuries and will be investigated for their ability to promote functional muscle regeneration in the future.

5.6 ACKNOWLEDGEMENTS

We thank Lyra Huynh, Cailin Gonyea, Giulio Cataldo, and Matthew Cannata for their assistance with preparing scaffolds and crosslinking. We also thank Cailin Gonyea for her help with Ki67 staining and imaging. This work was funded in part by NIH R15 HL137145 (GDP) and NSF DGE IGERT 1144804 (MEC).

5.7 REFERENCES

1. National Hospital Discharge Survey (NHDS). *Center for Disease Control* **2010**.
2. National Hospital Ambulatory Medical Care Survey Outpatient Department (NHAMCS_OP). *Center for Disease Control* **2010**.
3. National Hospital Ambulatory Medical Care Survey Emergency Department (NHAMCS_ED). *Center for Disease Control* **2010**.
4. National Ambulatory Medical Care Survey (NAMCS). *Center for Disease Control* **2010**.
5. Medical Expenditures Panel Survey (MEPS), Agency for Healthcare Research and Quality, U.S. Department of Health and Human Services, 1996-2011. **2011**.
6. Eckardt, A., Microsurgical reconstruction in the head and neck region: an 18-year experience with 500 consecutive cases. *Journal of Cranio-Maxillofacial Surgery* **2003,** *31* (4), 197-201.
7. Äärimaa, V., Rantanen, J., Heikkilä, J., Helttula, I. and Orava, S., Rupture of the Pectoralis Major Muscle. *Amer J of Sports Med* **2004,** *32* (5), 1256-1262.
8. Pochini, A. D., Andreoli, C.V., Belangero, P.S., Figueiredo, E.A., Terra, B.B., Cohen, C., Andrade, M.D., Cohen, M., Ejnisman, B., Clinical Considerations for the Surgical Treatment of Pectoralis Major Muscle Ruptures Based on 60 Cases: a Prospecitve Study and Literature Review. *Amer J of Sports Med* **2014,** *42* (1), 95-102.

9. Borselli, C.; Storrie, H.; Benesch-Lee, F.; Shvartsman, D.; Cezar, C.; Lichtman, J. W.; Vandenburgh, H. H.; Mooney, D. J., Functional muscle regeneration with combined delivery of angiogenesis and myogenesis factors. *Proc Natl Acad Sci U S A* **2010,** *107* (8), 3287-92.
10. Wolf, M. T.; Dearth, C. L.; Sonnenberg, S. B.; Loboa, E. G.; Badylak, S. F., Naturally derived and synthetic scaffolds for skeletal muscle reconstruction. *Adv Drug Deliv Rev* **2014,** *84*, 208-221.
11. Baker, H. B.; Passipieri, J. A.; Siriwardane, M.; Ellenburg, M. D.; Vadhavkar, M.; Bergman, C. R.; Saul, J. M.; Tomblyn, S.; Burnett, L.; Christ, G. J., Cell and Growth Factor-Loaded Keratin Hydrogels for Treatment of Volumetric Muscle Loss in a Mouse Model. *Tissue Eng Part A* **2017,** *23* (11-12), 572-584.
12. Passipieri, J. A.; Baker, H. B.; Siriwardane, M.; Ellenburg, M. D.; Vadhavkar, M.; Saul, J. M.; Tomblyn, S.; Burnett, L.; Christ, G. J., Keratin Hydrogel Enhances In Vivo Skeletal Muscle Function in a Rat Model of Volumetric Muscle Loss. *Tissue Eng Part A* **2017**.
13. Wang, L.; Cao, L.; Shansky, J.; Wang, Z.; Mooney, D.; Vandenburgh, H., Minimally invasive approach to the repair of injured skeletal muscle with a shape-memory scaffold. *Molecular therapy : the journal of the American Society of Gene Therapy* **2014,** *22* (8), 1441-9.
14. Silva, E. A.; Mooney, D. J., Spatiotemporal control of vascular endothelial growth factor delivery from injectable hydrogels enhances angiogenesis. *J Thromb Haemost* **2007,** *5* (3), 590-8.
15. Hammers, D. W., Sarathy, A., Pham, C.B., Drinnan, C.T., Farrar, R.P., and Suggs, L.J., Controlled Release of IGF-1 From a Biodegradable Matrix Improves Functional Recovery of Skeletal Muscle from Ischemia/Reperfusion. *Biotechnology and bioengineering* **2011,** *109* (4), 1051-1059.
16. Shvartsman, D.; Storrie-White, H.; Lee, K.; Kearney, C.; Brudno, Y.; Ho, N.; Cezar, C.; McCann, C.; Anderson, E.; Koullias, J.; Tapia, J. C.; Vandenburgh, H.; Lichtman, J. W.; Mooney, D. J., Sustained delivery of VEGF maintains innervation and promotes reperfusion in ischemic skeletal muscles via NGF/GDNF signaling. *Molecular therapy : the journal of the American Society of Gene Therapy* **2014,** *22* (7), 1243-53.
17. Ju, Y. M., Atala, A., Yoo, J. J., Lee, S. J., In situ regeneration of skeletal muscle tissue through host cell recruitment. *Acta Biomater* **2014,** *10*, 4332-4339.
18. Grasman, J. M.; Do, D. M.; Page, R. L.; Pins, G. D., Rapid release of growth factors regenerates force output in volumetric muscle loss injuries. *Biomaterials* **2015,** *72*, 49-60.
19. Marui, A.; Kanematsu, A.; Yamahara, K.; Doi, K.; Kushibiki, T.; Yamamoto, M.; Itoh, H.; Ikeda, T.; Tabata, Y.; Komeda, M., Simultaneous application of basic fibroblast growth factor and hepatocyte growth factor to enhance the blood vessels formation. *J Vasc Surg* **2005,** *41* (1), 82-90.
20. Husmann, I.; Soulet, L.; Gautron, J.; Martelly, I.; Barritault, D., Growth factors in skeletal muscle regeneration. *Cytokine Growth Factor Rev* **1996,** *7* (3), 249-58.
21. Folkman, J.; Klagsbrun, M.; Sasse, J.; Wadzinski, M.; Ingber, D.; Vlodavsky, I., A heparin-binding angiogenic protein--basic fibroblast growth factor--is stored within basement membrane. *The American journal of pathology* **1988,** *130* (2), 393-400.
22. Bashkin, P.; Doctrow, S.; Klagsbrun, M.; Svahn, C. M.; Folkman, J.; Vlodavsky, I., Basic fibroblast growth factor binds to subendothelial extracellular matrix and is released by heparitinase and heparin-like molecules. *Biochemistry* **1989,** *28* (4), 1737-43.
23. Sanes, J. R., The basement membrane/basal lamina of skeletal muscle. *J Biol Chem* **2003,** *278* (15), 12601-4.
24. Charge, S. B. P., Rudnicki, M.A., Cellular and Molecular Regulation of Muscle Regeneration. *Physiol Rev* **2004,** *84*, 209-238.
25. Cornelison, D. D.; Olwin, B. B.; Rudnicki, M. A.; Wold, B. J., MyoD(-/-) satellite cells in single-fiber culture are differentiation defective and MRF4 deficient. *Dev Biol* **2000,** *224* (2), 122-37.
26. Sheehan, S. M.; Allen, R. E., Skeletal muscle satellite cell proliferation in response to members of the fibroblast growth factor family and hepatocyte growth factor. *J Cell Physiol* **1999,** *181* (3), 499-506.

27. Jarvinen, T. A.; Jarvinen, T. L.; Kaariainen, M.; Kalimo, H.; Jarvinen, M., Muscle injuries: biology and treatment. *Am J Sports Med* **2005,** *33* (5), 745-64.
28. Cornelison, D. D.; Filla, M. S.; Stanley, H. M.; Rapraeger, A. C.; Olwin, B. B., Syndecan-3 and syndecan-4 specifically mark skeletal muscle satellite cells and are implicated in satellite cell maintenance and muscle regeneration. *Dev Biol* **2001,** *239* (1), 79-94.
29. Cornelison, D. D.; Wilcox-Adelman, S. A.; Goetinck, P. F.; Rauvala, H.; Rapraeger, A. C.; Olwin, B. B., Essential and separable roles for Syndecan-3 and Syndecan-4 in skeletal muscle development and regeneration. *Genes Dev* **2004,** *18* (18), 2231-6.
30. Do, M. K.; Suzuki, T.; Gerelt, B.; Sato, Y.; Mizunoya, W.; Nakamura, M.; Ikeuchi, Y.; Anderson, J. E.; Tatsumi, R., Time-coordinated prevalence of extracellular HGF, FGF2 and TGF-beta3 in crush-injured skeletal muscle. *Anim Sci J* **2012,** *83* (10), 712-7.
31. Nehls, V.; Schuchardt, E.; Drenckhahn, D., The effect of fibroblasts, vascular smooth muscle cells, and pericytes on sprout formation of endothelial cells in a fibrin gel angiogenesis system. *Microvasc Res* **1994,** *48* (3), 349-63.
32. Nillesen, S. T.; Geutjes, P. J.; Wismans, R.; Schalkwijk, J.; Daamen, W. F.; van Kuppevelt, T. H., Increased angiogenesis and blood vessel maturation in acellular collagen-heparin scaffolds containing both FGF2 and VEGF. *Biomaterials* **2007,** *28* (6), 1123-31.
33. Baird, A., Fibroblast growth factors: activities and significance of non-neurotrophin neurotrophic growth factors. *Curr Opin Neurobiol* **1994,** *4* (1), 78-86.
34. Unsicker, K.; Reichert-Preibsch, H.; Wewetzer, K., Stimulation of neuron survival by basic FGF and CNTF is a direct effect and not mediated by non-neuronal cells: evidence from single cell cultures. *Brain Res Dev Brain Res* **1992,** *65* (2), 285-8.
35. Sakiyama-Elbert, S. E.; Hubbell, J. A., Development of fibrin derivatives for controlled release of heparin-binding growth factors. *J Control Release* **2000,** *65* (3), 389-402.
36. Jungnickel, J.; Haase, K.; Konitzer, J.; Timmer, M.; Grothe, C., Faster nerve regeneration after sciatic nerve injury in mice over-expressing basic fibroblast growth factor. *J Neurobiol* **2006,** *66* (9), 940-8.
37. Simons, M.; Ware, J. A., Therapeutic angiogenesis in cardiovascular disease. *Nat Rev Drug Discov* **2003,** *2* (11), 863-71.
38. Simons, M.; Annex, B. H.; Laham, R. J.; Kleiman, N.; Henry, T.; Dauerman, H.; Udelson, J. E.; Gervino, E. V.; Pike, M.; Whitehouse, M. J.; Moon, T.; Chronos, N. A., Pharmacological treatment of coronary artery disease with recombinant fibroblast growth factor-2: double-blind, randomized, controlled clinical trial. *Circulation* **2002,** *105* (7), 788-93.
39. Lederman, R. J.; Mendelsohn, F. O.; Anderson, R. D.; Saucedo, J. F.; Tenaglia, A. N.; Hermiller, J. B.; Hillegass, W. B.; Rocha-Singh, K.; Moon, T. E.; Whitehouse, M. J.; Annex, B. H.; Investigators, T., Therapeutic angiogenesis with recombinant fibroblast growth factor-2 for intermittent claudication (the TRAFFIC study): a randomised trial. *Lancet* **2002,** *359* (9323), 2053-8.
40. Simons, M.; Bonow, R. O.; Chronos, N. A.; Cohen, D. J.; Giordano, F. J.; Hammond, H. K.; Laham, R. J.; Li, W.; Pike, M.; Sellke, F. W.; Stegmann, T. J.; Udelson, J. E.; Rosengart, T. K., Clinical trials in coronary angiogenesis: issues, problems, consensus: An expert panel summary. *Circulation* **2000,** *102* (11), E73-86.
41. Lee, K.; Silva, E. A.; Mooney, D. J., Growth factor delivery-based tissue engineering: general approaches and a review of recent developments. *J R Soc Interface* **2011,** *8* (55), 153-70.
42. Sakiyama-Elbert, S. E. a. H., J. A., Development of fibrin derivatives for controlled release of heparin-binding growth factors. *J Control Release* **1999,** *65*, 389-402.
43. Yang, H. S.; Bhang, S. H.; Hwang, J. W.; Kim, D. I.; Kim, B. S., Delivery of basic fibroblast growth factor using heparin-conjugated fibrin for therapeutic angiogenesis. *Tissue Eng Part A* **2010,** *16* (6), 2113-9.

44. Gillies, A. R.; Lieber, R. L., Structure and function of the skeletal muscle extracellular matrix. *Muscle & nerve* **2011,** *44* (3), 318-31.
45. Roghani, M.; Moscatelli, D., Basic fibroblast growth factor is internalized through both receptor-mediated and heparan sulfate-mediated mechanisms. *J Biol Chem* **1992,** *267* (31), 22156-62.
46. Rapraeger, A. C., Syndecan-regulated receptor signaling. *The Journal of cell biology* **2000,** *149* (5), 995-8.
47. Sakiyama-Elbert, S. E.; Hubbell, J. A., Controlled release of nerve growth factor from a heparin-containing fibrin-based cell ingrowth matrix. *J Control Release* **2000,** *69* (1), 149-58.
48. Laham, R. J.; Sellke, F. W.; Edelman, E. R.; Pearlman, J. D.; Ware, J. A.; Brown, D. L.; Gold, J. P.; Simons, M., Local perivascular delivery of basic fibroblast growth factor in patients undergoing coronary bypass surgery: results of a phase I randomized, double-blind, placebo-controlled trial. *Circulation* **1999,** *100* (18), 1865-71.
49. Ruel, M.; Laham, R. J.; Parker, J. A.; Post, M. J.; Ware, J. A.; Simons, M.; Sellke, F. W., Long-term effects of surgical angiogenic therapy with fibroblast growth factor 2 protein. *J Thorac Cardiovasc Surg* **2002,** *124* (1), 28-34.
50. Kumagai, M.; Marui, A.; Tabata, Y.; Takeda, T.; Yamamoto, M.; Yonezawa, A.; Tanaka, S.; Yanagi, S.; Ito-Ihara, T.; Ikeda, T.; Murayama, T.; Teramukai, S.; Katsura, T.; Matsubara, K.; Kawakami, K.; Yokode, M.; Shimizu, A.; Sakata, R., Safety and efficacy of sustained release of basic fibroblast growth factor using gelatin hydrogel in patients with critical limb ischemia. *Heart Vessels* **2016,** *31* (5), 713-21.
51. Ono, K.; Yanishi, K.; Ariyoshi, M.; Kaimoto, S.; Uchihashi, M.; Shoji, K.; Matoba, S., First-in-Man Clinical Pilot Study Showing the Safety and Efficacy of Intramuscular Injection of Basic Fibroblast Growth Factor With Atelocollagen Solution for Critical Limb Ischemia. *Circ J* **2018,** *83* (1), 217-223.
52. Marui, A.; Tabata, Y.; Kojima, S.; Yamamoto, M.; Tambara, K.; Nishina, T.; Saji, Y.; Inui, K.; Hashida, T.; Yokoyama, S.; Onodera, R.; Ikeda, T.; Fukushima, M.; Komeda, M., A novel approach to therapeutic angiogenesis for patients with critical limb ischemia by sustained release of basic fibroblast growth factor using biodegradable gelatin hydrogel: an initial report of the phase I-IIa study. *Circ J* **2007,** *71* (8), 1181-6.
53. Hwang, J. H.; Kim, I. G.; Piao, S.; Jung, A. R.; Lee, J. Y.; Park, K. D.; Lee, J. Y., Combination therapy of human adipose-derived stem cells and basic fibroblast growth factor hydrogel in muscle regeneration. *Biomaterials* **2013,** *34* (25), 6037-45.
54. Hill, E.; Boontheekul, T.; Mooney, D. J., Regulating activation of transplanted cells controls tissue regeneration. *Proc Natl Acad Sci U S A* **2006,** *103* (8), 2494-9.
55. Hagiwara, K.; Chen, G.; Kawazoe, N.; Tabata, Y.; Komuro, H., Promotion of muscle regeneration by myoblast transplantation combined with the controlled and sustained release of bFGFcpr. *J Tissue Eng Regen Med* **2016,** *10* (4), 325-33.
56. Doukas, J.; Blease, K.; Craig, D.; Ma, C.; Chandler, L. A.; Sosnowski, B. A.; Pierce, G. F., Delivery of FGF genes to wound repair cells enhances arteriogenesis and myogenesis in skeletal muscle. *Molecular therapy : the journal of the American Society of Gene Therapy* **2002,** *5* (5 Pt 1), 517-27.
57. Stratos, I.; Madry, H.; Rotter, R.; Weimer, A.; Graff, J.; Cucchiarini, M.; Mittlmeier, T.; Vollmar, B., Fibroblast growth factor-2-overexpressing myoblasts encapsulated in alginate spheres increase proliferation, reduce apoptosis, induce adipogenesis, and enhance regeneration following skeletal muscle injury in rats. *Tissue Eng Part A* **2011,** *17* (21-22), 2867-77.
58. Zisch, A. H., Schenk, U., Schense, J. C., Sakiyama-Elbert, S. E., and Hubbell, J. A., Covalently conjugated VEGF–fibrin matrices for endothelialization. *J Control Release* **2001,** *72*, 101-113.
59. Richardson, T. P., Peters, M. C., Ennett, A. B., and Mooney, D. J., Polymeric system for dual growth factor delivery. *Nature Biotechnology* **2001,** *19*, 1029-1034.
60. Sahni, A.; Baker, C. A.; Sporn, L. A.; Francis, C. W., Fibrinogen and fibrin protect fibroblast growth factor-2 from proteolytic degradation. *Thromb Haemost* **2000,** *83* (5), 736-41.

61. Cornwell, K. G.; Pins, G. D., Discrete crosslinked fibrin microthread scaffolds for tissue regeneration. *J Biomed Mater Res A* **2007,** *82* (1), 104-12.
62. Cornwell, K. G.; Pins, G. D., Enhanced proliferation and migration of fibroblasts on the surface of fibroblast growth factor-2-loaded fibrin microthreads. *Tissue Eng Part A* **2010,** *16* (12), 3669-77.
63. Duan, X.; Sheardown, H., Dendrimer crosslinked collagen as a corneal tissue engineering scaffold: Mechanical properties and corneal epithelial cell interactions. *Biomaterials* **2006,** *27* (26), 4608-4617.
64. Duan, X. D.; McLaughlin, C.; Griffith, M.; Sheardown, H., Biofunctionalization of collagen for improved biological response: Scaffolds for corneal tissue engineering. *Biomaterials* **2007,** *28* (1), 78-88.
65. Singh, S.; Wu, B. M.; Dunn, J. C., The enhancement of VEGF-mediated angiogenesis by polycaprolactone scaffolds with surface cross-linked heparin. *Biomaterials* **2011,** *32* (8), 2059-69.
66. van Wachem, P. B.; Plantinga, J. A.; Wissink, M. J.; Beernink, R.; Poot, A. A.; Engbers, G. H.; Beugeling, T.; van Aken, W. G.; Feijen, J.; van Luyn, M. J., In vivo biocompatibility of carbodiimide-crosslinked collagen matrices: Effects of crosslink density, heparin immobilization, and bFGF loading. *J Biomed Mater Res* **2001,** *55* (3), 368-78.
67. Smith, P. K.; Mallia, A. K.; Hermanson, G. T., Colorimetric method for the assay of heparin content in immobilized heparin preparations. *Anal Biochem* **1980,** *109* (2), 466-73.
68. Elahi, M. F.; Guan, G.; Wang, L.; King, M. W., Influence of Layer-by-Layer Polyelectrolyte Deposition and EDC/NHS Activated Heparin Immobilization onto Silk Fibroin Fabric. *Materials (Basel)* **2014,** *7* (4), 2956-2977.
69. Jee, K. S.; Dal Park, H.; Park, K. D.; Ha Kim, Y.; Shin, J. W., Heparin conjugated polylactide as a blood compatible material. *Biomacromolecules* **2004,** *5* (5), 1877-1881.
70. Grasman, J. M.; Page, R. L.; Dominko, T.; Pins, G. D., Crosslinking strategies facilitate tunable structural properties of fibrin microthreads. *Acta Biomater* **2012,** *8* (11), 4020-30.
71. Cornwell, K. G.; Downing, B. R.; Pins, G. D., Characterizing fibroblast migration on discrete collagen threads for applications in tissue regeneration. *J Biomed Mater Res A* **2004,** *71* (1), 55-62.
72. Grasman, J. M., Page, R. L., and Pins, G. D., Design of an In Vitro Model of Cell Recruitment for Skeletal Muscle Regeneration Using Hepatocyte Growth Factor-Loaded Fibrin Microthreads. *Tissue Eng Part A* **2017,** *23* (15-16), 773-783.
73. Sakiyama-Elbert, S. E., Incorporation of heparin into biomaterials. *Acta Biomater* **2014,** *10* (4), 1581-1587.
74. Wissink, M. J.; Beernink, R.; Pieper, J. S.; Poot, A. A.; Engbers, G. H.; Beugeling, T.; van Aken, W. G.; Feijen, J., Immobilization of heparin to EDC/NHS-crosslinked collagen. Characterization and in vitro evaluation. *Biomaterials* **2001,** *22* (2), 151-63.
75. Pieper, J. S.; Hafmans, T.; Veerkamp, J. H.; van Kuppevelt, T. H., Development of tailor-made collagen-glycosaminoglycan matrices: EDC/NHS crosslinking, and ultrastructural aspects. *Biomaterials* **2000,** *21* (6), 581-93.
76. Younesi, M.; Donmez, B. O.; Islam, A.; Akkus, O., Heparinized Collagen Sutures for Sustained Delivery of PDGF-BB: Delivery Profile and Effects on Tendon-derived Cells In-Vitro. *Acta Biomater* **2016,** *41*, 100-109.
77. Yang, H. S., La, W., Bhang, S.H., Jeon, J., Lee, J.H., and Kim, B., Heparin-conjugated Fibrin as an Injectable System for Sustained Delivery of Bone Morphogenic Protein-2. *Tissue Eng Part A* **2101,** *16* (4), 1225-1233.
78. Jeon, O.; Kang, S. W.; Lim, H. W.; Hyung Chung, J.; Kim, B. S., Long-term and zero-order release of basic fibroblast growth factor from heparin-conjugated poly(L-lactide-co-glycolide) nanospheres and fibrin gel. *Biomaterials* **2006,** *27* (8), 1598-607.
79. Schense, J. C. a. H., J. A., Cross-Linking Exogenous Bifunctional Peptides into Fibrin Gels with Factor XIIIa. *Bioconjugate Chem* **1999,** *10*, 75-81.

80. Patel, S., Kurpinski, K., Quigly, R., Gao, H., Hsiao, B. S., Poo, M., and Li, S., Bioactive Nanofibers: Synergistic Effects of Nanotopography and Chemical Signaling on Cell Guidance. *Nano Letters* **2007,** *7* (7), 2122-2128.
81. Sakiyama, S. E.; Schense, J. C.; Hubbell, J. A., Incorporation of heparin-binding peptides into fibrin gels enhances neurite extension: an example of designer matrices in tissue engineering. *Faseb J* **1999,** *13* (15), 2214-2224.
82. Maynard, H. D.; Hubbell, J. A., Discovery of a sulfated tetrapeptide that binds to vascular endothelial growth factor. *Acta Biomater* **2005,** *1* (4), 451-459.
83. Freeman, I.; Kedem, A.; Cohen, S., The effect of sulfation of alginate hydrogels on the specific binding and controlled release of heparin-binding proteins. *Biomaterials* **2008,** *29* (22), 3260-3268.
84. Shipp, E. L.; Hsieh-Wilson, L. C., Profiling the sulfation specificities of glycosaminoglycan interactions with growth factors and chemotactic proteins using microarrays. *Chem Biol* **2007,** *14* (2), 195-208.
85. Pye, D. A.; Vives, R. R.; Turnbull, J. E.; Hyde, P.; Gallagher, J. T., Heparan sulfate oligosaccharides require 6-O-sulfation for promotion of basic fibroblast growth factor mitogenic activity. *Journal of Biological Chemistry* **1998,** *273* (36), 22936-22942.
86. Jeon, O.; Ryu, S. H.; Chung, J. H.; Kim, B. S., Control of basic fibroblast growth factor release from fibrin gel with heparin and concentrations of fibrinogen and thrombin. *Journal of Controlled Release* **2005,** *105* (3), 249-259.
87. Jeon, O.; Song, S. J.; Yang, H. S.; Bhang, S. H.; Kang, S. W.; Sung, M. A.; Lee, J. H.; Kim, B. S., Long-term delivery enhances in vivo osteogenic efficacy of bone morphogenetic protein-2 compared to short-term delivery. *Biochem Bioph Res Co* **2008,** *369* (2), 774-780.
88. Sakiyama-Elbert, S. E. a. H., J. A., Controlled release of nerve growth factor from a heparin-containing fibrin-based cell ingrowth matrix. *J Control Release* **2000,** *69*, 149-158.
89. Wissink, M.; Beernink, R.; Poot, A.; Engbers, G.; Beugeling, T.; van Aken, W.; Feijen, J., Improved endothelialization of vascular grafts by local release of growth factor from heparinized collagen matrices. *J Control Release* **2000,** *64* (1-3), 103-14.
90. Pieper, J.; Hafmans, T.; van Wachem, P.; van Luyn, M.; Brouwer, L.; Veerkamp, J.; van Kuppevelt, T., Loading of collagen-heparan sulfate matrices with bFGF promotes angiogenesis and tissue generation in rats. *J Biomed Mater Res* **2002,** *62* (2), 185-94.
91. Allen, R. E.; Boxhorn, L. K., Regulation of skeletal muscle satellite cell proliferation and differentiation by transforming growth factor-beta, insulin-like growth factor I, and fibroblast growth factor. *J Cell Physiol* **1989,** *138* (2), 311-5.
92. Yanagiuchi, A.; Miyake, H.; Nomi, M.; Takenaka, A.; Fujisawa, M., Modulation of the microenvironment by growth factors regulates the in vivo growth of skeletal myoblasts. *BJU Int* **2009,** *103* (11), 1569-73.
93. Moutasim, K. A.; Nystrom, M. L.; Thomas, G. J., Cell migration and invasion assays. In *Cancer cell culture*, Springer: 2011; pp 333-343.
94. Rapraeger, A. C.; Krufka, A.; Olwin, B. B., Requirement of heparan sulfate for bFGF-mediated fibroblast growth and myoblast differentiation. *Science* **1991,** *252* (5013), 1705-1708.
95. Grover, C. N.; Gwynne, J. H.; Pugh, N.; Hamaia, S.; Farndale, R. W.; Best, S. M.; Cameron, R. E., Crosslinking and composition influence the surface properties, mechanical stiffness and cell reactivity of collagen-based films. *Acta Biomater* **2012,** *8* (8), 3080-3090.
96. Bax, D. V.; Davidenko, N.; Gullberg, D.; Hamaia, S. W.; Farndale, R. W.; Best, S. M.; Cameron, R. E., Fundamental insight into the effect of carbodiimide crosslinking on cellular recognition of collagen-based scaffolds. *Acta Biomater* **2017,** *49*, 218-234.
97. Neveux, I.; Doe, J.; Leblanc, N.; Valencik, M. L., Influence of the extracellular matrix and integrins on volume-sensitive osmolyte anion channels in C2C12 myoblasts. *Am J Physiol-Cell Ph* **2010,** *298* (5), C1006-C1017.

98. Clegg, C. H.; Linkhart, T. A.; Olwin, B. B.; Hauschka, S. D., Growth factor control of skeletal muscle differentiation: commitment to terminal differentiation occurs in G1 phase and is repressed by fibroblast growth factor. *The Journal of cell biology* **1987,** *105* (2), 949-56.
99. Yun, Y. R.; Lee, S.; Jeon, E.; Kang, W.; Kim, K. H.; Kim, H. W.; Jang, J. H., Fibroblast growth factor 2-functionalized collagen matrices for skeletal muscle tissue engineering. *Biotechnol Lett* **2012,** *34* (4), 771-8.
100. Sahni, A.; Sporn, L. A.; Francis, C. W., Potentiation of endothelial cell proliferation by fibrin(ogen)-bound fibroblast growth factor-2. *J Biol Chem* **1999,** *274* (21), 14936-41.
101. O'Brien, M. P.; Carnes, M. E.; Page, R. L.; Gaudette, G. R.; Pins, G. D., Designing Biopolymer Microthreads for Tissue Engineering and Regenerative Medicine. *Curr Stem Cell Rep* **2016,** *2* (2), 147-157.
102. Ornitz, D. M.; Itoh, N., The fibroblast growth factor signaling pathway. *Wiley Interdisciplinary Reviews: Developmental Biology* **2015,** *4* (3), 215-266.
103. Sakiyama-Elbert, S., Drug Delivery via Heparin Conjugates. In *Comprehensive Biomaterials*, Ducheyne, P.; Healy, K.; Hutmacher, D.; Grainger, D.; Kirkpatrick, C., Eds. Elsevier: Amsterdam, 2011; pp 333-338.

Chapter 6: Conclusions and Future Work

6.1 OVERVIEW

The goal of this thesis was to develop fibrin microthread scaffolds with anisotropic surface features, robust mechanical properties, and sustained release of FGF2 towards the ultimate goal of restoring function in volumetric muscle loss (VML) injuries. We developed a novel method to create aligned, grooved features on the surfaces of fibrin microthreads by etching microthreads in 2-(N-morpholino)ethane-sulfonic acid (MES) acidic buffer. We evaluated the effect of buffer pH on the generation of these features and found that etched microthreads improved myoblast alignment. We were also the first to implement an enzymatic crosslinking strategy using horseradish peroxidase (HRP) and hydrogen peroxide (H_2O_2) on fibrin microthreads. We evaluated the effect of varying HRP and H_2O_2 incorporation strategies by incorporating crosslinking agents during or after microthread production. HRP crosslinking enhanced scaffold mechanical properties, decreased the rate of plasmin-mediated degradation, and did not inhibit myoblast viability. Finally, we developed fibrin microthreads with a physiologically-relevant, sustained release of fibroblast growth factor 2 (FGF2) by covalently conjugating heparin to fibrin microthreads, mimicking native FGF2 sequestration, or by mixing FGF2 within microthreads prior to extrusion. FGF2-loaded microthreads enhance myoblast proliferation and outgrowth *in vitro.*

6.2 RESULTS AND CONCLUSIONS

6.2.1 Specific Aim 1: Create and characterize anisotropic surface topography on fibrin microthreads to enhance myoblast alignment

Myoblast alignment is an essential step towards myotube formation, which is guided *in vivo* by extracellular matrix (ECM) structure and submicron-scale grooves between adjacent muscle fibers.[1] During muscle repair, satellite cells (SCs) are guided by the basement membrane to facilitate aligned cell division, migration, and fusion into myofibers.[2, 3] To mimic these native

cues and regenerate functional muscle tissue, engineered scaffolds often impart aligned topographical features to induce myoblast alignment. Microthreads are discrete fibrous scaffolds that have a structure resembling native ECM fibrils, and have been shown to promote cellular alignment.[4] Fibrin microthread scaffolds mimic the morphological architecture of native muscle tissue and have demonstrated promise as an implantable scaffold for treating skeletal muscle injuries.[5, 6] While microthreads facilitate aligned muscle regeneration *in vivo*[5], an *in vitro* analysis revealed that only 40% of myoblasts on fibrin microthreads were aligned along the long axis of the microthread.[7] To improve myoblast alignment on fibrin microthreads, we developed and characterized a new method of etching the surface of fibrin microthreads to incorporate aligned, sub-micron grooves that improve myoblast alignment.

To generate aligned topographic features on the surface of fibrin microthreads, we placed microthreads into MES acidic buffer for 15 minutes and evaluated the effect of buffer pH on the generation of these features. Initial studies in our lab demonstrated that when microthreads were placed in MES buffer prior to carbodiimide crosslinking (EDC), they displayed anisotropically aligned groves on the surface of microthreads.[8] We found that MES buffer pH played an important role in regulating surface feature generation. Scanning electron microscopy (SEM) revealed that microthreads etched in MES for 15 minutes with pH 5.0 (MES 5.0) had aligned, grooved surface features parallel to the long axis of the microthread, whereas those etched in MES with pH 5.5 (MES 5.5) had amorphous surface features similar to control threads placed in deionized water (dH_2O). This finding was further substantiated with atomic force microscopy (AFM), and an anisotropy surface characterization analysis using fast fourier transform confirmed that all MES 5.0 microthreads had surface features that were anisotropic and consistent with the long axis of the microthreads. AFM also revealed that surface features on fibrin microthreads were on the sub-micron scale. Surface features were approximately 25-40 nm in height and 0.5 μm in width. These features are consistent with the 0.5 - 1 μm wide perimysial collagen bundles that run parallel to muscle fibers in native skeletal muscle ECM that play in important role in myofiber alignment.[1] These dimensions are also consistent with those reported in literature to promote myoblast alignment and myotube formation.[9-11] We hypothesize that anisotropic surface features are generated on MES 5.0 microthreads because the more acidic bath degrades fibrin on the microthread surface, exposing aligned interfibrillar structures within the microthread. An

important fabrication step in fibrin microthread production is uniaxial stretching.[7] Researchers have demonstrated that uniaxially stretched fibrin gel and microthread scaffolds have a high degree of interfibrillar alignment.[7, 12-15]

Despite marked changes in surface features, MES etched fibrin microthreads did not exhibit changes in scaffold tensile mechanical properties compared to control dH_2O microthreads. Scaffold mechanics are known to play an important role in myotube maturation.[16] All microthread conditions strained 23% - 27% before failure, which is consistent with the 10% - 30% strains experienced in native skeletal muscle. Control and etched microthreads had maximum tangent moduli (MTM) that ranged from 103 - 147 MPa. This is considerably higher than native skeletal muscle tissue which has a static stiffness of 12 kPa that increases up to 11.2 MPa during muscle contraction.[17] It has been demonstrated previously that substrates significantly stiffer than native muscle promoted the generation of enhanced myogenic differentiation via an upregulation in muscle creatine kinase and myogenin expression.[18, 19] The lack of significant changes to fibrin microthread mechanics with this surface etching technique is significant, because it allows us to tune scaffold topography independent of mechanics. This makes MES etching a versatile tool for modulating the structural features of fibrin microthreads.

MES 5.0 microthreads with anisotropic grooved surface features enhanced myoblast alignment compared to MES 5.5 microthreads. Cytoskeletal staining of filamentous actin revealed that myoblasts appeared elongated with aligned stress fibers consistent with the long axis of MES 5.0 single and bundled microthreads. A nuclear orientation analysis of myoblasts seeded on single microthreads revealed that myoblasts preferentially aligned on all microthread conditions. This finding is expected, as it has been previously reported that microthreads promote alignment of a variety of cell types, including fibroblasts[20], cardiomyocytes[21], and myoblasts.[7] We found that a significantly higher percentage of myoblasts (58%) were aligned within 15° of the thread long axis on MES 5.0 microthreads compared to MES 5.5 microthreads (36%). Aligned micropatterned and electrospun scaffolds with similar sub-micron sized features have been shown to promote enhanced myoblast alignment and myotube formation.[9-11]

In conclusion of *Specific Aim 1: Create and characterize anisotropic surface topography on fibrin microthreads to enhance myoblast alignment*, we developed and characterized a new method of etching the surface of fibrin microthreads to incorporate aligned, sub-micron grooves

by placing fibrin microthreads into MES acidic buffer. We evaluated the effect of buffer pH on the generation of these features. Surface characterization with AFM and SEM indicated the generation of aligned, sub-micron sized grooves on microthreads in MES buffer with pH 5.0. Microthreads etched with surface features had tensile mechanical properties comparable to controls, indicating that surface treatment does not inhibit scaffold bulk properties. Our data demonstrates that etching threads in MES buffer with pH 5.0 enhanced alignment and filamentous actin stress fiber organization of myoblasts on the surface of scaffolds. The ability to tune topographic features on the surfaces of scaffolds independent of mechanical properties provides a valuable tool for designing microthread-based scaffolds to enhance regeneration of functional muscle tissue.

6.2.2 Specific Aim 2: Enzymatically crosslink fibrin microthreads with horseradish peroxidase to enhance mechanical properties and decrease degradation rate while maintaining myoblast viability

This aim sought to further alter the biophysical cues of fibrin microthreads by generating a new method to enzymatically crosslink the scaffolds to enhance their mechanical properties and decrease their degradation rate. Uncrosslinked (UNX) fibrin microthreads are susceptible to rapid degradation by fibrinolytic proteases when implanted *in vivo* which greatly limits their clinical utility for promoting functional tissue regeneration.[6, 7, 20, 22] This motivated the development strategies to increase the structural stability and persistence of these scaffolds. Fibrin microthread mechanical properties have been modified through production and post-processing crosslinking techniques.[7, 20, 22] Increasing microthread uniaxial stretching during production yields scaffolds with significantly greater tensile strength and moduli, but does not decrease scaffold degradation rate.[7] Fibrin microthreads have also been crosslinked with ultraviolet (UV) light[20] and EDC,[22] which both enhanced scaffold mechanics. However, both strategies have distinct disadvantages. UV crosslinked fibrin microthreads attenuated fibroblast proliferation,[20] and EDC crosslinked microthreads did not degrade when implanted in an *in vivo* murine VML defect, which limited cell mediated scaffold remodeling.[5] Thus, we sought to develop a new strategy to crosslink fibrin microthreads that might significantly enhance their mechanics and prolong their degradation without inhibiting cellular viability.

We investigated dityrosine crosslinking of fibrin microthreads using an enzymatic reaction driven by HRP. Enzymatic HRP reactions have high specificity and occur in aqueous solutions with neutral pH, making them amenable to fibrin microthread modifications. HRP crosslinking of phenol-containing polymer scaffolds with H_2O_2 used as the substrate has enabled tunable scaffold mechanical properties and degradation rates while maintaining biocompatibility,[23, 24] but it had yet to be explored for crosslinking fibrin-based scaffolds. We examined the effect of varying HRP and H_2O_2 incorporation strategies on resulting crosslink densities, structural properties, and myoblast viability. The incorporation of crosslinking agents into the precursor solutions during extrusion of microthreads was considered a primary (1º) modification method, while soaking microthreads in a post-processing crosslinker bath was considered a secondary (2º) method of scaffold modification. Microthreads were enzymatically crosslinked through primary, secondary, or a combination of both approaches (1º/2º).

The incorporation of HRP and H_2O_2 through 1º and 2º methods resulted in the formation of covalent bonds between tyrosine residues of fibrin, which was confirmed by quantitative fluorescence microscopy and fourier transform infrared spectroscopy (FTIR). All fibrin microthreads crosslinked with HRP and H_2O_2 via primary and/or secondary methods exhibited increased fluorescence compared to UNX microthreads, suggesting dityrosine bond formation in these scaffolds. FTIR analyses further confirmed the formation of isodityrosine bonds on 1º HRP crosslinked microthreads, which are a less common product of this enzymatic reaction. Taken together, these results demonstrate that HRP-catalyzed crosslinking of fibrin microthreads occurs as hypothesized, and that the degree of crosslinking is dependent on crosslinker incorporation strategy. We hypothesize that differences in the extent of crosslinking observed with different incorporation strategies are due to the distribution of HRP and H_2O_2 within the microthreads. In 1º HRP crosslinked microthreads, HRP and H_2O_2 are evenly distributed through the microthread and added during polymerization, when polymer chain mobility is higher. In contrast, 2º HRP crosslinking relies on HRP and H_2O_2 diffusion through the microthreads and occurs after polymerization when polymer chain mobility is lower. Because of this, we hypothesize that 2º HRP crosslinking is primarily crosslinking the surface of the microthreads. We believe this may also explain our finding that 2º HRP crosslinked microthreads had a significantly lower swelling ratio than UNX microthreads.

HRP crosslinking yielded enhanced biophysical properties of microthreads, including improved tensile mechanical properties and resistance to plasmin-mediated degradation. All HRP crosslinked microthreads had significantly increased (1.5 - 3.5-fold higher) ultimate tensile strengths (UTS) compared to UNX microthreads. MTM were significantly higher in 1º/2º and 2º HRP crosslinked microthreads compared to UNX microthreads. The degree to which HRP crosslinking enhanced microthread mechanics is consistent with previous literature performing photochemical dityrosine crosslinking of fibrin scaffolds.[25, 26] HRP-catalyzed crosslinking further mediated the resistance of microthreads to plasmin-mediated proteolytic degradation. Despite significant dityrosine bond formation and enhanced tensile mechanics, 1º/2º and 2º HRP crosslinked microthreads did not have increased resistance to plasmin-mediated degradation compared to UNX microthreads. 1º HRP crosslinked microthreads, which exhibited the highest crosslink density, had prolonged degradation at early timepoints compared to UNX control microthreads. We hypothesize that the increased crosslink density of 1º HRP crosslinked microthreads inhibits plasmin from accessing its cleavage sites. Plasmin cleaves the β-chain and γ-chain of fibrin, which also have the most abundant tyrosine residues that would participate in crosslinking.[27] HRP crosslinking had a less pronounced effect on prolonging plasmin-mediated degradation than EDC crosslinking,[22] which would be expected as there are less tyrosine residues readily available for HRP crosslinking than amides, which are abundant in fibrin for EDC crosslinking.

Finally, we observed robust viability of myoblasts seeded on HRP crosslinked microthread bundles after three days in culture by performing LIVE/DEAD staining. All crosslinked microthreads regardless of HRP and H_2O_2 incorporation strategy demonstrated a high degree of viability, with only a few dead cells that could be identified on the surface of the microthread bundles. This is consistent with previously published work that demonstrated extended viability and proliferation of cells seeded on or encapsulated within HRP crosslinked scaffolds made of silk,[28, 29] HA,[30, 31] and gelatin,[32-35] among others. Despite reported biocompatibility of this crosslinking technique, immunogenicity and cytotoxicity of HRP and H_2O_2 remain concerns of this crosslinking method.[36] However, we hypothesize that we observed minimal cytotoxicity because HRP crosslinked microthreads are subsequently rinsed after crosslinking, removing any residual HRP and H_2O_2 from the scaffold before cells were seeded on the microthreads. This is

unlike hydrogel-based systems that encapsulate cells during hydrogel crosslinking, thus directly exposing cells to HRP and H_2O_2.

In conclusion of *Specific Aim 2: Enzymatically crosslink fibrin microthreads with horseradish peroxidase to enhance mechanical properties and decrease degradation rates while maintaining myoblast viability*, we reported findings of the first study investigating HRP crosslinking of a fibrin scaffold. We examined the effect of varying HRP and H_2O_2 incorporation strategies by using primary (1º) and secondary (2º) scaffold modification techniques to crosslink fibrin microthreads. The incorporation of crosslinking agents into the precursor solutions during extrusion of microthreads was considered a 1º modification method, while soaking microthreads in a post-processing crosslinker bath was considered a 2º method of scaffold modification. All fibrin microthreads crosslinked with HRP and H_2O_2 via 1º and/or 2º methods exhibited an increase in dityrosine crosslink density compared to UNX microthreads, demonstrated by scaffold fluorescence. FTIR indicated the formation of isodityrosine bonds in 1º HRP crosslinked microthreads. Characterization of tensile mechanical properties revealed that all HRP crosslinked microthreads were significantly stronger than UNX microthreads. 1º HRP crosslinked microthreads also demonstrated significantly slower degradation than UNX microthreads, suggesting that incorporating HRP and H_2O_2 during extrusion yields scaffolds with increased resistance to proteolytic degradation. Finally, myoblasts seeded on HRP crosslinked microthreads retained a high degree of viability, demonstrating that HRP crosslinking yields biocompatible scaffolds suitable for tissue engineering. This work will facilitate the rational design of enzymatically crosslinked fibrin microthreads with tunable structural properties, enabling their application for engineered tissue constructs with varied mechanical and structural properties, including skeletal muscle.

6.2.3 Specific Aim 3: Develop fibrin microthreads with fibroblast growth factor 2 (FGF2) release profiles to enhance myoblast proliferation and outgrowth

FGF2's pleiotropic effect on promoting myogenesis, angiogenesis, and innervation make it an ideal growth factor for treating VML injuries. FGF2 is present in muscle tissue 2-8 days after injury, highlighting the need for sustained release of FGF2.[37] To mitigate challenges with FGF2 delivery such as supraphysiological dosing and its short *in vivo* half-life,[38, 39] bioinspired

conjugation strategies have been investigated using heparin to mimic sequestration of FGF2 in the ECM.[40-43] While the therapeutic potential of sustained FGF2 delivery to VML defects has been demonstrated, it has primarily been performed in hydrogel scaffolds, which lack biophysical cues such as mechanical support and aligned contact guidance.[44-46] The physiologically-relevant, sustained delivery of FGF2 from scaffolds with robust mechanical properties and topographic alignment cues has yet to be explored for treating VML injuries.

The goal of this aim was to develop an instructive fibrin microthread scaffold with physiologically-relevant, sustained release of FGF2. To accomplish this, we coupled heparin to fibrin microthreads, creating a biomimetic conjugation strategy recapitulating FGF2 sequestration in the basement membrane. Heparin sodium salt was either passively adsorbed or covalently coupled to fibrin microthreads in increasing concentrations from 0 to 1000 μg/mL. Passively adsorbed heparin likely binds to fibrin primarily through electrostatic interactions.[47] Carbodiimide crosslinking was employed to create a covalent amide bond between the carboxyl groups of heparin and the amine groups of fibrin, producing a stable bond with no residues from the crosslinking reaction in the bond structure.[48] Toluidine blue staining and FTIR were used to confirm heparin incorporation to fibrin scaffolds. Both passively adsorbed (UNX HEP) and covalently conjugated (EDC HEP) conditions demonstrated increasing toluidine blue dye uptake with increasing concentrations of heparin from 0 to 1000 μg/mL, which was quantified with a pixel intensity analysis. FTIR was used to evaluate an increase in amide bond and sulfone ($-SO_3$) peaks as a result of heparin incorporation onto the microthreads. All microthreads covalently coupled with heparin appeared to have higher amide and sulfone peaks than UNX microthreads, despite challenges seeing clear differences in overlapping peaks. This data may indicate the presence of heparin on these scaffolds. Other studies have also demonstrated an increasing amount of conjugated heparin on collagen scaffolds by increasing the heparin concentration of the crosslinking solution.[48, 49]

In addition to heparin conjugated microthreads, we evaluated whether co-incorporation of FGF2 within the fibrin microthread scaffolds by mixing prior to extrusion (co-inc) would yield sustained release of FGF2. Fibrin is an ideal scaffold material for incorporating FGF2, as it binds with high affinity to FGF2 and protects it from proteolytic degradation.[50] Co-inc fibrin microthreads yielded sustained release of FGF2 over the course of five days, at which point the

scaffolds were largely degraded and FGF2 release was attenuated. A linear regression analysis of FGF2 release kinetics through the first 5 days showed that co-inc microthreads achieved zero-order release kinetics of FGF2 ($R^2 = 0.94$). We hypothesize that FGF2 release was mediated by a combination of hydrolysis, bulk degradation, dissociation of FGF2 from fibrin, and diffusion through the microthread. Co-inc microthreads had the smallest total cumulative FGF2 release compared to microthreads passively adsorbed with FGF2, which is likely due to differences in the initial loading strategies.

Fibrin microthreads covalently conjugated with heparin also demonstrated sustained release of FGF2 over one week. Concentrations of 100 and 1000 μg/mL heparin appeared to yield more sustained release and higher cumulative FGF2 delivery compared to EDC microthreads with no heparin. Yang et al. observed similar sustained release of FGF2 from a fibrinogen scaffold conjugated with heparin via EDC crosslinking.[40] After a crush injury, FGF2 is present in muscle tissue 2-8 days after injury, and peaks at 6-8 days;[37] this highlights the need for a scaffold capable of providing sustained release of FGF2 over the course of one week. We hypothesize FGF2 release from heparin conjugated fibrin microthreads occurs through a combination of FGF2 dissociation from heparin and degradation of fibrin.[41, 42]

Microthreads passively adsorbed with 1000 μg/mL heparin (UNX HEP 1000) had the highest total FGF2 release, which was 2.75-fold higher than EDC microthreads with the same 1000 μg/mL heparin concentration (EDC HEP 1000). However, UNX HEP 1000 microthreads appeared to have a greater initial burst release of FGF2 compared to EDC HEP 1000, which may be a result of the non-covalent attachment of heparin. Yang et al. compared FGF2 release from fibrin hydrogels containing free and EDC conjugated heparin, and found that fibrin hydrogels containing free heparin had less sustained release than heparin conjugated fibrinogen, and exhibited a higher initial burst release within the first few days.[40] The sustained release of FGF2 from UNX microthreads may be due to the high binding affinity FGF2 has for fibrin, allowing FGF2 to bind with specificity to saturate UNX microthreads, mediating its sustained release from the scaffold. We hypothesize that differences in cumulative release between fibrin microthread conditions is likely a result of differences in initial FGF2 binding as well as release mechanisms and should be investigated in the future.

A Transwell®-based proliferation assay was performed to evaluate whether FGF2 released from fibrin microthreads remained bioactive by measuring its ability to stimulate myoblast proliferation over the course of four days. At each timepoint, there was no significant difference in the percent of $Ki67^+$ myoblasts between FGF2-loaded fibrin microthread conditions, although they appeared to stimulate higher percent $Ki67^+$ myoblasts on days 2-4 compared to serum free medium (SFM) and UNX no FGF2 control conditions. All FGF2 loaded microthreads stimulated myoblast proliferation comparable to 5 ng/mL FGF2 supplemented SFM, suggesting that our incorporation strategies did not inhibit FGF2 bioactivity. The percent of $Ki67^+$ myoblasts significantly increased from day 1 to day 4 in all microthread conditions passively adsorbed with FGF2, including UNX, EDC, and EDC HEP 10, 100, and 1000 microthreads, indicating that FGF2 was able to release and stimulate proliferation over a prolonged time. Hoechst count was also used to determine fold changes in cell number normalized to SFM at each timepoint. Co-inc microthreads, as well as UNX and EDC crosslinked microthreads with 10, 100, and 1000 μg/mL heparin and passively adsorbed with FGF2 all had heightened normalized cell number, ranging from a ~1.1 to 2.5-fold increase over those cultured in SFM. Additionally, normalized myoblast cell number remained elevated over four days in all FGF2 loaded microthreads.

To assess the ability of FGF2 that remains bound on fibrin microthreads to stimulate myoblast proliferation and migration, we performed a three dimensional (3D) cellular outgrowth assay. Myoblast outgrowth was observed as several leading myoblasts furthest out on the microthread, which were followed by a more confluent layer of cells. Myoblast outgrowth rate on fibrin microthreads was linear for all conditions (R^2 values for each condition ranged from $0.92 < R^2 < 0.99$) and was highest on co-inc and UNX HEP 1000 microthreads (both 145 μm/day). Although not significantly different, there appeared to be a trend where outgrowth was higher on UNX microthreads compared to EDC crosslinked microthreads with the same heparin concentration. Researchers demonstrated that EDC crosslinking of collagen films reduced C2C12 binding and spreading, which they hypothesize is due to EDC crosslinking using the functional groups necessary for integrin-mediated cellular attachment.[51, 52] Finally, to uncouple which cellular mechanism is primarily contributing to the myoblast outgrowth observed on FGF2-loaded fibrin microthreads, we performed Ki67 staining of myoblasts on fibrin microthreads from the 3D outgrowth assays. All conditions, regardless of FGF2 incorporation strategy, showed minimal

expression of $Ki67^+$ nuclei. Thus, we may conclude that the outgrowth observed on fibrin microthreads is driven by myoblast migration, rather than proliferation.

In conclusion, the goal of *Specific Aim 3: Develop fibrin microthreads with fibroblast growth factor 2 release profiles to enhance myoblast proliferation and outgrowth* was to develop an instructive fibrin microthread scaffold with physiologically-relevant, sustained release of FGF2. To accomplish this, we coupled heparin to fibrin microthreads, creating a biomimetic conjugation strategy. We also evaluated whether incorporation of FGF2 within the fibrin microthreads by mixing prior to extrusion would yield sustained release of FGF2. We hypothesized that heparin conjugated and co-incorporated fibrin microthreads would provide sustained release of FGF2 from the scaffold and enhance *in vitro* myoblast proliferation and outgrowth. Toluidine blue staining and FTIR confirmed heparin conjugation to fibrin microthreads by demonstrating increased dye uptake and amide bond peaks, respectively. FGF2 release kinetics revealed that fibrin microthreads conjugated with heparin had sustained release over one week and delivered a higher total amount of FGF2 than microthreads without heparin conjugation. A Transwell®-based proliferation assay demonstrated that FGF2 released from fibrin microthread scaffolds was bioactive, stimulating myoblast proliferation over a period of four days *in vitro*. Finally, a 3D outgrowth assay demonstrated that co-inc and heparin conjugated microthreads may enhance myoblast outgrowth. Sustained release of FGF2 from fibrin microthreads addresses limitations in the field and it will enable the development of a scaffold that synergistically provides biochemical and biophysical cues. We anticipate that the combined effect of fibrin microthread mechanical properties, topographic alignment cues, and FGF2 will be an effective scaffold to enhance the regeneration of functional muscle tissue in VML injuries.

6.3 FUTURE WORK

The goal of this thesis was to develop fibrin microthread scaffolds with instructive biophysical and biochemical cues which direct the cellular processes that will ultimately enhance functional muscle regeneration in VML injuries. We accomplished this by developing microthreads with sub-micron anisotropic surface features, robust mechanical properties, and physiologically-relevant, sustained release of FGF2. Moving forward, we are interested in combining the strategies developed herein and evaluating this microthread scaffold in an *in vivo*

VML defect to investigate its ability to facilitate functional muscle regeneration. Fibrin microthread biophysical properties can be further developed by additional tuning of HRP crosslinking, altering microthread diameter, and incorporating microthreads into a composite scaffold. The addition of biochemical cues such as multi-growth factor delivery and cell-laden microthreads may also be worth investigating and are also discussed herein. Finally, the development of a multi-cellular *in vitro* outgrowth assay will be beneficial in creating a more predictive *in vitro* model of how fibrin microthreads will facilitate myogenesis, angiogenesis, innervation, and ECM deposition upon implantation.

6.3.1 Evaluate fibrin microthreads in an in vivo VML defect

Before making additional modifications to fibrin microthreads, we are first interested in combining the methods described in this thesis to ultimately develop an off-the-shelf scaffold with anisotropic surface features, robust mechanical properties, and sustained release of FGF2. We envision this scaffold to include several different types of discrete microthreads combined into one microthread bundle, which could then be implanted into a VML defect. The implantation of fibrin microthread bundles in VML defects remains a limitation of this proposed method, and an alternative composite-based scaffold is addressed in detail in Section 6.3.2. To evaluate functional muscle regeneration *in vivo*, we plan on using a murine *tibialis anterior* (TA) partial resection injury model, which has been previously described and used to assess fibrin microthreads *in vivo*.[5, 6] Using this same defect model, timepoints of 14 and 60 days, and functional assessment methodology allows results from these studies to be directly compared to previous work assessing fibrin microthread scaffolds.

Before creating a scaffold that combines several types of microthreads, we first need to evaluate individual conditions from each aim alone to assess their ability to promote *in vivo* functional muscle regeneration. From aim 1, we are interested in evaluating MES 5.0 microthreads in an *in vivo* VML defect, as they enhanced myoblast alignment *in vitro*. By evaluating these scaffolds *in vivo*, we can determine their ability to promote cellular infiltration, aligned differentiation, and tetanic contractile force. We would also like to assess 1° HRP crosslinked microthreads from aim 2 because they had the most di- and isodityrosine bonds formed, the highest resistance to *in vitro* plasmin-mediated degradation, and enhanced mechanical properties. By

evaluating this scaffold *in vivo*, we can further assess its degradation and biocompatibility *in vivo*. Finally, we want to assess both EDC HEP 1000 and UNX HEP 1000 microthreads *in vivo*, as these scaffolds had the highest heparin adsorption. UNX HEP 1000 microthreads had the highest FGF2 release and stimulated the highest *in vitro* myoblast outgrowth rate. EDC HEP 1000 microthreads also had sustained FGF2 release, despite being less total release than UNX HEP 1000 microthreads. Evaluating EDC HEP 1000 microthreads *in vivo* will also better inform us about the scaffold biocompatibility, especially when compared directly to UNX HEP 1000 microthreads. An *in vivo* study will also allow for a more thorough investigation of how these scaffolds influence myoblast response, as well as angiogenesis, fibrosis, and innervation. An injury with no treatment and treatment with control UNX fibrin microthreads will serve as controls for these experiments.

After a thorough characterization of individual microthread scaffolds is performed, future work can then address the delivery of combinations of microthreads in an *in vivo* VML defect. We would be interested in evaluating the combination of MES 5.0 microthreads, 1° HRP crosslinked microthreads, and UNX HEP 1000 FGF2 microthreads as one bundled microthread scaffold. It would also be interesting to make 1° HRP crosslinked microthreads and assess whether they can be subsequently etched or passively adsorbed with heparin and FGF2. This would allow us to generate one microthread with alignment cues, enhanced mechanics, and sustained FGF2 delivery, and eliminate the need to create microthread bundles that consist of various microthreads.

6.3.2 Further enhancing biophysical cues: Microthread structural modifications

In specific aim 2, we demonstrated that the structural properties of fibrin microthreads could be altered through HRP-mediated enzymatic crosslinking, whereby incorporating HRP and H_2O_2 during microthread extrusion or in a post-processing crosslinker bath resulted in varying degrees of crosslinking and microthread structural properties. To further modulate the degree of HRP-mediated crosslinking, tensile mechanics, and enzymatic degradation, other aspects of this crosslinking reaction can be varied. Future work varying fibrinogen, HRP, and H_2O_2 concentrations will enable the development of more robust changes in fibrin microthread tensile mechanics and degradation kinetics. Other researchers demonstrated that tunable scaffold mechanics and degradation were achieved by altering H_2O_2 concentration,[53] percent concentration of composite components,[29] and delivery method.[54] Further modifications of HRP crosslinking

may allow for a greater range of microthread ultimate tensile strengths and moduli, enabling the application of these scaffolds to an array of target tissues that possess varying structures, mechanical demands, and functions. Tunable mechanical stiffnesses of biomaterial scaffolds regulate cellular processes including adhesion, proliferation, migration, and differentiation.[55] Additionally, hierarchically assembling these microthreads into complex 3D scaffolds such as composites, braids, and bundles enable further optimization of scaffold mechanics and mimic tissue-specific ECM architectures including skeletal muscle, ventricular myocardium, tendon, ligament, or skin.[4]

We found that HRP crosslinked microthreads supported myoblast viability, which is consistent with previous literature demonstrating extended cell viability and proliferation of cells on or within HRP crosslinked scaffolds.[28-35, 56-58] However, concerns remain regarding the immunogenicity and cytotoxicity of HRP and H_2O_2, which may be more prevalent upon scaffold implantation.[36] Future work should focus on replacing plant-derived HRP with a human peroxidase such as myeloperoxidase. Myeloperoxidase has been shown to crosslink tyrosine residues in the presence of H_2O_2.[59] Human-derived catalysts such as hematin could also be used to catalyze dityrosine crosslinking.[60-62] Myeloperoxidase may also be a more effective catalyst, as previously researchers have shown it was ten times more effective than HRP as a catalyst of crosslinking bovine serum albumin (BSA).[63] Additionally, future studies to further characterize myoblast seeding efficiency, proliferation, and metabolic activity may better elucidate their interaction with HRP crosslinked fibrin microthreads.

Additional methods to alter microthread mechanics independent of crosslinking could also be explored in future studies. Our lab has previously demonstrated that altering the degree to which microthreads are uniaxially stretched during their production yields scaffolds with varying tensile strengths and stiffnesses.[7] Preliminary work in the Pins lab sought to alter fibrin microthread diameter by altering the diameter of the polyethylene tubing which combine the fibrinogen and thrombin solutions prior to being drawn into a HEPES buffer bath. Preliminary studies used conventional 0.86 mm inner diameter (ID) tubing, as well as large 1.67 mm and small 0.38 mm ID tubing. Large diameter tubing created microthreads with a hydrated diameter of approximately 300 microns, while small microthreads had a hydrated diameter of 44 microns (**Figure 6.1 A, B**). Interestingly, microthreads with different diameters also demonstrated varying tensile mechanics.

Small diameter microthreads had the highest UTS and MTM, while large diameter microthreads had a lower UTS and MTM compared to small and normal diameter microthreads (**Figure 6.1 C, D**). We hypothesize that changes in scaffold mechanics are likely due to the degree of interfibrillar alignment of the fibrin within microthreads, which we hypothesize is lower in large diameter microthreads and higher in small diameter microthreads. We hypothesize that interfibrillar alignment is primarily a function of uniaxial stretching and could be assessed with SEM, as demonstrated previously.[13, 15] Upon further investigation, altering microthread diameter may serve as an additional production parameter that can be varied to yield scaffolds with altered mechanics, and could be exploited to create scaffolds for a range of tissues with varying mechanical demands.

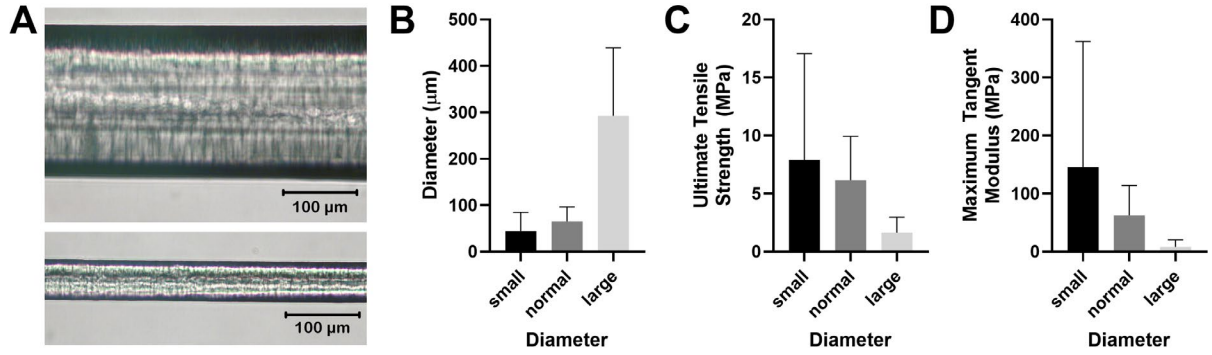

Figure 6.1. Fibrin microthreads with varying diameter. (A) Brightfield image of hydrated large diameter (top) and small diameter (bottom) microthreads. (B) Diameter, (C) Ultimate tensile strength, and (D) Maximum tangent modulus of fibrin microthreads with small, normal, and large diameters made with 0.38, 0.86, and 1.67 mm I.D. tubing, respectively (Mean ± SD; N ≥ 1).

In addition to their enhanced tensile mechanics, smaller diameter fibrin microthreads may also promote enhanced myoblast alignment. Hwang et al. generated poly(lactic-co-glycolic acid) (PLGA) microfibers with diameters ranging from 10 to 250 µm and assessed their ability to promote fibroblast alignment.[64] They found that cellular alignment increases with decreasing microfiber diameter. Low 10 µm diameter microfibers yielded mean cell angle of 3° within the long axis of the microfiber, whereas fibers with 250 µm diameter had a 38° mean orientation. This work demonstrates the importance of microfiber diameter in directing cellular orientation, with fibers on the same size scale as those reported in our pilot study. Myoblast alignment is critical for myotube formation and functional muscle regeneration; enhancing the ability of myoblasts to align on fibrin microthreads likely strengthens their regenerative potential. Small diameter microthreads

may serve as an alternative strategy to obtain a higher degree of myoblast alignment on fibrin microthreads than MES etching, which was described in specific aim 1 of this thesis. However, it should be noted that small diameter fibrin microthreads made with the same co-extrusion method will likely remain on the micron-scale, unless other methods to generate these are developed such as electrospinning, which can create microthreads with nanoscale diameters. MES etching generates anisotropic surface grooves on the sub-micron scale, which better recapitulate the size scale of native ECM fibrils and have been shown to promote enhanced myoblast alignment and myotube formation.[9-11] Additionally, MES etching of small diameter microthreads may provide more robust cellular alignment than what we demonstrated in this thesis.

Other strategies to enhance myoblast alignment on fibrin microthreads other than surface topography could also be explored. Mechanical and electrical stimulation have demonstrated success in recapitulating skeletal muscle structure and function.[65] Native skeletal muscle tissue receives electric signals from motor neurons via neuromuscular junctions, initiating muscle contraction. Electrical stimulation has been shown to further enhance myoblast alignment, contractile protein expression, and contractility when used in conjunction with anisotropically aligned electrospun scaffolds.[66, 67] Future work incorporating electrical stimulation into fibrin microthread culture may serve as a method to further enhance myoblast alignment on these scaffolds. In addition to electrical signals, skeletal muscle experiences mechanical strains during development that play an important role in myogenesis. A range of mechanical strain regimes applied to tissue engineered skeletal muscle constructs have resulted in enhanced myogenic outcomes.[68] There is promising potential in combining electrical and mechanical stimulation regimes with anisotropically aligned scaffolds towards the goal of further enhancing myoblast maturation, alignment, and differentiation. Preliminary work in our lab is focused on providing these instructive mechanical and electrical cues to fibrin microthread scaffolds.

Future work to develop composite scaffolds of fibrin microthreads encapsulated within a hydrogel or film may also allow for further mechanical tunability, easier handling and implantation, and a more efficient strategy to incorporate cells within the scaffold. Our lab previously developed a composite scaffold consisting of aligned fibrin microthreads encapsulated within a fibrin hydrogel.[21] By increasing the number of threads within the composite (and thus the microthread volume fraction), Chrobak et al. were able to significantly increase the moduli of the

scaffolds. They also demonstrated that cells could be encapsulated within the fibrin hydrogel portion of the composite, creating an efficient strategy for seeding a microthread-based scaffold. Furthermore, they demonstrated that encapsulated cardiomyocytes within 100 μm of a fibrin microthread preferentially aligned in the direction of the microthread. Taken together, fibrin microthreads within composite scaffolds can create mechanically tunable scaffolds and promote regional cellular alignment. Composite scaffolds with encapsulated microthreads may serve as a more efficient strategy for treating the large size-scale VML injuries. Previous pre-clinical *in vivo* studies filled the VML defect by individually placing microthreads to pack the wound,[5, 6] which is not scalable for clinical-sized defects. Additionally, current strategies to seed fibrin microthreads[6, 69-72] may not be as efficient as delivering hydrogel-encapsulated cells, which is known to be a highly efficient delivery method.

6.3.3 Further enhancing biochemical cues: Multi-growth factor dual delivery

Growth factors are among some of the most commonly investigated biologic molecules to treat VML injuries because they play an instrumental role in facilitating native skeletal muscle regeneration.[73] While delivery of a single growth factor has shown promising results for promoting skeletal muscle regeneration and angiogenesis, this strategy represents a highly simplified version of the complex, spatiotemporal presentation of multiple factors during regeneration. Toward the goal of recapitulating *in vivo* regeneration, researchers investigated the synergistic presentation of multiple growth factors.[74] We hypothesize that we can further enhance fibrin microthread biochemical cues and improve myoblast proliferation, migration, and differentiation through the strategic temporal incorporation of an additional growth factor along with FGF2.

Researchers investigated the co-stimulatory effect of FGF2 in combination with hepatocyte growth factor (HGF)[75, 76] or insulin-like growth factor (IGF-1).[77, 78] Sheehan et al. showed that the co-stimulatory effect of HGF and FGF2 enhanced SC proliferation *in vitro* significantly more than either of the factors alone.[75] Hill et al. implanted alginate scaffolds containing SCs, HGF, and FGF2 into murine tibialis anterior (TA) laceration injuries to assess their ability to promote muscle regeneration.[79] Myoblasts delivered on scaffolds releasing both HGF and FGF2 had notably higher engraftment into the regenerating muscle compared to myoblasts delivered via bolus injection or acellular scaffolds loaded with HGF and FGF2. In addition to promoting myogenesis, the co-

stimulatory effect of HGF and FGF2 has also been shown to promote angiogenesis. Marui et al. found that the co-release of HGF and FGF2 from collagen microspheres yielded higher capillary density, maturation, and perfusion than either factor alone in an ischemic injury.[76] Despite these promising findings, the enhanced myogenic and angiogenic capability of HGF and FGF2 co-delivery has yet to be explored for treating VML injuries. Our laboratory delivered HGF from fibrin microthread scaffolds, and found that after 60 days implanted into a murine TA VML defect, they enhanced force production, recovering 200% of force relative to post-injury levels.[5] Future studies could incorporate HGF onto microthreads with this incorporation strategy, which demonstrated pre-clinical success for treating VML. These could be delivered alongside co-inc or heparin conjugated FGF2 microthreads developed in this thesis.

The co-delivery of FGF2 and IGF-1 from fibrin microthreads is also a promising future direction of this work. The Christ lab evaluated the co-stimulatory effect of keratin hydrogels loaded with FGF2 and IGF-1 for the treatment of VML defects in rat mouse latissimus dorsi (LD) VML defects.[78] Acellular keratin hydrogels loaded with FGF2 and IGF-1 enabled significantly improved recovery of contractile force compared to treatment with scaffolds loaded with either FGF2 or IGF-1 alone.[78] Because IGF-1 stimulates both proliferation and differentiation of SCs during skeletal muscle regeneration,[73, 80-83] we hypothesize that a sustained release of this factor from fibrin microthreads would enhance its ability to participate in myogenesis. Future work could develop strategies to provide sustained release of IGF-1 from fibrin microthreads, so the co-stimulatory effect of FGF2 and IGF-1 from fibrin microthreads can be realized for treating VML injuries. Taken together, past work demonstrates that FGF2 in combination with HGF or IGF-1 has a co-stimulatory effect in promoting myogenesis and angiogenesis. By further developing growth factor incorporation strategies on fibrin microthreads, the release of multiple growth factors in a spatiotemporal manner that mimics *in vivo* presentation can be achieved, and will likely enhance regenerative outcomes.[74, 84]

6.3.4 Utilizing fibrin microthreads for efficient cell delivery

While acellular fibrin microthreads have demonstrated success in promoting endogenous skeletal muscle regeneration through the recruitment of host cells,[5] it remains uncertain whether an acellular strategy has the potential to facilitate full functional recovery after the large-scale

injuries incurred from VML.[85, 86] Researchers hypothesize that limited host SC infiltration is the primary limitation to the success of acellular strategies, which was demonstrated after implantation of an acellular ECM scaffold into a murine VML defect.[86] Because of this, researchers often develop scaffolds to deliver SCs, myoblasts, or stem cells to VML defects. Scaffolds with strategic biophysical and biochemical signaling cues creates a synthetic microenvironment conducive for cell survival and engraftment upon transplantation. Delivered cells can then provide host cells with paracrine signaling and/or participate in regeneration.[87]

It has been well demonstrated that fibrin microthreads can be efficiently seeded with muscle derived progenitor cells (MDPCs),[6] mesenchymal stem cells,[69, 88] and induced pluripotent stem cells (iPS)[71] through static and dynamic seeding methods. Furthermore, fibrin microthreads served as an efficient cell delivery method to murine acute myocardial infarcts[70, 71, 88] and VML defects.[6] Fibrin microthreads seeded with MDPCs restored function in a mouse TA partial resection VML injury.[6] Implanted cells were found to migrate into the host tissue, and mice treated with cell-seeded fibrin microthreads had significantly reduced collagen deposition and higher muscle area compared to injuries that received no treatment. At four months post treatment, mice receiving treatment with MDPC-loaded microthreads had significant improvements in tetanic force generation compared to untreated injuries. This study suggests that fibrin microthreads in combination with MDPCs are a promising scaffold for treating VML defects.

Encapsulating myoblasts within fibrin microthreads may serve as an alternative, more efficient cell delivery system that better directs myoblast alignment and differentiation.[13] Keijdener et al. recently demonstrated less dense fibrin microthreads with lower fibrinogen concentrations (10 mg/mL vs. 70 mg/mL reported by our laboratory) can support encapsulated endothelial cells, fibroblasts, and Schwann cells.[13] They found that 30% and 60% stretching of microthreads after extrusion induced alignment of the fibrin fibrils parallel to the long axis of the microthread. When cells were extruded within fibrin microthreads (final concentration of 3×10^6 – 5×10^6 cells/mL), 60% stretching induced a small but significant decrease in cell viability, where ~7-11% of encapsulated cells were dead, depending on cell type. 60% stretching of cell-laden microthreads induced 75% alignment of fibroblasts within 20° of the long axis of the microthread. Based on these results, we hypothesize myoblasts could be successfully encapsulated within fibrin microthreads and stretching could induce alignment without detrimentally impacting

cell viability. We have conducted preliminary proof-of-concept work demonstrating that C2C12 myoblasts can be incorporated within fibrin microthreads by mixing a cell suspension with the 70 mg/mL fibrinogen solution prior to co-extrusion with 40 U/mL thrombin (**Figure 6.2**). Final cell concentrations of 0, 0.5×10^6, and 1×10^6 cells/mL were evaluated. We demonstrated that cells were evenly distributed throughout the fibrin microthreads.

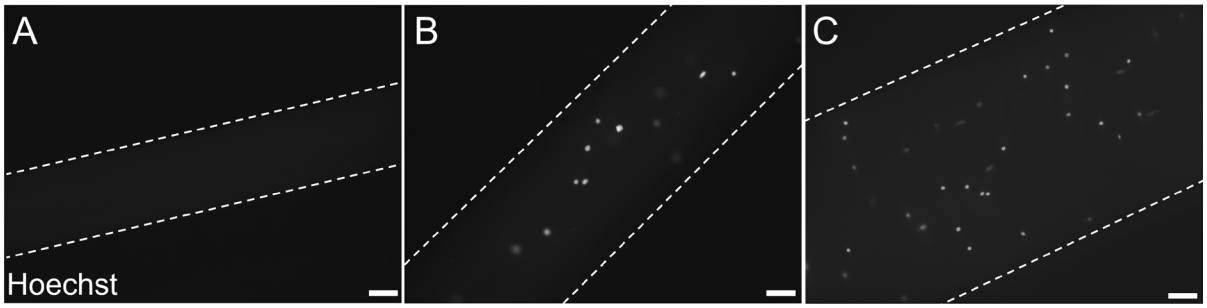

Figure 6.2. Myoblasts encapsulated within fibrin microthreads. C2C12 myoblasts were pre-loaded with Hoechst and encapsulated within fibrin microthreads by mixing cell suspensions with fibrinogen prior to co-extrusion. Final cell concentrations of 0, 0.5×10^6, and 1×10^6 cells/mL (A, B, and C, respectively) were evaluated and demonstrated even distribution of cells throughout the microthreads. Scale bar is 100 μm.

Based on the results from the Keijdener et al. study, we are interested in investigating the effect of fibrinogen concentration, cell concentration, and degree of stretching on encapsulated myoblast viability and alignment. More specifically, myoblast viability could be evaluated with LIVE/DEAD staining and a metabolic assay such as an MTT, while alignment could be assessed by immunostaining for filamentous actin and evaluating nuclear orientation. Other researchers developed C2C12-laden gelatin methacrylate microfibers, and they found that uniaxial strain of these fibers induced C2C12 alignment and differentiation into aligned myotubes.[89] Thus, future work could also evaluate extended culture time of myoblast-encapsulated microthreads to determine whether they will induce the formation of aligned and mature myotubes. This could be performed by quantifying myosin heavy chain (MyHC) in samples with a Western blot or reverse transcription polymerase chain reaction (RT-qPCR). Immunostaining for MyHC would also allow for an assessment of myotube alignment, width, length, and myogenic index. Overall, myoblast-laden fibrin microthreads may serve as an alternative method of incorporating cells that is able to maintain cell viability, induce cellular alignment, and promote aligned myotube formation. In addition to myoblasts, future work could also investigate the use of additional cell types that are

essential to VML regeneration, such as endothelial cells, neurons, or fibroblasts to generate a co-culture system.[90-95] Ultimately, these scaffolds may allow for more efficient cellular delivery to VML injuries, enhancing transplanted cell participation in regeneration and ultimately improving functional outcomes.

6.3.5 Development of a multi-cellular outgrowth assay

The *in vitro* cellular outgrowth assay developed by our lab is a useful tool for predicting *in vivo* cellular ingrowth onto fibrin microthreads scaffolds after skeletal muscle injury and subsequent scaffold implantation.[96, 97] Further development of this model may elucidate the response of other cell types to fibrin microthreads, including macrophages, endothelial cells, neurons, and fibroblasts. Many of these cell types play an important role in regulating various phases of skeletal muscle regeneration. Creating a more complex *in vitro* model with multiple cell types could allow for the study of multi-cellular interactions and paracrine signaling and may ultimately serve as a more predictive model of skeletal muscle regeneration.

Researchers have utilized co-cultures of myoblasts and neurons to assess neuromuscular junction (NMJ) formation, maturation, and signaling.[98-100] While both 2D and 3D co-culture systems can generate NMJs, Bakooshli et al. demonstrated that 3D co-cultures of MDPCs and iPS-derived motor neurons had upregulated epsilon acetylcholine receptor (AChR) subunit protein and activity, indicating a transition to a more mature phenotype than those cultured in 2D.[98] Furthermore, the addition of sera from patients with myasthenia gravis, a congenital disease caused by mutations in AChR genes, to the 3D co-culture system enabled the study of this disease. This study emphasizes the important role of 3D culture in more accurately recapitulating the native cellular microenvironment and highlights the application of 3D cellular assays towards disease modelling and drug screening applications. We hypothesize that co-culture of myoblasts and neurons within our cellular outgrowth assay may serve as a better predictor of multi-cellular interactions in response to fibrin microthreads than other conventionally used migration assays such as a 2D scratch assay or a Transwell® migration assay. Determining muscle- and nerve-specific protein regulation with Western blotting or immunofluorescence would indicate how this co-culture system influences myogenic differentiation and AChR formation and clustering. Additionally, it would be interesting to compare the 3D microthread-based co-culture system with

a 2D co-culture system to determine differences in the number and size of AChR clusters, MyHC expression, rapsyn expression, and calcium handling by transfecting myoblasts with GCaMP6, a fluorescent calcium indicator. To isolate the effect of paracrine signaling from one cell type to another, a Transwell®-based assay could be used to isolate cell types while allowing for secreted molecules to diffuse and act on the other cell type.

Vascularized muscle constructs have also been developed through the co-culture of myoblasts and endothelial cells and have demonstrated successful outcomes upon implantation into VML defects.[101] Because endothelial cells play an important role in facilitating muscle regeneration, it would be interesting to investigate their response, alone or in tandem with myoblasts, to fibrin microthreads. Kurpinski et al. demonstrated that aligned poly(l-lactide) (PLLA) nanofibers significantly enhanced endothelial cell migration and infiltration into the scaffold *in vitro* and in a murine *in vivo* dermal wound model.[102] Moreover, endothelial cell infiltration was further enhanced when aligned nanofibers were covalently conjugated with heparin via EDC crosslinking. Based on the results of this study, we anticipate heparin and FGF2-modified fibrin microthreads will stimulate endothelial cell migration. Further characterization of endothelial cell migration when cultured with myoblasts and/or pericytes may elucidate the multi-cellular response to these cells, including the effects of paracrine signaling between cell types, and the formation of more mature, pericyte-stabilized vasculature.

6.4 FINAL CONCLUSIONS

In this thesis, we developed fibrin microthreads with strategic biophysical and biochemical cues that direct cellular processes to ultimately enhance the functional regeneration of skeletal muscle in VML injuries. Specifically, we developed and characterized a novel method of etching aligned, sub-micron grooves onto microthreads by placing them in MES acidic buffer. AFM and SEM analyses indicated that this technique generated aligned, sub-micron sized grooves on microthreads in MES buffer with pH 5.0. Microthreads etched with surface features had tensile mechanical properties comparable to controls, indicating that surface treatment does not inhibit scaffold bulk properties. Microthreads etched in MES buffer with pH 5.0 enhanced alignment and filamentous actin stress fiber organization of myoblasts on the surface of scaffolds. The ability to tune topographic features on the surfaces of scaffolds independent of mechanical properties

provides a valuable tool for designing microthread-based scaffolds to enhance regeneration of functional muscle tissue.

To modulate fibrin microthread tensile mechanical properties and degradation rates, we developed an enzymatic crosslinking strategy for fibrin microthreads and examined the effect of varying HRP and H_2O_2 incorporation strategies. Mixing crosslinking reagents into microthread precursor solutions prior to extrusion was considered a 1º modification method, while soaking microthreads in a post-processing crosslinker bath was considered a 2º method of scaffold modification. Microthreads crosslinked via 1º and/or 2º methods exhibited an increase in dityrosine crosslink density compared to UNX microthreads. All HRP crosslinked microthreads were significantly stronger than UNX microthreads, and 1º HRP crosslinked microthreads also demonstrated significantly slower degradation than UNX microthreads. Myoblasts seeded on all HRP crosslinked microthreads retained a high degree of viability, indicating that HRP crosslinking yields biocompatible scaffolds suitable for skeletal muscle tissue engineering.

Finally, we developed fibrin microthreads with physiologically-relevant, sustained release of FGF2. We covalently conjugated heparin to fibrin microthreads, creating a biomimetic conjugation strategy mimicking native sequestration in the ECM. We also incorporated FGF2 within fibrin microthreads by mixing prior to extrusion. We confirmed heparin conjugation to fibrin microthreads by demonstrating increased dye uptake and amide bond peaks with increasing heparin concentration, respectively. FGF2 release kinetics revealed that fibrin microthreads conjugated with heparin had sustained release over one week and delivered a higher total amount of FGF2 than microthreads without heparin conjugation. A Transwell® proliferation assay demonstrated that FGF2 released from fibrin microthread scaffolds was bioactive, as it was able to stimulate myoblast proliferation over the course of four days *in vitro*. A 3D outgrowth assay demonstrated that co-inc and heparin conjugated microthreads may enhance myoblast outgrowth. Sustained release of FGF2 from fibrin microthreads addresses limitations in the field of scaffold that synergistically provides biochemical and biophysical cues. We anticipate that the combined effect of fibrin microthread mechanical properties, topographic alignment cues, and FGF2 will be an effective scaffold to enhance the cell-mediated regeneration of functional muscle tissue in VML injuries. Future work to further modulate the biophysical and biochemical cues of these scaffolds may enable more robust skeletal muscle regeneration.

6.5 REFERENCES

1. Gillies, A. R.; Lieber, R. L., Structure and function of the skeletal muscle extracellular matrix. *Muscle & nerve* **2011,** *44* (3), 318-31.
2. Serrano, A. L.; Munoz-Canoves, P., Regulation and dysregulation of fibrosis in skeletal muscle. *Experimental cell research* **2010,** *316* (18), 3050-8.
3. Webster, M. T.; Manor, U.; Lippincott-Schwartz, J.; Fan, C. M., Intravital Imaging Reveals Ghost Fibers as Architectural Units Guiding Myogenic Progenitors during Regeneration. *Cell stem cell* **2016,** *18* (2), 243-52.
4. O'Brien, M. P.; Carnes, M. E.; Page, R. L.; Gaudette, G. R.; Pins, G. D., Designing Biopolymer Microthreads for Tissue Engineering and Regenerative Medicine. *Curr Stem Cell Rep* **2016,** *2* (2), 147-157.
5. Grasman, J. M.; Do, D. M.; Page, R. L.; Pins, G. D., Rapid release of growth factors regenerates force output in volumetric muscle loss injuries. *Biomaterials* **2015,** *72*, 49-60.
6. Page, R. L.; Malcuit, C.; Vilner, L.; Vojtic, I.; Shaw, S.; Hedblom, E.; Hu, J.; Pins, G. D.; Rolle, M. W.; Dominko, T., Restoration of Skeletal Muscle Defects with Adult Human Cells Delivered on Fibrin Microthreads. *Tissue Eng Part A* **2011,** *17* (21), 2629-2640.
7. Grasman, J. M.; Pumphrey, L. M.; Dunphy, M.; Perez-Rogers, J.; Pins, G. D., Static axial stretching enhances the mechanical properties and cellular responses of fibrin microthreads. *Acta Biomater* **2014,** *10* (10), 4367-76.
8. Grasman, J. M. Designing Fibrin Microthread Scaffolds for Skeletal Muscle Regeneration. Doctoral dissertation, Worcester Polytechnic Institute, Worcester, MA, 2015.
9. Choi, J. S.; Lee, S. J.; Christ, G. J.; Atala, A.; Yoo, J. J., The influence of electrospun aligned poly(epsilon-caprolactone)/collagen nanofiber meshes on the formation of self-aligned skeletal muscle myotubes. *Biomaterials* **2008,** *29* (19), 2899-906.
10. Huang, N. F., Patel, S., Thakar, R.G., Wu, J., Hsiao, B.S., Chu, B., Lee, R.J., and Li, S., Myotube Assembly on Nanofibrous and Micropatterned Polymers. *Nano Letters* **2006,** *6* (3), 537-542.
11. Wang, P. Y.; Yu, H. T.; Tsai, W. B., Modulation of alignment and differentiation of skeletal myoblasts by submicron ridges/grooves surface structure. *Biotechnology and bioengineering* **2010,** *106* (2), 285-94.
12. Brown, A. E.; Litvinov, R. I.; Discher, D. E.; Purohit, P. K.; Weisel, J. W., Multiscale mechanics of fibrin polymer: gel stretching with protein unfolding and loss of water. *Science* **2009,** *325* (5941), 741-4.
13. Keijdener, H.; Konrad, J.; Hoffmann, B.; Gerardo-Nava, J.; Rutten, S.; Merkel, R.; Vazquez-Jimenez, J.; Brook, G. A.; Jockenhoevel, S.; Mela, P., A bench-top molding method for the production of cell-laden fibrin micro-fibers with longitudinal topography. *J Biomed Mater Res B Appl Biomater* **2020,** *108* (4), 1198-1212.
14. Matsumoto, T.; Sasaki, J.; Alsberg, E.; Egusa, H.; Yatani, H.; Sohmura, T., Three-dimensional cell and tissue patterning in a strained fibrin gel system. *PLOS ONE* **2007,** *2* (11), e1211.
15. Zhang, S.; Liu, X.; Barreto-Ortiz, S. F.; Yu, Y.; Ginn, B. P.; DeSantis, N. A.; Hutton, D. L.; Grayson, W. L.; Cui, F. Z.; Korgel, B. A.; Gerecht, S.; Mao, H. Q., Creating polymer hydrogel microfibres with internal alignment via electrical and mechanical stretching. *Biomaterials* **2014,** *35* (10), 3243-51.
16. Engler, A. J.; Griffin, M. A.; Sen, S.; Bonnemann, C. G.; Sweeney, H. L.; Discher, D. E., Myotubes differentiate optimally on substrates with tissue-like stiffness: pathological implications for soft or stiff microenvironments. *The Journal of cell biology* **2004,** *166* (6), 877-87.
17. Caiozzo, V. J., Plasticity of skeletal muscle phenotype: mechanical consequences. *Muscle & nerve* **2002,** *26* (6), 740-68.
18. Boontheekul, T.; Hill, E. E.; Kong, H. J.; Mooney, D. J., Regulating myoblast phenotype through controlled gel stiffness and degradation. *Tissue Eng* **2007,** *13* (7), 1431-42.

19. Gilbert, P. M.; Havenstrite, K. L.; Magnusson, K. E.; Sacco, A.; Leonardi, N. A.; Kraft, P.; Nguyen, N. K.; Thrun, S.; Lutolf, M. P.; Blau, H. M., Substrate elasticity regulates skeletal muscle stem cell self-renewal in culture. *Science* **2010,** *329* (5995), 1078-81.
20. Cornwell, K. G.; Pins, G. D., Discrete crosslinked fibrin microthread scaffolds for tissue regeneration. *J Biomed Mater Res A* **2007,** *82* (1), 104-12.
21. Chrobak, M. O.; Hansen, K. J.; Gershlak , J. R.; Vratsanos, M.; Kanellias, M.; Gaudette, G. R.; Pins, G. D., Design of a Fibrin Microthread-Based Composite Layer for Use in a Cardiac Patch. *ACS Biomater. Sci. Eng.* **2017,** *3* (7), 1394–1403.
22. Grasman, J. M.; Page, R. L.; Dominko, T.; Pins, G. D., Crosslinking strategies facilitate tunable structural properties of fibrin microthreads. *Acta Biomater* **2012,** *8* (11), 4020-30.
23. Bae, J. W.; Choi, J. H.; Lee, Y.; Park, K. D., Horseradish peroxidase-catalysed in situ-forming hydrogels for tissue-engineering applications. *J Tissue Eng Regen Med* **2015,** *9* (11), 1225-32.
24. Khanmohammadi, M.; Dastjerdi, M. B.; Ai, A.; Ahmadi, A.; Godarzi, A.; Rahimi, A.; Ai, J., Horseradish peroxidase-catalyzed hydrogelation for biomedical applications. *Biomater Sci* **2018,** *6* (6), 1286-1298.
25. Elvin, C. M.; Brownlee, A. G.; Huson, M. G.; Tebb, T. A.; Kim, M.; Lyons, R. E.; Vuocolo, T.; Liyou, N. E.; Hughes, T. C.; Ramshaw, J. A.; Werkmeister, J. A., The development of photochemically crosslinked native fibrinogen as a rapidly formed and mechanically strong surgical tissue sealant. *Biomaterials* **2009,** *30* (11), 2059-65.
26. Syedain, Z. H.; Bjork, J.; Sando, L.; Tranquillo, R. T., Controlled compaction with ruthenium-catalyzed photochemical cross-linking of fibrin-based engineered connective tissue. *Biomaterials* **2009,** *30* (35), 6695-701.
27. Henschen, A.; Lottspeich, F.; Kehl, M.; Southan, C., Covalent structure of fibrinogen. *Ann N Y Acad Sci* **1983,** *408*, 28-43.
28. Partlow, B. P.; Hanna, C. W.; Rnjak-Kovacina, J.; Moreau, J. E.; Applegate, M. B.; Burke, K. A.; Marelli, B.; Mitropoulos, A. N.; Omenetto, F. G.; Kaplan, D. L., Highly tunable elastomeric silk biomaterials. *Adv Funct Mater* **2014,** *24* (29), 4615-4624.
29. Raia, N. R.; Partlow, B. P.; McGill, M.; Kimmerling, E. P.; Ghezzi, C. E.; Kaplan, D. L., Enzymatically crosslinked silk-hyaluronic acid hydrogels. *Biomaterials* **2017,** *131*, 58-67.
30. Wang, L. S.; Lee, F.; Lim, J.; Du, C.; Wan, A. C. A.; Lee, S. S.; Kurisawa, M., Enzymatic conjugation of a bioactive peptide into an injectable hyaluronic acid-tyramine hydrogel system to promote the formation of functional vasculature. *Acta Biomater* **2014,** *10* (6), 2539-2550.
31. Toh, W. S.; Lim, T. C.; Kurisawa, M.; Spector, M., Modulation of mesenchymal stem cell chondrogenesis in a tunable hyaluronic acid hydrogel microenvironment. *Biomaterials* **2012,** *33* (15), 3835-45.
32. Lim, T. C.; Toh, W. S.; Wang, L. S.; Kurisawa, M.; Spector, M., The effect of injectable gelatin-hydroxyphenylpropionic acid hydrogel matrices on the proliferation, migration, differentiation and oxidative stress resistance of adult neural stem cells. *Biomaterials* **2012,** *33* (12), 3446-55.
33. Wang, L. S.; Du, C.; Toh, W. S.; Wan, A. C.; Gao, S. J.; Kurisawa, M., Modulation of chondrocyte functions and stiffness-dependent cartilage repair using an injectable enzymatically crosslinked hydrogel with tunable mechanical properties. *Biomaterials* **2014,** *35* (7), 2207-17.
34. Wang, L. S.; Chung, J. E.; Chan, P. P.; Kurisawa, M., Injectable biodegradable hydrogels with tunable mechanical properties for the stimulation of neurogenesic differentiation of human mesenchymal stem cells in 3D culture. *Biomaterials* **2010,** *31* (6), 1148-57.
35. Sakai, S.; Hirose, K.; Taguchi, K.; Ogushi, Y.; Kawakami, K., An injectable, in situ enzymatically gellable, gelatin derivative for drug delivery and tissue engineering. *Biomaterials* **2009,** *30* (20), 3371-7.
36. Lee, F.; Bae, K. H.; Kurisawa, M., Injectable hydrogel systems crosslinked by horseradish peroxidase. *Biomed Mater* **2016,** *11* (1), 014101.

37. Do, M. K.; Suzuki, T.; Gerelt, B.; Sato, Y.; Mizunoya, W.; Nakamura, M.; Ikeuchi, Y.; Anderson, J. E.; Tatsumi, R., Time-coordinated prevalence of extracellular HGF, FGF2 and TGF-beta3 in crush-injured skeletal muscle. *Anim Sci J* **2012,** *83* (10), 712-7.
38. Simons, M.; Bonow, R. O.; Chronos, N. A.; Cohen, D. J.; Giordano, F. J.; Hammond, H. K.; Laham, R. J.; Li, W.; Pike, M.; Sellke, F. W.; Stegmann, T. J.; Udelson, J. E.; Rosengart, T. K., Clinical trials in coronary angiogenesis: issues, problems, consensus: An expert panel summary. *Circulation* **2000,** *102* (11), E73-86.
39. Simons, M.; Ware, J. A., Therapeutic angiogenesis in cardiovascular disease. *Nat Rev Drug Discov* **2003,** *2* (11), 863-71.
40. Yang, H. S.; Bhang, S. H.; Hwang, J. W.; Kim, D. I.; Kim, B. S., Delivery of basic fibroblast growth factor using heparin-conjugated fibrin for therapeutic angiogenesis. *Tissue Eng Part A* **2010,** *16* (6), 2113-9.
41. Jeon, O.; Ryu, S. H.; Chung, J. H.; Kim, B. S., Control of basic fibroblast growth factor release from fibrin gel with heparin and concentrations of fibrinogen and thrombin. *Journal of Controlled Release* **2005,** *105* (3), 249-259.
42. Sakiyama-Elbert, S. E.; Hubbell, J. A., Development of fibrin derivatives for controlled release of heparin-binding growth factors. *J Control Release* **2000,** *65* (3), 389-402.
43. Folkman, J.; Klagsbrun, M.; Sasse, J.; Wadzinski, M.; Ingber, D.; Vlodavsky, I., A heparin-binding angiogenic protein--basic fibroblast growth factor--is stored within basement membrane. *The American journal of pathology* **1988,** *130* (2), 393-400.
44. Zisch, A. H., Schenk, U., Schense, J. C., Sakiyama-Elbert, S. E., and Hubbell, J. A., Covalently conjugated VEGF–fibrin matrices for endothelialization. *J Control Release* **2001,** *72*, 101-113.
45. Borselli, C.; Storrie, H.; Benesch-Lee, F.; Shvartsman, D.; Cezar, C.; Lichtman, J. W.; Vandenburgh, H. H.; Mooney, D. J., Functional muscle regeneration with combined delivery of angiogenesis and myogenesis factors. *Proc Natl Acad Sci U S A* **2010,** *107* (8), 3287-92.
46. Richardson, T. P., Peters, M. C., Ennett, A. B., and Mooney, D. J., Polymeric system for dual growth factor delivery. *Nature Biotechnology* **2001,** *19*, 1029-1034.
47. Sakiyama-Elbert, S. E., Incorporation of heparin into biomaterials. *Acta Biomater* **2014,** *10* (4), 1581-1587.
48. Wissink, M. J.; Beernink, R.; Pieper, J. S.; Poot, A. A.; Engbers, G. H.; Beugeling, T.; van Aken, W. G.; Feijen, J., Immobilization of heparin to EDC/NHS-crosslinked collagen. Characterization and in vitro evaluation. *Biomaterials* **2001,** *22* (2), 151-63.
49. Younesi, M.; Donmez, B. O.; Islam, A.; Akkus, O., Heparinized Collagen Sutures for Sustained Delivery of PDGF-BB: Delivery Profile and Effects on Tendon-derived Cells In-Vitro. *Acta Biomater* **2016,** *41*, 100-109.
50. Sahni, A.; Baker, C. A.; Sporn, L. A.; Francis, C. W., Fibrinogen and fibrin protect fibroblast growth factor-2 from proteolytic degradation. *Thromb Haemost* **2000,** *83* (5), 736-41.
51. Grover, C. N.; Gwynne, J. H.; Pugh, N.; Hamaia, S.; Farndale, R. W.; Best, S. M.; Cameron, R. E., Crosslinking and composition influence the surface properties, mechanical stiffness and cell reactivity of collagen-based films. *Acta Biomater* **2012,** *8* (8), 3080-3090.
52. Bax, D. V.; Davidenko, N.; Gullberg, D.; Hamaia, S. W.; Farndale, R. W.; Best, S. M.; Cameron, R. E., Fundamental insight into the effect of carbodiimide crosslinking on cellular recognition of collagen-based scaffolds. *Acta Biomater* **2017,** *49*, 218-234.
53. Lee, F.; Chung, J. E.; Kurisawa, M., An injectable enzymatically crosslinked hyaluronic acid-tyramine hydrogel system with independent tuning of mechanical strength and gelation rate. *Soft Matter* **2008,** *4* (4), 880-887.
54. Kurisawa, M.; Chung, J. E.; Yang, Y. Y.; Gao, S. J.; Uyama, H., Injectable biodegradable hydrogels composed of hyaluronic acid-tyramine conjugates for drug delivery and tissue engineering. *ChemComm* **2005,** (34), 4312-4314.

55. Handorf, A. M.; Zhou, Y.; Halanski, M. A.; Li, W. J., Tissue stiffness dictates development, homeostasis, and disease progression. *Organogenesis* **2015,** *11* (1), 1-15.
56. Sakai, S.; Hirose, K.; Moriyama, K.; Kawakami, K., Control of cellular adhesiveness in an alginate-based hydrogel by varying peroxidase and H(2)O(2) concentrations during gelation. *Acta Biomater* **2010,** *6* (4), 1446-52.
57. Jin, R.; Moreira Teixeira, L. S.; Dijkstra, P. J.; Karperien, M.; van Blitterswijk, C. A.; Zhong, Z. Y.; Feijen, J., Injectable chitosan-based hydrogels for cartilage tissue engineering. *Biomaterials* **2009,** *30* (13), 2544-51.
58. Jin, R.; Moreira Teixeira, L. S.; Dijkstra, P. J.; Zhong, Z.; van Blitterswijk, C. A.; Karperien, M.; Feijen, J., Enzymatically crosslinked dextran-tyramine hydrogels as injectable scaffolds for cartilage tissue engineering. *Tissue Eng Part A* **2010,** *16* (8), 2429-40.
59. Heinecke, J. W.; Li, W.; Francis, G. A.; Goldstein, J. A., Tyrosyl radical generated by myeloperoxidase catalyzes the oxidative cross-linking of proteins. *J Clin Invest* **1993,** *91* (6), 2866-72.
60. Sakai, S.; Moriyama, K.; Taguchi, K.; Kawakami, K., Hematin is an Alternative Catalyst to Horseradish Peroxidase for In Situ Hydrogelation of Polymers with Phenolic Hydroxyl Groups In Vivo. *Biomacromolecules* **2010,** *11* (8), 2179-2183.
61. Ke, Z.; Huang, Q., Haem-assisted dityrosine-cross-linking of fibrinogen under non-thermal plasma exposure: one important mechanism of facilitated blood coagulation. *Sci Rep* **2016,** *6*, 26982.
62. Akkara, J. A.; Wang, J. Z.; Yang, D. P.; Gonsalves, K. E., Hematin-catalyzed polymerization of phenol compounds. *Macromolecules* **2000,** *33* (7), 2377-2382.
63. Sampson, J. B.; Ye, Y.; Rosen, H.; Beckman, J. S., Myeloperoxidase and horseradish peroxidase catalyze tyrosine nitration in proteins from nitrite and hydrogen peroxide. *Archives of biochemistry and biophysics* **1998,** *356* (2), 207-213.
64. Hwang, C. M.; Park, Y.; Park, J.; Lee, K.; Sun, K.; Khademhosseini, A.; Lee, S. H., Controlled cellular orientation on PLGA microfibers with defined diameters. *Biomedical microdevices* **2009,** *11* (4), 739-746.
65. Qazi, T. H.; Mooney, D. J.; Pumberger, M.; Geißler, S.; Duda, G. N., Biomaterials based strategies for skeletal muscle tissue engineering: Existing technologies and future trends. *Biomaterials* **2015,** *53*, 502-521.
66. Liao, I. C.; Liu, J. B.; Bursac, N.; Leong, K. W., Effect of Electromechanical Stimulation on the Maturation of Myotubes on Aligned Electrospun Fibers. *Cellular and molecular bioengineering* **2008,** *1* (2-3), 133-145.
67. Chen, M. C.; Sun, Y. C.; Chen, Y. H., Electrically conductive nanofibers with highly oriented structures and their potential application in skeletal muscle tissue engineering. *Acta Biomater* **2013,** *9* (3), 5562-72.
68. Somers, S. M.; Spector, A. A.; DiGirolamo, D. J.; Grayson, W. L., Biophysical Stimulation for Engineering Functional Skeletal Muscle. *Tissue Eng Part B Rev* **2017,** *23* (4), 362-372.
69. Proulx, M. K.; Carey, S. P.; DiTroia, L. M.; Jones, C. M.; Fakharzadeh, M.; Guyette, J. P.; Clement, A. L.; Orr, R. G.; Rolle, M. W.; Pins, G. D.; Gaudette, G. R., Fibrin microthreads support mesenchymal stem cell growth while maintaining differentiation potential. *J Biomed Mater Res A* **2011,** *96A* (2), 301-312.
70. Tao, Z. W.; Favreau, J. T.; Guyette, J. P.; Hansen, K. J.; Lessard, J.; Burford, E.; Pins, G. D.; Gaudette, G. R., Delivering stem cells to the healthy heart on biological sutures: effects on regional mechanical function. *Journal of tissue engineering and regenerative medicine* **2017,** *11* (1), 220-230.
71. Hansen, K. J.; Laflamme, M. A.; Gaudette, G. R., Development of a Contractile Cardiac Fiber From Pluripotent Stem Cell Derived Cardiomyocytes. *Front Cardiovasc Med* **2018,** *5*, 52.
72. Guyette, J. P., Fakharzadeh, M., Burford, E. J., Tao, Z.-W., Pins, G. D., Rolle, M. W. and Gaudette, G. R. , A novel suture-based method for efficient transplantation of stem cells. *J Biomed Mater Res* **2013,** *101A*, 809-818.

73. Husmann, I.; Soulet, L.; Gautron, J.; Martelly, I.; Barritault, D., Growth factors in skeletal muscle regeneration. *Cytokine Growth Factor Rev* **1996,** *7* (3), 249-58.
74. Chen, F. M.; Zhang, M.; Wu, Z. F., Toward delivery of multiple growth factors in tissue engineering. *Biomaterials* **2010,** *31* (24), 6279-308.
75. Sheehan, S. M.; Allen, R. E., Skeletal muscle satellite cell proliferation in response to members of the fibroblast growth factor family and hepatocyte growth factor. *J Cell Physiol* **1999,** *181* (3), 499-506.
76. Marui, A.; Kanematsu, A.; Yamahara, K.; Doi, K.; Kushibiki, T.; Yamamoto, M.; Itoh, H.; Ikeda, T.; Tabata, Y.; Komeda, M., Simultaneous application of basic fibroblast growth factor and hepatocyte growth factor to enhance the blood vessels formation. *J Vasc Surg* **2005,** *41* (1), 82-90.
77. Passipieri, J. A.; Baker, H. B.; Siriwardane, M.; Ellenburg, M. D.; Vadhavkar, M.; Saul, J. M.; Tomblyn, S.; Burnett, L.; Christ, G. J., Keratin Hydrogel Enhances In Vivo Skeletal Muscle Function in a Rat Model of Volumetric Muscle Loss. *Tissue Eng Part A* **2017**.
78. Baker, H. B.; Passipieri, J. A.; Siriwardane, M.; Ellenburg, M. D.; Vadhavkar, M.; Bergman, C. R.; Saul, J. M.; Tomblyn, S.; Burnett, L.; Christ, G. J., Cell and Growth Factor-Loaded Keratin Hydrogels for Treatment of Volumetric Muscle Loss in a Mouse Model. *Tissue Eng Part A* **2017,** *23* (11-12), 572-584.
79. Hill, E.; Boontheekul, T.; Mooney, D. J., Regulating activation of transplanted cells controls tissue regeneration. *Proc Natl Acad Sci U S A* **2006,** *103* (8), 2494-9.
80. Charge, S. B. P., Rudnicki, M.A., Cellular and Molecular Regulation of Muscle Regeneration. *Physiol Rev* **2004,** *84*, 209-238.
81. Allen, R. E.; Boxhorn, L. K., Regulation of skeletal muscle satellite cell proliferation and differentiation by transforming growth factor-beta, insulin-like growth factor I, and fibroblast growth factor. *J Cell Physiol* **1989,** *138* (2), 311-5.
82. Engert, J. C.; Berglund, E. B.; Rosenthal, N., Proliferation precedes differentiation in IGF-I-stimulated myogenesis. *The Journal of cell biology* **1996,** *135* (2), 431-40.
83. Coolican, S. A.; Samuel, D. S.; Ewton, D. Z.; McWade, F. J.; Florini, J. R., The mitogenic and myogenic actions of insulin-like growth factors utilize distinct signaling pathways. *J Biol Chem* **1997,** *272* (10), 6653-62.
84. Cezar, C. A.; Mooney, D. J., Biomaterial-based delivery for skeletal muscle repair. *Adv Drug Deliv Rev* **2015,** *84*, 188-97.
85. Badylak, S. F.; Dziki, J. L.; Sicari, B. M.; Ambrosio, F.; Boninger, M. L., Mechanisms by which acellular biologic scaffolds promote functional skeletal muscle restoration. *Biomaterials* **2016,** *103*, 128-36.
86. Corona, B. T.; Greising, S. M., Challenges to acellular biological scaffold mediated skeletal muscle tissue regeneration. *Biomaterials* **2016,** *104*, 238-46.
87. Sicari, B. M., Londono, R., and Badylak, S. F., Strategies for skeletal muscle tissue engineering: seed vs. soil. *J. Mater. Chem. B* **2015,** *3*, 7881-7895.
88. Hansen, K. J.; Favreau, J. T.; Guyette, J. P.; Tao, Z.-W.; Coffin, S. T.; Cunha-Gavidia, A.; D'Amore, B.; Perreault, L. R.; Fitzpatrick, J. P.; DeMartino, A., Functional effects of delivering human mesenchymal stem cell-seeded biological sutures to an infarcted heart. *BioResearch open access* **2016,** *5* (1), 249-260.
89. Chen, X.; Du, W.; Cai, Z.; Ji, S.; Dwivedi, M.; Chen, J.; Zhao, G.; Chu, J., Uniaxial Stretching of Cell-Laden Microfibers for Promoting C2C12 Myoblasts Alignment and Myofibers Formation. *ACS Appl Mater Interfaces* **2020,** *12* (2), 2162-2170.
90. Li, M. T.; Ruehle, M.; Stevens, H.; Servies, N.; Willett, N.; Karthikeyakannan, S.; Warren, G. L.; Guldberg, R.; Krishnan, L. N., Skeletal myoblast-seeded vascularized tissue scaffolds in the treatment of a large volumetric muscle defect in the rat biceps femoris muscle. *Tissue Eng Part A* **2017**.
91. Nakayama, K. H.; Quarta, M.; Paine, P.; Alcazar, C.; Karakikes, I.; Garcia, V.; Abilez, O. J.; Calvo, N. S.; Simmons, C. S.; Rando, T. A.; Huang, N. F., Treatment of volumetric muscle loss in mice using nanofibrillar scaffolds enhances vascular organization and integration. *Commun Biol* **2019,** *2*.

92. Gilbert-Honick, J.; Iyer, S. R.; Somers, S. M.; Lovering, R. M.; Wagner, K.; Mao, H. Q.; Grayson, W. L., Engineering functional and histological regeneration of vascularized skeletal muscle. *Biomaterials* **2018,** *164*, 70-79.
93. Koffler, J.; Kaufman-Francis, K.; Shandalov, Y.; Egozi, D.; Pavlov, D. A.; Landesberg, A.; Levenberg, S., Improved vascular organization enhances functional integration of engineered skeletal muscle grafts. *Proc Natl Acad Sci U S A* **2011,** *108* (36), 14789-94.
94. Shandalov, Y.; Egozi, D.; Koffler, J.; Dado-Rosenfeld, D.; Ben-Shimol, D.; Freiman, A.; Shor, E.; Kabala, A.; Levenberg, S., An engineered muscle flap for reconstruction of large soft tissue defects. *Proc Natl Acad Sci U S A* **2014,** *111* (16), 6010-5.
95. Lee, J.; Jun, I.; Park, H. J.; Kang, T. J.; Shin, H.; Cho, S. W., Genetically engineered myoblast sheet for therapeutic angiogenesis. *Biomacromolecules* **2014,** *15* (1), 361-72.
96. Cornwell, K. G.; Downing, B. R.; Pins, G. D., Characterizing fibroblast migration on discrete collagen threads for applications in tissue regeneration. *J Biomed Mater Res A* **2004,** *71* (1), 55-62.
97. Grasman, J. M., Page, R. L., and Pins, G. D., Design of an In Vitro Model of Cell Recruitment for Skeletal Muscle Regeneration Using Hepatocyte Growth Factor-Loaded Fibrin Microthreads. *Tissue Eng Part A* **2017,** *23* (15-16), 773-783.
98. Bakooshli, M. A.; Lippmann, E. S.; Mulcahy, B.; Iyer, N.; Nguyen, C. T.; Tung, K.; Stewart, B. A.; van den Dorpel, H.; Fuehrmann, T.; Shoichet, M., A 3D culture model of innervated human skeletal muscle enables studies of the adult neuromuscular junction. *Elife* **2019,** *8*, e44530.
99. Umbach, J. A.; Adams, K. L.; Gundersen, C. B.; Novitch, B. G., Functional neuromuscular junctions formed by embryonic stem cell-derived motor neurons. *PLOS ONE* **2012,** *7* (5), e36049.
100. Kim, J. H.; Kim, I.; Seol, Y.-J.; Ko, I. K.; Yoo, J. J.; Atala, A.; Lee, S. J., Neural cell integration into 3D bioprinted skeletal muscle constructs accelerates restoration of muscle function. *Nature communications* **2020,** *11* (1), 1-12.
101. Gilbert-Honick, J.; Grayson, W., Vascularized and Innervated Skeletal Muscle Tissue Engineering. *Advanced healthcare materials* **2020,** *9* (1), e1900626.
102. Kurpinski, K. T.; Stephenson, J. T.; Janairo, R. R. R.; Lee, H.; Li, S., The effect of fiber alignment and heparin coating on cell infiltration into nanofibrous PLLA scaffolds. *Biomaterials* **2010,** *31* (13), 3536-3542.